# DEVELOPMENT OF IMPROVED METHODS FOR THE ANALYSIS OF METALLOPORPHYRINS IN COALS, SEDIMENTS AND OILS

**WARREN GAVIN PRETORIUS**

**Nat. Higher Dip. Anal. Chem., Masters Diploma Anal. Chem.**

Submitted to the University of Plymouth in partial fulfilment
for the degree of:

**DOCTOR OF PHILOSOPHY**

Department of Environmental Sciences,
University of Plymouth,
Drake Circus,
Plymouth,
Devon,
GREAT BRITAIN

February 1994

i

This thesis is dedicated to my late grandfather Jack Derrick

Webster and to the late Desmond Gervais

"...He's dead now and I am left,
    Bereft, wondering
    To what stream I could take whom and
    Kneel like that, and say:
    Taste how sweet it is."

Sweetwater, Guy Butler

## ABSTRACT

## Development of improved methods for the analysis of metalloporphyrins in coals, sediments and oils

A high temperature gas chromatography (HTGC)-inductively coupled plasma-mass spectrometry (ICP-MS) interface was successfully developed which allowed the analysis of metalloporphyrins (Retention Index >6000), with detection limits of less than 1 nanogram on column. The system was used together with conventional HTGC-flame ionization detection and HTGC-mass spectrometry (MS) for the analysis of geoporphyrin fractions from Julia Creek, Serpiano, Marl Slate and Green River shales. This allowed the rapid fingerprinting of the metals chelated to the porphyrins in these samples. Previously unreported titanium porphyrins were detected in two of these shales, the Marl Slate and Julia Creek. An iron porphyrin fraction from Bagworth coal was also examined for the first time using both HTGC-ICP-MS and HTGC-MS and the distributions of the ETIO porphyrins calculated.

The HTGC method was found to be useful only for qualitative scanning of the geoporphyrin fractions. This was due to problems with the stability of the gas chromatographic columns used for these analyses. The columns used were found to last between 5 and 10 injections, after which the porphyrins appeared as broad humps, slowly eluting off the column.

A high performance liquid chromatography (HPLC)-ICP-MS method was developed to allow the quantitative analysis of geoporphyrins, which was not possible with the HTGC-ICP-MS method. The HPLC-ICP-MS interface used allowed good chromatographic separation to be achieved, with less than 10 % loss in column efficiency. This system was used for the quantitative analysis of gallium and nickel porphyrins from coals and shales respectively. The qualitative distributions obtained for the geoporphyrins using HPLC-ICP-MS showed good agreement with the HPLC-UV/VIS results.

A GC-Low Pressure-ICP-MS interface was designed and constructed and the analysis of metalloporphyrins attempted. The metalloporphyrins were not successfully eluted through the GC-LP-ICP-MS system. However, a number of more volatile organometallic compounds were analysed (tetraethyl lead, ferrocene and tetrabutyl tin). Interestingly the system also produced fragment molecular ions of chlorobenzene, bromobenzene and iodobenzene at low plasma powers (~10 W), using the carrier gas as the plasma gas (helium). Thus the system could be used to obtain both atomic and molecular spectra, which has not been achieved previously.

# ACKNOWLEDGMENTS

## AUTHORS DECLARATION:

At no time during the registration for the degree of Doctor of Philosophy has the author been registered for any other University award.

This study was financed with the aid of the Foundation for Research Development (South Africa) and University of Plymouth.

Signed.. _W. Pretorius_ ..........

Date......23/03/94.............

v

# CONTENTS:

# CHAPTER 1: INTRODUCTION

## CHAPTER 4: HPLC ANALYSIS OF GEOPORPHYRINS

# CHAPTER 5: GC-LOW PRESSURE-ICP-MS:

# CHAPTER 6: CONCLUSIONS AND SUGGESTIONS FOR

## FUTURE WORK

# CHAPTER 7: EXPERIMENTAL

# LIST OF ABBREVIATIONS AND SYMBOLS:

| | |
|---|---|
| A | Ampere |
| AED | atomic emission detection |
| amu | atomic mass unit |
| Ar | Argon |
| °C | degrees celsius |
| Cl | Chloride |
| CI | chemical ionization |
| cm | centimetre (x $10^{-2}$ m) |
| Cu | Copper |
| $C_{18}$ | octadecylsilane |
| DC | direct current |
| DCM | dichloromethane |
| DCP | direct current plasma |
| DPEP | desoxophylloerythroetioporphyrin |
| ECD | electron capture detector |
| EI | electron impact |
| Et | ethyl ($-C_2H_5$) |
| ETIO | ETIO porphyrin |
| Fe | Iron |
| FID | flame ionization detector |
| FTIR | fourier transform infra red spectroscopy |
| Ga | Gallium |
| GC | gas chromatography |
| HCl | hydrochloric acid |
| He | Helium |
| HPLC | high performance liquid chromatography |
| hrs | hours |
| HTGC | high temperature gas chromatography |
| ICP | inductively coupled plasma |
| ICP-MS | inductively coupled plasma-mass spectrometry |
| i.d. | internal diameter |
| iso. | isothermal |
| kPa | kilopascal (x $10^3$ Pa) |
| kW | kilowatt (x $10^3$ W) |
| LC | liquid chromatography |
| LOD | limit of detection |
| m | Metre |
| mbar | millibar (x $10^{-3}$ bar) |
| Me | methyl ($-CH_3$) |
| mg | milligram (x $10^{-3}$ g) |
| MHz | mega hertz |
| MIP | microwave induced plasma |
| min | minute |
| ml | millilitre (x $10^{-3}$ L) |
| mm | millimetre (x $10^{-3}$ m) |
| Mn | Manganese |
| MS | mass spectrometry |
| m/z | mass to charge ratio |
| n/a | not applicable |
| ng | nanogram (x $10^{-9}$ g) |
| Ni | Nickel |
| nm | nanometre (x $10^{-9}$ m) |

| | |
|---|---|
| o.d. | outer diameter |
| OEP | octaethylporphyrin |
| pg | picogram (x $10^{-12}$ g) |
| ppm | parts per million (mg/L or $\mu$g/g) |
| RF | radio frequency |
| RI | retention index |
| RSD | relative standard deviation |
| Ret. time | retention time |
| s | second |
| SEC | size exclusion chromatography |
| SFC | supercritical fluid chromatography |
| SIR | selected ion recording |
| Temp. | temperature |
| TIC | total ion current |
| TLC | thin layer chromatography |
| torr | torr (133 Pa) |
| TPP | tetraphenyl porphyrin |
| $\mu$A | microampere (x $10^{-6}$ A) |
| $\mu$g | microgram (x $10^{-6}$ g) |
| $\mu$L | microlitre (x $10^{-6}$ L) |
| $\mu$s | microsecond (x $10^{-6}$ s) |
| UV/VIS | ultraviolet-Visible spectroscopy |
| V | volt |
| V=O | Vanadyl |
| W | Watt |
| Zn | Zinc |

# LIST OF FIGURES

# LIST OF TABLES

# 1.0 INTRODUCTION:

## 1.1 Origins of Metalloporphyrins in the geosphere:

In 1934 Alfred Treibs first identified metalloporphyrins in a number of bitumens and oils [1]. This was the first evidence that fossil fuels were of biological origin and has been cited as the beginning of organic geochemistry [2].

Desoxyphylloerythroetioporphyrin (DPEP) and etioporphyrin (ETIO) are the two major groups of geoporphyrins. These occur as pseudo-homologous series extending from $C_{25}$ to $C_{33}$ (in some cases to $C_{37}$). The DPEP and ETIO porphyrins usually occur as nickel ($Ni^{+2}$) and vanadyl ($V=O^{+2}$) complexes in oils, oil shales and sediments, in concentrations of > 10 $\mu g/g$ [2]. Other metals identified in geoporphyrins are copper ($Cu^{+2}$) in porphyrins from recent sediments [3] and iron ($Fe^{+3}$), gallium ($Ga^{+3}$) and manganese ($Mn^{+2}$) in porphyrins from coals [4,5].

The majority of the investigations of geoporphyrins have concerned the identification of geoporphyrin precursors. Treibs, proposed a scheme for the conversion of chlorophyll-a to DPEP and ETIO porphyrins [6]. The scheme was later modified by Corwin and has since been modified further (Figure 1.1)[7]. Although chlorophyll-a is still proposed as the major source of geoporphyrins, chlorophyll-b and -c, along with some of the bacteriochlorophylls also contribute [2].

1
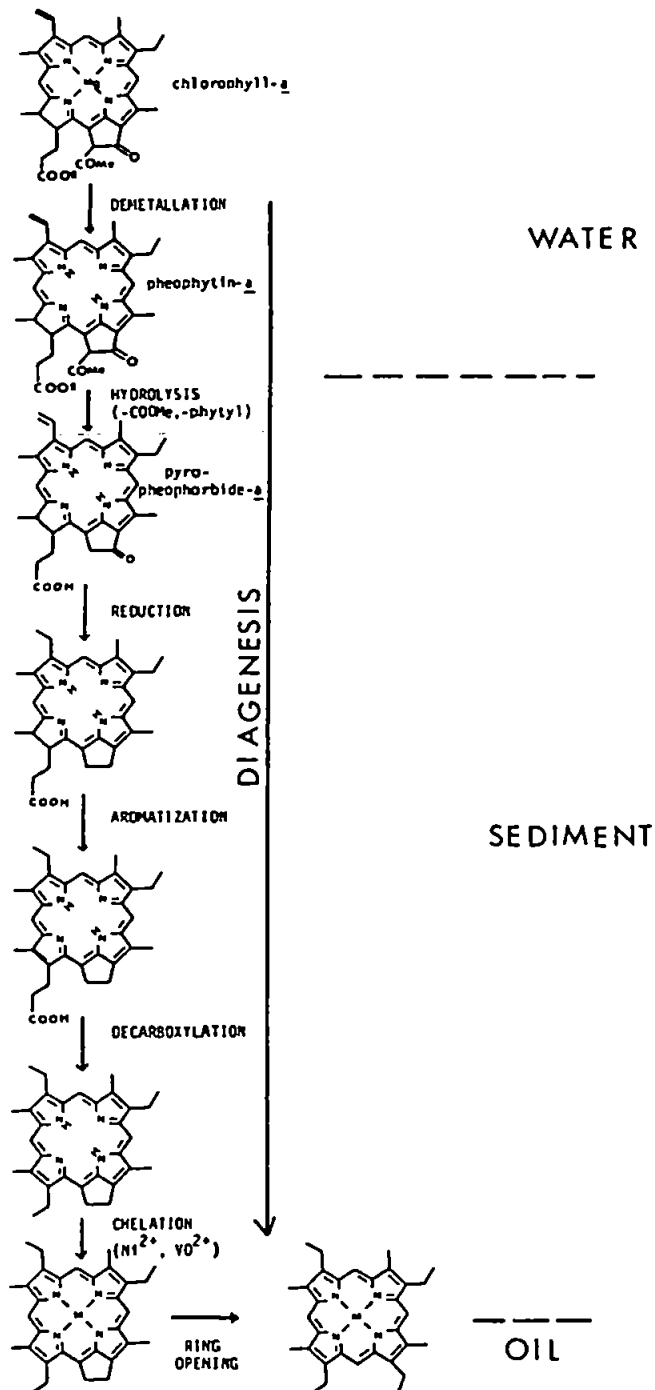
**Figure 1.1:** Treibs-Corwin scheme for geochemical conversion of chlorophyll-a to $C_{32}$ metalloporphyrins (from [2]).

The occurrence of ETIO porphyrins has been proposed to be due to oxidative cleavage rather than thermal scission of the isocyclic ring of the DPEP macrocycle [8]. However, recent laboratory degradation studies of vanadyl porphyrins at different temperatures seem to support the hypothesis of thermal scission [9].

The formation of iron and gallium porphyrins in coals has been proposed to take a different route whereby haems were also considered to be important precursors (Figure 1.2) [10].

Geoporphyrins have been used in oil exploration to provide oil-source rock and oil-oil correlations [11,12] and as oil maturity indicators [13]. They have also been proposed as palaeoenvironmental indicators, indicating oxic/anoxic conditions and other parameters in the sediment-water interface [14].

The presence of nickel and vanadyl complexes in oils causes problems in refining processes, such as catalyst poisoning and unwanted side reactions during catalytic cracking. This has led to interest in metal speciation and a need for quantitative information [15].

The use of porphyrins as markers has been somewhat limited by the applicability of the analytical techniques, the development of new techniques is likely to lead to better utilization of these molecules as markers.

Chlorophyll a
large amount
chemically less stable

Cytochrome c
a small amount
chemically more stable

?

DIAGENESIS
(Lignite stage)

Mesoporphyrin IX
$C_{32}$ diCOOH

$-CO_2$

$-CO_2$

$C_{32}$ mono COOH

$-CO_2$

Cycloetioporphyrin III
$C_{32}$, minor in bituminous
coals

Etioporphyrin III
$C_{32}$ (lignites and
bituminous coals)

CATAGENESIS
(Bituminous coal stage)

$-C_2H_5$    $-CH_3$

$C_{29}$ ⟵ $C_{30}$ ⟵ $C_{31}$
     $-CH_3$    $-CH_3$

$C_{28}$ ⟶ $C_{27}$ ⟶ $C_{26}$ etc

Bituminous Cracking Progression
(dotted lines on structure above)

$C_{32}$ Isomer
(not yet recognised in coals)

**Figure 1.2:** Proposed scheme of chemical changes in natural porphyrins during diagenesis and catagenesis of humic coal deposits. Chlorophyll-a and cytochrome-c are taken as examples of chlorophylls and haems respectively (from [10]).

4

## 1.2 Analysis of Geoporphyrins:

Over the last 60 years many analytical techniques have been applied to the analysis of geoporphyrins. Table 1.1 shows the major techniques applied to geoporphyrin analysis and the amount of material required.

Whilst an overview of the most important techniques used is provided here, for more detailed information the reader is referred to recent reviews [46,47]. A brief review of chromatographic-element selective techniques applied to geoporphyrins is also included in the respective chromatographic sections.

### 1.2.1 UV/VIS Spectroscopy:

UV-VIS spectroscopy was the first method used to identify metalloporphyrins in oils and bitumens [1] and is still one of the most widely used methods for identification and quantification of porphyrins [10,13,48].

Metalloporphyrins and free-base porphyrins have very different absorption spectra. The free-base spectra are characterised by four absorption maxima between 450 and 650 nm, whereas the metalloporphyrins have three absorption maxima, a Soret band usually at ~400 nm and $\alpha$ and $\beta$ bands at between 500 and 600 nm [49]. Thus free-base porphyrins can be distinguished from metallated porphyrins.

5

| Technique | Amount Required | Use, information gained and comments | Ref. |
|---|---|---|---|
| Column LC | ~ 100mg to 100g | Separation of porphyrins from matrix. Separation of free-base and metalloporphyrins | 16 |
| TLC | ~1-100mg | Separation of different metalloporphyrins and crude structural separations. | 16 |
| HPLC ($SiO_2$) | ~100ng | Separation of structural types, homologues of free-base porphyrins only. | 17 |
| HPLC ($C_3H_6NH_2$) | ~100ng | Separation of nickel and vanadyl porphyrins. | 18 |
| HPLC ($C_{18}$) | ~100ng | Separation of structural types, homologues and isomers of nickel and vanadyl porphyrins. | 19, 20 |
| SEC | ~100ng | Molecular weight distributions of geoporphyrins. | 21 |
| HPLC-MS | ~100ng | Separation of structural types, homologues and isomers of free-base porphyrins. Molecular formula obtained. | 22 |
| HPLC-ICP-AES/GFAA | ~1-10$\mu$g | Separation of vanadyl and nickel porphyrins with element selective detection. | 23-26 |
| GC | ~100ng | Separation of structural types, co-elution of homologues and isomers occurs. Normal temperature GC requires the use of silicon derivatives of geoporphyrins. | 27-29 |
| GC-MS | ~1$\mu$g | Separation of structural types, homologues and isomers by mass chromatography. Silicon derivatives used. | 29-32 |
| HTGC | ~1-5$\mu$g | Separation of structural types. Co-elution of homologues and isomers. | 33, 34 |

**Table 1.1:** Analytical techniques used for the analysis of geoporphyrins (modified from [51])

| | | | |
|---|---|---|---|
| HTGC-MS | ~1-5$\mu$g | Separation of structural types, homologues and isomers by mass chromatography. Molecular formula obtained. | 34 |
| HTGC-AED | ~1$\mu$g-200mg | Speciation information on metalloporphyrins. | 35-37 |
| SFC/SFC-MS | ~1$\mu$g-10$\mu$g | Essentially minimal separation of geoporphyrins. Co-elution can be seen with mass-chromatography. | 38, 39 |
| UV/Visible | ~5$\mu$g | Structural type and chelating metal identified. | 40 |
| EI Probe MS | ~1$\mu$g | Structural type and molecular formula. | 41 |
| CI (H$_2$) Probe-MS | ~1$\mu$g | Structural information on $\beta$-alkyl substituents. | 42 |
| $^1$H NMR and $^1$H nOe NMR | ~100$\mu$g-1mg | Structural information on $\beta$-alkyl and meso substituents. Unambiguous structures for unsymmetrical porphyrins. | 43, 44 |
| X-ray crystallography | ~10$\mu$g | Complete structure, if good single crystal can be obtained. | 45 |

Table 1.1 (continued)

The wavelengths of the metalloporphyrin absorption maxima depend on the nature of the chelated metal. For example, the nickel porphyrins have Soret bands at 390 nm, 514 nm ($\alpha$) and 550 nm ($\beta$) and vanadyl porphyrins at 405, 530 and 570 nm respectively. The extinction coefficient of the absorption maxima vary, depending on the porphyrin macrocycle (e.g. DPEP < ETIO). The $\alpha/\beta$ ratio varies according to the porphyrin macrocycle type (e.g. for nickel ETIO ratio ~3 and nickel DPEP ratio ~2) [49].

Knowledge of  the extinction coefficient allows approximate quantification of the porphyrins in a mixture from the UV/VIS spectra. The type of porphyrin, the chelated metal and the type of macrocycle or mixture can be identified.

## 1.2.2. Mass Spectrometry:

Hood *et al.* obtained the first mass spectrum of nickel ETIO porphyrin in 1960 [50]. Since then probe mass spectra of porphyrins have become one of the most important means of identifying geoporphyrins.

When mass spectra of geoporphyrins are obtained using electron impact (EI) at low ionizing voltage (16 eV), molecular ions are produced almost exclusively [51,52]. This makes the interpretation of the mass spectra fairly simple, since the molecular masses of the porphyrin homologues are well known and can be correlated directly with the mass spectral data. The distribution patterns of the homologous/pseudo homologous

series can be obtained from the mass spectra. Mass spectra give limited information on the structure of the porphyrin macrocycles (i.e. ETIO or DPEP). Figure 1.3 shows the probe mass spectrum for Boscan crude obtained at 16 eV.

Chemical ionization (CI) of porphyrins causes extensive fragmentation of the porphyrin macrocycle, which results in a complex spectrum [47]. Thus CI has been far less utilised compared with EI [42,52].

Distillation of impurities from the porphyrin fraction during the probe MS analysis can serve as an in situ method of purification. This is achieved by heating the probe to ~200°C and allowing the lighter hydrocarbons to distil from the sample. When this is complete the probe temperature can be raised to the sublimation temperature of the porphyrins and a mass spectrum of the porphyrins obtained [51].

## 1.2.3. High Performance Liquid Chromatography:

HPLC methods for the analysis of geoporphyrins have included both normal-phase and reverse-phase methods [17-26]. Both have advantages and disadvantages. The major advantage of reverse phase methods is that the porphyrins are analysed intact, whereas the normal phase methods require demetallation for good resolution. Methods used to date are shown in Table 1.1.

Geoporphyrins were first analysed by normal-phase HPLC by Hajibrahim *et al.* in 1978 [17]. This work showed that the ETIO

9
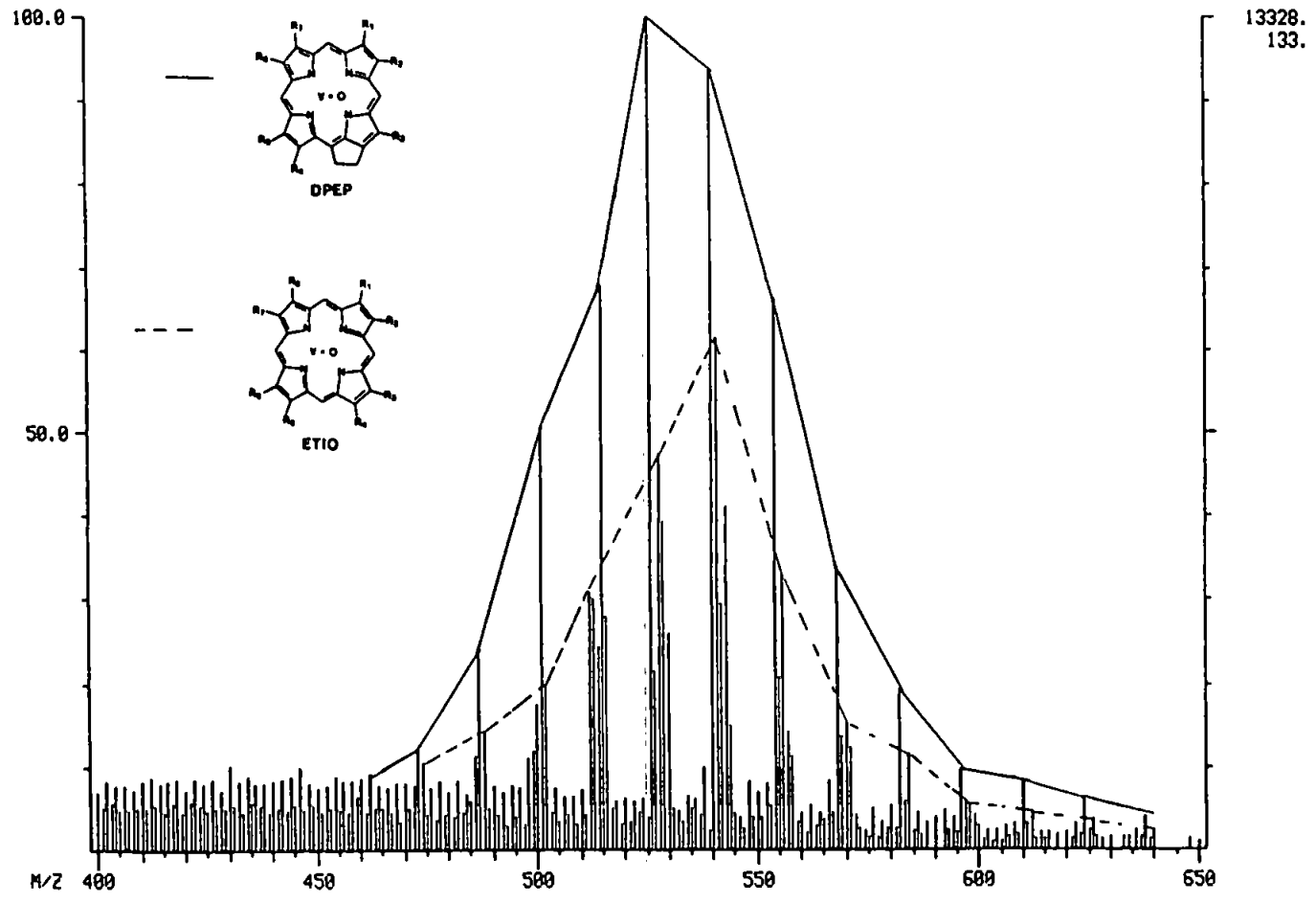
**Figure 1.3:** Probe mass spectrum of vanadyl porphyrin fraction of Boscan crude at 16eV.

and DPEP series could be separated with a 5 $\mu$m silica column and that the different homologues or pseudohomologues could be separated. This allowed the structure and distribution of numerous geoporphyrins in various geological samples to be determined by several workers [53-55]. The normal phase method became the most widely used method, however such analyses required the demetallation of the geoporphyrins with methanesulphonic acid. The acid treatment resulted in loss of material and was probably responsible for the degradation of the porphyrin macrocycle [56].

Xu *et al.* used normal phase aminopropyl silica to separate both nickel and vanadyl porphyrins, but resolution of porphyrin macrocycles was not investigated [18].

The use of reverse phase $C_{18}$ separations for the direct analysis of intact metalloporphyrins was initially attempted by Hajibrahim *et al.*, but this only separated the nickel from the vanadyl porphyrins on the basis of their respective polarities [17]. In this study no attempt was made to optimise the mobile phase and diameter of the packing material [17]. Fish *et al.* used reverse phase $C_{18}$ for the separation of nickel and vanadyl porphyrins and obtained better resolution than that obtained by Hajibrahim *et al.*, but did not investigate the resolution between the different porphyrins macrocycles [25,26].

Sundararaman investigated the separation of vanadyl porphyrins using reverse phase $C_{18}$ and showed that ETIO and DPEP could be

separated [20]. The method also separated homologues, pseudohomologues and positional isomers as illustrated in Figure 1.4. The resolution of this method was improved later by increasing the column length [57]. Boreham et al. separated nickel porphyrins using reverse phase $C_{18}$ and obtained separation of ETIO/DPEP, homologues/pseudo homologues and positional isomers [19].

Size exclusion chromatography (SEC) has been applied to the analysis of both vanadyl and nickel porphyrins [22,58]. The SEC separations have shown the existence of large porphyrins (molecular mass > 1000), but the use of this technique remains rather limited.

HPLC-MS has been limited to the analysis of free-base geoporphyrins [22,58]. This is probably largely due to the difficulties involved with the use of thermospray interfaces for metalloporphyrin analysis.

HPLC has been coupled to various element selective detectors for the analysis of nickel and vanadyl geoporphyrins [21,23-26]. Fish et al. used both SEC and reverse phase $C_{18}$ HPLC in combination with graphite furnace atomic absorption for the direct analysis of both nickel and vanadyl porphyrins in various oils and shales [25,26]. de Waal et al. used both SEC and reverse phase $C_{18}$ HPLC in combination with ICP-AES for the analysis of vanadyl and nickel porphyrins in various oils and asphaltenes [23,24].
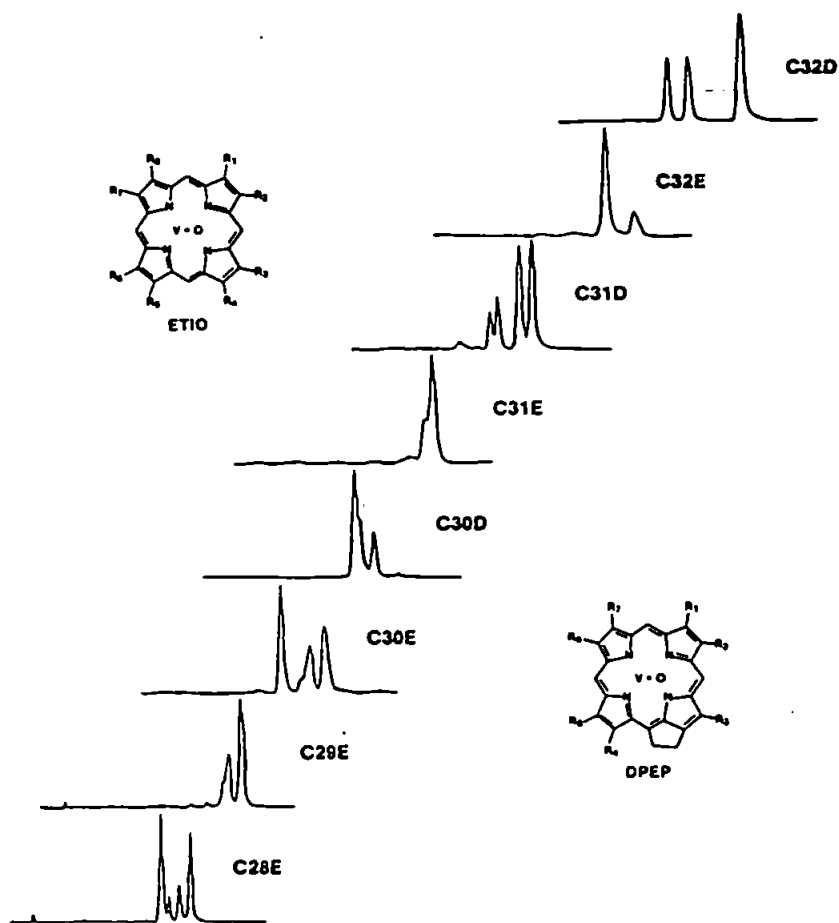
**Figure 1.4:** Chromatograms showing the resolution of structural isomers within each carbon number and porphyrin type for vanadyl porphyrins (250 mm x 4.6 mm i.d. Hypersil $C_{18}$ (3 $\mu$m), 1 ml/min, 45% methanol, 45% acetonitrile and 10% water). D= DPEP, E=ETIO [20]

## 1.2.4. Gas Chromatographic analysis of geoporphyrins:

The use of GC for the analysis of geoporphyrins can be divided into the analysis of derivatized geoporphyrins and the direct analysis of metallated geoporphyrins.

## 1.2.4.1. Derivatization of geoporphyrins for GC analysis:

Boylan et al. first reported the use of silicon derivatization of porphyrins for GC analysis [59]. The method was first applied to geoporphyrins in 1968 [27], allowing the analysis of Boscan crude oil and Green River Shale porphyrins. This method was further refined and applied to GC-MS by Gill [60].

The derivatisation steps are shown in Figure 1.5. The method, like normal phase HPLC, relies on the demetallation of the total geoporphyrin fraction, followed by derivatization. The derivatized silicon porphyrins have retention indices of ~3500 (normally ~6000 for porphyrins), which allows the analysis of these under normal GC conditions. Figure 1.6 shows the improved resolution obtained by Gill for Boscan crude, compared with that of Boylan et al. using packed GC columns [27,60]. This method has been applied to a number of geoporphyrins samples and is still the only practical routine GC analysis method for geoporphyrins [55].

## 1.2.4.2. Direct gas chromatography of geoporphyrins:

The first attempts at gas chromatographic analysis of

14
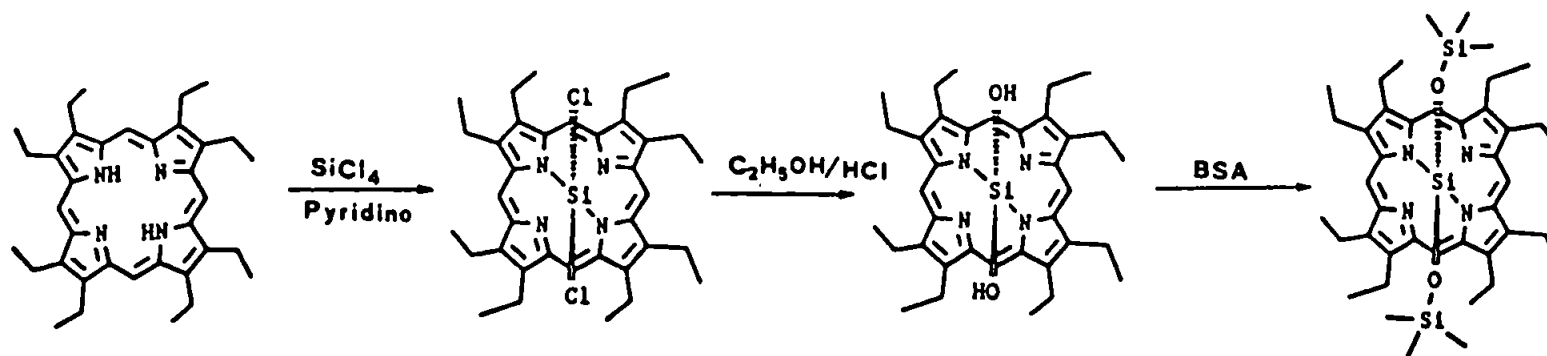
Figure 1.5: Derivatization scheme for demetallated porphyrins to silicon porphyrins, used in GC analysis. BSA= N,O Bis(trimethylsilyl) acetamide (from [38]).

BOSCAN  PETROPORPHYRIN

$(70-135 \times 10^6$ YRS)

a

column-$\frac{1}{8}$'x10' ss
coating-J%Apiezon L on
     rough glass beads
temp. programmed  225→250°C
     at 1°/min.
flow-15ml/min. N$_2$
qty.-1 µg.

E.C.D

time    (hrs)

2hrs.                    1hr.

b

Relative Intensity

Kovats Retention Index
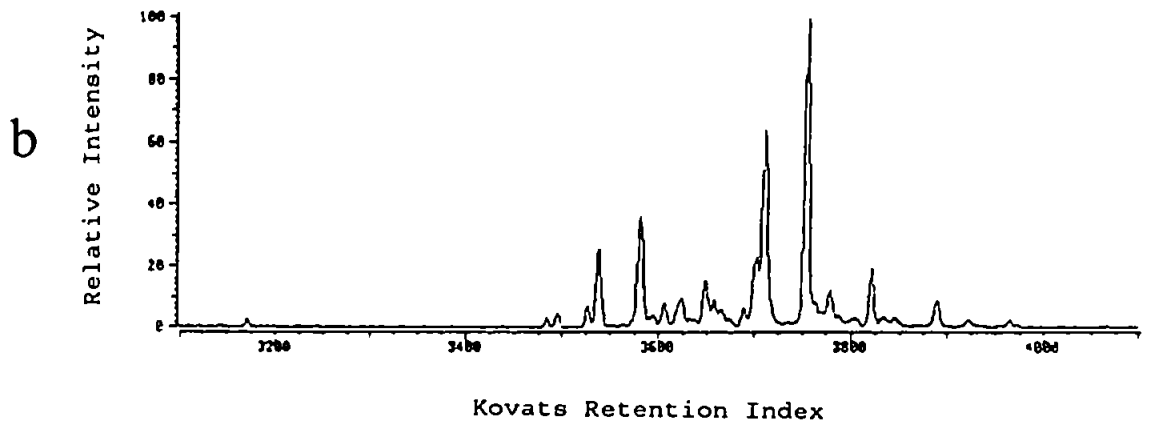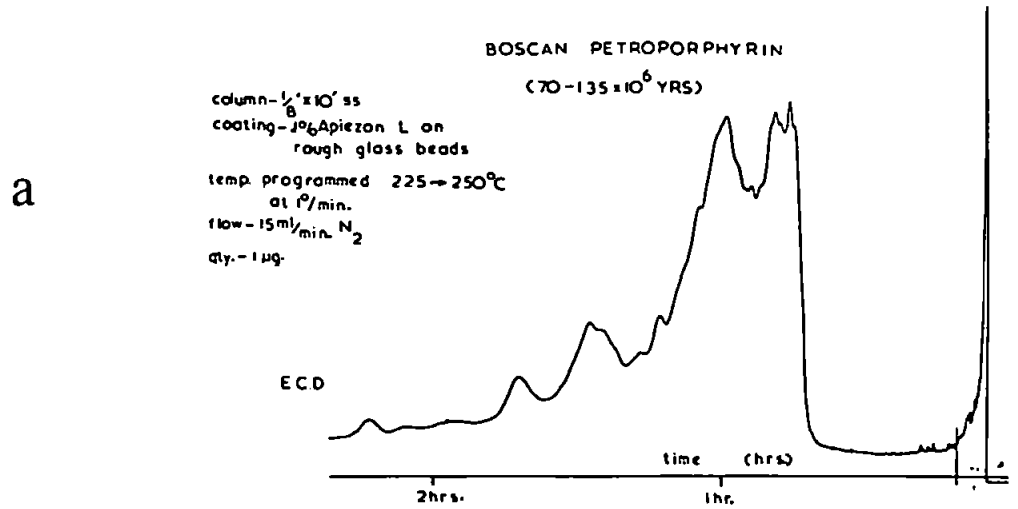
**Figure 1.6:** Chromatograms of Derivatized Boscan geoporphyrins.

(a) Packed column, as

bis(trimethylsiloxy)silicon(IV)porphyrins [27]

(b) Capillary GC, on 25 m X 0.3 mm OV-1 column, 2-

5 µg on column as

bis(t-butyldimethylsiloxy)silicon(IV)porphyrins

[28].

porphyrins led to the development of so-called hyperpressure-gas chromatography, which was the beginning of supercritical fluid chromatography (SFC) [61-63]. Therefore it is arguable whether this can be classified as the first "gas chromatographic" analysis of porphyrins.

Marriott et al. obtained arguably the first gas chromatographic analysis of porphyrins [33], using a 6 m, 0.30 mm i.d. (0.15 $\mu$m, OV-1) (Hewlett Packard) column, shown in Figure 1.7.

In 1983 Gallegos et al. analysed a vanadyl geoporphyrin sample from Messel Shale by GC-MS [64]. This showed that DPEP could be separated from ETIO porphyrins, but the resolution was disappointing.

Blum et al. analysed a number of shale samples using high temperature gas chromatography (> 350°C) with custom made glass columns and investigated the separation of geoporphyrins on various phases [39]. Figure 1.8 shows the separation of the nickel porphyrin fraction of Marl Slate on a number of different phases. The chromatograms show that both apolar and polar phases give good separation of the geoporphyrins, with only the selectivity varying. Blum recommended the use of the apolar phases for the separation of the geoporphyrins, because of the higher elution temperatures of the geoporphyrin on the polar columns. The higher elution temperatures were probably a result of the $\pi$ interactions between the phenyl rings associated with the stationary phase and the extended $\pi$
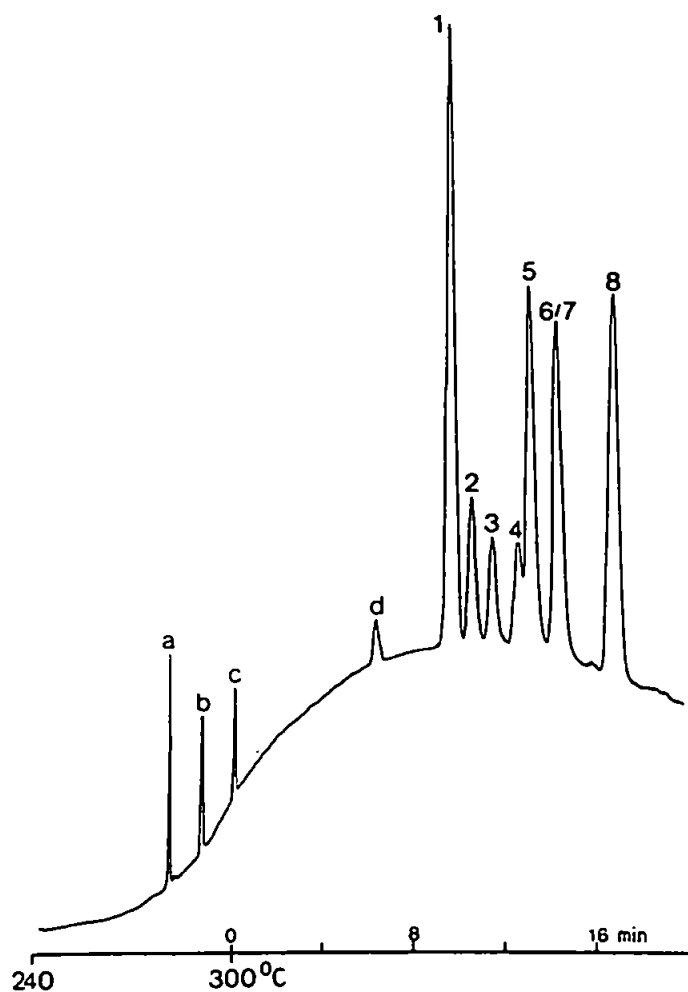
**Figure 1.7:** Capillary GC of n-alkanes and metalloporphyrins on 6 m x 0.3 mm i.d., OV-1). a= $n$-$C_{42}$, b= $n$-$C_{44}$, c= $n$-$C_{50}$, 1= Cu AETIO I, 2= Ni AETIO I, 3= V=O AETIO I, 4= Co AETIO I, 5= Cu OEP, 6= Ni OEP, 7= V=O OEP, 8= Co OEP [33]

a   PS 347.5 (100% methyl, -OH terminal)
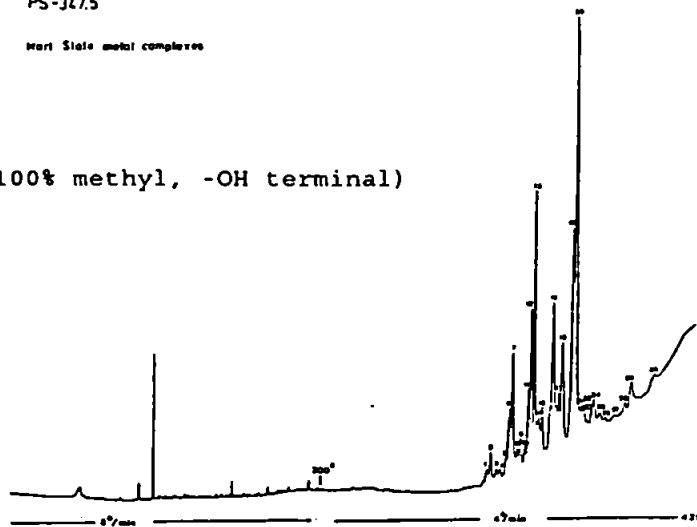
PS-090

Marl Slate metal complexes

b   PS-90 (80% methyl, 20% phenyl, -CH₃O terminal)
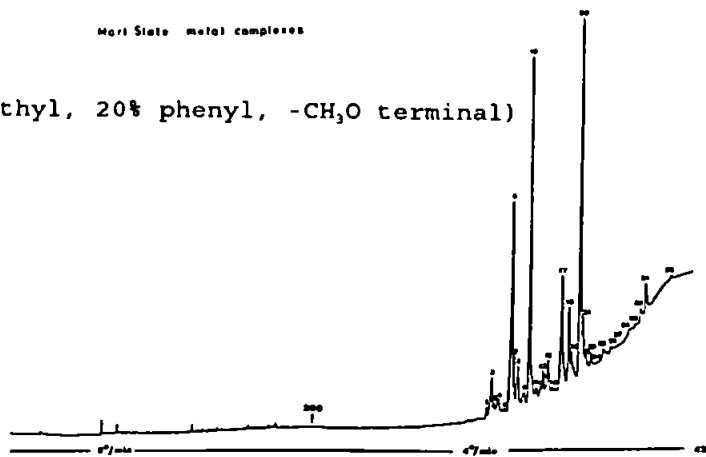
OV-61-OH

Marl Slate metal complexes

c   OV-61-OH (67% methyl, 33% phenyl, -OH terminal)
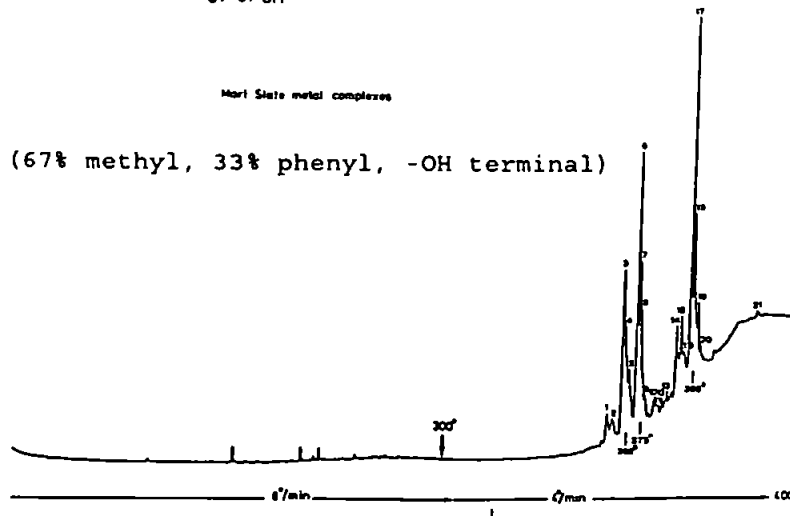
**Figure 1.8:**  Capillary GC of Marl Slate nickel porphyrins on 20
m x 0.3 mm i.d. (0.15 μm film thickness) columns
coated with the phases indicated [38].

electron system of the porphyrin molecule [38].

The glass capillary columns used by Blum, lasted on average, 20-30 injections. This included attempts to prolong the column life by the removal of the first few coils of the glass columns and the use of silica retention gaps [39].

The first separation of geoporphyrins on a commercially available column was reported in 1983 but more recently several workers have reported separation of geoporphyrins on commercial high temperature columns [35-37,65].

The major advantage that HTGC analysis of porphyrins has over the HPLC or GC (normal temperature i.e. >350°C) method is that HTGC-MS can be performed directly on geoporphyrins with no need for demetallation or derivatization [39].

The use of HTGC-AED for the analysis of geoporphyrins has been described in a number of papers [35-37]. Quimby *et al.* examined various nickel, iron and vanadyl porphyrins in a number of oils, using a 5 m, 0.53 mm (0.15 $\mu$m, methylsiloxane) column [36]. Hausler *et al.* used HTGC-AED with a 12 m, 0.53 mm (0.15 $\mu$m, methylsiloxane) aluminium clad column for the analysis of nickel porphyrins in various crude oils [35].

## 1.3 Inductively coupled plasma-Mass spectrometry:

The idea of coupling a plasma source to a mass spectrometer

arose from initial experiments with electrical discharges, chemical reactors and flames as sources for the mass spectrometry. These experiments involved sampling ions directly from these various sources into a mass spectrometer [66,67]. The possibility of plasma sources began with experiments in the early 1960's using a DC plasma as the source [68]. The logical progression to inductively coupled plasma (ICP) and microwave induced plasma (MIP) sources was made in the late 1970's [69]. This culminated in the manufacture of the first commercial instrument in 1983.

## 1.3.1. Instrumentation:

The following sub-sections of 1.3.1. give a brief description of the component parts of an ICP-MS. This description is largely based on the VG PlasmaQuad II instrument (Figure 1.9). A more detailed description of ICP-MS instrumentation is available in reference [69].

## 1.3.1.1. Sample introduction:

Samples analysed by ICP-MS are usually aqueous solutions, but can be gaseous or solids (in the case of slurry nebulization or laser ablation) [70-72]. The sample solution is aspirated and converted into an aerosol by a v-groove or concentric nebulizer. The aerosol droplets are filtered *via* a Scott double pass spray chamber, with the larger droplets going to waste. Only about 1-3 % of the aspirated sample solution finally reaches the plasma with a standard nebulization system.

Inductively Coupled          Sampling                              Mass Spectrometer
       Plasma                 Interface

                           Skimmer
                           Cone

                    Sampling                  Ion Lenses          Quadrupole Mass              Ion
RF Induction Coil    Cone              (including photon stop)         filter               Detector

              O  O

Plasma Torch  O  O  O

                    Rotary                                     High Vacuum
RF Power            pump                                         pumps
                                                                                          Signal
                                                                                          Handling
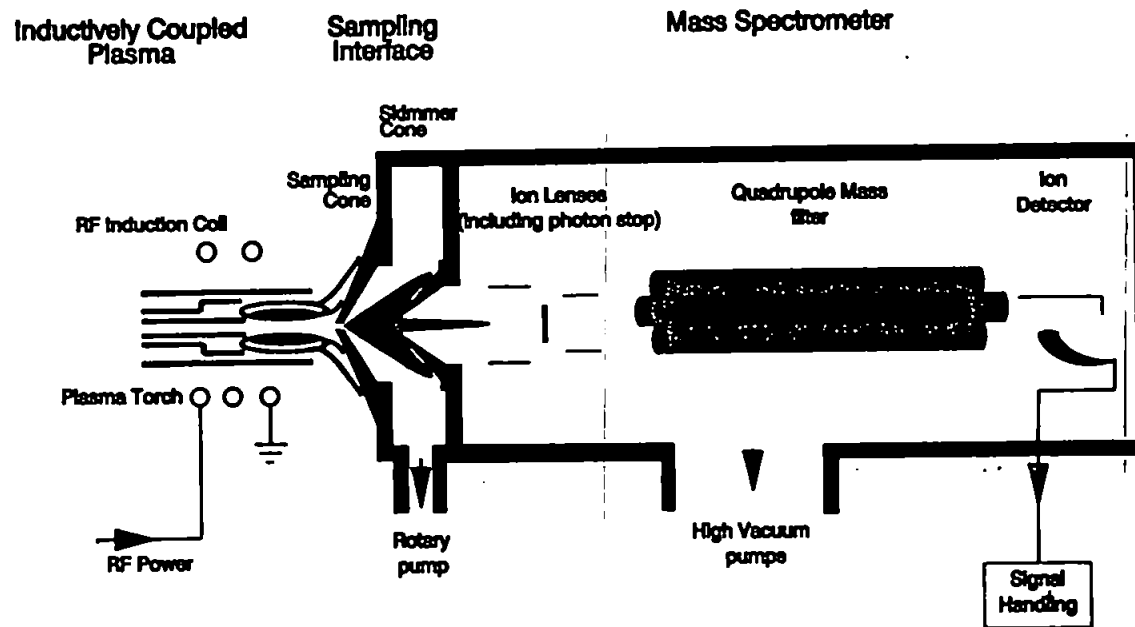
**Figure 1.9:   Diagrammatic representation of a VG ICP-MS**

## 1.3.1.2. Plasma generation:

The plasma is typically generated by a 1.5 kW, 27.12 MHz radio frequency generator in a Fassel design torch (1 mm injector diameter), via a 3 turn load coil. The typical argon flow rates are between 16-18 L/min total.

## 1.3.1.3. ICP-MS interface:

The plasma gas is sampled into the low pressure (~3 mbar) expansion stage *via* the nickel sampler cone (usually 1 mm aperture). The sampled gas reaches the speed of sound in less than one aperture diameter, and rapid expansion of the gases causes a drop in temperature and inhibits reactions occurring in the sampled plasma gas. This adiabatic expansion results in the formation of a "free jet", bounded by a shock wave known as "barrel shock". The temperature in the centre of the free jet is ~200 K and this helps to cool the skimmer cone, since the surrounding gas is still hot. A second shock wave known as the "Mach disc" is formed perpendicularly across the axis of the "free jet" at a distance determined by the pressure differential between the expansion stage and the plasma as well as the aperture diameter of the sampler cone. Beyond the Mach disc the flow becomes subsonic and the extracted gas mixes with surrounding gas. The tip of the nickel skimmer cone is mounted upstream of the Mach disc, sampling gas from within the barrel shock region. The pressure behind the skimmer cone is low enough to ensure that the mean free path of the sampled ions is greater than the system dimensions. A slide valve is

situated behind the expansion stage and this isolates the high
vacuum of the mass spectrometer from the expansion stage, when
the instrument is not in use [73].

### 1.3.1.4. Ion lenses:

The extracted ions form an ion beam behind the skimmer cone and
these ions are focused at the entrance of the quadrupole mass
spectrometer by means of a set of electrostatic lenses. These
lenses include a photon stop to prevent photons impinging upon
the detector and contributing to random background.

Ions entering the quadrupole travel relatively slowly along the
axis of the rods and have a relatively low energy (typically
a couple of eV). This ensures that the ions experience an
adequate number of RF cycles to obtain good resolution and good
ion transmission at high masses. The energy of the ions
entering the quadrupole is due mainly to the DC potential
difference between the source and the quadrupole rods. The
energy of the ions can thus be optimised by varying this
potential (called pole bias potential).

### 1.3.1.5. Quadrupole mass spectrometer:

The quadrupole has a set of pre- and post rods which are
operated at the same potential as the main rods but the DC
component is omitted.  These rods are used to improve the
extraction field.

The quadrupole acts as a mass filter, whereby only ions of a single mass to charge ratio (m/z) are transmitted. Ions of other m/z are deflected and lost. The transmitted m/z is determined by the amplitude of both the RF and DC potentials applied to the quadrupole rods by the RF generator. The RF generator potentials are controlled electronically and the mass range may be scanned rapidly (e.g. 3000 amu/second).

Quadrupoles are usually limited to a resolution of unit mass, although complete resolution of peaks half a mass unit apart is possible. The PlasmaQuad II quadrupole is limited to a mass range of 0-256 amu.

### 1.3.1.6. Detector:

A continuous dynode channel electron multiplier is used for detection in ICP-MS. This is capable of counting ion pulses at rates above $10^6$ counts/s (1 MHz) and has a naturally low background (~ 1 count/s). However these detectors suffer from saturation at high counting rates, variable dead time and hysteresis. Dead time and saturation limit the detector to count rates below 1 MHz, which corresponds to an analyte concentration of $1\mu g/ml$. These detectors also suffer from fatigue, which limits the detector lifetime.

### 1.3.1.7. Data handling and processing:

The output of the ion detector is initially stored in a multichannel analyzer in the multiscaler mode. This allows

rapid data acquisition which is not limited by the data handling system. The drawback to this system is that time is wasted in scanning blank regions of the spectrum, although this can be overcome by simply skipping those regions.

The software for the ICP-MS allows various options for data acquisition, including scanning the whole spectrum, single ion monitoring with time and multi-ion monitoring with time. The last two methods are of particular interest for chromatographic work and will be discussed further in later chapters (Chapters 3,4,5).

## 1.4. Interferences in ICP-MS:

There are two basic types of interference encountered in ICP-MS, namely isobaric and polyatomic interference.

Isobaric interference arise from the overlapping of isotopes of different elements. These interferences are usually solved by the use of a different mass for the determination of the element.

Polyatomic interferences arise from the combination of argon, water, air and sample matrices, and are usually limited to below mass 80 ($Ar^{2+}$). The exception to the 80 mass limit is the formation of metal oxides, but these can usually be overcome by varying the plasma conditions. Table 1.2 shows a list of the most polyatomic interferences encountered in ICP-MS [73].

| Mass (m/z): | Interference: |
|---|---|
| 17 | $^{16}OH^+$ |
| 18 | $^{16}OH_2^+$ |
| 19 | $^{16}OH_3^+$ |
| 20 | $^{18}OH_2^+$ |
| 21 | $^{18}OH_3^+$ |
| 28 | $^{14}N^{14}N^+$, $^{12}C^{16}O^+$ |
| 29 | $^{14}N^{14}NH^+$, $^{12}C^{16}OH^+$ |
| 30 | $^{14}N^{16}O^+$ |
| 31 | $^{14}N^{16}OH^+$ |
| 32 | $^{16}O^{16}O^+$, $^{32}S^+$ |
| 33 | $^{16}O^{16}OH^+$, $^{33}S^+$, $^{32}SH^+$ |
| 34 | $^{16}O^{18}O^+$, $^{33}SH^+$, $^{34}S^+$ |
| 35 | $^{16}O^{18}OH^+$, $^{34}SH^+$, $^{35}Cl^+$ |
| 36 | $^{36}Ar^+$, $S^{36+}$, $^{35}ClH^+$ |
| 37 | $^{36}ArH^+$, $S^{36}H^+$, $^{37}Cl^+$ |
| 38 | $Ar^{38+}$, $^{37}ClH^+$ |
| 39 | $Ar^{38}H^+$ |
| 40 | $^{40}Ar^+$ |
| 41 | $^{40}ArH^+$ |
| 42 | $^{40}ArH_2^+$ |
| 44 | $^{12}C^{16}O^{16}O^+$ |
| 45 | $^{12}C^{16}O^{16}OH^+$ |
| 46 | $^{14}N^{16}O^{16}O^+$, $^{32}S^{14}N^+$ |
| 47 | $^{33}S^{14}N^+$ |
| 48 | $^{34}S^{14}N^+$, $^{32}S^{16}O^+$ |

**Table 1.2:** List of polyatomic interferences encountered in ICP-MS [73]

27

| | |
|---|---|
| 49 | $^{33}SO^{14+}$, $^{35}Cl^{14}N^+$ |
| 50 | $^{36}Ar^{14}N^+$, $^{34}SO^{14+}$ |
| 51 | $^{37}Cl^{14}N^+$, $^{35}Cl^{16}O^+$ |
| 52 | $^{40}Ar^{12}C^+$, $^{36}Ar^{16}O^+$, $S^{3616}O^+$, $^{35}Cl^{16}OH^+$ |
| 53 | $^{37}Cl^{16}O^+$ |
| 54 | $^{40}Ar^{14}N^+$, $^{37}Cl^{16}OH^+$ |
| 56 | $^{40}Ar^{16}O^+$ |
| 64 | $^{32}S^{16}O^{16}O^+$, $^{32}S^{32}S^+$ |
| 65 | $^{33}S^{16}O^{16}O^+$, $^{32}S^{32}S^+$ |
| 66 | $^{34}S^{16}O^{16}O^+$, $^{32}S^{34}S^+$ |
| 67 | $^{35}Cl^{16}O^{16}O^+$ |
| 68 | $^{40}Ar^{14}N^{14}N^+$, $S^{3616}O^{16}O^+$, $^{32}SS^{36+}$ |
| 69 | $^{37}Cl^{16}O^{16}O^+$ |
| 70 | $^{40}Ar^{14}N^{16}O^+$ |
| 71 | $^{36}Ar^{35}Cl^+$ |
| 72 | $^{36}Ar^{36}Ar^+$, $^{40}Ar^{32}S^+$ |
| 73 | $^{40}Ar^{33}S^+$, $^{36}Ar^{35}Cl^+$ |
| 74 | $^{36}ArAr^{38+}$, $^{40}Ar^{34}S^+$ |
| 75 | $^{40}Ar^{35}Cl^+$ |
| 76 | $^{36}Ar^{40}Ar^+$, $^{40}ArS^{36+}$ |
| 77 | $^{36}Ar^{40}ArH^+$, $^{40}Ar^{37}Cl^+$ |
| 78 | $^{38}Ar^{40}Ar^+$ |
| 79 | $^{38}Ar^{40}ArH^+$ |
| 80 | $^{40}Ar^{40}Ar^+$, $^{32}S^{16}O^{16}O^{16}O^+$ |

**Table 1.2 (continued)**

## 1.5. HPLC-ICP-MS:

The speciation of numerous elements in real samples has been performed using LC-ICP-MS [74-101]. The coupling of LC to ICP-MS has resulted in a low detection limit (low ppb) and element selective detection.

Conventional LC-MS employs a thermospray desolvation interface or electrospray sample introduction system, but with LC-ICP-MS the interface is simplified and pneumatic nebulization is the standard method of sample introduction for ICP-MS.

Thus the normal method for interfacing LC to ICP-MS is to transfer the LC eluent to the nebulizer of the ICP system *via* a short length of narrow bore (0.5 mm) PTFE tubing. The nebulizer employed is usually a standard concentric-type nebulizer with a Scott double-pass spray chamber (single pass spray chambers are also sometimes employed). This produces a LC-ICP-MS system with acceptable chromatographic resolution and the loss in column efficiency due to the coupling is usually less than 10 % [74].

Problems with interfacing LC with ICP-MS arise when mobile phases with high concentrations of organic solvents are used. These mobile phases result in high solvent vapour loading of the nebulizer gas. This in turn results in high reflected power to the RF generator, due to the unstable plasma. If the reflected power becomes too great the RF generator will cut out in order to prevent damage to the circuits, and the plasma

extinguishes. The mobile phases typically used in reverse phase HPLC (methanol and acetonitrile) often result in the above mentioned plasma conditions and RF cut outs.

The solvent loading of the nebulizer gas can be reduced by cooling the spray chamber. For very volatile solvents this does not reduce the solvent loading sufficiently and a desolvation membrane must be employed. However, even with a desolvation membrane, mobile phases are usually limited to pure methanol or up to 20 % acetonitrile in water [75].

A further effect of high concentrations of organic solvents in the mobile phase is the deposition of carbon on the cones and in extreme cases, on the lens stack [74]. This reduces the sensitivity and precision of the system, because of the detrimental effect on ion focusing and hence ion transmission to the mass spectrometer. Carbon deposition can be reduced by mixing oxygen into the nebulizer gas (typically 1-3 % v/v). This is a trade-off, because although the signal is stabilized and the sensitivity improved, the oxygen oxidizes the nickel cones, reducing their lifetime.

Table 1.3 summarizes most of the publications to date, in which LC has been interfaced with ICP-MS. Typically, the standard interface described earlier has been used, but the major exceptions are the use of ultrasonic nebulizers and direct injection nebulizers (DIN) [76,77,99,100]. Ultrasonic nebulization results in improved transport efficiency as up to 35 % of the sample is delivered into the plasma (compared with

| Elements: | Chromatography: | Interface: | Comments: | Ref: |
|---|---|---|---|---|
| Number of elements including As, Se | Reverse phase (RP) $C_{18}$ 5mM sodium pentane sulphonate/5% MeOH (1.5 ml/min) | 0.25 mm i.d. s/steel tube (20 cm), continuous-flow ultrasonic neb. | 35% transport efficiency, aerosol heated to 100°C and passed through condenser at 0°C | 76,77 |
| Cd, Co | SEC, 0.12 M tris HCl (0.75 ml/min) | 0.3 mm i.d. PTFE, neb. cross flow, Scott type spray chamber | Evaluated different configuration of tubing and aerosol transport | 78 |
| Pb | RP $C_{18}$, 10 mM sodium dodecyl sulphonate, 5% MeOH, 2.5% acetic acid (3.0 ml/min) | 0.25 mm i.d. PTFE, other details not stated | / | 79 |
| Hg | RP $C_{18}$, 60 mM ammonium acetate, 0.005% mercaptoethanol, 3% ACN (1 ml/min) | PTFE tubing from column to plasma torch, neb. and spray chamber not stated | Spraychamber cooled to 8°C, post column cold vapour generation also used | 80 |
| P,S | RP $C_{18}$, 5 mM TEA $NO_3$, 2% MeOH (1.4 ml/min) 10 mM TEA Br, 5% MeOH (1.6 ml/min) 10 mM TEA Br, 1% ACN (1.2 ml/min) | Same as ref 76,77 except s/steel used | / | 81 |

Table 1.3: HPLC-ICP-MS systems employed to date:

| Sn | Cation exchange, 100 mM ammonium acetate, 80% MeOH, 20% water (1.5 ml/min) | Details not stated | / | 82 |
|---|---|---|---|---|
| As | RP $C_{18}$, 10 mM tetraethyl ammonium hydroxide, MeOH (0.75 ml/min) | Details not stated | / | 83 |
| As | RP $C_{18}$, 5 mM tetrabutyl ammonium hydroxide, 5% MeOH (1 ml/min) anion exchange, 25 mM sodium dihydrogen phosphate, 5% MeOH (1 ml/min) cation exchange, 50 mM dodecyl sulphonate, 5% MeOH, 2.5% acetic acid (1 ml/min) | PTFE transfer line, other details not stated | / | 84 |
| Cd | SEC, 120 mM tris HCl (0.75 ml/min) | As in ref. 78 | As ref. 78 | 85 |
| As | RP $NH_2$, 15 mM ammonium dihydrogen phosphate, 1.5 mM ammonium acetate, 30% MeOH (1 ml/min) | 0.25 mm i.d. Flexon tubing (60 cm), concentric neb., Scott double pass spray chamber | Aluminium sampler cone, spray chamber cooled to -5°C, 2% oxygen in neb. gas | 86 |
| Sn | $C_{18}$, 100 mM (negatively charged surfactant), 3% acetic acid, 3% propanol (1 ml/min) | 0.25 mm i.d. PTFE tubing (40 cm), concentric neb., Scott-type spraychamber | Spraychamber cooled to 5°C, switching valve post HPLC column, tapered injector plasma torch | 87 |

Table 1.3 (continued)

| | | | | |
|---|---|---|---|---|
| Au | Anion exchange, 20 mM to 200 mM tris (hydroxymethyl)amino methane, gradient over 15 min (1 ml/min) SEC, 25 mM tris HCl (1 ml/min) | 0.25 mm i.d. PTFE (100 cm), concentric neb., Scott double pass spray chamber | / | 88 |
| Halogens, P and S | Anion exchange | Details not stated | / | 89 |
| As | Anion exchange, 5 mM phthalic acid (1 ml/min) | 0.5 mm i.d. PTFE (70 cm), concentric neb., Scott type spray chamber | Spray chamber cooled to 5°C | 90 |
| Pb, Fe, Zn and Mg | SEC, 100 mM tris HCl (0.5 ml/min) | 0.3 mm i.d. PTFE (120 cm), cross flow neb., Scott double pass spray chamber | $Fe^{54}$ used ($ArO^+$, $Fe^{56}$), protein standards used for SEC | 91 |
| Sn | Cation exchange, 300 mM ammonium citrate, 70% MeOH, 30% water (1 ml/min) | 0.5 mm i.d. tubing, concentric neb., spray chamber type not stated | Spray chamber cooled | 92 |
| Pb | RP $C_{18}$, 5 mM sodium pentane sulphonate, gradient 30% (3 min) to 90% MeOH over 10 min (1 ml/min) | 0.25 mm i.d. PTFE (40 cm), concentric neb., Scott double pass spray chamber | Spray chamber cooled to -9°C | 93,94 |

Table 1.3 (continued)

| | | | | |
|---|---|---|---|---|
| Rare earth metals | Cation exchange, gradient 75 to 100 mM (12 min), 100 to 250 mM lactic acid in 40 min (1 ml/min) | 0.3 mm i.d. PTFE, concentric neb., Scott double pass spraychamber | Peltier cooling of spraychamber to 0°C | 95 |
| Zn | RP $C_8$, 100 mM ammonium acetate, 0.1% trifluoroacetic acid (0.5 ml/min) SEC, 120 mM tris HCl (0.75 ml/min) | Transfer tubing not stated, de Galan neb., Scott double pass spray chamber | / | 96 |
| Cd | Anion exchange, 50 mM carbonate buffer, 2% propanol (1 ml/min) | 0.5 mm Polyex tubing (71 cm), concentric neb., Scott type double pass spray chamber | Spray chamber cooled to 5°C, Ar-He plasma (20% He) | 97 |
| Rare earth elements | RP $C_{18}$ (Picotag column), 400 mM 2-hydroxy-2-methylpropanoic acid, 20 mM octane sulphonic acid, 5% MeOH (0.5 ml/min) | As in ref. 80 | Spray chamber cooled to 8°C | 98 |
| Sn, As | RP $C_{18}$ (Microbore), 5 mM heptyltriethyl ammonium phosphate, 5% MeOH (30 $\mu$L/min) 5 mM heptane sulphonate, 25% MeOH (30 $\mu$L/min) | DIN neb. (micro-concentric pneumatic neb.) | Positioned 3-4 mm from base of plasma, 100% transport efficiency, used up to 70% ACN, encountered signal drift at 70% ACN | 99 |

**Table 1.3 (continued)**

34

| Hg, Pb | RP C18 (Microbore), 5mM ammonium pentane sulphonate, 20% ACN (100 $\mu$L/min) | DIN as in ref. 99 | Used up to 40% ACN | 100 |
|---|---|---|---|---|
| Mn, Al, Fe, Ni, Cu, Zn, Cd, La | SEC, 200 mM ammonium acetate (0.3 ml/min) | Conditions not stated | / | 101 |

**Table 1.3 (continued)**

1-3 % for normal systems). This is possible because a condenser is placed between the nebulizer and the plasma torch thereby reducing the solvent loading to tolerable levels. The DIN has been used in conjunction with microbore HPLC and has allowed nebulization of mobile phases containing up to 70 % acetonitrile without extinguishing the plasma [99].

Thus, the coupling of normal phase HPLC to ICP-MS can be realized if an efficient desolvation system is used. Unfortunately, the desolvation systems such as those used with traditional HPLC-MS have not been used with HPLC-ICP-MS to date. These systems rely on thermospray aerosol formation, which cannot be used for the determination of metalloporphyrins on a routine basis [102].

1.6. GC-ICP-MS:

The advantages offered by GC-ICP-MS include very good analyte transport efficiency, stable plasma source and few polyatomic interferences due to the absence of solution nebulization. The major disadvantage is the rather limited range of compounds which can be analysed. To date only halogenated organic molecules, organo-lead, organo-tin and a few other volatile organometallic compounds have been determined (Table 1.4). However many of these organometallics are toxic and all are relevant from an environmental viewpoint [110].

The first publication on GC-ICP-MS appeared in 1986 and described the use of a packed GC column with argon as carrier

| Sample: | Chromatography: | Interface: | Comments: | Ref: |
|---|---|---|---|---|
| Organotin compounds | Packed column (length not stated) 3% OV-1 on Chromasorb W (mesh 80-100) Carrier gas: Ar (8 ml/min), $O_2$ (2 ml/min) | 50 cm length of glass lined s/steel tubing (o.d., i.d. not stated), heating method not stated | Interface kept at 250°C, $O_2$ introduced midway between GC and torch, detection limits 3-6.5 ng tin on column | 103 |
| Organic compounds containing C, H, N, O, S, Cl, Br, I, P, B, Si | Packed column (length not stated) 10% dodecyl phthalate or 10% Carbowax 20M, both on Chromasorb W (80-100 mesh) carrier gas: Ar (25 ml/min) | Length of glass lined s/steel tube (2 mm o.d., 0.4 mm i.d.) length not stated, resistively heated with Variac | Interface kept at 150 or 250°C, tube inserted to within 20 mm of plasma (dead volume ~ 0.08 ml), detection limits 0.001 to 400 ng/s | 104 |
| Organotin and organo-chlorine compounds | Packed column 175 cm (2 mm i.d.) 6% OV 101 on Chromasorb AW-DCMS (80-100 mesh) carrier gas: Ar (10 ml/min) | 90 cm length of glass lined s/steel tubing (3.1 mm o.d., 1.5 mm i.d.), heated with heating tape controlled by Variac | Special sheathing gas interface with three way valve for GC and solution nebulization with one interface, detection limits: Cl 2.1 ng, Sn 4.5-12 pg | 105, 106 |

Table 1.4: GC-ICP-MS systems employed to date:

| | | | |
|---|---|---|---|
| Organo-tin, organo-lead and nickel | 5-25 m HT-5, 0.32 mm (0.1 $\mu$m carboborane phase) capillary column<br>Carrier gas: He (2 ml/min) | 60 cm length of aluminum rod (25 mm i.d.) with longitudinal slot for inserting capillary column, Heated with heating tape controlled with Variac, S/steel tube resistively heated inserted into injector tube of plasma torch | First use of capillary column, Used He as carrier gas<br>Detection limits: Pb 0.7 pg/s; Sn 6.5 pg/s | 107, 108 |
| Bromo-nonane | DB-5 40 m, 0.25 mm (0.25 $\mu$m 55 phenyl methylsiloxane) capillary column<br>Carrier gas: He (3.0 ml/min) | Heated transfer line, modified sampling cone arrangement (2.0 mm oriface), modified silica torch | Used low pressure plasma system to produce plasma at powers between 200-350 W, with both He and Ar | 109 |

Table 1.4 (continued)

38

gas [103]. The interface was a heated stainless steel glass-lined tube, which employed an oxygen bleed into the injector gas to prevent carbon deposition on the cones arising from large amounts of sample injected onto the GC column. This system was used to determine organotin compounds [$Sn(CH_3)(C_5H_{11})_3$ to $Sn(CH_3)_3(C_5H_{11})$] but the detection limits were disappointing (3-10 ng on column as tin).

Since 1986 only three papers have been published on packed GC-ICP-MS (Table 1.4). Included in these are two publications by Peters *et al.*, who used a dual interface system thus allowing the use of both gas phase GC samples and nebulized aqueous samples [105,106]. This interface employed a sheathing gas flow to facilitate the use of nebulized aerosols and to supplement the GC carrier gas flow. The first use of capillary GC coupled to ICP-MS was reported by Kim *et al.* in 1992 [107,108]. The use of capillary columns resulted in much improved resolution and detection limits. Whereas previous GC-ICP-MS systems had employed argon as the GC carrier gas Kim *et al.*, used helium. The interface employed a demountable torch, which also allowed the injector to be removed. A stainless steel tube was mounted in the injector, which was resistively heated to ensure that the capillary column was heated to within 20 mm of the plasma. With this design analytes with retention indices up to 3400 could be analysed routinely.

**1.7 Aims of the present study:**

The use of ICP coupled techniques for the analysis of

geoporphyrins has been limited to the use of atomic emission detection (coupled to GC or HPLC) [21,23-26,35-37]. The main aim of this study is to develop a HTGC-ICP-MS technique and to apply it to the analysis of geoporphyrins. The second aim is to develop a HPLC-ICP-MS system and apply it to the analysis of geoporphyrins. Alternative GC-ICP-MS systems (i.e. GC coupled to low pressure ICP-MS) will be developed and analysis of geoporphyrins attempted.

# 2.0 DEVELOPMENT OF HTGC-ICP-MS INTERFACE:

## 2.1 Introduction:

The coupling of capillary GC to ICP-MS was first described by Kim et al. [108]. That system was validated by the analysis of various certified reference materials containing tetraethyl lead and a number of organotin compounds. This allowed the analysis of environmental samples containing these analytes [109]. However the GC-ICP-MS interface described by Kim et al. limited application of the method to compounds with retention indices of less than ~ 3400 [2], whereas metalloporphyrins typically have retention indices of ~ 6000 [60].

The interface used by Kim (Figure 2.1) consisted of a heated aluminium rod and a demountable plasma torch with injector insert. The injector had a stainless steel tube mounted inside, which was resistively heated. This served to ensure even heating across the interface from the gas chromatograph to the plasma torch. Two problems were encountered with this interface. Firstly, an aluminium clad capillary column was used which conducted current and when passed through the stainless steel injector insert became welded to the wall of the stainless steel tube. This caused the column to break and the application of further heating to facilitate elution of higher boiling point compounds was therefore pointless. Secondly, the argon injector gas (flow typically 1.0-1.5 L/min) cooled the stainless steel insert mounted in the injector. This increased

MS     PLASMA TORCH          TRANSFER LINE          GC
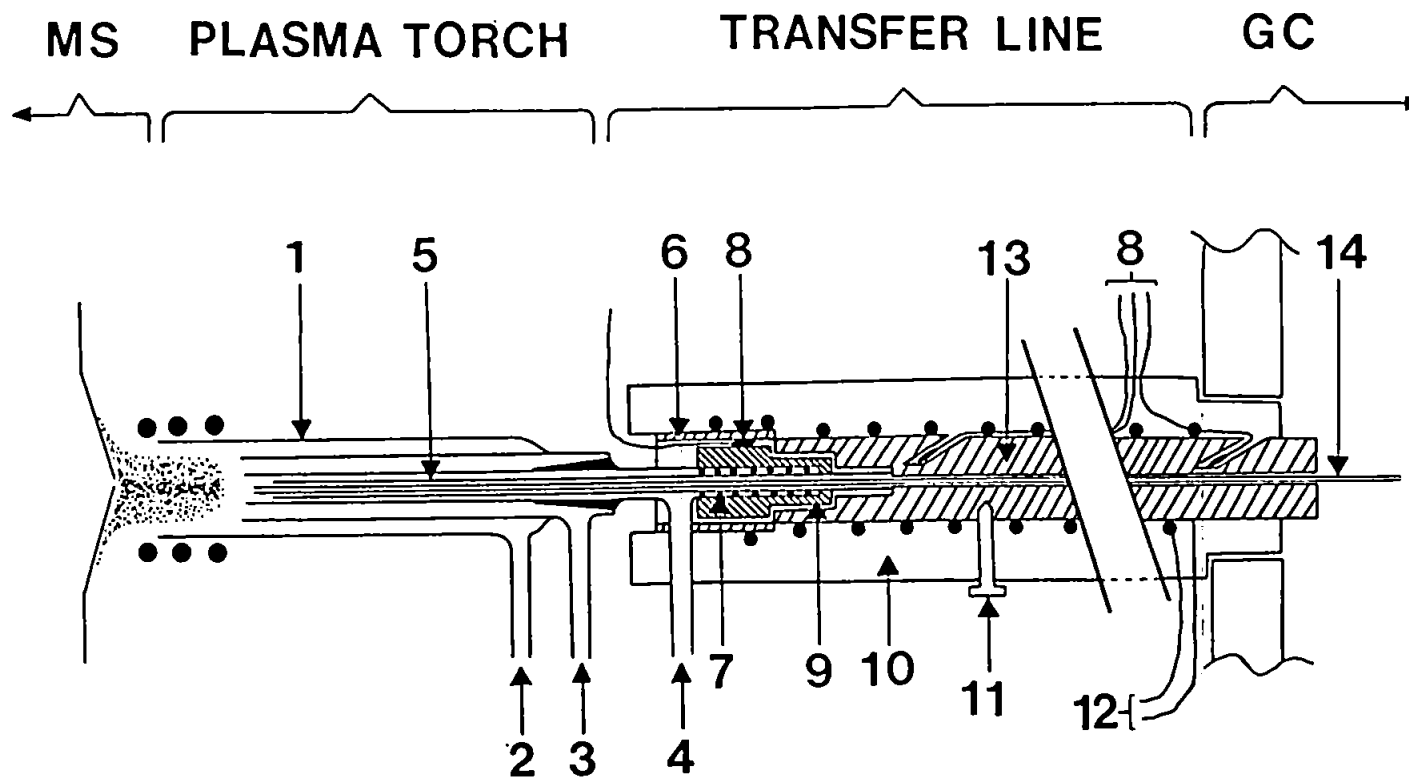


**Figure 2.1:**  Mark II Interface: 1. demountable ICP torch; 2. cooling; 3. auxiliary; 4. injector gas; 5. stainless steel tube; 6. aluminium colar; 7. graphite tape; 8. Thermocouples; 9. stainless steel reducing union; 10. industrial pipe lagging; 11. earthing point; 12. heater leads to variable voltage supply; 13. aluminium bar; 14. capillary GC column

the likelihood of "cold spots" which would cause porphyrins to condense in the column. Indeed metalloporphyrins were found, by Kim, in the last 15 cm of the column, but whether this was due to adsorption or condensation was unclear [111].

In addition to these problems the interface was also somewhat cumbersome and required two people at least 2-3 hours to assemble. Ideally, a system capable of assembly by one person in less than a hour, with minimum modifications to the instrument, is required.

Thus the aims of the current work were:

1. To develop an interface capable of eluting metalloporphyrins. This would start with heating the injector gas.
2. To redesign the interface. This would be aimed at reducing the time, and increasing ease, of installation.

## 2.2 Instrumentation:

### 2.2.1 Gas chromatography:

A Carlo Erba HRGC 5300 (HT-Simdist) gas chromatograph (Fisons, Instruments), equipped with an on-column injector and high temperature flame ionization detector was used. The GC was also equipped with a CP-CF 516 (constant flow-constant pressure unit), which ensured a constant gas flow rate during oven

temperature programming.

The capillary columns used, unless otherwise stated were; HT-5 (carborane-methyl siloxane phase) aluminium clad fused silica columns (12 m x 0.32 mm I.D. x 0.1 $\mu$m film thickness) supplied by S.G.E. or DB-1 HT (methyl-siloxane) polyimide-coated fused silica columns (15 m x 0.32 mm I.D. x 0.1 $\mu$m film thickness) supplied by J&W. The polyimide coating was capable of withstanding temperatures of up to 400°C for short periods of time (~ 15 minutes). The carrier gas used throughout was helium (Air Products). Typical flow rates were 3-3.5 ml/min, unless otherwise stated. Helium was filtered to remove oxygen and water, using in-line filters.

The FID response was recorded with a Shimadzu C-R3A integrator or on Unicam 4880 software with a Philips PU 6030 data capture unit.

## 2.2.2 Inductively coupled plasma-mass spectrometry:

The instrument used was a VG PlasmaQuad II (VG Elemental, Winsford, U.K.). The modifications to the ICP-MS were as described by Kim [111].

The ICP-MS was tuned in two different ways; firstly with 100 $\mu$g/L metallic mercury, generated using tin(II) chloride dissolved in hydrochloric acid [108]; secondly with argon purge

over $Hg^0$ in a Dreschel bottle (the concentration of $Hg^0$ in the argon was approximately 5 $\mu$g/L). The use of the second method approximated more closely to the actual conditions in the plasma during GC-ICP-MS operation and was generally preferred to the first method of tuning.

Table 2.1 describes typical ICP-MS operating conditions.

## 2.3 Interface Design:

Successive GC-ICP-MS interfaces designed by Kim [4] were denoted Marks I-III respectively. Further modifications made by the present author are therefore numbered Mark IV-VII.

### 2.3.1 Mark IV interface:

Initial experiments to investigate the hypothesis that the argon plasma gas was causing cold spots where the metalloporphyrins were condensing, involved the use of the Mark III interface designed by Kim (Figure 2.1) but with an argon pre-heater. The argon pre-heater was constructed using a coiled nichrome wire mounted in a ¼ inch silica tube. The nichrome coil was heated using a Variac (0-240 V, 4 A). The design and heating profile are shown in Figure 2.2. The pre-heater was mounted outside the ICP-MS and the injector gas was introduced via a ⅛ inch stainless steel tube 20 cm long. The tube was lagged with glass fibre insulation. The electronic noise from this arrangement created numerous electronic spikes which made the interpretation of the data impossible. Thus a re-think of

| | |
|---|---|
| Cooling gas | 15 L/min |
| Auxiliary gas | 1.0 L/min |
| Injector gas | 1.33 L/min |
| Forward power | 1500 W |
| Reflected power | < 5 W |
| Mode | Time Resolved Analysis |
| Dwell time | Typically 1280 $\mu$s |
| No. of scans | Typically < 900 |
| Data acquisition time | Typically < 10 min |

**Table 2.1:** ICP-MS operating conditions

a

7
4
6
5
3
2
1

b

Temperature (°C)
450
200 W maximum
400
350
300
250
200
150
40    50    60    70    80    90    100    110    120
Variac voltage
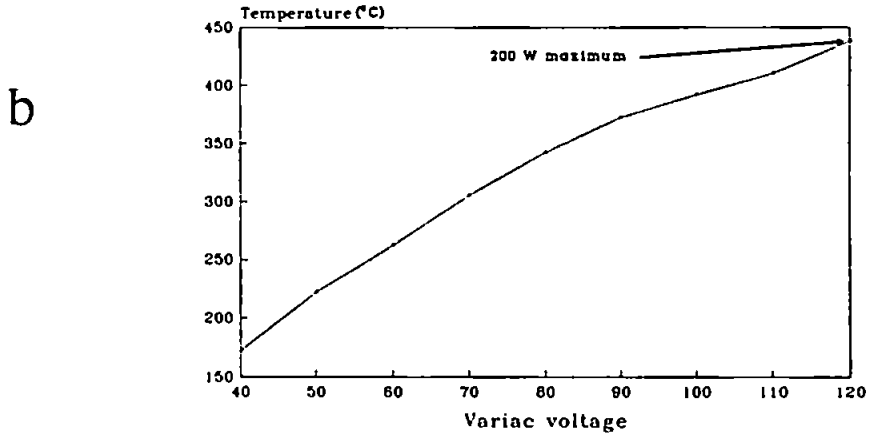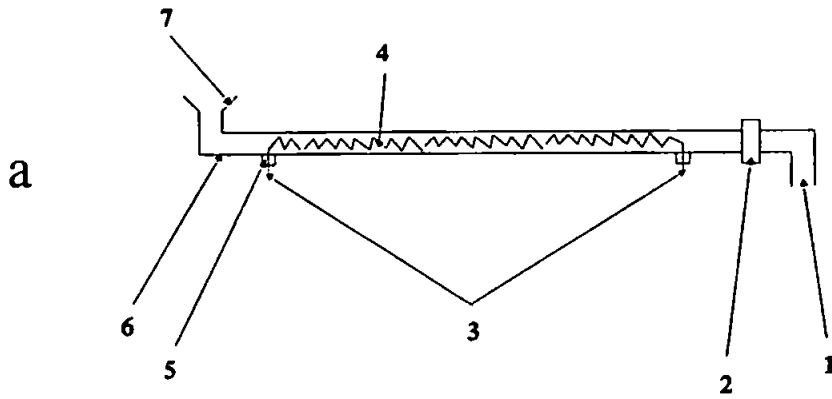
**Figure 2.2:** (a) Argon heater: 1. argon inlet; 2. stainless steel union; 3. nichrome wire connectors; 4. nichrome wire coils; 5. ceramic paste; 6. ¼ inch silica tubing; 7. cup joint

(b) Heating profile of argon heater using Variac and argon flow of 1.5 L/min

the interface design was required.

The re-design of the interface resulted in a version in which a heated sheathing gas was used. The new design consisted of a $\frac{1}{4}$ inch silica tube 85 cm long, with a T-joint at the GC oven (approx. 80 mm from the end) and a ball joint at the torch end, to which a standard Fassel torch with a 1 mm injector was connected (Figure 2.3). The temperature profile along the transfer line and torch was monitored off-line using a thermocouple. The temperature was maintained at ~ 400°C throughout the transfer line, but in the torch dropped to 200°C within 30 mm of the transfer line/torch union. The inside of the torch injector was deactivated by silanisation with hexamethyldisilazane ($(CH_3)_2SiNHSi(CH_3)_3$) to prevent adsorption of porphyrins onto the silica walls.

The Mark IV interface was initially tested with nickel dithiocarbamate (retention index ~ 3400), which eluted successfully through the system. The resultant chromatographic peak was symmetrical; with a base peak width of ~ 7 seconds. Subsequent analysis of metalloporphyrins was also partially successful.
The temperature at the argon inlet seems to have been crucial. Only above 390°C did the metalloporphyrins elute from the column. Figure 2.5 illustrates the temperature profile at various points along the transfer line.

However, although zinc OEP Cl, nickel OEP and iron OEP Cl were chromatographed, peak shapes were poor as a result of
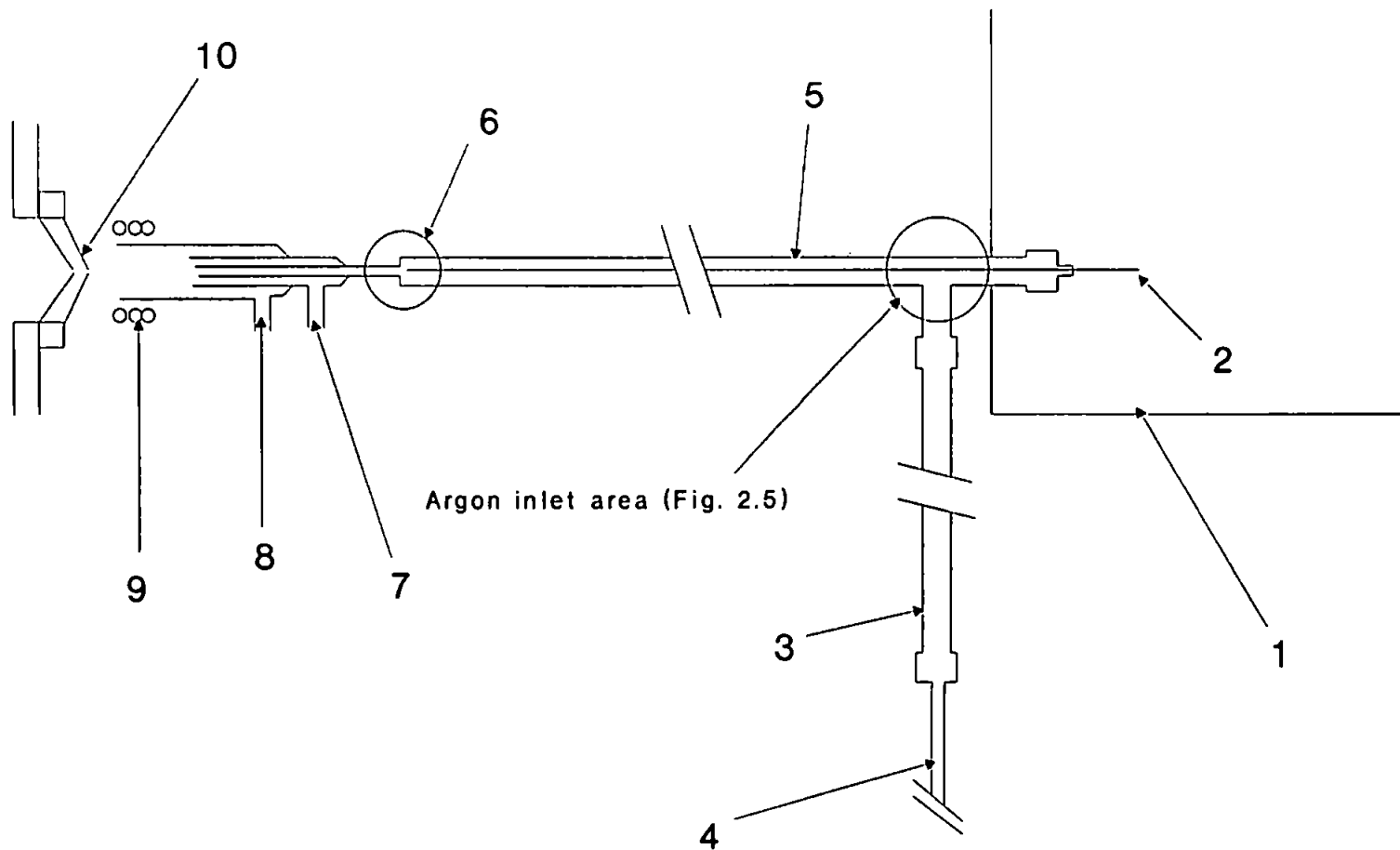
**Figure 2.3:** Mark IV interface: 1. GC oven; 2. capillary column; 3. argon heater; 4. argon injector gas; 5. ¼ inch silica tube transfer-line; 6. end of capillary column; 7. cooling; 8. auxiliary; 9. load coil; 10. ICP-MS interface

considerable band broadening (Figure 2.4). Deactivation of the torch injector had obviously reduced the adsorption effects sufficiently for metalloporphyrins to elute through the interface, but the silica may not have been completely deactivated.

The broadening and adsorption effects may also have been caused by the large dead volume (approx. 5 ml) resulting from the fact that the GC column ended ~ 120 mm from the plasma. The result was poor peak shapes and high detection limits. Estimated detection limits for metalloporphyrins with the Mark IV interface are given in Table 2.2.

Although the Mark IV interface served to illustrate that injector gas temperature was a crucial factor in the elution of the metalloporphyrins, subsequent attempts to improve the interface were unsuccessful. This, combined with the difficulty of assembling the interface, led to the design and manufacture of a different interface (Mark V).

## 2.3.2 Mark V interface:

Argon gas temperature was the most important point of concern when the new interface was designed. The distance between the argon pre-heater and the injector insert was the crucial factor, since the heat capacity of argon is low. A modification
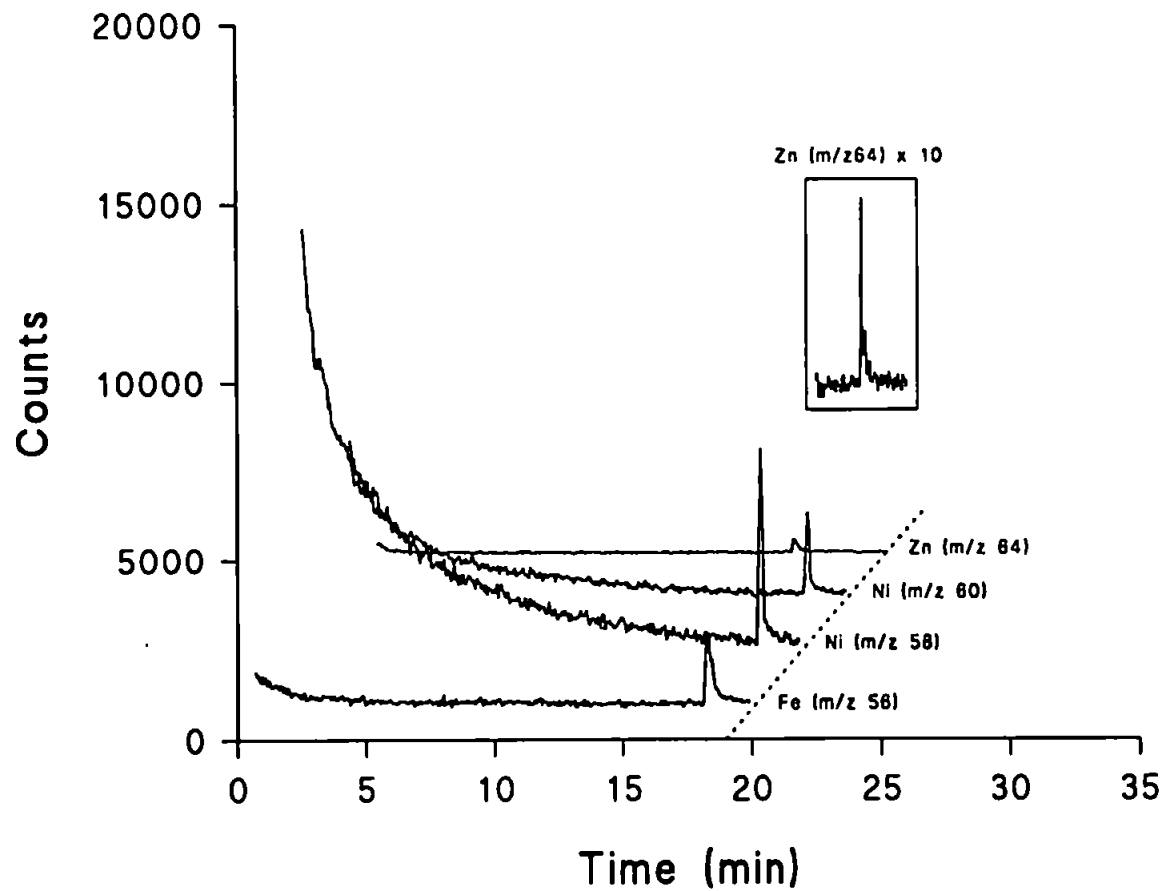
**Figure 2.4:** Selected ion recording chromatograms of m/z 56 (Fe), m/z 58 (Ni), m/z 60 (Ni) and m/z 64 (Zn). GC program 60°C to 350°C at 20°C/min, 350°C to 410°C at 10°C/min. Monitored from 350°C
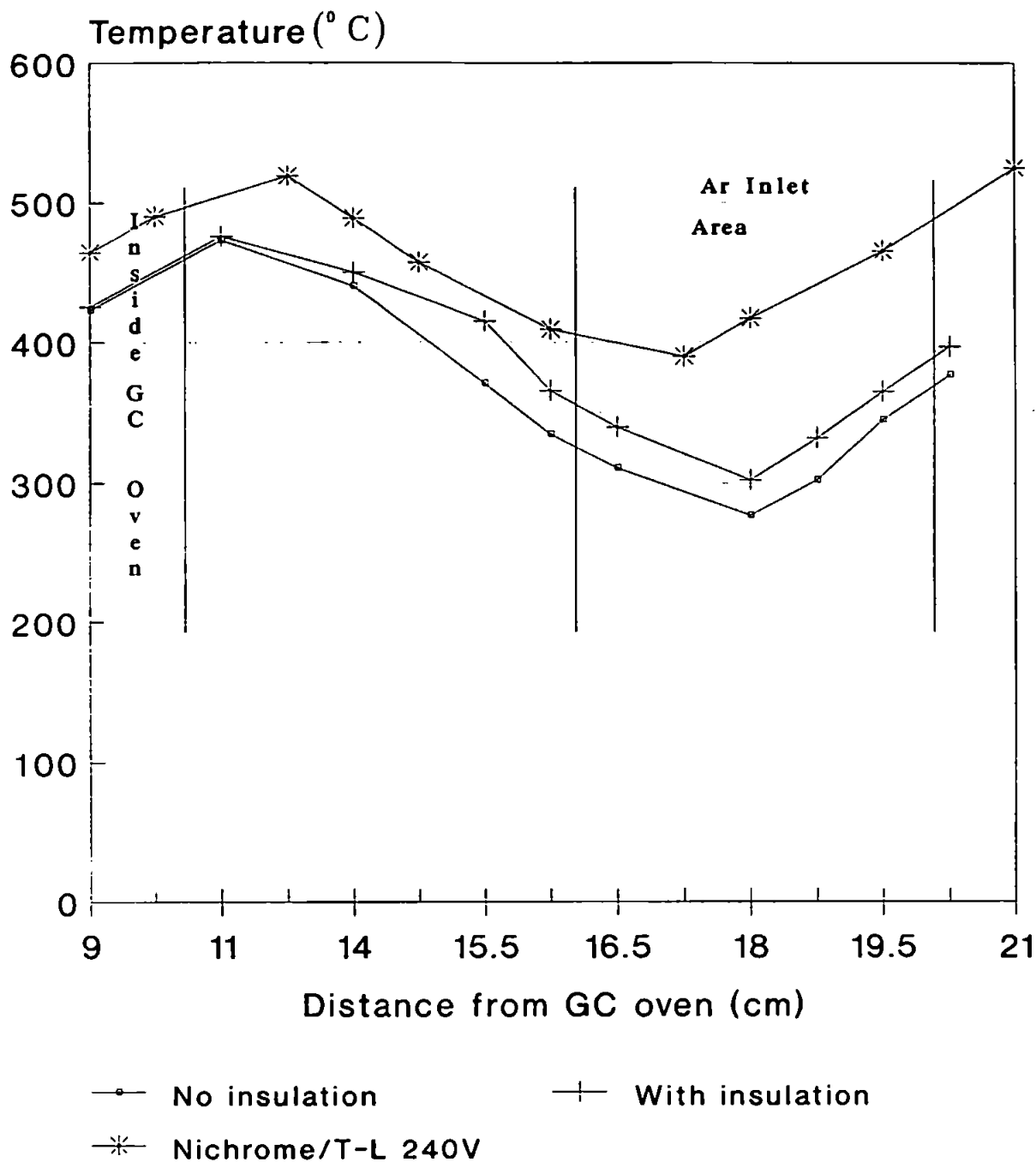
**Figure 2.5:** Temperature variation across the argon injector gas inlet on transfer-line.

to the demountable torch was necessary, which involved the addition of a side arm onto the injector insert. The argon pre-heater was shortened to 500 mm and was fitted to the injector insert by means of a ball and cup joint. As in Kim's original design [111] a stainless steel tube was mounted inside the transfer line, but was insulated with industrial pipe lagging. This ensured that the temperature from the end of the transfer line to the argon injector inlet was maintained above 390°C. This interface is shown in Figure 2.6.

The Mark V interface resulted in improved peak shapes (dead volume was reduced to ~ 0.7 ml) and detection limits for a number of synthetic porphyrins (Figure 2.7, Table 2.2). The detection limits were improved by a factor of ~5, compared with the Mark IV interface. Even so, these do not approach typical LOD's, for other organometallic species. For example, for ferrocene the detection limit was approximately 1-2 pg on-column, whereas 100 pg on-column (Table 2.2, Mn OEP Cl) was the best estimated detection limit for any of the metalloporphyrins. There are a number of possible reasons for this; firstly, metalloporphyrin peaks are broad (15-25 seconds base peak width) compared with many earlier eluting analytes (e.g. ferrocene) which have base peak widths typically of 3-5 seconds at base of peak. Secondly, the elution of the porphyrins from the column may not be quantitative (see Chapter 3, Section 3.7). Finally, a further restriction was placed on the peak shape by the time resolved software of the ICP-MS instrument. This software was not designed for gas chromatographic use and to keep the data files to a reasonable

a

b

Copper connectors
Stainless Steel Insert
Silica insert
Aluminium rod
Ar heater
Ceramic cement
Heating tape and insulation
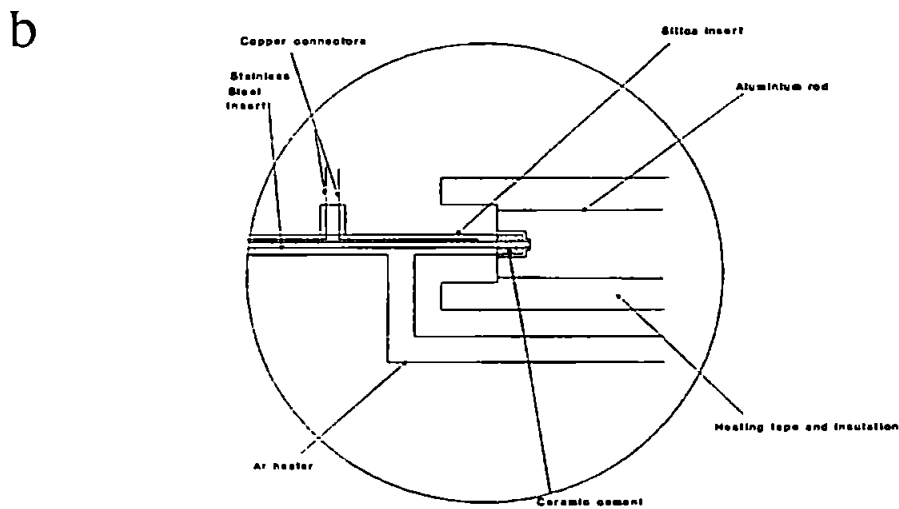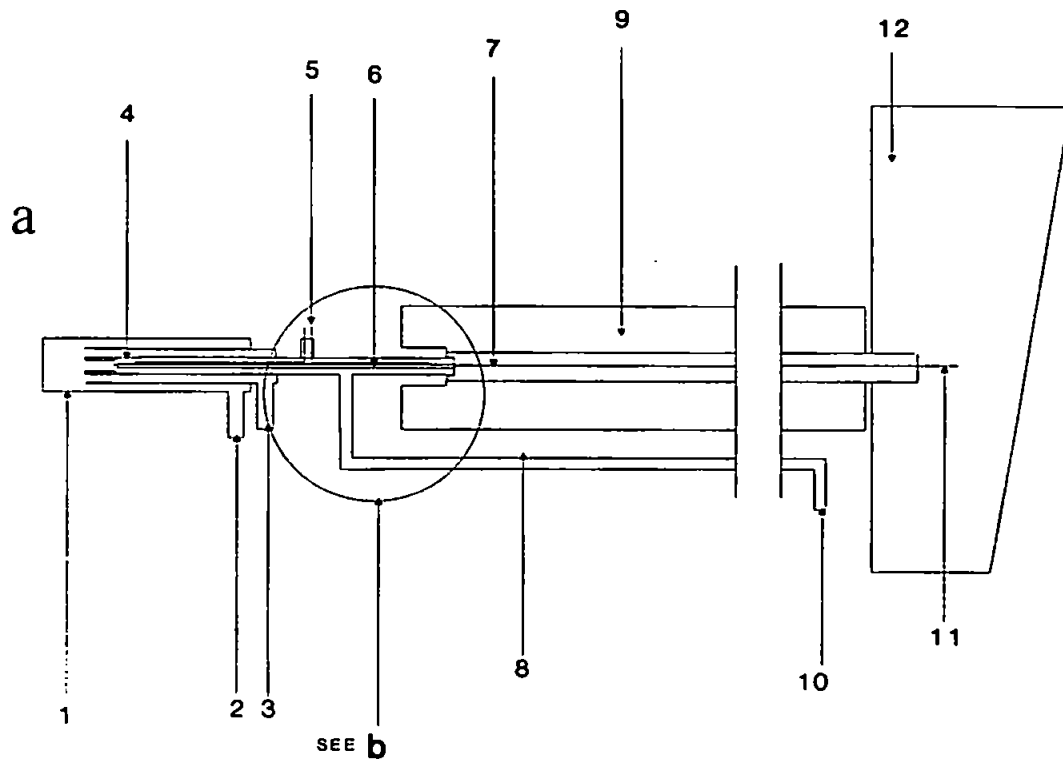
Figure 2.6:  (a) Mark V interface: 1. plasma demountable torch;
2. cooling gas inlet; 3. auxiliary; 4.
stainless steel insert; 5. outlet for copper
leads (sealed with ceramic paste); 6.
copper wire leads; 7. aluminium rod; 8. argon
heater; 9. Insulation; 10. injector gas
inlet; 11. capillary column; 12. GC oven

(b) Expanded view of transfer line coupling
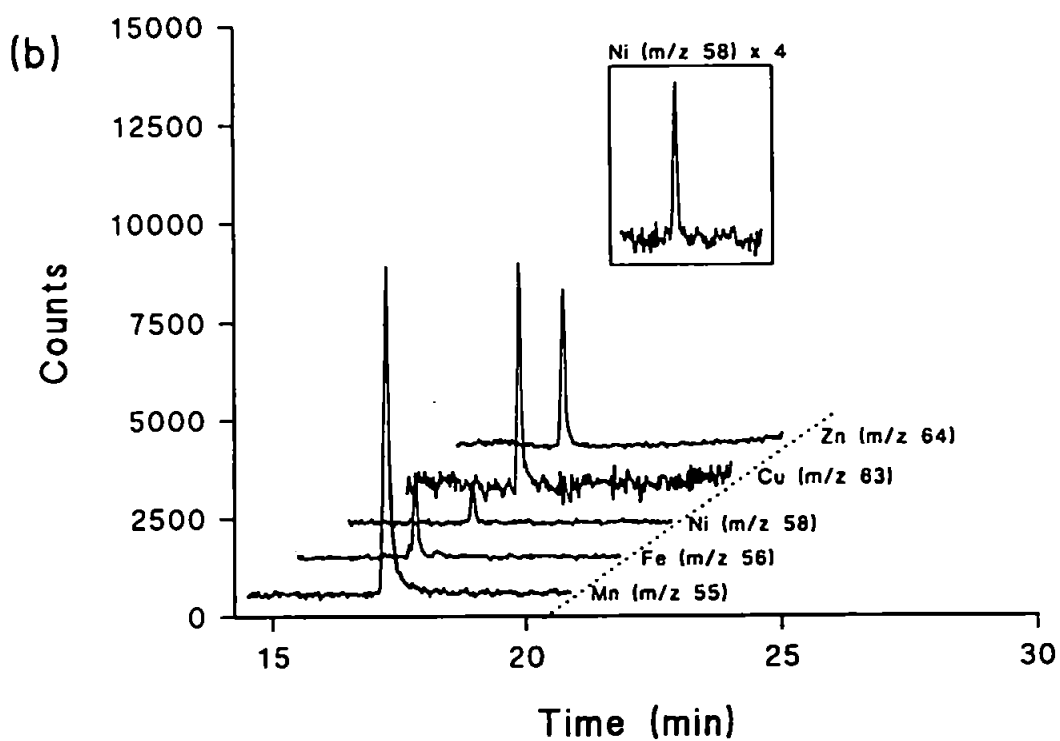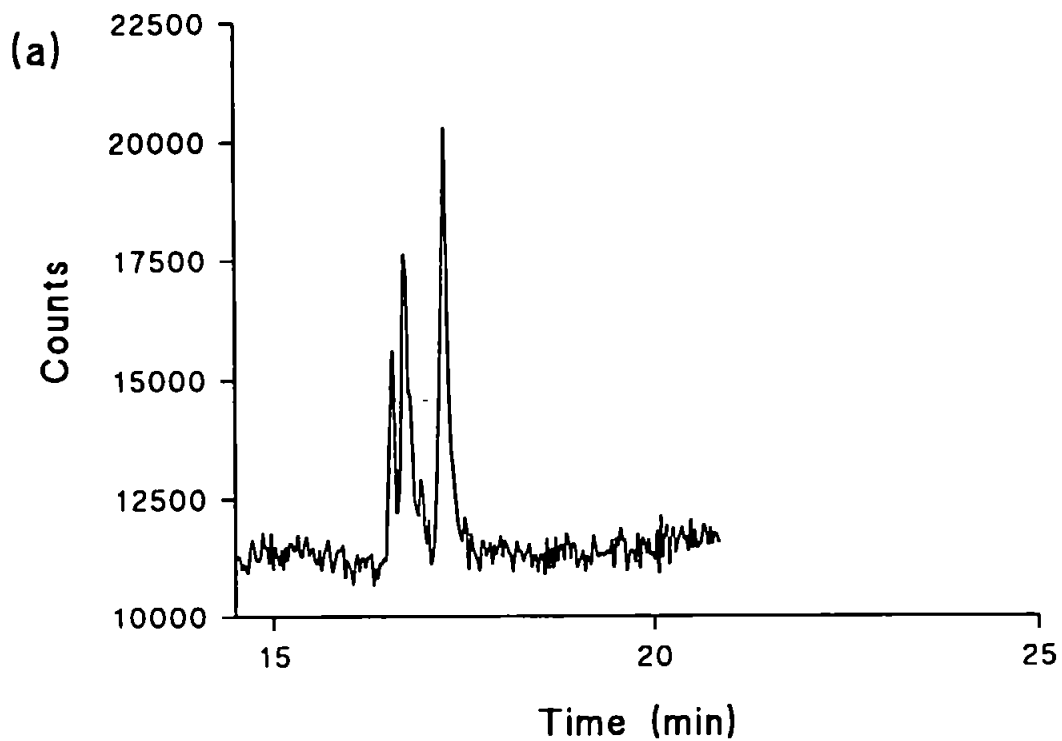
Figure 2.7: (a)  Total ion current of (b).

(b)  Selected ion recording chromatograms of m/z 55 (Mn), m/z 56 (Fe), m/z 58 (Ni), m/z 63 (Cu) and m/z 64 (Zn). GC program 60°C to 350°C at 20°C/min, 350°C to 410°C at 12°C/min, 1 minute isothermal hold. Monitored from 350°C

| Synthetic Metalloporphyrin | Retention Index | Mark IV Detection Limit[1] | Mark V Detection Limit[1] |
|---|---|---|---|
| Vanadyl OEP | 6280 | n/d | 0.51 |
| Manganese OEP Cl | 6022 | n/d | 0.10 |
| Iron OEP Cl | 6213 | 1.6 | 0.30 |
| Nickel OEP | 6266 | 2.5 | 0.51 |
| Copper OEP | 6692 | n/d | 0.55 |
| Zinc OEP Cl | 6114 | 0.5 | 0.14 |

1. Estimated detection limits given in ng on-column calculated at $3\sigma$

**Table 2.2:** Detection Limits for Synthetic Metalloporphyrins:

size (< 3.0 megabytes), a relatively long scan time of between 0.8-1.2 s was necessary.

In an attempt to improve peak shapes the GC column was extended to within 5 mm of the plasma (normally the column extended only to within ~ 15 mm of the plasma). Unexpectedly this resulted in peak broadening which was probably caused by slow elution of the metalloporphyrins from the tip of the column. Thus any slight variation in elution temperature to below 390°C would then cause broadening. The peak broadening observed, illustrated the need for even heating across the length of the interface.

Although the Mark V interface allowed the analysis of metalloporphyrins with acceptable peak shapes and detection limits, there are some problems associated with it. Assembly of the interface required two people and was a delicate procedure because the capillary column had a fragile pivot point (where the transfer-line joined the injector insert). Also, reconstruction of the injector insert was required each time the interface was assembled. The silica insert was broken after each disassembly of the interface (again due to the fragile pivot point between the injector and transfer line). In addition, slight variations in the different injector inserts and stainless steel tubes introduced "hot spots" into the metal tube and capillary column. Re-design of the interface to make it a one component system would have introduced the risk of breaking the plasma torch and was therefore rejected. The problem of the aluminium column welding to the stainless

steel tube was also encountered. This led to the interface being unreliable and each insert could only be used once and for about 10-15 injections.


## 2.3.3 Mark VI interface:

The problems of high detection limits, peak broadening and the practical disadvantages involved with the Mark IV and V interfaces discussed above led to the design of the Mark VI interface. It was decided to attempt to resistively heat a stainless steel capillary column, rather than persist with the heated aluminium bar, but to maintain the argon pre-heating introduced in the Mark IV interface.

Resistive heating of a stainless steel capillary column [85 cm long Chrompack column, 0.5 mm (i.d.) X 0.8 mm (o.d.); coated with 0.1 $\mu$m of Simdist-CB methyl siloxane equivalent] required the use of a 0.5 kW transformer where the input voltage to the transformer was controlled with a Variac (0-240 V, 3 A). The temperature of the stainless steel capillary was monitored along the entire length of the column and was found to be uniform (Figure 2.8). The column was insulated with a glass fibre sleeve and mounted in the injector insert. The capillary thus extended from inside the GC oven to 20 mm from the plasma. The argon pre-heater described in Section 2.3.2 was used. The interface is shown in Figure 2.9.

Examination of a mixture of ~ 500 $\mu$g/ml nickel OEP, manganese

Temperature (°C) vs Variac voltage
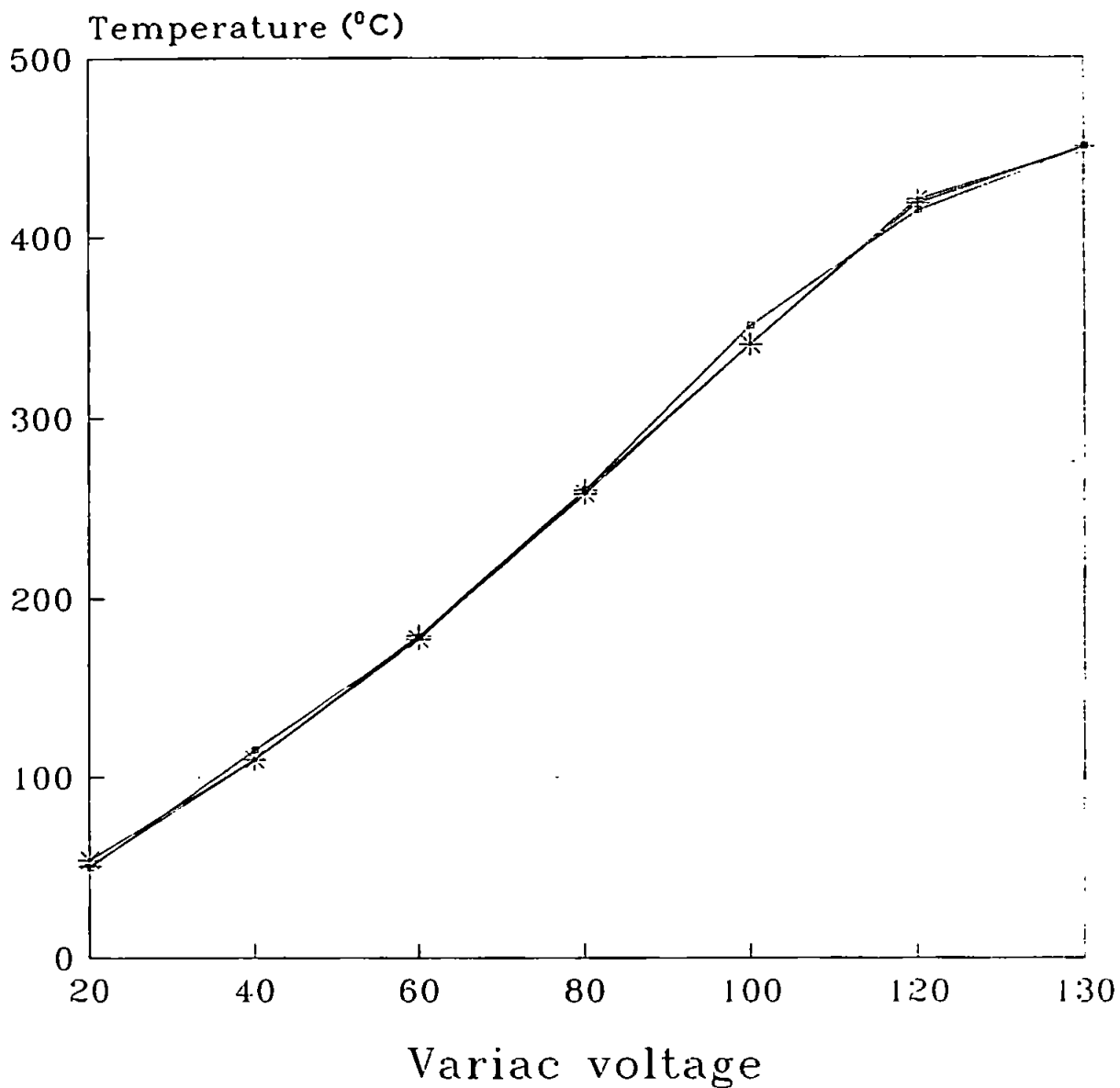
Legend:
—◻— 45cm (middle)        —+— 5cm (from left)
—✳— 5cm (from right)

(using 30 V, 20 Amp. system)

**Figure 2.8:**  Heating profile of a 0.5 mm x 0.8 mm stainless steel capillary 90 cm in length using 0.5 kW transformer, with variac control of input voltage.
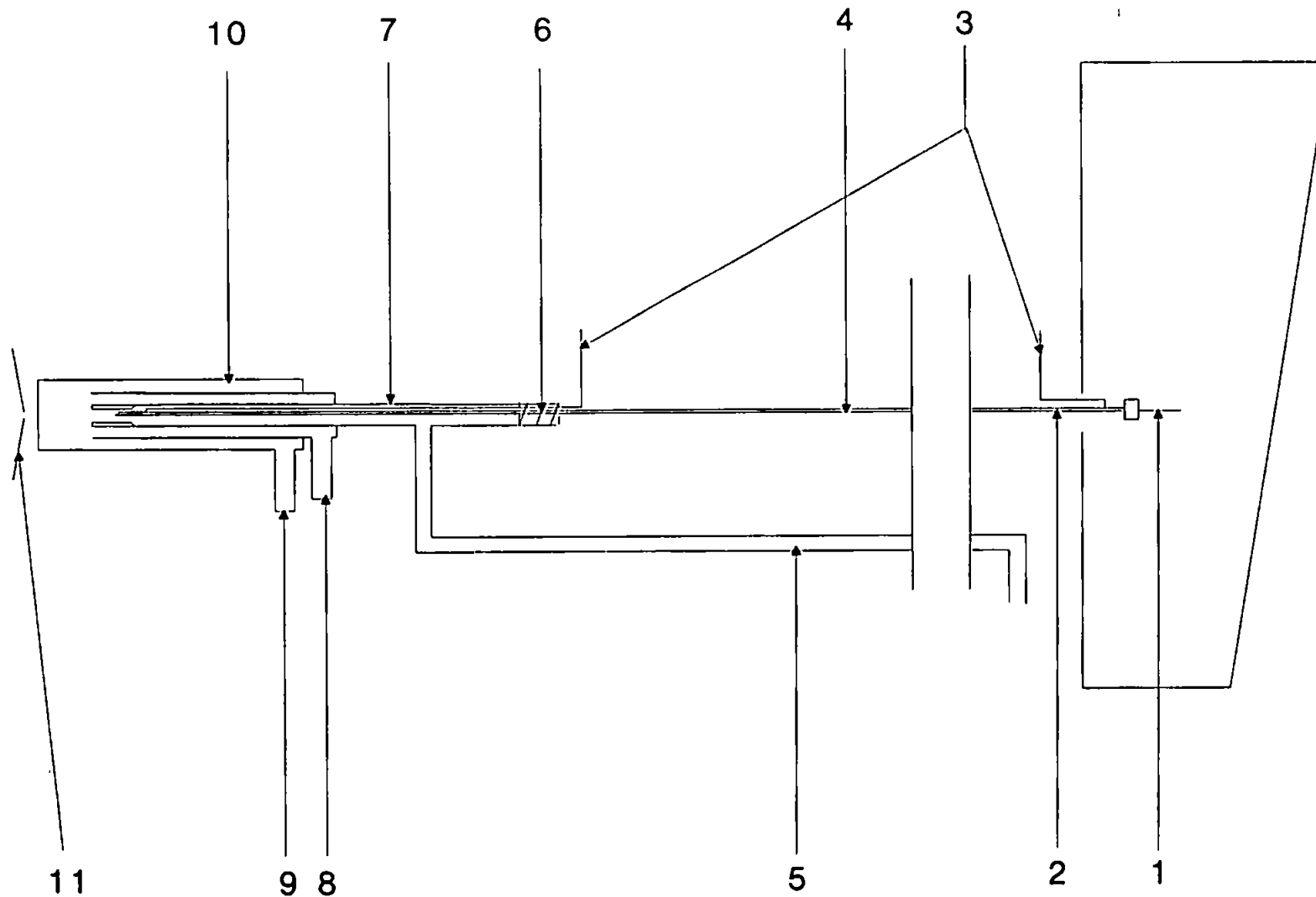
**Figure 2.9:** Mark VI interface: 1. capillary column; 2. zero dead volume stainless steel glass lined union; 3. copper connectors to transformer; 4. Chrompack capillary column; 5. argon heater; 6. ceramic paste; 7. injector insert; 8. cooling; 9. auxialry; 10. demountable torch; 11. ICP-MS interface

OEP Cl, iron OEP Cl, copper OEP and zinc OEP Cl with this interface gave disappointing results. Elution of the porphyrins was erratic and only zinc OEP was routinely eluted with nickel OEP only occasionally observed. The poor elution of porphyrins was attributed to retention on the Simdist CB stationary phase and/or inner metal surfaces of the Chrompack column.

Previously these columns were used mainly for simulated distillation analysis of apolar alkanes [112-114]. Only two reports discuss the use of these columns for metalloporphyrin analysis [37,115]. Zeng *et al.* showed that both nickel and vanadyl porphyrins could be eluted from this column using GC-AED [37]. However, though not emphasised by the authors, the amount injected on to the column were very large. For instance, 200 mg of Boscan crude oil in tetrahydrofuran (an unusually large volume of 1 ml was injected on-column) was introduced into a 5 m column, the total internal volume of which was only 1.96 ml, corresponding to ca. 280 $\mu$g of porphyrins onto the column. The porphyrin "peaks" exhibited extremely poor shapes and resembled "humps". It seems extremely likely that the porphyrins were not eluting quantitatively from the column, since the normal sensitivity of GC-AED to metals is typically in the order of picograms [36]. Taking this into consideration the work of Zeng *et al.* with the Chrompack columns would seem to be consistent with the poor elution characteristics observed by the present author.

## 2.3.4 Mark VII interface:

The resistively heated Chrompack column indicated that the zinc porphyrin could be eluted and that the problem with the system was the chromatographic column not the interface. Hence a 90 cm length of stainless steel column (uncoated) was substituted for the Chrompack column with a 1 m length of DB-1 ht (0.32 i.d x 0.45 o.d.) capillary column inserted into a length of blank stainless steel column.

This interface was successfully used to elute the metalloporphyrins (Figure 2.10). Detection limits were not rigorously determined, but were in the same order as those obtained with interface the Mark V. The peak shape was comparable to those obtained using interface the Mark V. The rigorous determination of the detection limits was not pursued due to the irreproducible chromatography of the porphyrins through the columns used (Chapter 3, Section 3.7).

The advantage of this interface was that the construction and installation could be performed in less than one hour, by one person and the transfer-line could be heated very rapidly to the required temperature (typically 420°C) with an accuracy of ± 10°C. This is in contrast to the previous system, in which the transfer-line took over 45 minutes to heat up to 380°C.

## 2.4 Conclusions:

The Mark IV-VII interfaces showed, for the first time that

**(a)**

*Counts* (y-axis): 0, 20000, 40000, 60000, 80000, 100000, 120000, 140000

*Time (min.)* (x-axis): 16.5, 18.5, 20.5, 22.5, 24.5

**(b)**

*Counts* (y-axis): 0, 20000, 40000, 60000, 80000, 100000

Ni (m/z 58)

Cu (m/z 63)

Zn (m/z 64)

Fe (m/z 56)

Mn (m/z 55)

*Time (min.)* (x-axis): 16.5, 18.5, 20.5, 22.5, 24.5, 26.5, 28.5, 30.5
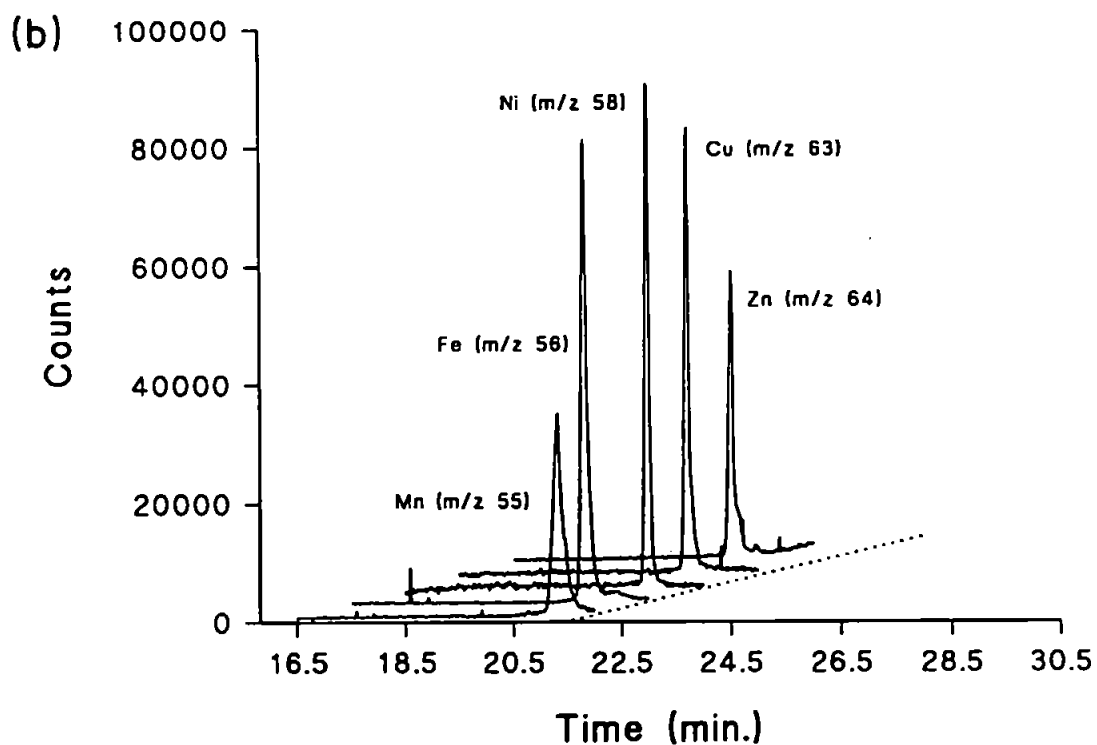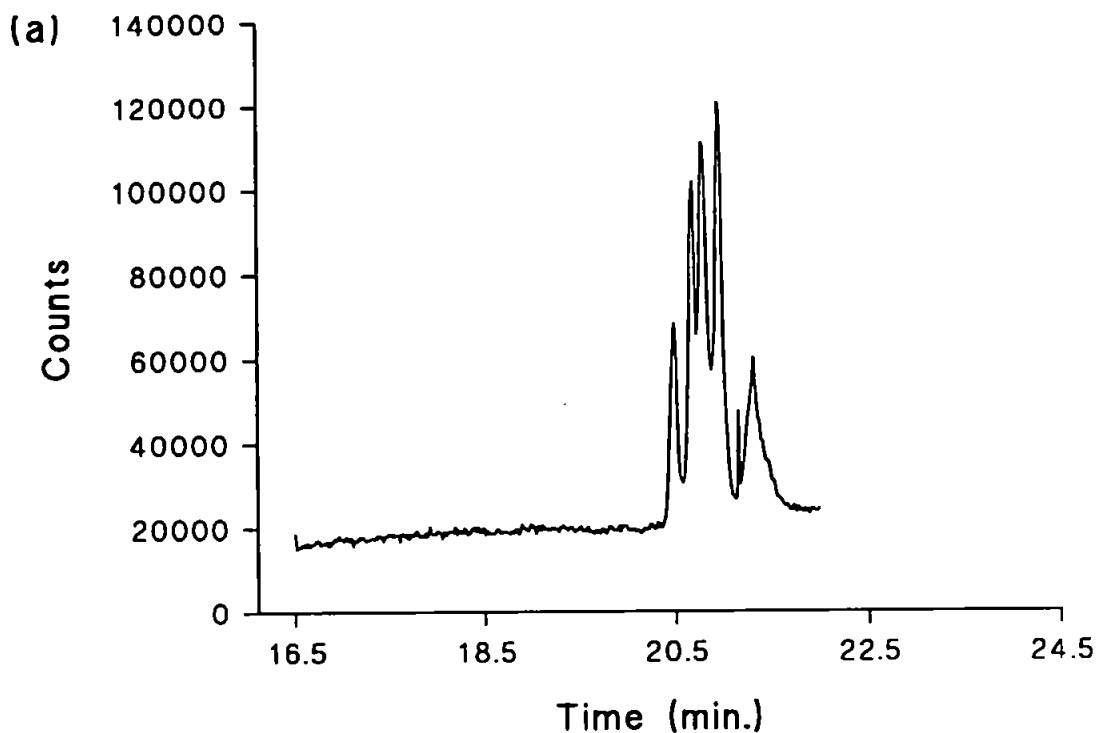
**Figure 2.10:** (a) Total ion current of (b).

(b) Selected ion recording chromatograms of m/z 55 (Mn), m/z 56 (Fe), m/z 58 (Ni), m/z 63 (Cu) and m/z 64 (Zn). GC program 50°C to 350°C at 18°C/min, 350°C to 402°C at 10°C/min. Monitored from 350°C

metalloporphyrins could be analysed by GC-ICP-MS, effectively extending the retention index of the system to >6000.

Both Mark V and VII interfaces gave acceptable peak shapes and detection limits for the metalloporphyrins; these interfaces were subsequently used for the analysis of geoporphyrins (Chapter 3).

The Mark VII interface represented a significant advance on Marks I-V for the analysis of organometals, since the interface could be constructed and installed in a short period. In addition, the power supply could be modified so that the transfer-line could use the same temperature program rate as the GC oven.

# 3.0 HTGC ANALYSIS OF GEOPORPHYRINS:

## 3.1 Introduction:

The majority of studies of geoporphyrins to date have used either HPLC-UV/VIS or probe-MS as methods of analysis for the metallated species [116-119]. However, the use of high temperature gas chromatography (HTGC) for the rapid analysis of metallated geoporphyrins (typical analysis time 50-60 minutes) has also been demonstrated by a few workers [34-37,64,65,120,121]. Whilst HTGC produces chromatograms which are characteristic for each sample, use has been limited by the restricted availability of suitable high temperature columns, the first of which only became commercially available around 1988 [35-37].

HTGC-MS has also been used occasionally for the analysis of metallated geoporphyrins. For example Gallegos *et al.* used a commercially available DB-1 column for this purpose but, like previous studies, this work concentrated on the characterization of porphyrin macrocycle distributions, rather than the metals chelated to the porphyrins [65]. The geoporphyrins were assumed to be chelated with metals which commonly occur in the geosphere (i.e. nickel and vanadium).

HTGC analysis of intact geoporphyrins with element selective detectors has been restricted to the use of the commercially available GC-atomic emission detection (AED) [35-37]. The focus

of these studies has been the quantification of the nickel, iron and vanadyl porphyrins [35-37]. Investigation of other metalloporphyrins appears to have been neglected.

Chicarelli *et al.* produced tentative evidence for the presence of metalloporphyrins other than those already known [123], on the basis of off-line analysis of liquid chromatographic fractions from various oil shales using ICP-MS. Fractions were shown to contain significant amounts of iron, cobalt, copper, manganese, zinc and titanium as well as nickel and vanadium. No on-line speciation studies were conducted but this study did highlight the need for direct on-line element selective analysis of metalloporphyrins [122].

ICP-MS would appear to offer the sensitivity required for such studies and would also provide isotopic information [123,124].

This chapter describes the use of HTGC coupled to flame ionization detection (FID), mass spectrometry (MS) and ICP-MS for the analysis of metallated geoporphyrins. The chromatographic behaviour of the geoporphyrins on commercially available columns (HT-5 and DB-1 ht) is also discussed.

## 3.2 Analysis of Julia Creek Oil Shale:

Julia Creek oil Shale contains both nickel and vanadyl porphyrins [19,45,125-128], both of which have been studied herein using HTGC with FID, MS and ICP-MS detection. The UV/VIS

quantification data for the vanadyl and nickel porphyrins is shown in Chapter 7.

## 3.2.1.   HTGC-FID:

The HTGC-FID chromatogram (with HT-5 column) of the nickel porphyrin fraction shown in Figure 3.1 comprised 8 peaks (RI 6034-6895; Table 3.1). The chromatogram provides a "fingerprint" of the nickel porphyrin fraction and is similar to that obtained by Blum *et al.* with non-polar PS 347.5 stationary phase [129]. The major peak (RI 6895) represents 49.8 % of the total integrated area.

Examination of vanadyl geoporphyrin fraction on HT-5 stationary phase showed that the porphyrins were not separated but eluted as a bimodal "hump" (Figure 3.2 (b)). This was at first mistaken for column bleed, but increasing the concentration of the porphyrins, showed the "humps" to be the vanadyl porphyrins.

Re-examination of the vanadyl fraction (Figure 3.2 (a)) on DB-1 ht stationary phase produced a chromatogram which contained 11 peaks (RI 5519-6007, Table 3.2). The major peak (RI 5788) represented 71.8 % of the total integrated area. The separation obtained for the vanadyl fraction on the DB-1 ht phase was similar to that obtained by Blum *et al.* with PS 347.5 phase [129].
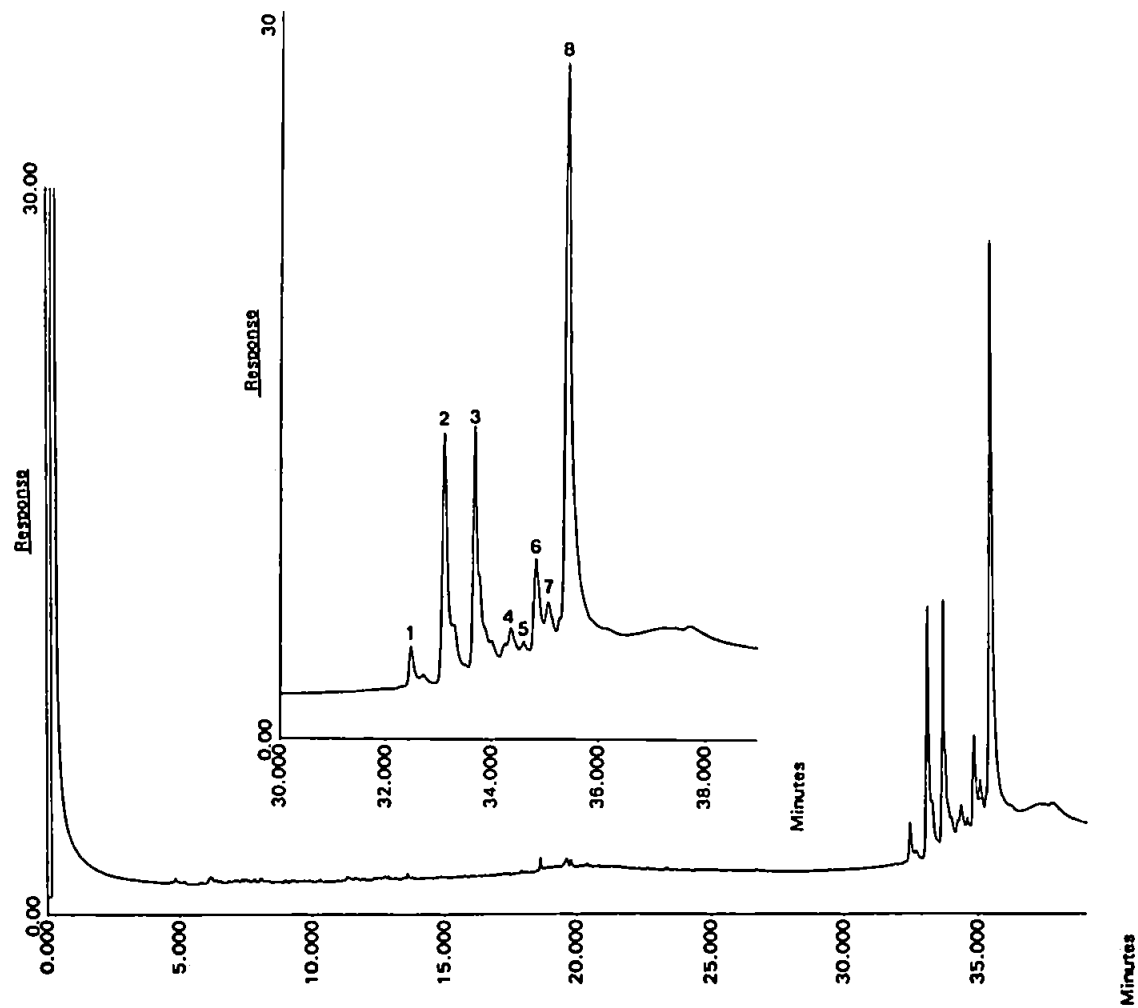
**Figure 3.1:** HTGC-FID of Julia Creek nickel Porphyrins (2.4 μg on column, 12 m HT-5 (0.32 mm; 0.10 μm film thickness), 50 to 410°C at 10°C/min, 3 min isothermal
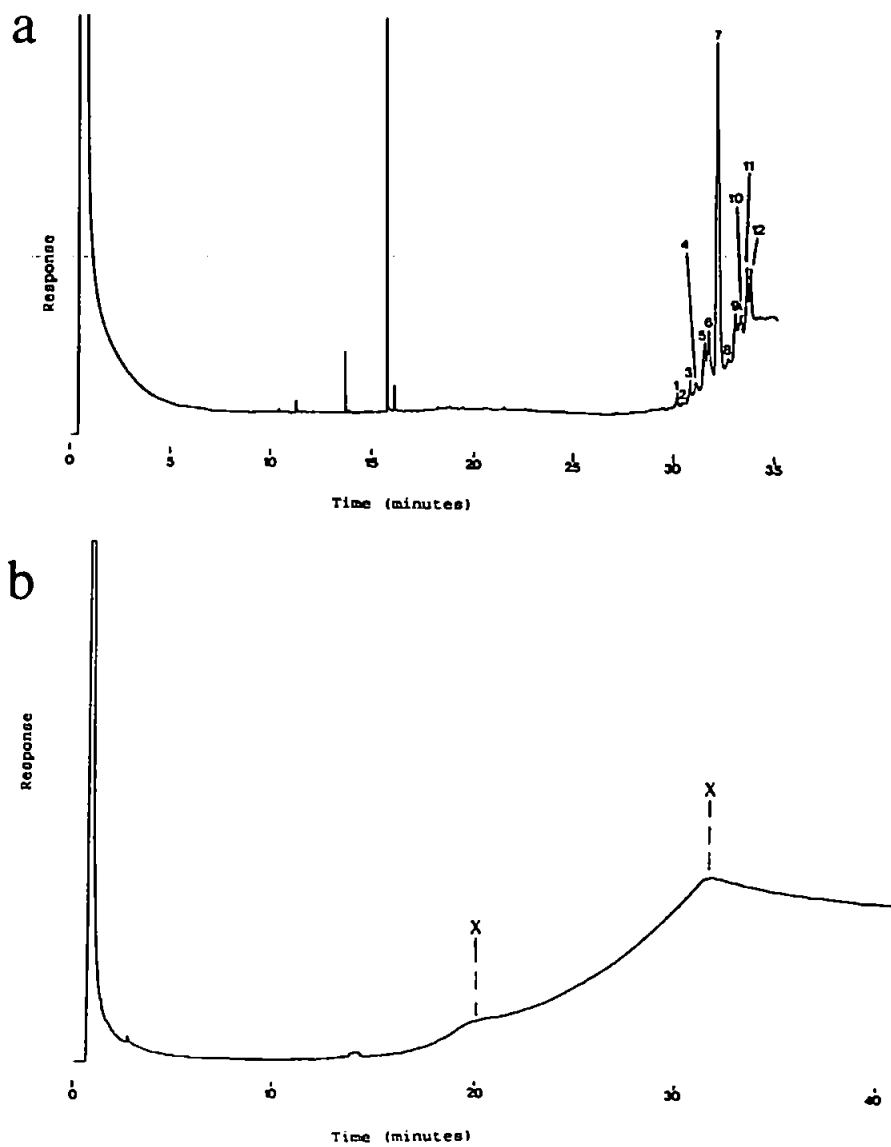
**Figure 3.2:** HTGC-FID of Julia Creek vanadyl porphyrins

(a) 0.7 μg on column; 15 m DB-1 ht (0.32 mm; 0.10 μm film), 50 to 400°C at 10°C/min

(b) 3.7 μg on column; 25 m HT-5 (0.32 mm; 0.10 μm film), 60 to 350°C at 15°C/min, 350 to 410°C at 5°C/min, X = vanadyl porphyrin "peaks"

| Retention Time (min) | Retention Index | Integrated Area (%) | Elution Temp. (°C) |
|---|---|---|---|
| 32.47 (1) | 6032 | 1.80 | 374 |
| 32.71 (2) | 6219 | 18.39 | 377 |
| 33.67 (3) | 6387 | 17.14 | 386 |
| 34.37 (4) | 6592 | 2.28 | 393 |
| 34.60 (5) | 6660 | 0.34 | 396 |
| 34.82 (6) | 6727 | 6.20 | 398 |
| 35:05 (7) | 6792 | 3.74 | 400 |
| 35.40 (8) | 6895 | 49.84 | 404 |

**Table 3.1:** Retention data and integrated areas of the Julia Creek nickel porphyrins

| Retention Time (min) | Retention Index | Integrated Area (%) | Elution Temp. (°C) |
|---|---|---|---|
| 30.29 (1) | 5519 | 1.95 | 352 |
| 30.53 (2) | 5552 | 0.48 | 355 |
| 30.92 (3) | 5604 | 2.20 | 359 |
| 31.20 (4) | 5642 | 2.16 | 362 |
| 31.61 (5) | 5697 | 3.20 | 366 |
| 31.84 (6) | 5728 | 4.80 | 368 |
| 32.29 (7) | 5788 | 71.86 | 373 |
| 32.80 (8) | 5857 | 1.05 | 378 |
| 33.19 (9) | 5910 | 3.74 | 381 |
| 33.44 (10) | 5943 | 2.15 | 384 |
| 33.74 (11) | 5983 | 2.79 | 387 |
| 33.92 (12) | 6007 | 3.46 | 389 |

**Table 3.2:** Retention data and integrated areas of the Julia Creek vanadyl porphyrins

## 3.2.2. Probe-MS and HTGC-MS:

Whilst HTGC-FID analysis of the porphyrin fractions produced simple chromatograms (Figures 3.1, 3.2), probe-MS revealed the hidden complexity of the porphyrin mixtures and the extensive co-elution that occurs in the HTGC-FID chromatograms.

The probe-MS spectrum for the nickel porphyrin fraction reveals the presence of two pseudohomologues series of porphyrin macrocycle with a distribution as indicated in Figure 3.6. The different macrocycles are discussed below.

Three or more porphyrin macrocycles commonly occur in the geoporphyrin mixtures. Porphyrins are classified according to the degree of unsaturation (Figure 3.3) [130]. Porphyrin macrocycles with only saturated alkyl substituents are classed together as A [A = (A)ETIO; Figure 3.3 (a)] porphyrins, i.e. with a molecular formula conforming to $C_{20+n}H_{14+2n}N_4$. Other porphyrin macrocycles are classed according to their degree of extra unsaturation, hence DPEP (as well as cyclopropano, butano-etioporphyrins) are classed as A-2 [A minus two; Figure 3.3 (b)] i.e. $C_{20+n}H_{12+2n}N_4$. The dicycloethano, propano, butano-etioporphyrins are classed as A-4 porphyrins [Figure 3.3 (c)] i.e. $C_{20+n}H_{10+2n}N_4$. Thus the classes are separated by two degrees of unsaturation i.e. A, A-2, A-4, A-6, A-8. The most commonly occurring are the A, A-2 and the A-4 classes.

Porphyrins are unusual in that under electron impact ionization almost exclusively molecular ions are produced [52]. This

71

A $(C_{20+n} H_{14+2n} N_4)$
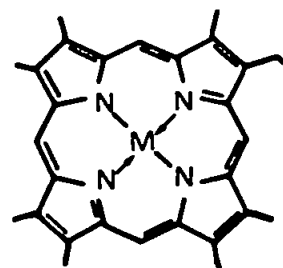
A-2 one extra degree of unsaturation

$(C_{20+n} H_{12+2n} N_4)$
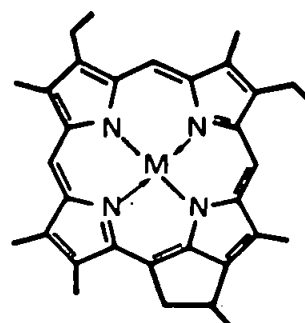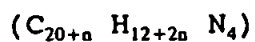
A-4 two extra degrees of unsaturation

$(C_{20+n} H_{10+2n} N_4)$
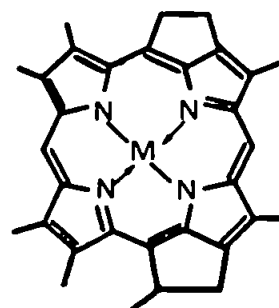
Figure 3.3: Geoporphyrin macrocycle classification [130]

facilitates resolution of the various classes of porphyrins by mass chromatography of the molecular ions.

The conditions used for HTGC-MS and probe-MS are shown in Chapter 7 (Table 7.2).

HTGC-MS chromatograms along with mass spectra for the nickel porphyrins of Julia Creek oil shale are shown in Figures 3.4 and 3.5. The DB-1 ht column provided poorer chromatographic resolution (Figure 3.4) than the HT-5 (Figure 3.5), hence subsequent nickel porphyrin fractions were analysed using only the HT-5 phase.

Probe-MS (Figure 3.6) and HTGC-MS spectra (Figure 3.5) confirmed the presence of A, A-2 and A-4 classes in the nickel porphyrin fraction. Mass chromatography of the molecular ions also confirmed the presence of A, A-2 and A-4 porphyrins (Table 3.3), for the purpose of illustration the mass chromatography for these are shown in Figure 3.7. The molecular ions are illustrated for nickel and vanadyl geoporphyrins, by the molecular mass Table in appendix A. In this work probe-MS and HTGC-MS were compared, to investigate whether all the porphyrins eluted from the column. The majority of the porphyrins were of the A-2 type with a carbon number distribution from $C_{26}$ to $C_{33}$ with the maximum at $C_{32}$. The A class extended from $C_{26}$ to $C_{32}$ with the majority occurring between $C_{30}$ and $C_{32}$. The A-4 class were distributed from $C_{27}$ to $C_{32}$, $C_{31}$ was the most abundant.

## Julia Creek Total Ion Current
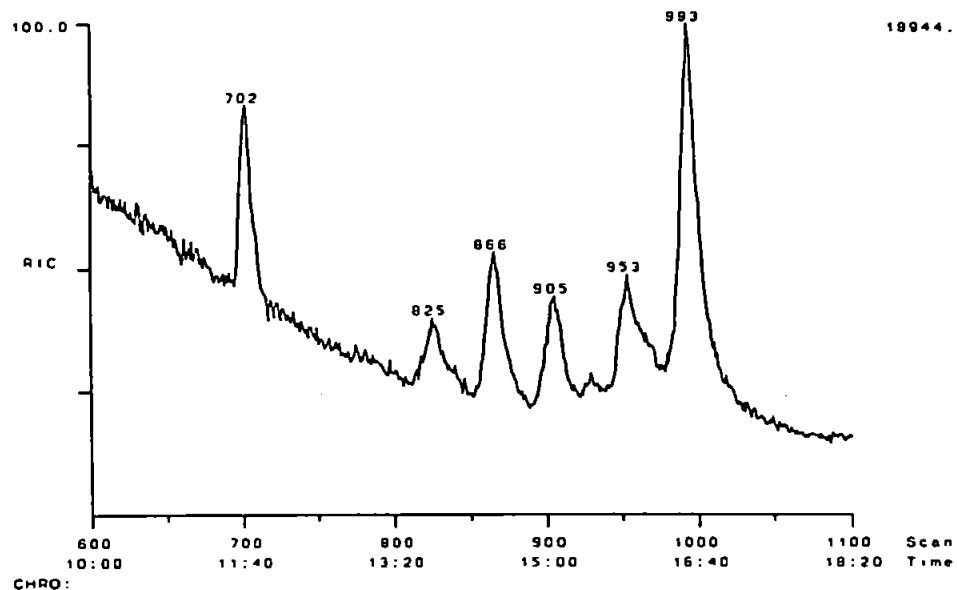


## Scan 865



**Figure 3.4:** HTGC-MS of Julia Creek nickel Porphyrins (3.5 $\mu$g on column), 15 m DB-1 ht, 40 to 350°C at 15°C/min, 350 to 390 at 10°C/min, ~1 min isothermal; chromatogram shown from 350°C, selected mass spectra shown (peak at scan 702 contamination)

Scan 953



Scan 993
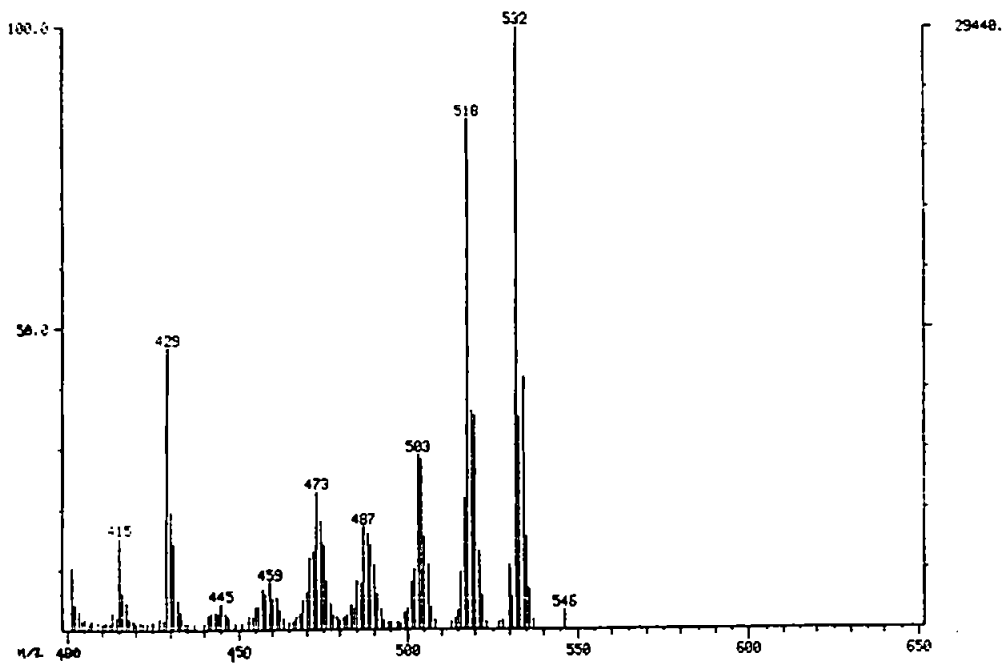


**Figure 3.4:** continued

## Julia Creek Total Ion Current
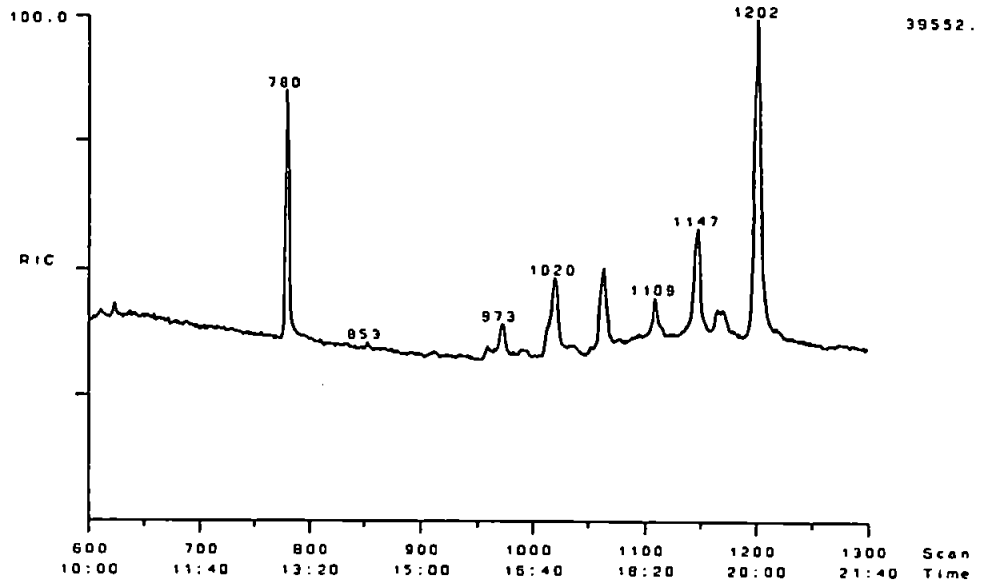


## Scan 1020
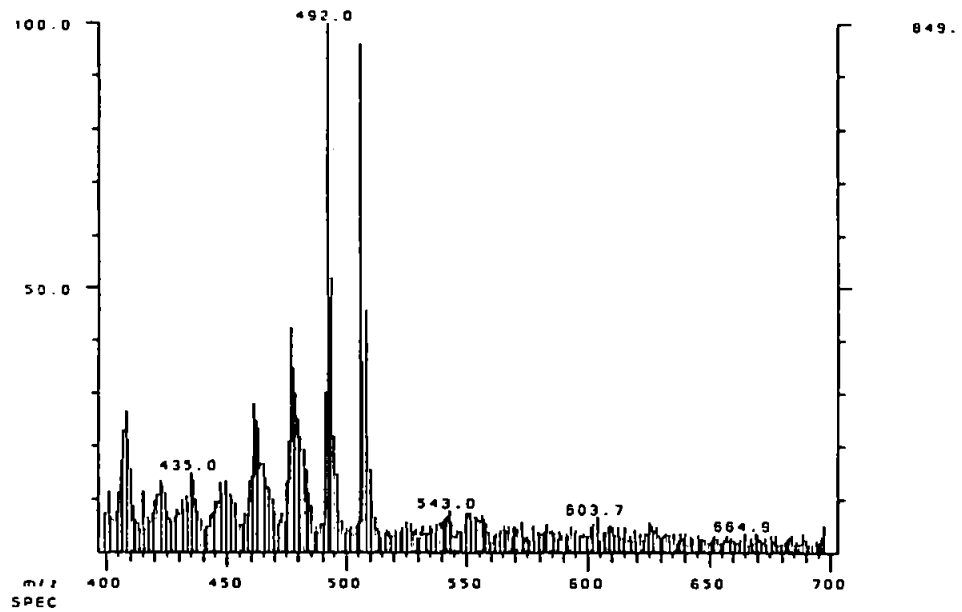


**Figure 3.5:** HTGC-MS of Julia Creek nickel porphyrins (3.0 μg on column), 12m HT-5, 40 to 350°C at 15°C/min, 350 to 410°C at 5°C/min. Chromatogram shown from 350°C, selected mass spectra shown (peak at scan 780 contamination)

**Scan 1147**
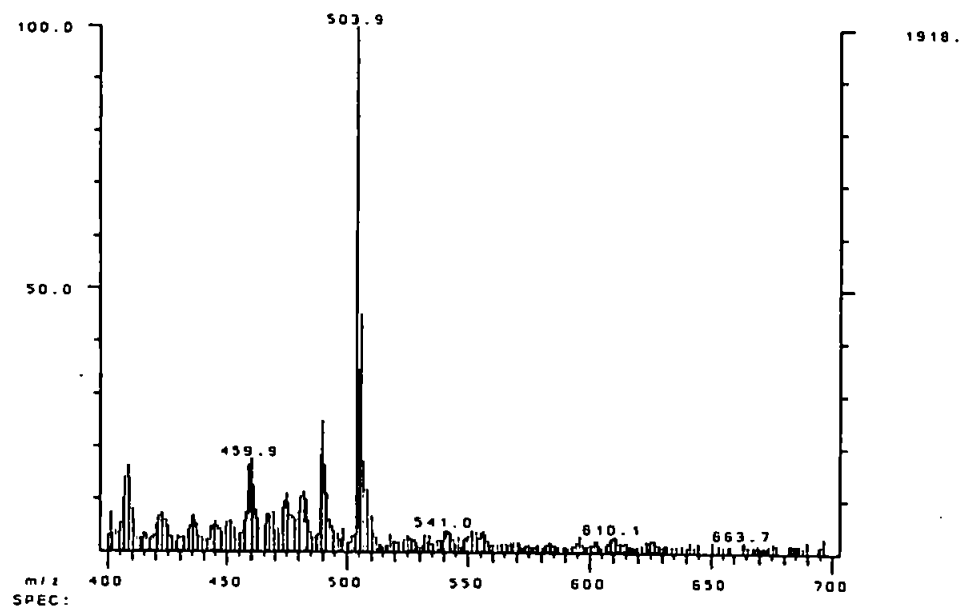


**Scan 1202**
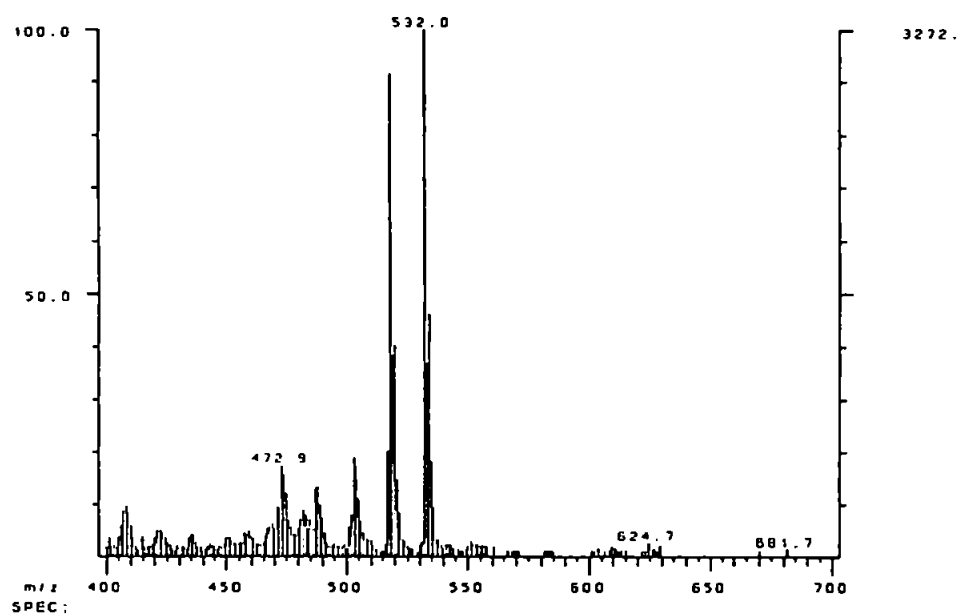


**Figure 3.5:** continued
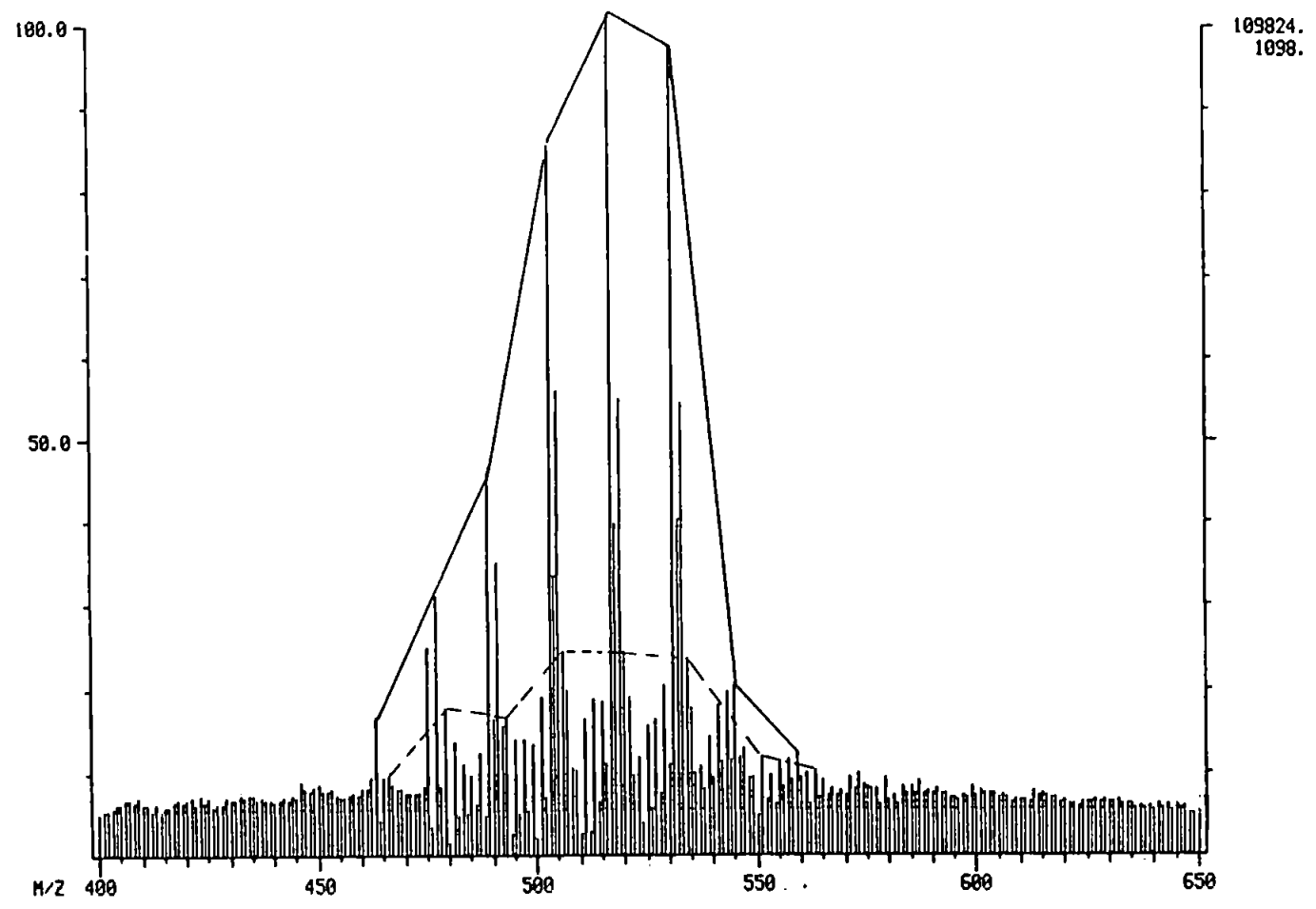
**Figure 3.6:** Probe mass spectrum of Julia Creek nickel porphyrins at 16eV; -- A macrocycles, —
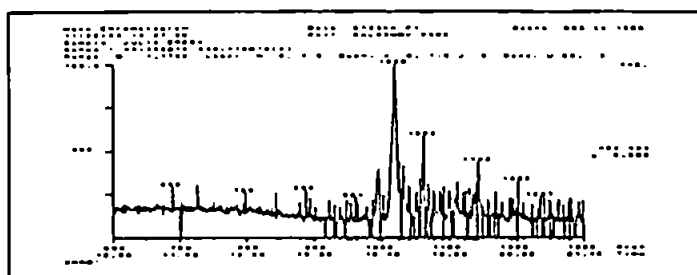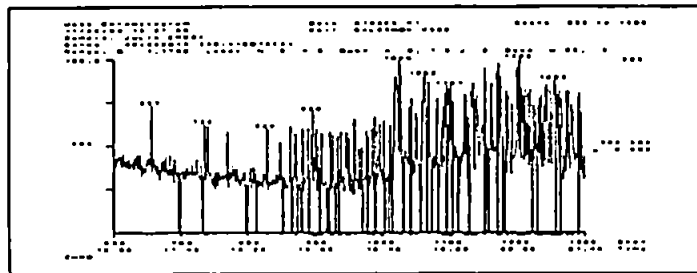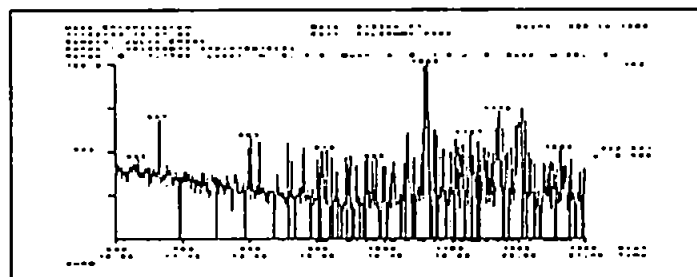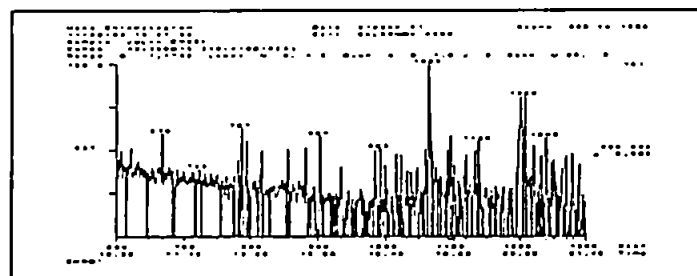
A-2 macrocycles

**Figure 3.7:** Single mass chromatograms obtained from HTGC-MS (Figure 3.5), showing A ($C_{29}$-$C_{32}$), A-2 ($C_{27}$-$C_{34}$) and A-4 ($C_{26}$-$C_{31}$) macrocycles present in Julia Creek nickel porphyrin fraction
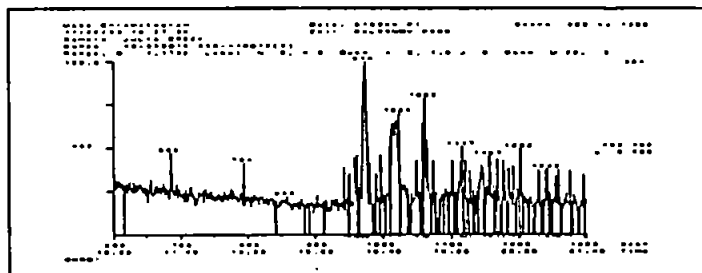
C$_{27}$ A-2
(m/z 462)
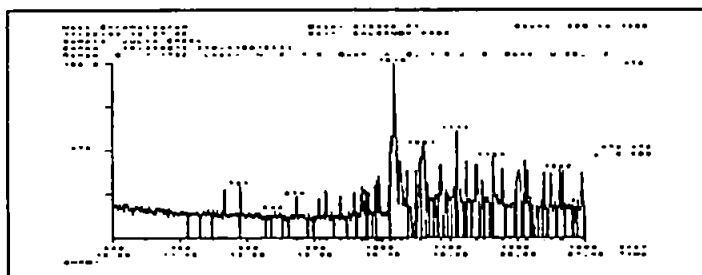
C$_{28}$ A-2
(m/z 476)
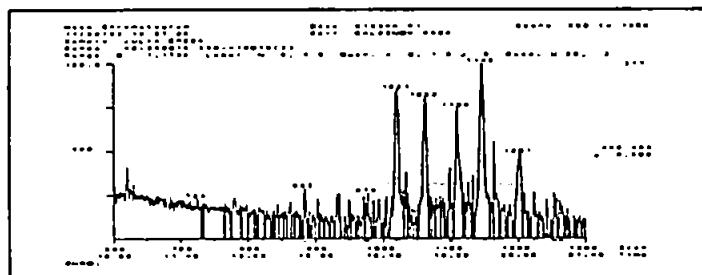
C$_{29}$ A-2
(m/z 490)
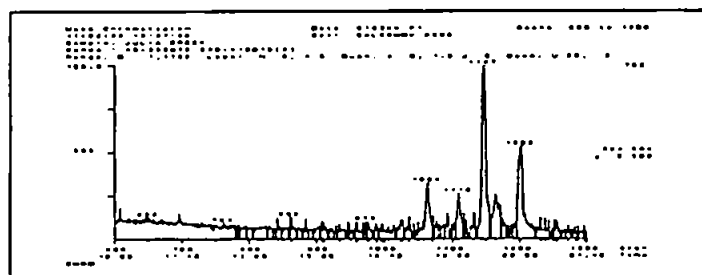
C$_{30}$ A-2
(m/z 504)

Figure 3.7: A-2 C$_{27}$ to C$_{30}$
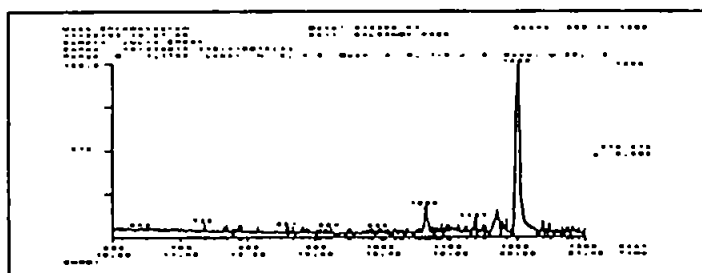
C$_{31}$ A-2
(m/z 518)
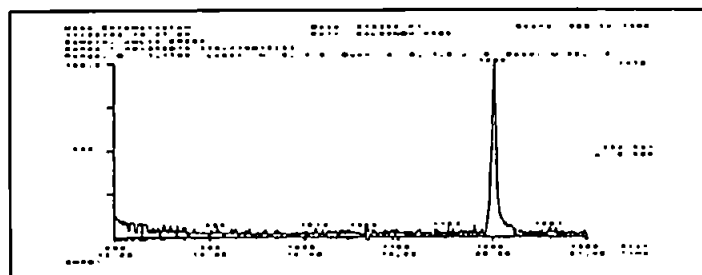
C$_{32}$ A-2
(m/z 532)
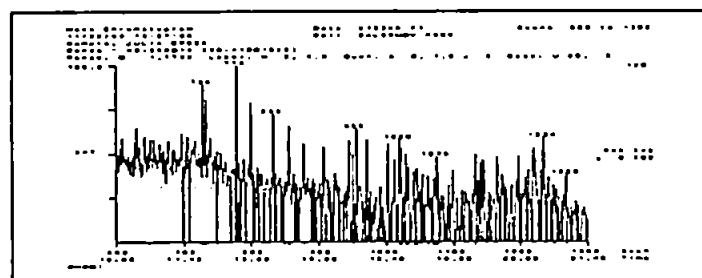
C$_{33}$ A-2
(m/z 546)
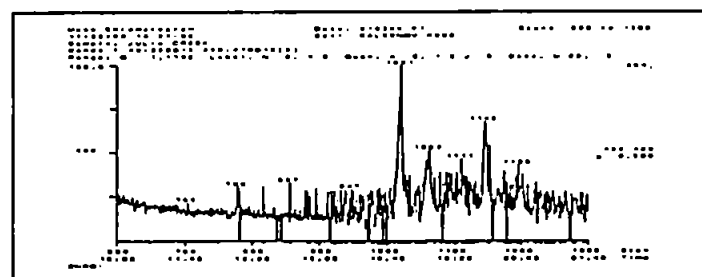
C$_{34}$ A-2
(m/z 560)

Figure 3.7: A-2 C$_{31}$ to C$_{34}$
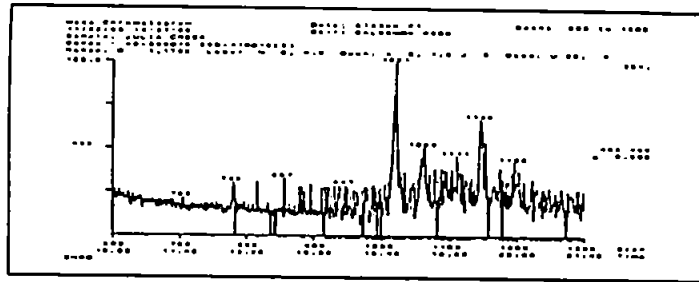
$C_{26}$ A-4
(m/z 460)
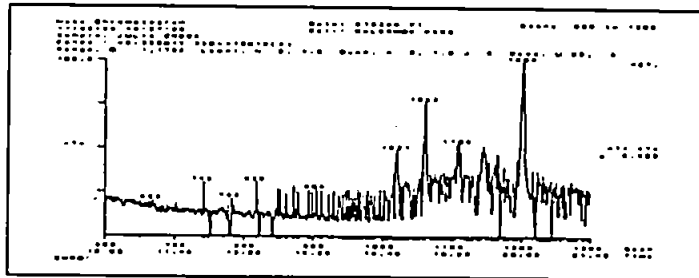
$C_{27}$ A-4
(m/z 474)
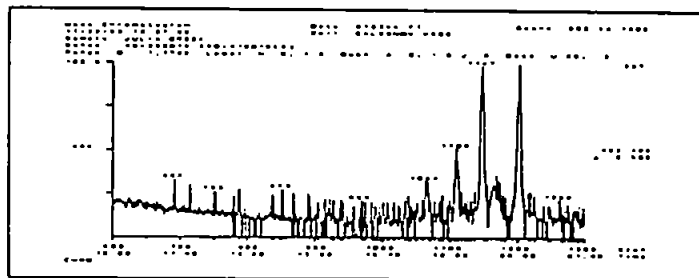
$C_{28}$ A-4
(m/z 488)
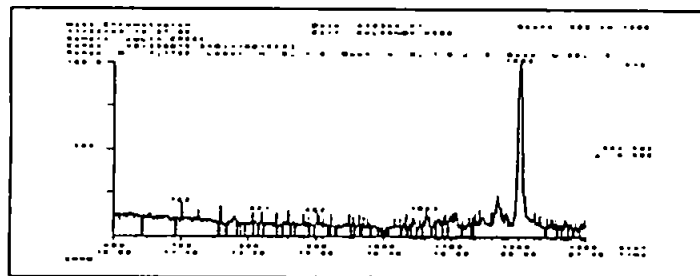
$C_{30}$ A-4
(m/z 502)
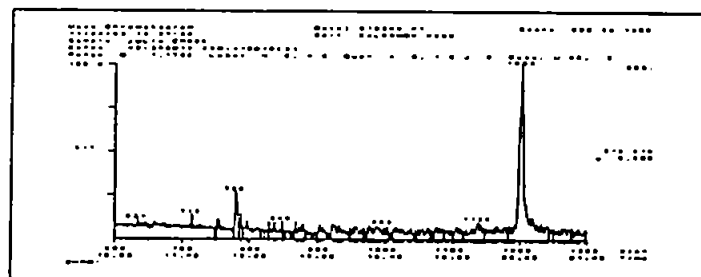
$C_{31}$ A-4
(m/z 516)

Figure 3.7: A-4 $C_{26}$ to $C_{31}$

| Retention Time/ Scan no. | Macrocycle Type and Molecular Ion Observed |
|---|---|
| 16.21 (973) | $C_{29}$A (494), $C_{27}$ A-2 (462), $C_{28}$ A-4 (474) |
| 17.00 (1020) | $C_{29}$ A (494), $C_{27}$ A-2 (462), $C_{28}$ A-2 (476), $C_{29}$ A-2 (490), $C_{30}$ A- 2 (504), $C_{34}$ A-2 (560), $C_{27}$ A-4 (460), $C_{28}$ A-4 (474) |
| 19.25 (1055) | $C_{31}$ A (522), $C_{32}$ A (536), $C_{29}$ A-2 (490), $C_{30}$ A-2 (504), $C_{31}$ A-2 (518), $C_{34}$ A-2 (560), $C_{27}$ A-4 (460), $C_{28}$ A-4 (474) |
| 18.48 (1109) | $C_{29}$ A-2 (490), $C_{30}$ A-2 (504), $C_{28}$ A-4 (474), $C_{29}$ A-4 (488) |
| 19.11 (1147) | $C_{31}$ A (522), $C_{29}$ A-2 (490), $C_{30}$ A-2 (504), $C_{31}$ A-2 (518), $C_{34}$ A-2 (560), $C_{27}$ A-4 (460), $C_{28}$ A-4 (474), $C_{29}$ A-4 (488) |
| 19.45 (1167) | $C_{31}$ A (522), $C_{32}$ A (536), $C_{27}$ A-2 (462), $C_{29}$ A-2 (490), $C_{34}$ A-2 (560), $C_{27}$ A-4 (460), $C_{28}$ A-4 (474), $C_{29}$ A-4 (488) |
| 20.03 (1202) | $C_{32}$ A (536), $C_{29}$ A-2 (490), $C_{30}$ A-2 (504), $C_{31}$ A-2 (518), $C_{32}$ A-2 (532), $C_{28}$ A-4 (474), $C_{28}$ A-4 (474), $C_{29}$ A-4 (488) |

Table 3.3: Nickel porphyrin distribution in HTGC-MS chromatogram of Julia Creek oil shale

The nickel porphyrin mixture consisted of 18 porphyrin macrocycles, but the total number of porphyrin isomers from this distribution is much larger [52]. Estimates of the number of isomers in simple mixtures containing only one class of porphyrin macrocycle distributed from $C_{28}$ to $C_{34}$ have suggested that up to 1080 isomers are possible [52]. This estimate included simplifications made on the basis of experimental observations. The number of isomers possible with porphyrins of higher unsaturation has not been attempted, but the number would be substantially larger [52]. This provides an explanation for the extensive co-elution of various porphyrin macrocycles observed using mass chromatography.

The nickel fraction of Julia Creek is thus a complex mixture of porphyrin macrocycles with the A-2 $C_{31}$ and $C_{32}$ macrocycles as major components [19,34].

Results of probe-MS and HTGC-MS (DB-1 ht phase) of the vanadyl fraction are shown in Figures 3.8 and 3.9. The mass spectra again indicate co-elution of the various macrocycles A, A-2 and A-4, as illustrated in Table 3.4. The distribution of the various classes of porphyrin macrocycles obtained using the HTGC-MS and probe-MS data agree. Mass chromatograms of molecular ions for the A and A-2 macrocycles are shown in Figure 3.10 and Table 3.4.

The A class macrocycles are distributed from $C_{28}$ to $C_{32}$ (maximum $C_{32}$), A-2 macrocycles from $C_{27}$ to $C_{33}$ (maximum $C_{31}$) and A-4 macrocycles range $C_{26}$ to $C_{33}$ (maximum $C_{31}$). The A-2 macrocycles
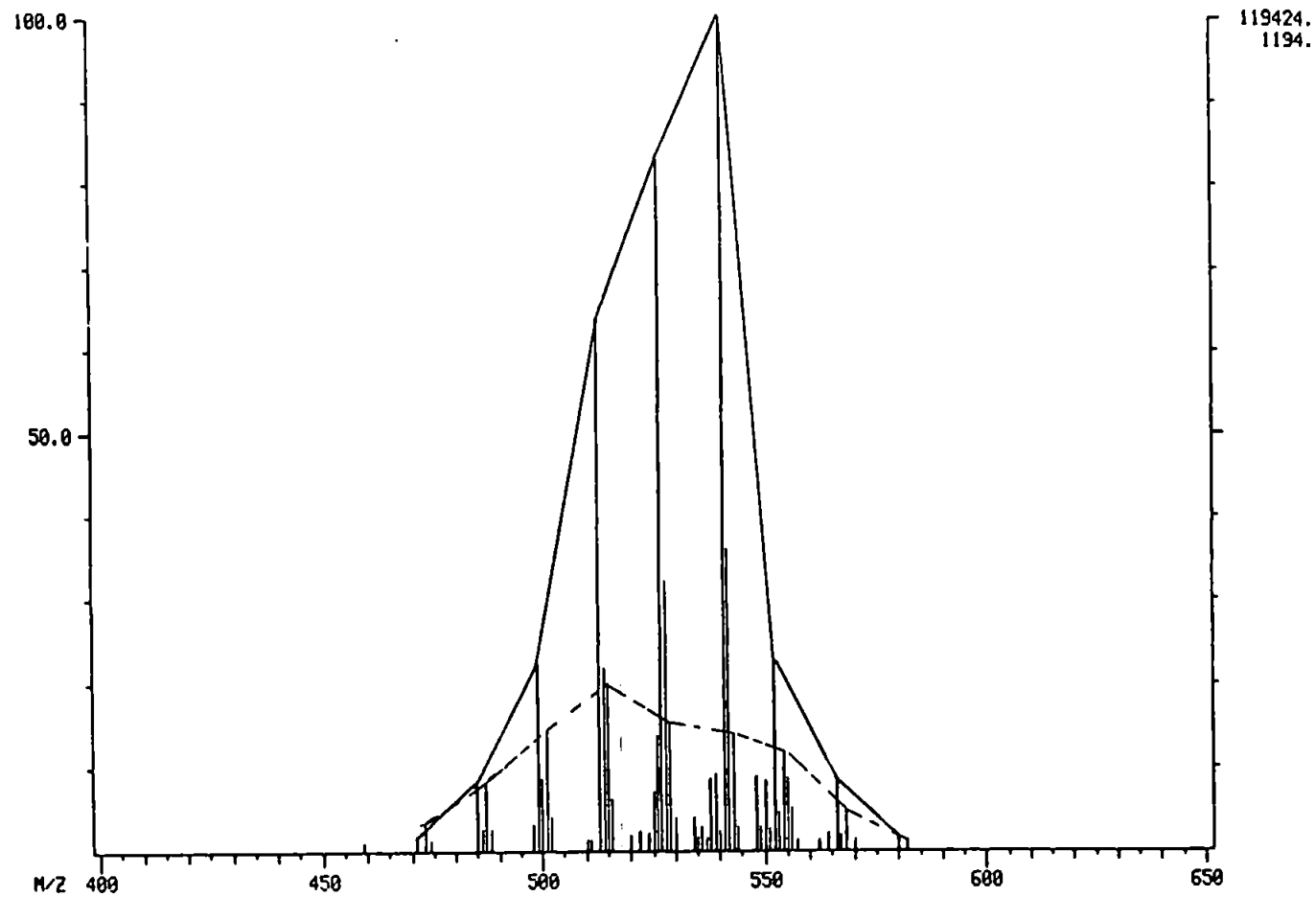
**Figure 3.8:** Probe mass spectrum of Julia Creek vanadyl porphyrins at 16eV; -- A macrocycles, — A-2 macrocycles
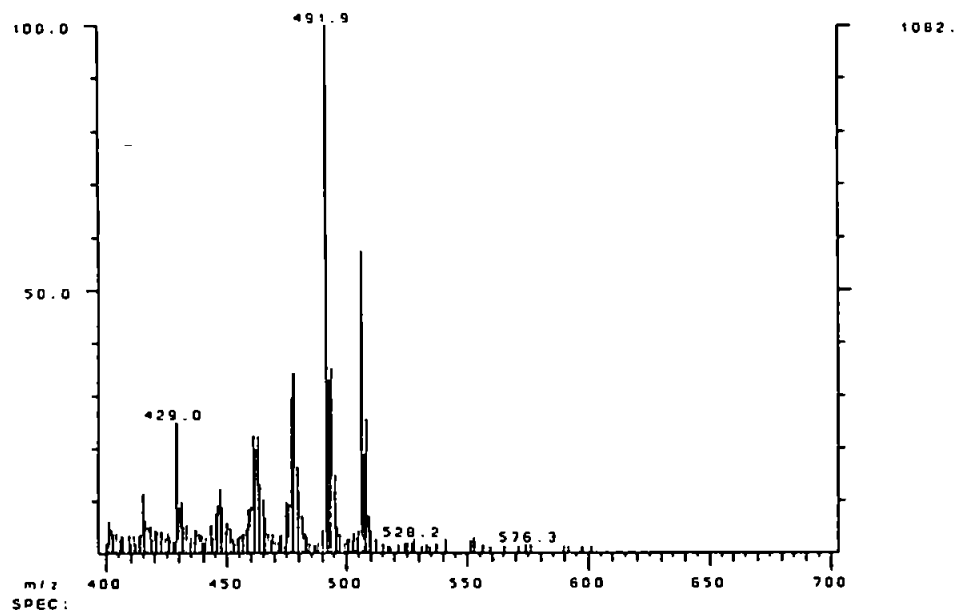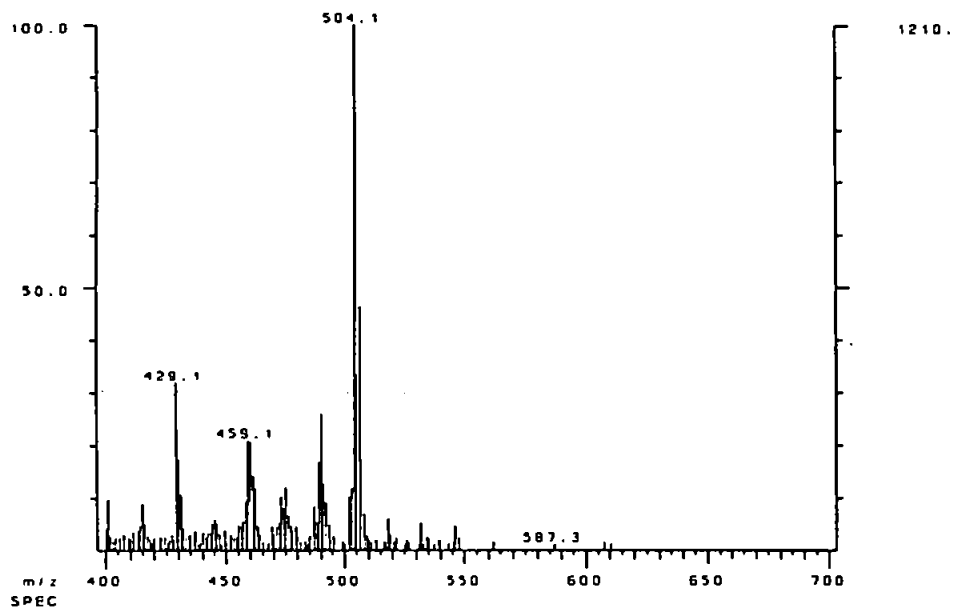
**Figure 3.9:** HTGC-MS of Julia Creek vanadyl Porphyrins (0.5 µg on column), 15 m DB-1 ht, 40 to 300°C at 15°C/min, 300 to 390 at 10°C/min, ~4 min isothermal; chromatogram shown from 150°C, all mass spectra shown
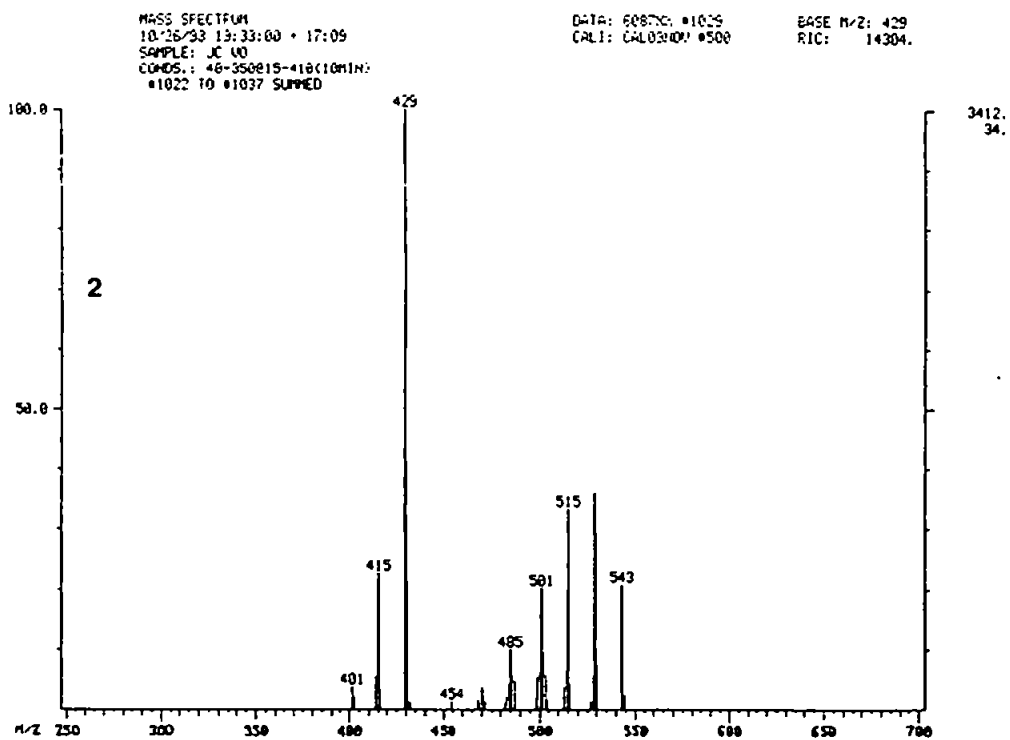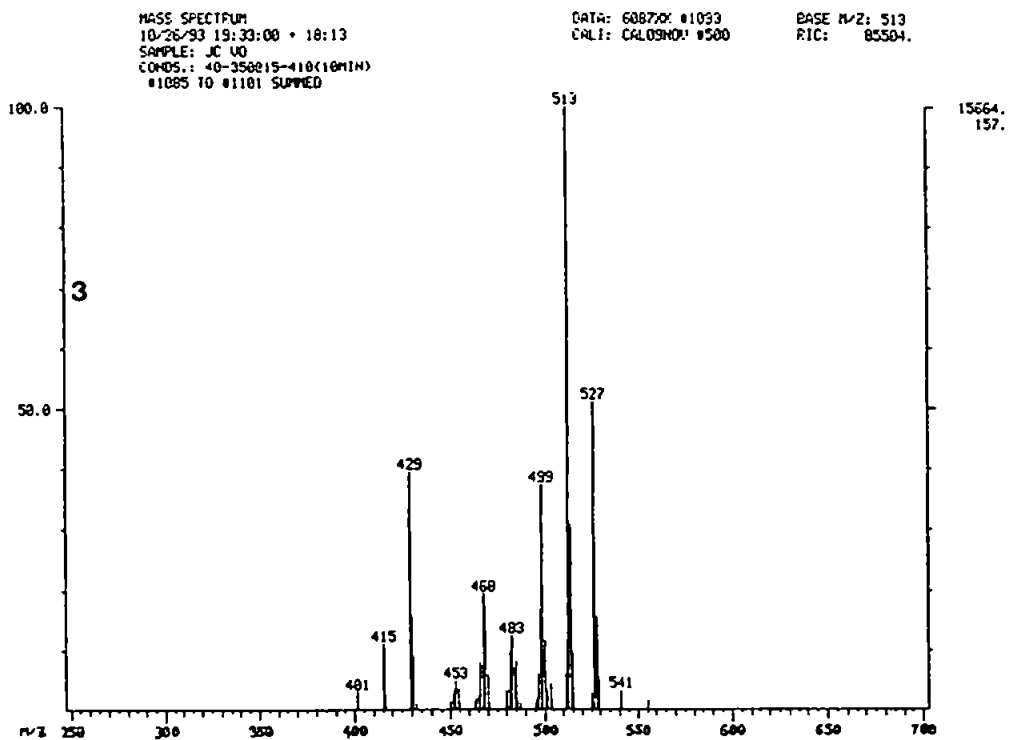
Figure 3.9: continued
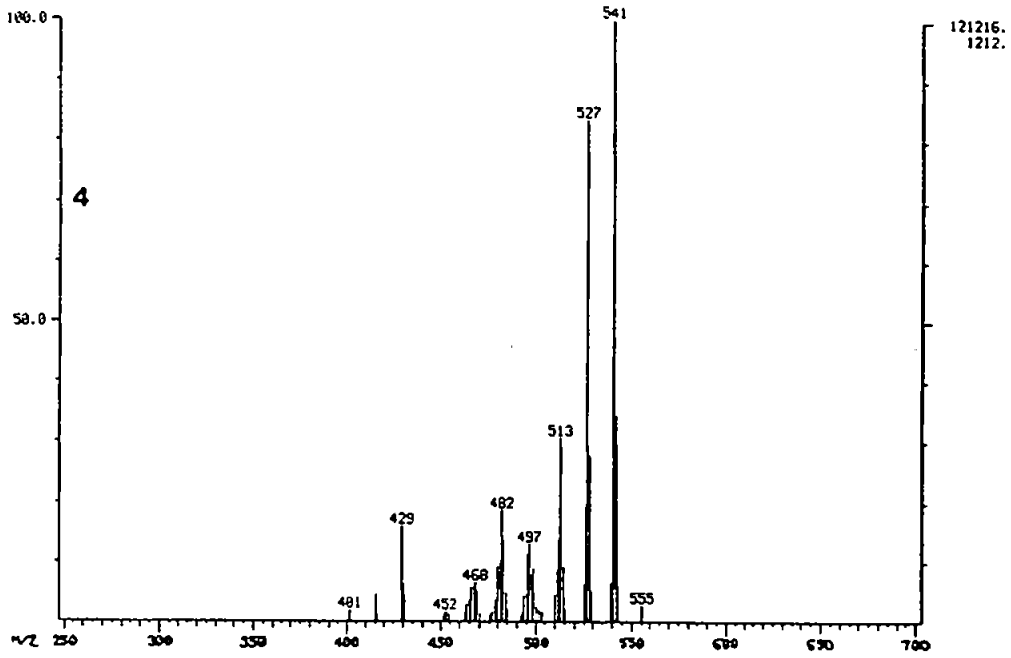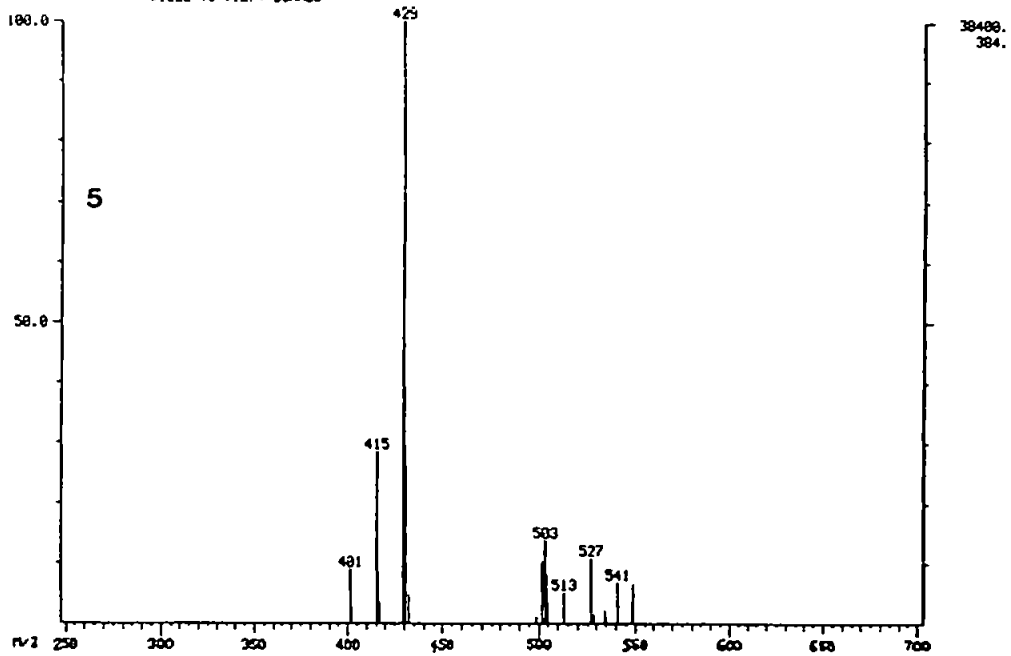
**Figure 3.9:** continued
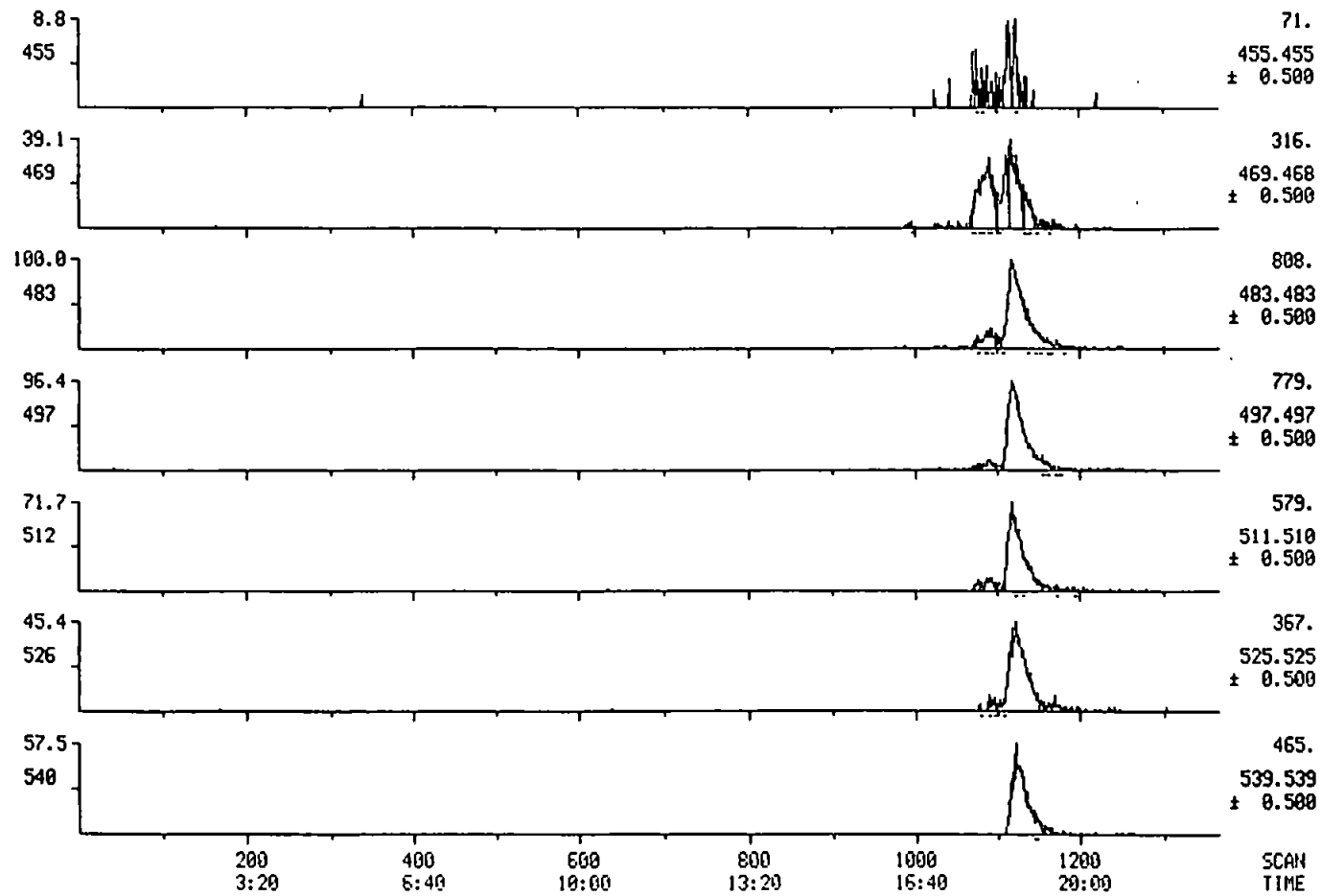
Figure 3.10:  A-4 $C_{26}$ to $C_{32}$
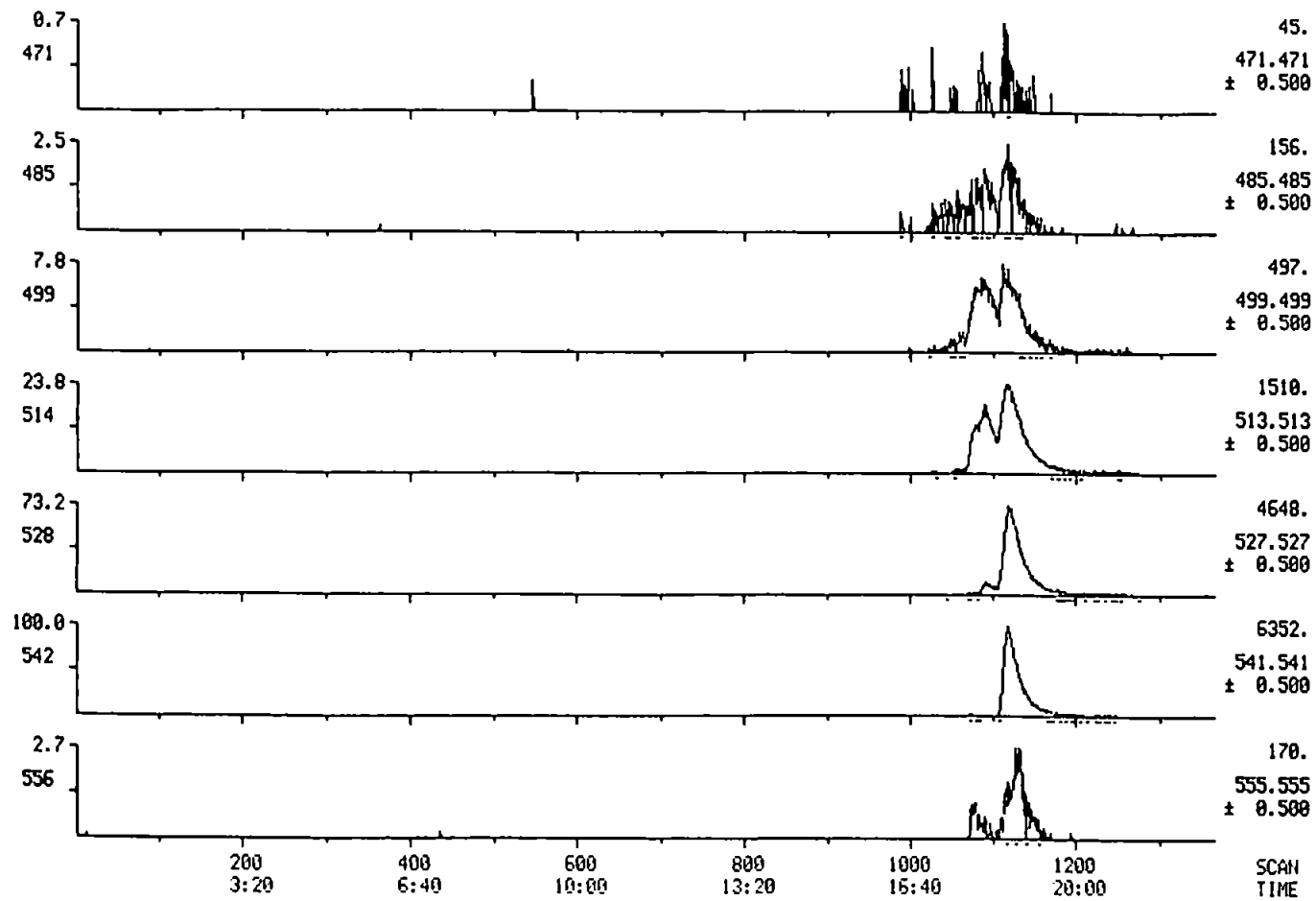
**Figure 3.10:** A-2 $C_{27}$ to $C_{33}$
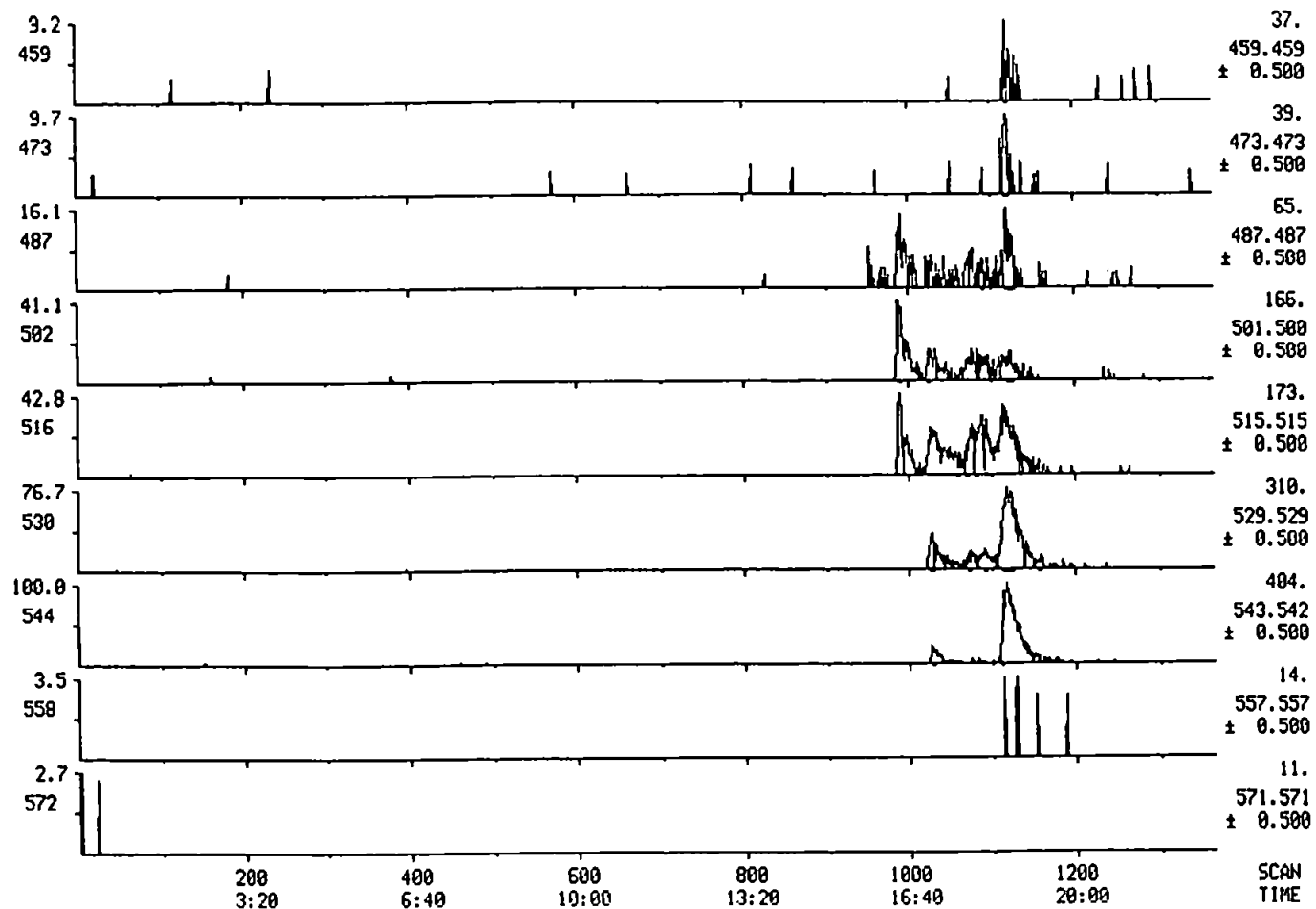
**Figure 3.10:** Single mass chromatograms obtained from HTGC-MS (Figure 3.9), showing A ($C_{26}$-$C_{32}$, above), A-2 ($C_{27}$-$C_{33}$) and A-4 ($C_{26}$-$C_{32}$) macrocycles present in Julia Creek nickel porphyrin fraction

| Retention Time/peak no. | Macrocycle Type and Molecular Ion Observed |
| --- | --- |
| 16.50 (1) | $C_{28}$ A (487), $C_{29}$ A (501), $C_{30}$ A (515), |
| 17.41 (2) | $C_{28}$ A (487), $C_{29}$ A (501), $C_{30}$ A (515), $C_{31}$ A (529), $C_{32}$ A (543) |
| 18.17 (3) | $C_{28}$ A (487), $C_{29}$ A (501), $C_{30}$ A (515), $C_{31}$ A (529), $C_{28}$ A-2 (485), $C_{29}$ A-2 (499), $C_{30}$ A-2 (513), $C_{31}$ A-2 (527) |
| 18.63 (4) | $C_{26}$ A (459), $C_{27}$ A (473), $C_{28}$ A (487), $C_{29}$ (501), $C_{30}$ A (515), $C_{31}$ A (529), $C_{32}$ A (543), $C_{27}$ A-2 (471), $C_{28}$ A-2 (485), $C_{29}$ A-2 (499), $C_{30}$ A-2 (513), $C_{31}$ A-2 (527), $C_{32}$ A-2 (541), $C_{33}$ A-2 (555) |

**Table 3.4:** Vanadyl porphyrin distribution in HTGC-MS chromatogram of Julia Creek oil shale

make up the majority of the porphyrins, the $C_{32}$, $C_{31}$ and $C_{30}$ being the most abundant.

Thus in both the nickel and vanadyl fractions the most abundant macrocycles are the A-2 (DPEP) $C_{30}$-$C_{32}$ series. The mass chromatographic runs were not integrated for two reasons, firstly, the main aim of this study was examination of the metals chelated by the geoporphyrins and not at the absolute macrocycle distributions. Secondly, the elution of the porphyrins from the columns used was erratic and selective adsorption by the column would lead to misleading results. The distributions of the macrocycles are discussed by Blum *et al.* [34].

### 3.2.3 HTGC-ICP-MS:

The nickel and vanadyl porphyrin fractions of Julia Creek Oil Shale were analysed using HTGC-ICP-MS. Selected ion recording of m/z 48 (Ti), 51 (V), 56 (Fe), 58 (Ni) and 64 (Zn) was performed for both fractions. HTGC-ICP-MS conditions are shown in Chapter 2 (Table 2.1).

The nickel fraction was analysed using a 25 m (HT-5) column (Figure 3.11). The distribution of the peaks are shown in Table 3.5 (p. 100). One component dominates the nickel (m/z 58) distribution and represents 64 % of the total area. The increased resolution obtained with this column is illustrated by the appearance of a shoulder on the main peak (trailing edge

93
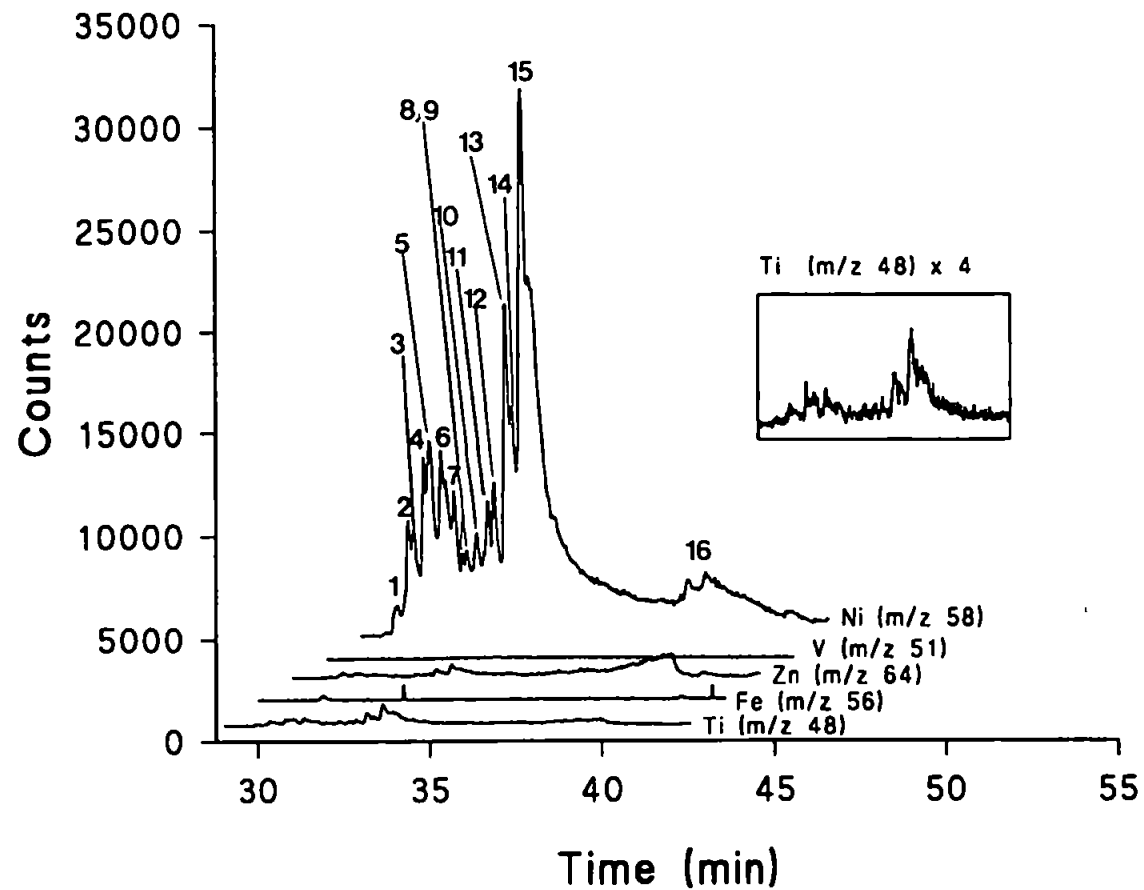
**Figure 3.11:** HTGC-ICP-MS of Julia Creek nickel porphyrins (3.3 µg on column), 25 m HT-5, 60 to 350°C at 10°C/min, 350 to 410 at 4.5°C/min, ~0.5 min isothermal; chromatogram monitored from 350°C

of 15, Figure 3.11) which could represent one of the multi-components of this peak. The chromatogram is consistent with the probe-MS and HTGC-FID/MS findings, namely that the macrocycle distribution is largely dominated by $C_{30}, C_{31}$ and $C_{32}$ A-2 type porphyrins. These three macrocycles co-elute in both the chromatograms of nickel and vanadyl porphyrins as one major peak.

The selected ion recordings also indicate the presence of Ti (m/z 48) and Zn (m/z 64). The elution patterns of these chromatograms are essentially identical to those of the nickel fraction. The zinc peaks could result from trans-metallation of the nickel porphyrins during sample work-up, probably on the activated silica during column chromatography [131]. The titanium peaks are more likely to be authentic [122,132,133]. The total area of the titanium and zinc peaks compared with the total area of the nickel (m/z 58) fraction was 8.1 % (m/z 64) and 3.9 % (m/z 48), respectively. This is a significant amount since the ratio of vanadyl porphyrins to nickel porphyrins in Julia Creek is 30:1 (Chapter 7).

Titanium porphyrins have not been reported in geological samples previously, although Chicarelli *et al.* speculated on their presence in several shales on the basis of off-line liquid chromatography followed by direct nebulization ICP-MS. The shales that Chicarelli *et al.* studied Julia Creek Oil Shale and Marl Slate [122] and speculated on the presence of titanium poprhyrins. Mango *et al.* commented on the catalytic activity of transition metals in catalysing reactions under diagenetic

conditions and mentioned titanium as one of the possible transition metal catalysts [132]. Other workers have suggested that the poisoning of coal liquefaction catalysts could be due, in part, to the presence of titanium porphyrins [133].

The nickel porphyrin fraction was also examined on a new 12 m HT-5 column with selected ion recording of the major isotopes of all the first row transition metals (Figure 3.12). Although only nickel was present, the chromatogram does reveal the potential of the HTGC-ICP-MS as an element selective GC detector.

The vanadyl porphyrin fraction was analysed using this method, with selected ion recording of m/z 48, 51, 56, 58 and 64 (Figure 3.13 and 3.14). The HT-5 phase again produced the bimodal "hump" (Figure 3.14), observed in the HTGC-FID chromatograms, whilst the DB-1 ht phase (Figure 3.13) separated the porphyrins into 4 peaks (distributions shown in Table 3.6). The separation on the DB-1 ht obtained for the HTGC-ICP-MS and HTGC-MS (Figure 3.13) was not as good as that obtained for the HTGC-FID [of Figure 3.2 (a)] due to deterioration of the DB-1 ht column (for further discussion see Section 3.7).

HTGC-ICP-MS revealed only vanadyl porphyrins in to be present, with the major peak representing 74 % of the total area. The chromatogram is consistent with the results obtained by probe-MS, HTGC-FID and HTGC-MS, which also indicated one component (~71 % of the total integrated area). The major constituents indicated by probe-MS and HTGC-MS were $C_{30}$, $C_{31}$ and
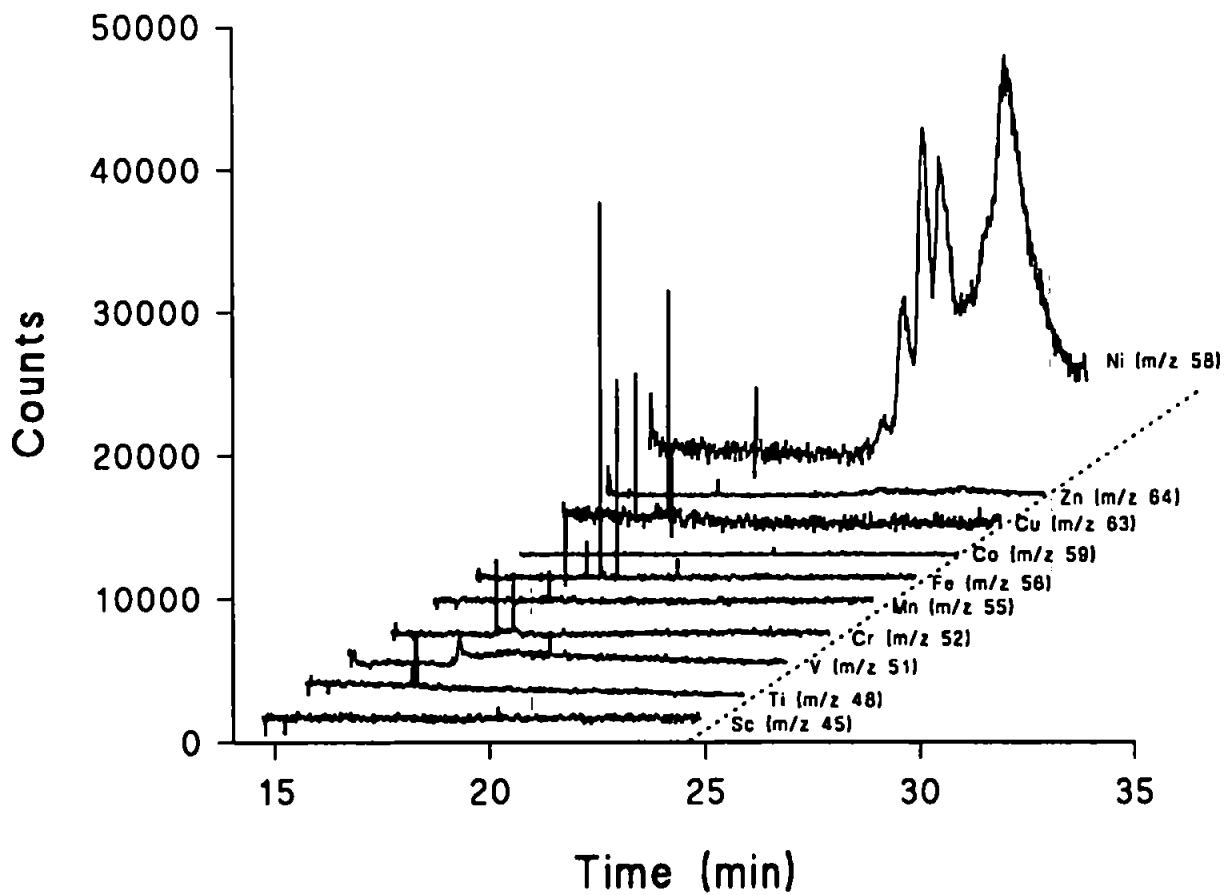
**Figure 3.12:** HTGC-ICP-MS of Julia Creek nickel porphyrins (1.9 μg on column), 12 m HT-5, 60 to 350°C at 20°C/min, 350 to 410 at 6°C/min, ~0.5 min isothermal. Chromatogram monitored from 350°C
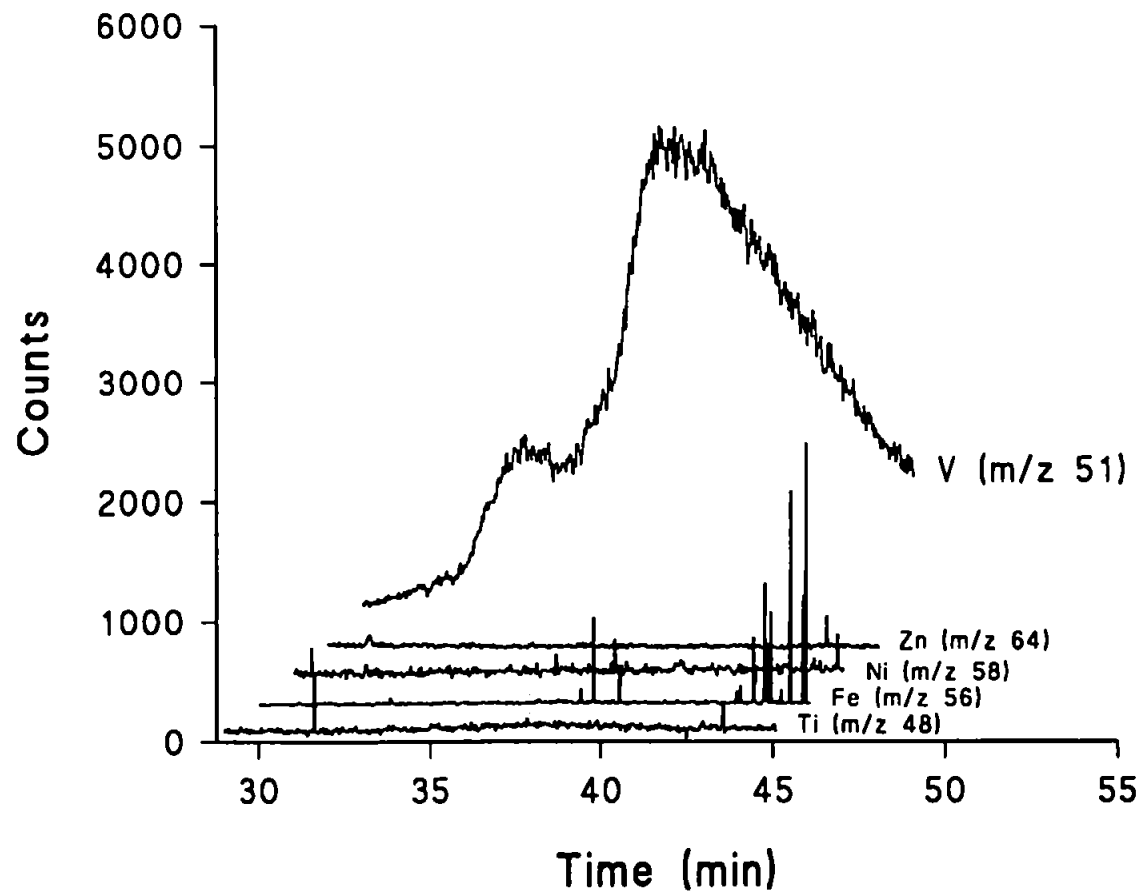
**Figure 3.13:** HTGC-ICP-MS of Julia Creek vanadyl porphyrins (2.4 $\mu$g on column), 25 m HT-5, GC conditions as in Figure 3.11; chromatogram monitored from 350°C

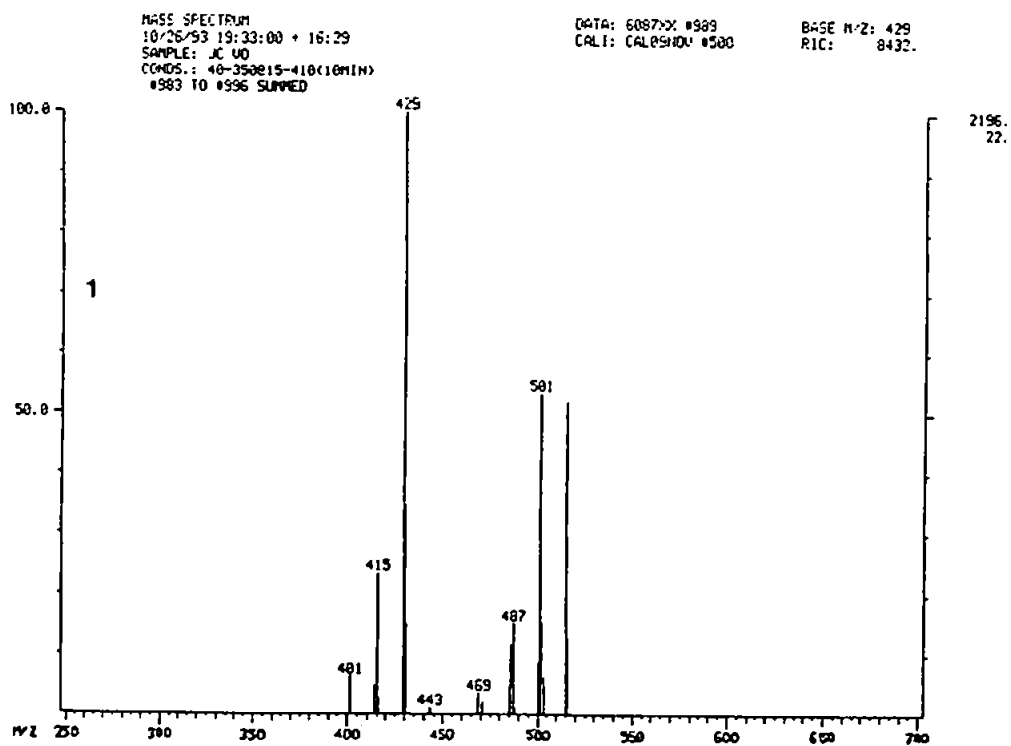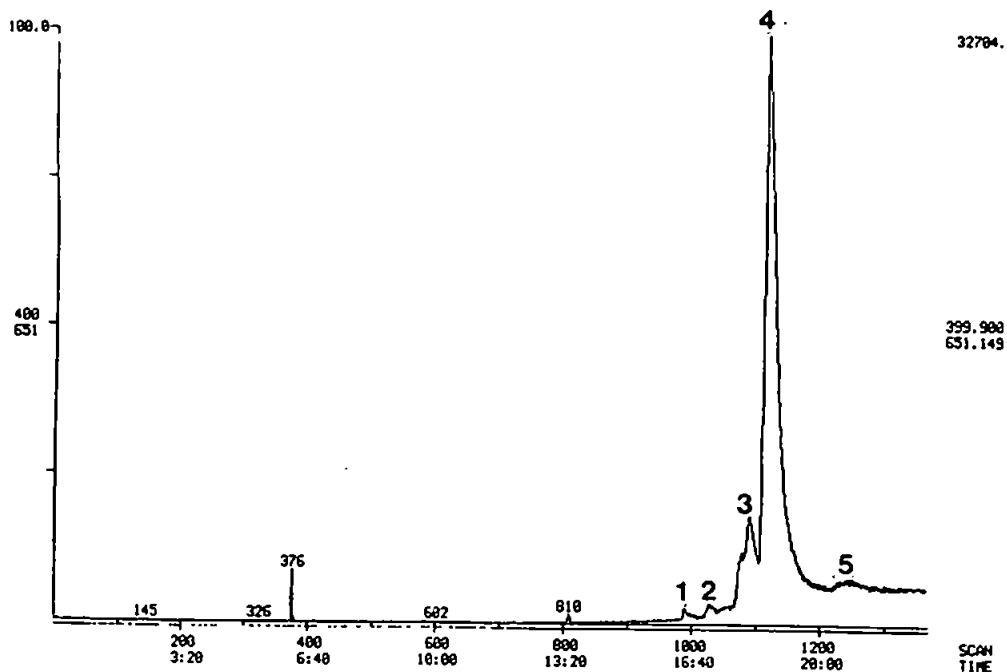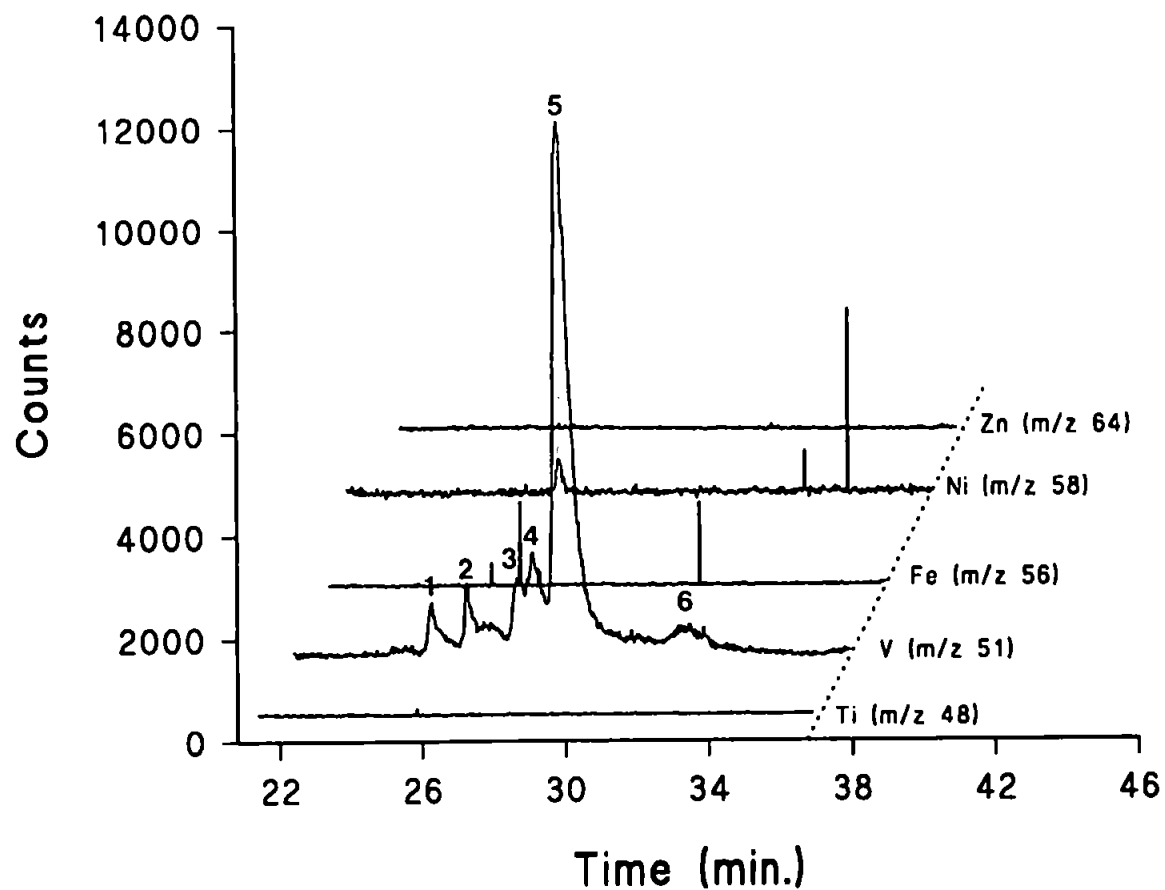**Figure 3.14:** HTGC-ICP-MS of Julia Creek vanadyl porphyrins (0.6 μg on column), 15 m DB-1 ht, 60°C to 320°C at 12°C/min, 320°C to 380°C at 4.5°C/min, 2 min isothermal; monitored from 320°C

| Retention Time (min) | Integrated area (%) |
|---|---|
| 31.4 (1) | 1.08 |
| 31.7 (2) | 1.74 |
| 31.9 (3) | 1.18 |
| 32.1 (4) | 2.49 |
| 32.3 (5) | 4.09 |
| 32.7 (6) | 2.93 |
| 33.0- (7) | -2.51 |
| 33.3 (8) | 0.51 |
| 33.4 (9) | 0.72 |
| 33.7 (10) | 1.82 |
| 34.0 (11) | 2.38 |
| 34.2 (12) | 3.16 |
| 34.5 (13) | 9.11 |
| 34.7 (14) | 1.54 |
| 35.0 (15) | 64.16 |
| 37.1 (16) | 21.53 |

**Table 3.5:** HTGC-ICP-MS retention and integration data for Julia Creek nickel porphyrins shown in Figure 3.11

| Retention time | Integrated area (%) |
|---|---|
| 25.2 (1) | 5.36 |
| 26.2 (2) | 7.84 |
| 27.8 (3) | 2.91 |
| 28.1 (4) | 4.03 |
| 28.9 (5) | 74.96 |
| 32.0 (6) | 4.90 |

**Table 3.6:** HTGC-ICP-MS retention and integration data for Julia Creek vanadyl porphyrins shown in Figure 3.13

100

$C_{32}$ A-2 type macrocycles, which co-elute as one peak in the HTGC-FID, -MS and -ICP-MS chromatograms.

## 3.3. Analysis of Serpiano Oil Shale:

Serpiano oil shale contains both nickel and vanadyl porphyrins [55] which were analysed using HTGC with FID, MS and ICP-MS detection and quantified by UV/VIS (see Chapter 7). The only exception was that the vanadyl porphyrins were not examined by HTGC-MS due to the problems associated with the DB-1 ht column (as discussed in section 3.7).

### 3.3.1. HTGC-FID:

The chromatogram for the nickel porphyrin fraction [Figure 3.15 (a)] contains 7 peaks (RI 6043 - 6858). The major peak (RI 6858) represents 75 % of the total integrated area. The distribution, relative areas and the retention times/indices are shown in Table 3.7.

The chromatogram for the vanadyl porphyrin fraction [Figure 3.16 (a)] contains 10 peaks (RI 5520 - 6084). The major peak (RI 5747) represents 65 % of the total integrated area. The distribution, relative areas and retention times/indices are shown in Table 3.8.

### 3.3.2. Probe-MS and HTGC-MS:

**Figure 3.15:** HTGC of Serpiano nickel porphyrins on 12 m HT-5

(a) HTGC-FID conditions as in Figure 3.1 (2.7 $\mu$g on column)

(b) HTGC-MS conditions as in Figure 3.5 (3.1 $\mu$g on column)

(c) HTGC-ICP-MS conditions as in Figure 3.12 (3.7$\mu$g on column)
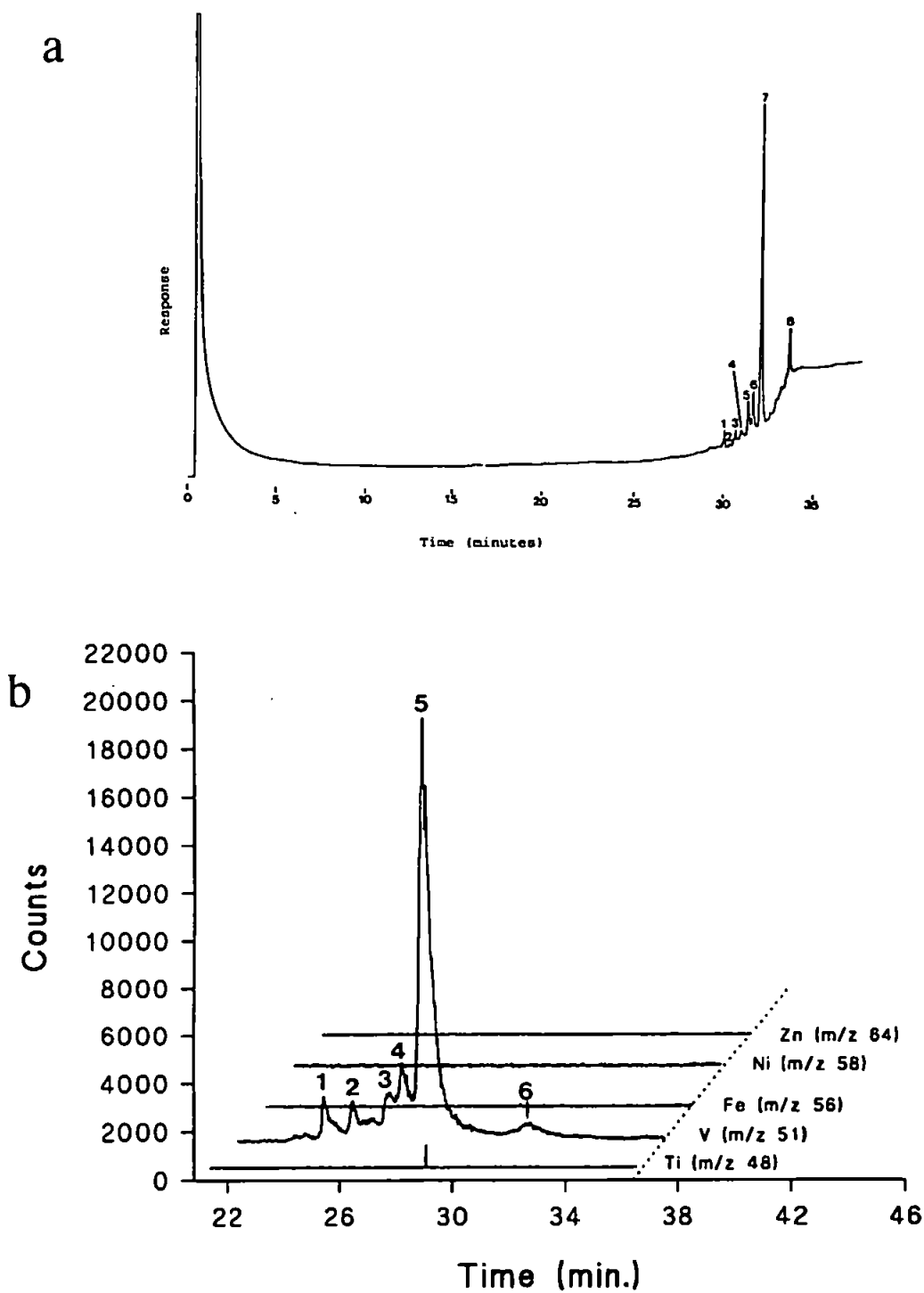
Figure 3.16: HTGC of Serpiano vanadyl porphyrins on 15 m DB-1ht

(a) HTGC-FID conditions as in Figure 3.2(a)(0.5 μg on column)

(b) HTGC-ICP-MS conditions as in Figure 3.14 (0.4 μg on column)

| Retention Time (min) | Retention Index | Integrated   Area (%) | Elution Temp. (°C) |
|---|---|---|---|
| 32.52 (1) | 6043 | 0.18 | 375 |
| 33.15 (2) | 6218 | 4.81 | 382 |
| 33.73 (3) | 6378 | 3.60 | 387 |
| 34.43 (4) | 6578 | 1.90 | 394 |
| 34.88 (5) | 6698 | 8.54 | 398 |
| 35.12 (6) | 6766 | 6.22 | 401 |
| 35.46 (7) | 6858 | 74.75 | 404 |

**Table 3.7:** Retention data and integrated areas of the Serpiano
nickel porphyrins

| Retention Time (min) | Retention Index | Integrated Area (%) | Elution Temp. (°C) |
|---|---|---|---|
| 30.27 (1) | 5520 | 3.93 | 353 |
| 30.54 (2) | 5556 | 0.46 | 355 |
| 30.92 (3) | 5607 | 3.07 | 359 |
| 31.23 (4) | 5649 | 2.39 | 361 |
| 31.58 (5) | 5654 | 4.60 | 365 |
| 31.84 (6) | 5688 | 5.79 | 368 |
| 32.28 (7) | 5747 | 64.68 | 373 |
| 33.91 (8) | 5966 | 12.89 | 389 |

**Table 3.8:** Retention data and integrated areas of the Serpiano
vanadyl porphyrins

The nickel porphyrin fraction was examined by probe-MS and HTGC-MS as shown in Figure 3.17 and 3.18 [Figure 3.16 (b)]. The probe-MS and HTGC-MS data confirmed the presence of A, A-2 and A-4 macrocycle types. This was further confirmed by mass chromatography using the relevant molecular ion masses (Table 3.9). The majority of the nickel fraction was found to consist of $C_{27}$ - $C_{33}$ A-2 macrocycles ($C_{31}$ maximum). A type macrocycles $C_{27}$-$C_{32}$ (maximum $C_{31}$) and A-4 macrocycles $C_{28}$-$C_{30}$ (maximum $C_{29}$). The A and A-4 macrocycle contribution to the total porphyrin distribution of the nickel fraction was small, which could be seen from both the probe-MS and HTGC-MS analysis. Co-eluting is again evident with the $C_{30}$ to $C_{32}$ A-2 macrocycles co-elution as the major peak on the HTGC-MS trace (Table 3.9; retention time 19.66).

The vanadyl porphyrin fraction was not analysed using HTGC-MS, but probe-MS and HTGC-FID did allow the identification of certain macrocycles. The probe-mass spectrum is shown in Figure 3.19. The majority of the porphyrins are A-2, distributed from $C_{26}$ to $C_{32}$ (maximum $C_{30}$).

### 3.3.3. HTGC-ICP-MS:

The nickel and vanadyl porphyrin fractions were both analysed by HTGC-ICP-MS. The nickel fraction was examined using selected ion recording for all the first row transition metals as shown in Figure 3.15 (c) and 3.20. The vanadyl fraction was analysed using selected ion recording for m/z 48 (Ti), 51 (V), 56 (Fe),
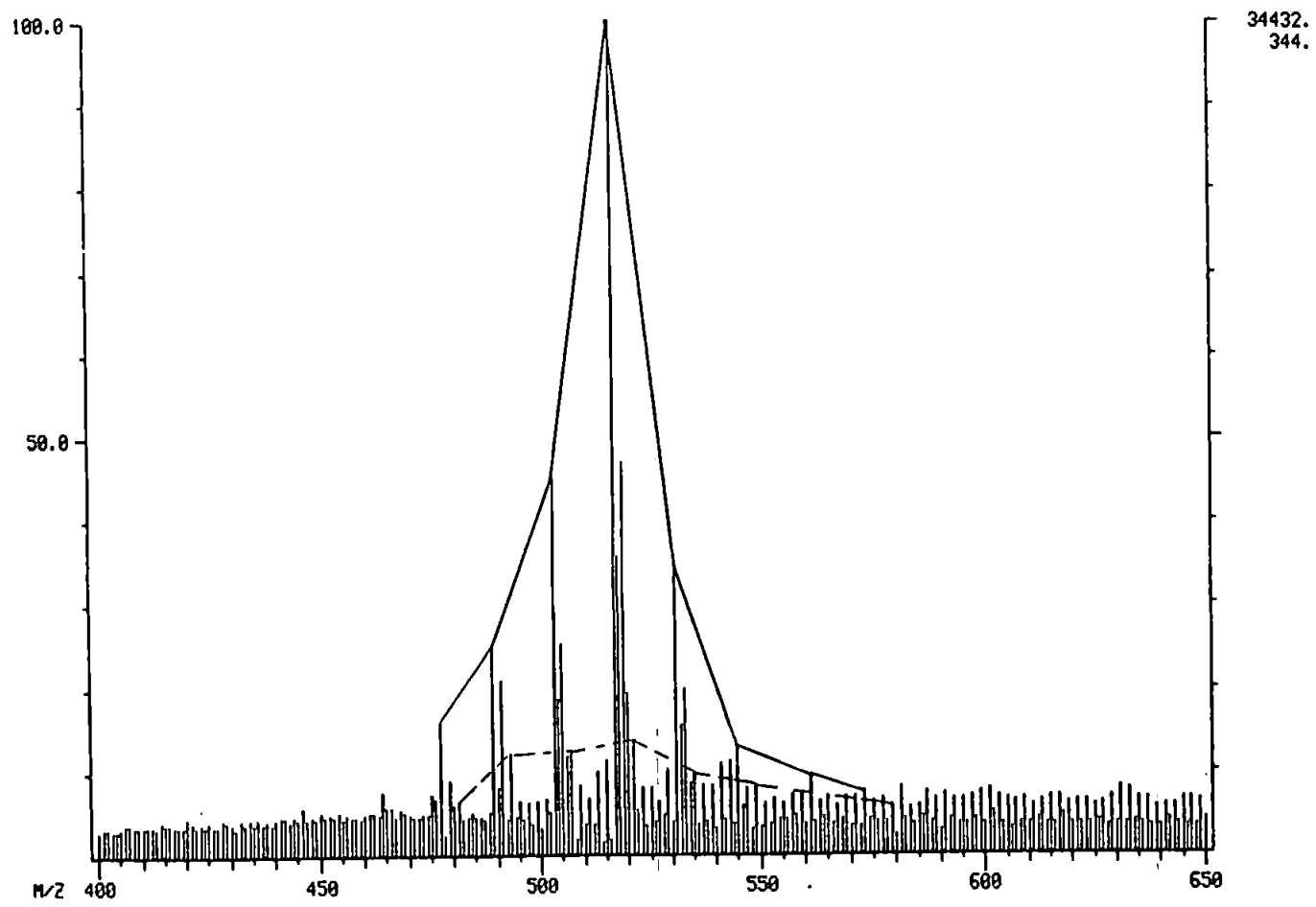
**Figure 3.17:** Probe mass spectrum of Serpiano nickel porphyrins at 16eV; -- A macrocycles, — A-2 macrocycles

## Serpiano Total Ion Current
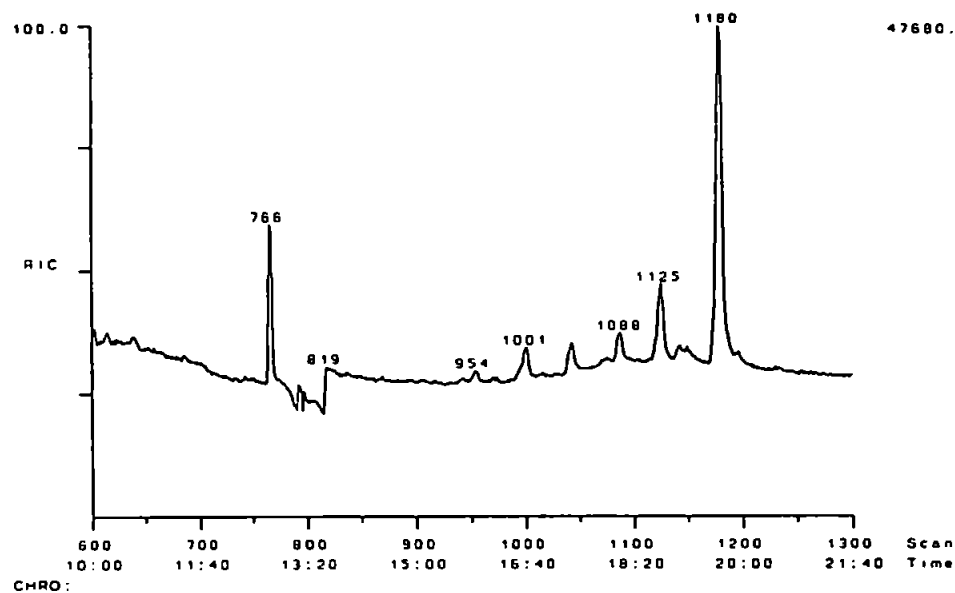


## Scan 1001
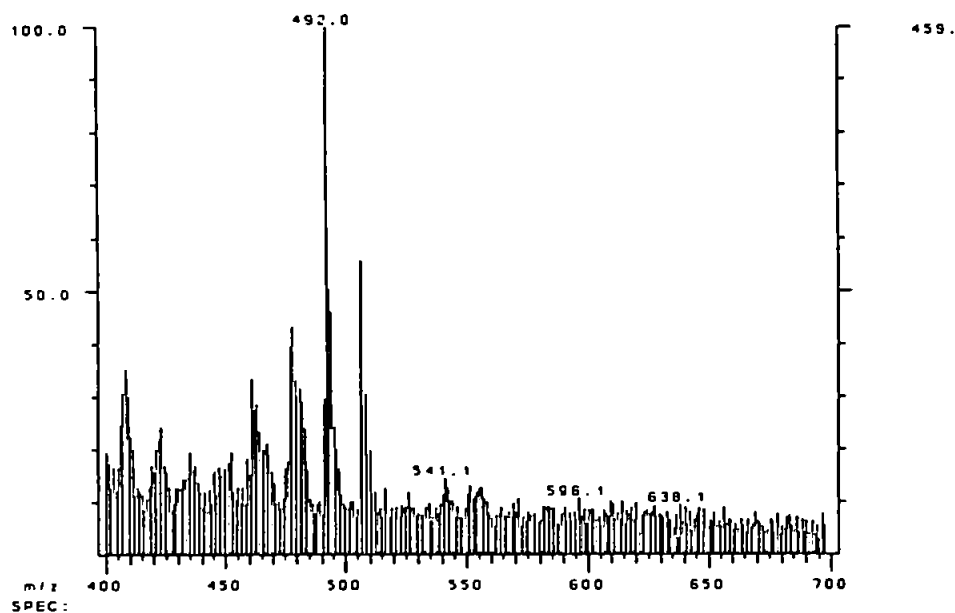


**Figure 3.18:** HTGC-MS of Serpiano nickel porphyrins (3.0 μg on column), conditions as in Figure 3.5, selected mass spectra shown

Scan 1123
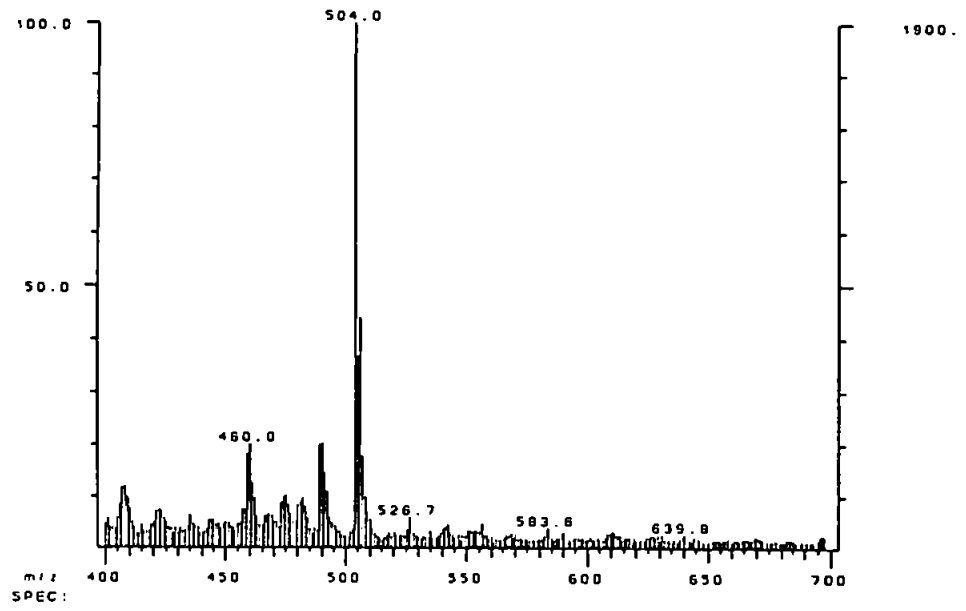


Scan 1179
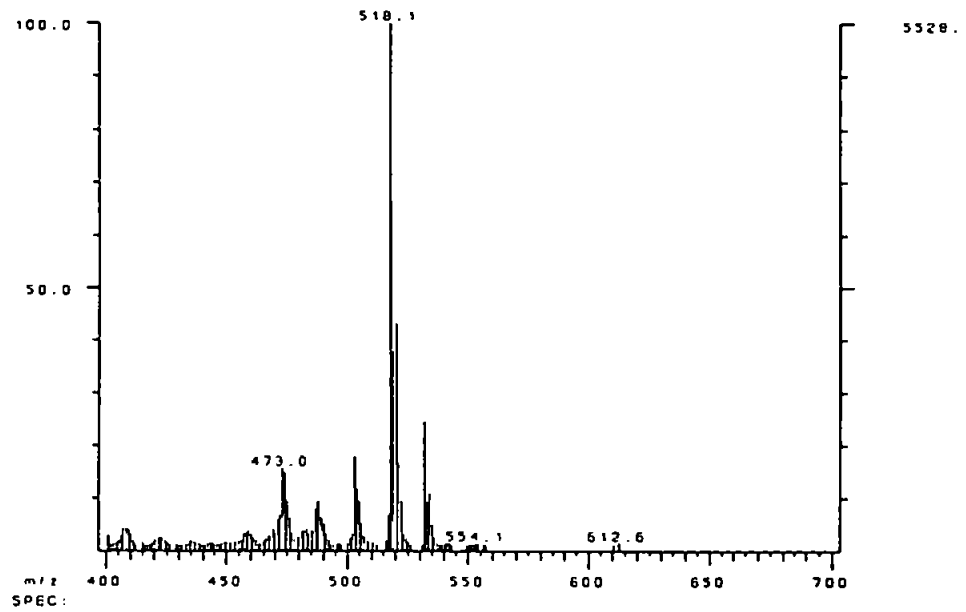


**Figure 3.18:** continued
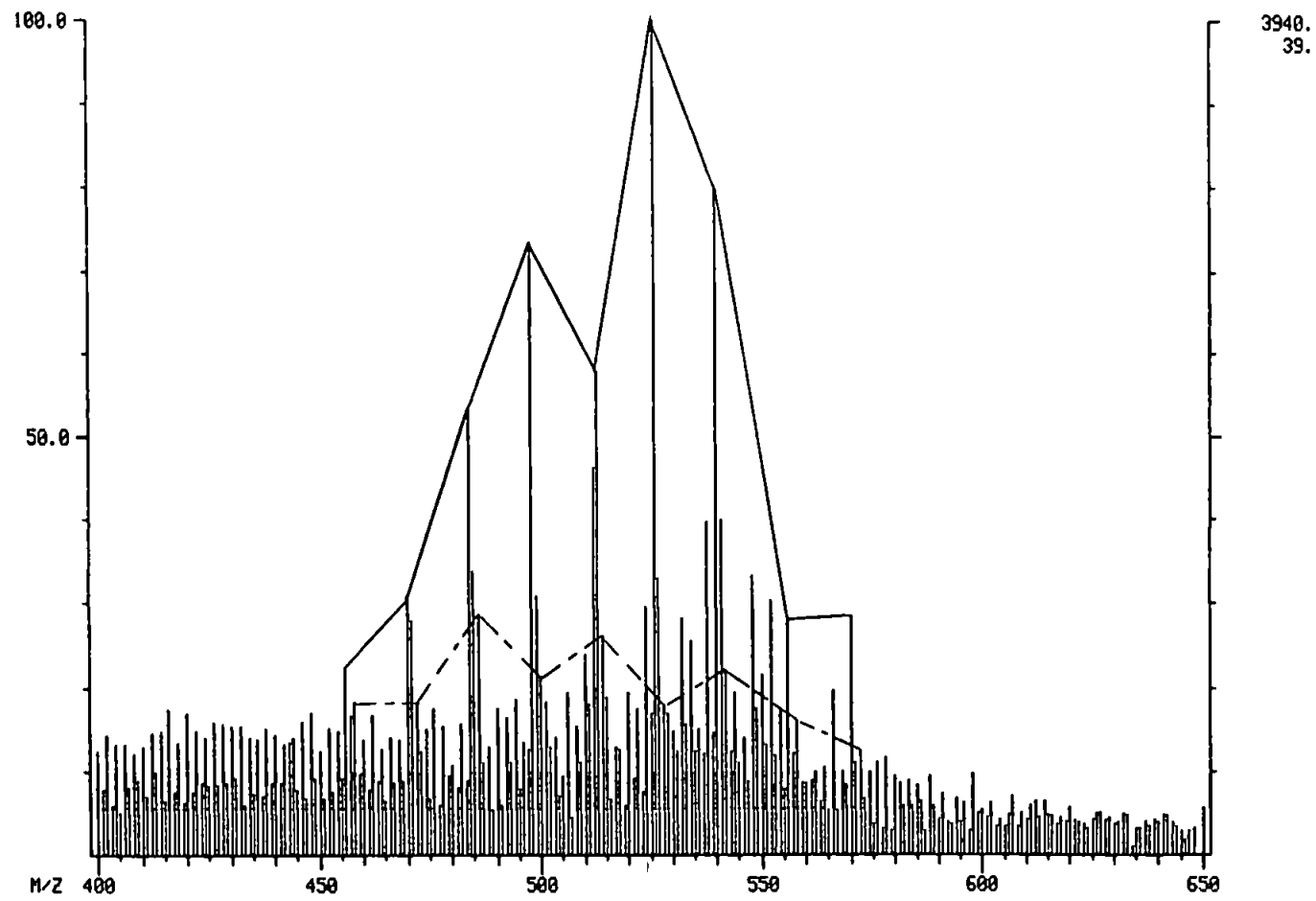
**Figure 3.19:** Probe mass spectrum of Serpiano vanadyl porphyrins at 16eV; -- A macrocycles, —— A-2 macrocycles

| Retention Time/ Scan no. | Macrocycle Type and Molecular Ion Observed |
|---|---|
| 15.90 (954) | $C_{27}$ A (466), $C_{28}$ A (480), $C_{26}$ A-2 (448) |
| 16.68 (1001) | $C_{29}$ A (494), $C_{29}$ A (494), $C_{30}$ A (508), $C_{26}$ A-2 (448), $C_{27}$ A-2 (462), $C_{28}$ A-2 (476) |
| 17.38 (1043) | $C_{29}$ A (494), $C_{30}$ A (508), $C_{31}$ A (522), $C_{32}$ A (536), $C_{27}$ A-2 (462), $C_{28}$ A-2 (476), $C_{29}$ A-2 (490) |
| 18.13 (1088) | $C_{29}$ A (494), $C_{30}$ A (508), $C_{28}$ A-2 (476), $C_{29}$ A-2 (490), $C_{30}$ A-2 (504) |
| 18.75 (1125) | $C_{28}$ A (480), $C_{29}$ A (494), $C_{30}$ A (508), $C_{28}$ A-2 (476), $C_{29}$ A-2 (490), $C_{30}$ A-2 (504), $C_{28}$ A-4 (474), $C_{29}$ A-4 (488) |
| 19.66 (1180) | $C_{27}$ A (466), $C_{28}$ A (480), $C_{29}$ A (494), $C_{30}$ A (508), $C_{31}$ A (522), $C_{32}$ A (536), $C_{27}$ A-2 (462), $C_{28}$ A-2 (476), $C_{29}$ A-2 (490), $C_{30}$ A-2 (504), $C_{31}$ A-2 (518), $C_{32}$ A-2 ($5_{32}$), $C_{33}$ A-2 (546), $C_{28}$ A-4 (474), $C_{29}$ A-4 (488), $C_{30}$ A-4 (502), $C_{31}$ A-4 (516) |

**Table 3.9:** Nickel porphyrin distribution in HTGC-MS chromatogram of Serpiano oil shale
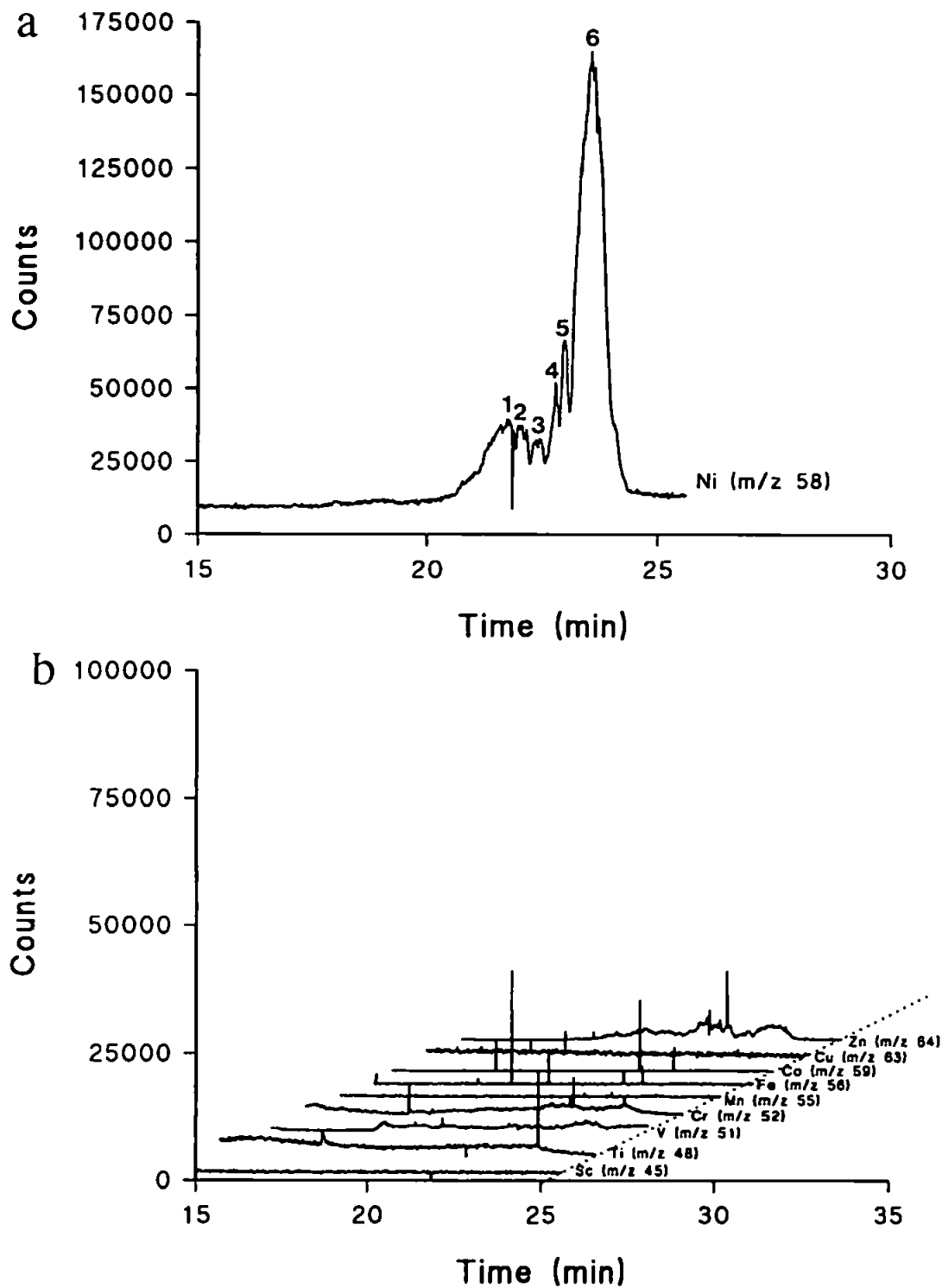
**Figure 3.20:** HTGC-ICP-MS of Serpiano nickel (3.7 $\mu$g on column) porphyrins, conditions as in Figure 3.12; (a) nickel (m/z 58), (b) other first row transition metals

58 (Ni) and 64 (Zn,Cu) as shown in Figure 3.16 (b).

The nickel fraction resembled the HTGC-FID and HTGC-MS chromatograms, with 6 peaks present. Chromatography was performed with a new HT-5 column (see Section 3.7). The major peak on the chromatogram made up 80 % of the integrated area of the nickel porphyrins in HTGC-ICP-MS chromatogram (Table 3.10). This compares well with the FID data which show 75 % of the area corresponding to this peak. The other selected ion chromatograms showed that no other first row transition metals were present in this nickel fraction (refer Section 3.7).

The selected ion chromatogram of the vanadyl fraction gave a chromatogram similar to that obtained with the HTGC-FID. The chromatogram contained 6 peaks, the major peak contributed 78 % of the integrated area of the vanadyl porphyrin fraction [Figure 3.16 (b); Table 3.11]. Selected ion chromatograms show no Ti (m/z 48), Fe (m/z 56), Ni (m/z 58) or Zn (m/z 64) to be present.

## 3.4. Analysis of Marl Slate:

The nickel fraction of the Marl slate was examined using HTGC with HTGC-FID, HTGC-MS and HTGC-ICP-MS detection.

### 3.4.1. HTGC-FID:

| Retention time | Integrated area (%) |
|---|---|
| 21.8 (1) | 10.57 |
| 22.2 (2) | 2.52 |
| 22.5 (3) | 1.72 |
| 22.9 (4) | 1.82 |
| 23.2 (5) | 3.41 |
| 23.8 (6) | 79.94 |

**Table 3.10:** HTGC-ICP-MS retention and integration data

for Serpiano nickel porphyrins shown in Figure 3.20

(c)

| Retention time | Integrated area (%) |
|---|---|
| 24.4 (1) | 6.19 |
| 25.5 (2) | 4.13 |
| 26.8 (3) | 2.66 |
| 27.2 (4) | 4.27 |
| 27.9 (5) | 78.43 |
| 32.0 (6) | 4.11 |

**Table 3.11:** HTGC-ICP-MS retention and integration data

for Serpiano vanadyl porphyrins

shown in Figure 3.16 (b)

The HTGC-FID chromatogram of the nickel porphyrin fraction is shown in Figure 3.21 (a). The chromatogram consisted of 18 peaks (RI 6064 - 7303). The major peaks contributed 14 % (6064), 24 % (6231) and 18 % (6705) of the total integrated area of the nickel fraction (Table 3.12). The chromatogram obtained with the HT-5 phase was similar to that obtained by Blum et al. (Figure 1.8 (a)) with the PS 347.5 phase.

The Marl Slate nickel fraction showed a larger distribution of nickel porphyrins than either of the previous shales.

## 3.4.2. Probe-MS and HTGC-MS:

Probe-MS and HTGC-MS data are shown in Figures 3.22 and 3.23. These results confirm the presence of the A, A-2 and A-4 macrocycles in the nickel fraction. Mass chromatography also confirmed these to be present (Table 3.13). A type $C_{26}-C_{32}$ (maximum $C_{30}$), A-2 type $C_{26}-C_{33}$ (maximum $C_{31}$ and $C_{32}$) and A-4 type $C_{29}-C_{32}$ (maximum $C_{30}$). The A-2 macrocycles again made up the majority of the porphyrins.

The problem of co-elution was emphasised in this nickel porphyrin fraction with the A ($C_{28}-C_{32}$) and A-2 ($C_{26}-C_{30}$) co-eluting in one peak (Figure 3.23; scan 1058). Similar co-elution is also observed in Julia Creek and Serpiano oil shales, but was more apparent in the Marl Slate due to the relatively higher proportions of A (ETIO) macrocycles.
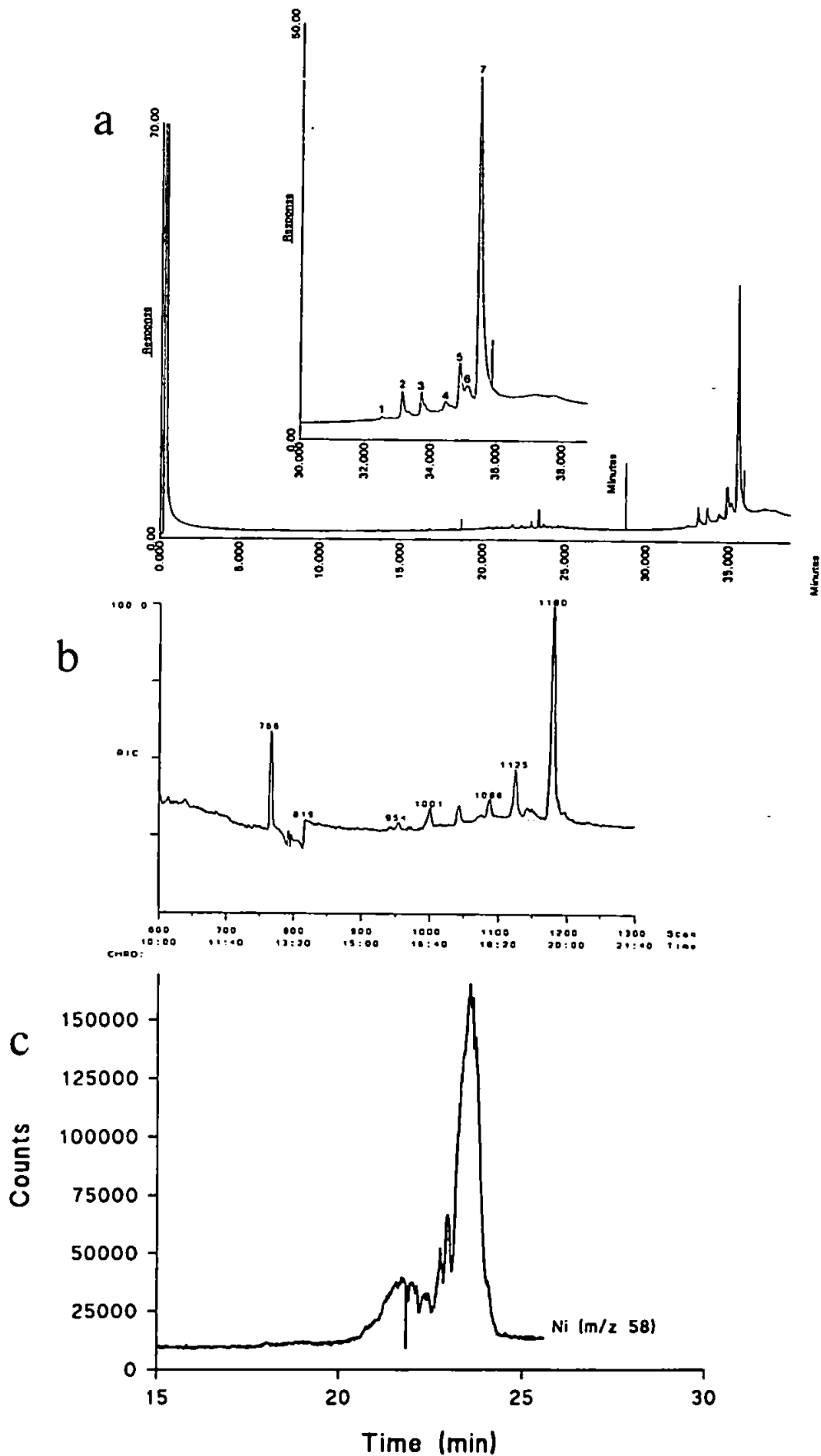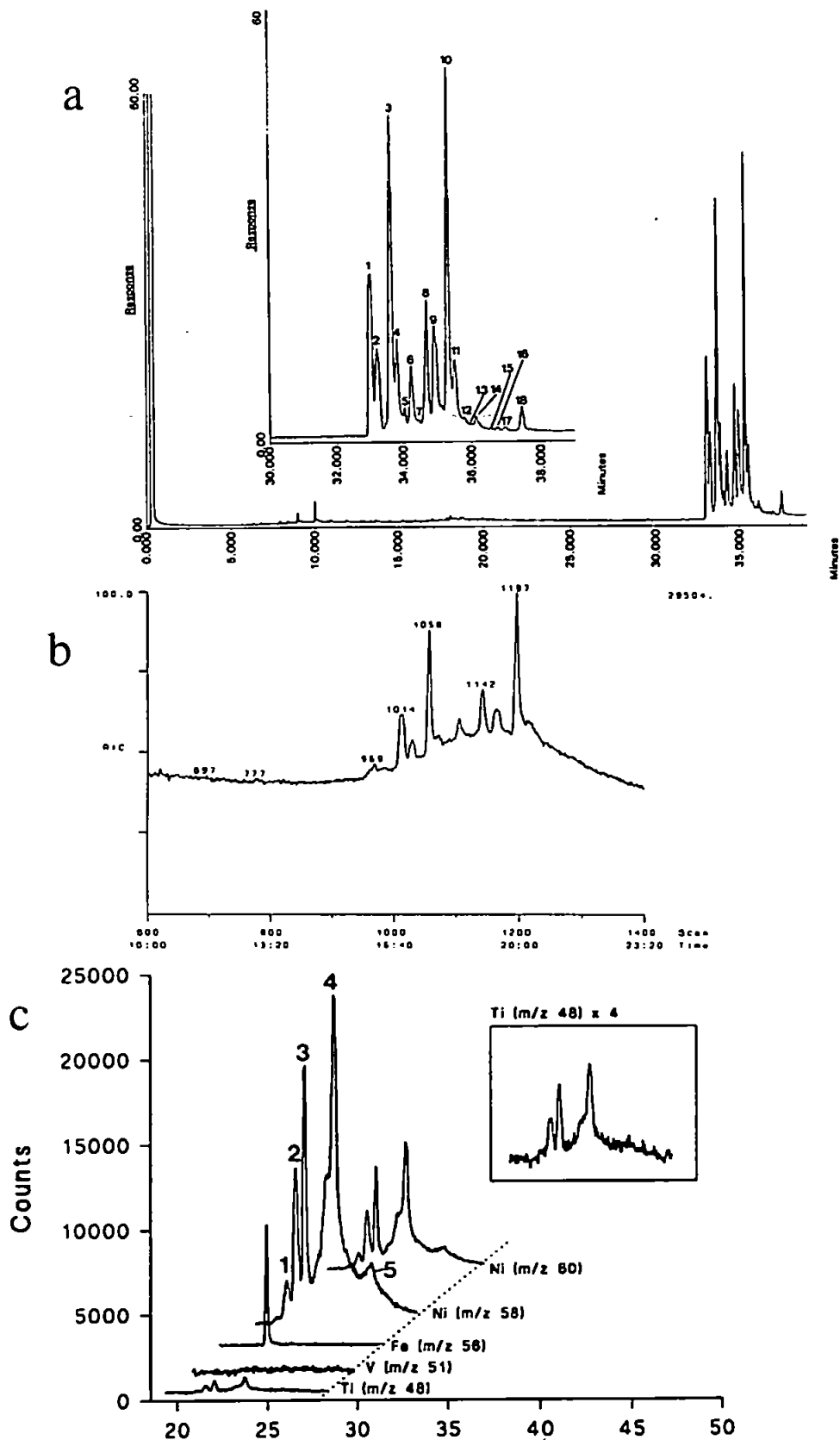
**Figure 3.21:** HTGC of Marl Slate nickel porphyrins on 12 m HT-5

(a) HTGC-FID conditions as in Figure 3.1 (3.4μg on column)

(b) HTGC-MS conditions as in Figure 3.5 (3.2μg on column)

(c) HTGC-ICP-MS on 9 m HT-5, 50°C to 350°C at 15°C/min, 350°C to 410°C at 10°C/min, ~2.8 min isothermal, monitored from 350°C (2.9 μg and 10 ng iron OEP on column)

| Retention Time (min) | Retention Index | Integrated Area (%) | Elution Temp. (°C) |
|---|---|---|---|
| 33.04 (1) | 6064 | 14.52 | 380 |
| 33.21 (2) | 6113 | 8.10 | 383 |
| 33.63 (3) | 6231 | 24.64 | 386 |
| 33.82 (4) | 6283 | 6.63 | 388 |
| 34.04 (5) | 6345 | 1.07 | 390 |
| 34.24 (6) | 6399 | 4.50 | 392 |
| 34.46 (7) | 6462 | 0.17 | 394 |
| 34.71 (8) | 6532 | 7.70 | 397 |
| 34.93 (9) | 6593 | 7.00 | 399 |
| 35.32 (10) | 6705 | 18.62 | 403 |
| 35.52 (11) | 6759 | 4.20 | 405 |
| 35.81 (12) | 6840 | 0.07 | 408 |
| 35.95 (13) | 6881 | 0.05 | 410 |
| 36.13 (14) | 6930 | 0.69 | 410 (iso.) |
| 36.57 (15) | 7053 | 0.03 | 410 (iso.) |
| 36.74 (16) | 7102 | 0.13 | 410 (iso.) |
| 36.98 (17) | 7168 | 0.23 | 410 (iso.) |
| 37.46 (18) | 7303 | 1.62 | 410 (iso.) |

**Table 3.12:** Retention data and integrated areas of the Marl Slate nickel porphyrins
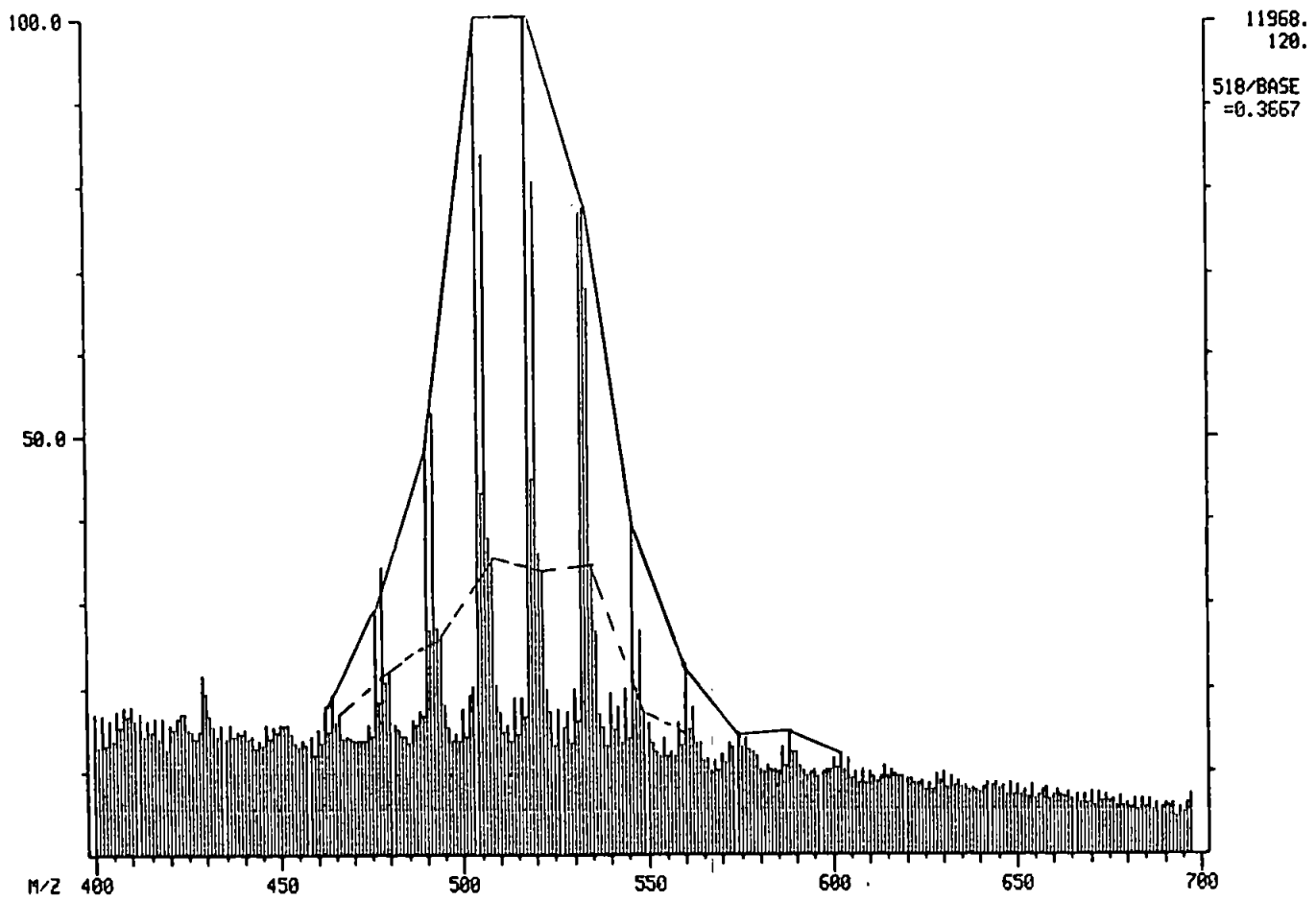
**Figure 3.22:** Probe mass spectrum of Marl Slate porphyrins at 16eV; -- A macrocycles, — A-2 macrocycles

## Marl Slate Total Ion Current
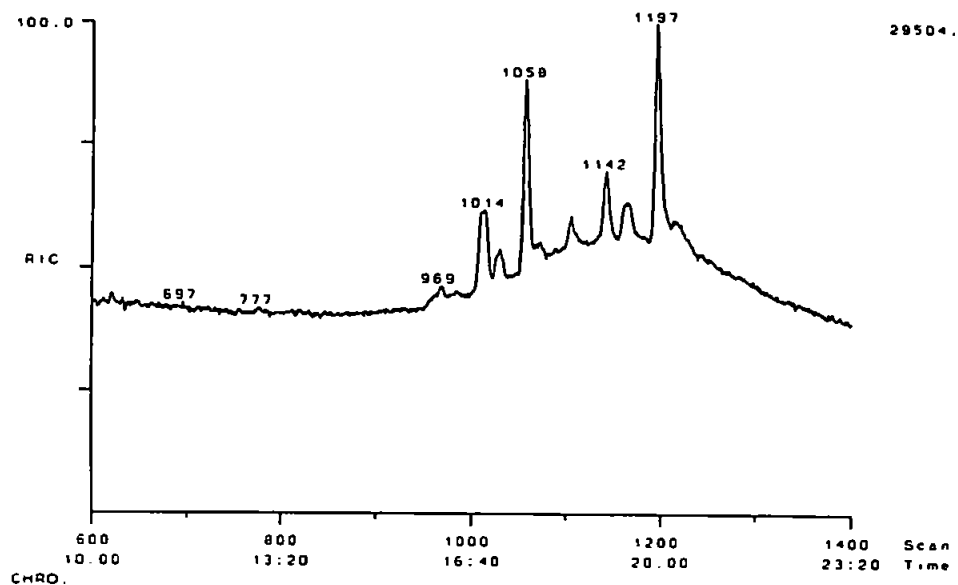


## Scan 1014
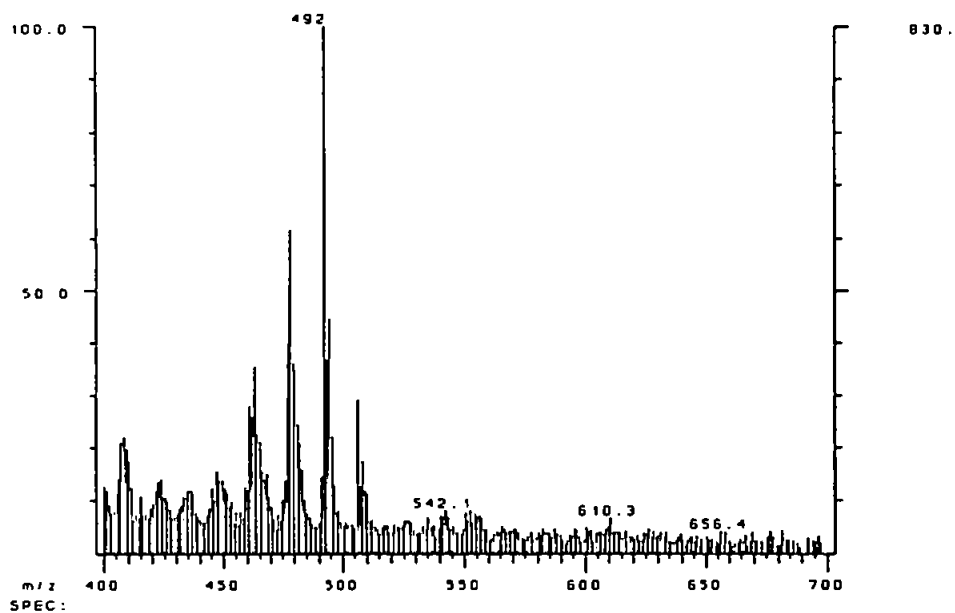


**Figure 3.23:** HTGC-MS of Marl Slate nickel porphyrins (4.0 μg on column), conditions as in Figure 3.5, selected mass spectra shown

## Scan 1058
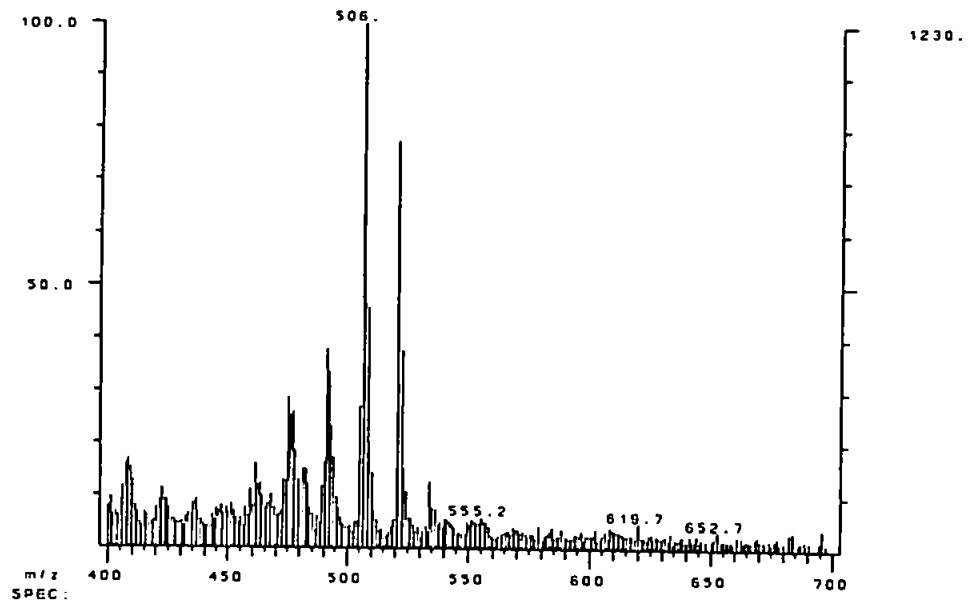


## Scan 1197



**Figure 3.23: continued**

119

| Retention Time/ Scan no. | Macrocycle Type and Molecular Ion Observed |
|---|---|
| 16.15 (969) | $C_{26}$ A (452), $C_{27}$ A (466), $C_{28}$ A (480), $C_{26}$ A-2 (448) |
| 16.90 (1014) | $C_{27}$ A (466), $C_{28}$ A (480), $C_{29}$ A (494), $C_{30}$ A (508), $C_{26}$ A-2 (448), $C_{27}$ A-2 (462), $C_{28}$ A-2 (476), $C_{29}$ A-2 (490) |
| 17.63 (1058) | $C_{28}$ A (480), $C_{29}$ A (494), $C_{30}$ A (508), $C_{31}$ A (522), $C_{32}$ A (536), $C_{26}$ A-2 (448), $C_{27}$ A-2 (462), $C_{28}$ A-2 (476), $C_{29}$ A-2 (490), $C_{30}$ A-2 (504), $C_{28}$ A-4 (474) |
| 18.40 (1104) | $C_{29}$ A (494), $C_{30}$ A (508), $C_{28}$ A-2 (476), $C_{29}$ A-2 (490), $C_{30}$ A-2 (504) |
| 19.03 (1142) | $C_{31}$ A (522), $C_{32}$ A (536), $C_{27}$ A-2 (462), $C_{28}$ A-2 (476), $C_{29}$ A-2 (490), $C_{30}$ A-2 (504), $C_{31}$ A-2 (518), $C_{33}$ A-2 (546), $C_{29}$ A-4 (488), $C_{31}$ A-4 (516) |
| 19.30 (1158) | $C_{31}$ A (522), $C_{32}$ A (536), $C_{33}$ A (550), $C_{27}$ A-2 (462), $C_{28}$ A-2 (476), $C_{29}$ A-2 (490), $C_{30}$ A-2 (504), $C_{33}$ A-2 (546), $C_{31}$ A-4 (516) |
| 19.95 (1197) | $C_{29}$ A (494), $C_{30}$ A (508), $C_{31}$ A (522), $C_{32}$ A (536), $C_{28}$ A-2 (476), $C_{29}$ A-2 (490), $C_{30}$ A-2 (504), $C_{31}$ A-2 (518), $C_{32}$ A-2 (5$_{32}$), $C_{33}$ A-2 (546), $C_{29}$ A-4 (488), $C_{30}$ A-4 (502), $C_{31}$ A-4 (516), $C_{32}$ A-4 (530) |

Table 3.13: Nickel porphyrin distribution in HTGC-MS chromatogram of Marl Slate

### 3.4.3. HTGC-ICP-MS:

The nickel fraction was analysed using selected ion recording of m/z 48 (Ti), 51 (V), 56 (Fe), 58 (Ni) and 60 (Ni) as shown in Figure 3.21 (c). The selected ion chromatograms of m/z 58 and 60 showed the presence of nickel, the ratio of the total integrated areas of these chromatograms was 0.734 (m/z 58) : 0.266 (m/z 60) which compares well to the natural ratio of 0.722 : 0.278. The selected ion recording at m/z 48 suggests the presence of titanium porphyrins.The amounts are significant at, 3.4 % of total $^{58}$Ni integrated area, since the ratio of vanadyl to nickel porphyrins in Marl Slate is about 1:2 [13].

The chromatogram [Figure 3.21 (c)] contained 5 peaks with the major peak contributing 63 % of the total integrated area (Table 3.14). The distribution was not the same as that obtained on the HTGC-FID chromatogram, but the HTGC-ICP-MS work was performed on a shorter column (~9 m) than HTGC-FID (12 m). The HTGC-FID chromatogram of the Marl Slate on the shorter column is shown in Figure 3.24. The qualitative match of this chromatogram with that obtained with the HTGC-ICP-MS is quite good (Section 3.7).

### 3.5. Analysis of Green River Shale:

The Green River Shale fraction analysed contained both nickel and vanadyl porphyrins. The mixture was analysed using HTGC-FID, HTGC-MS and HTGC-ICP-MS.
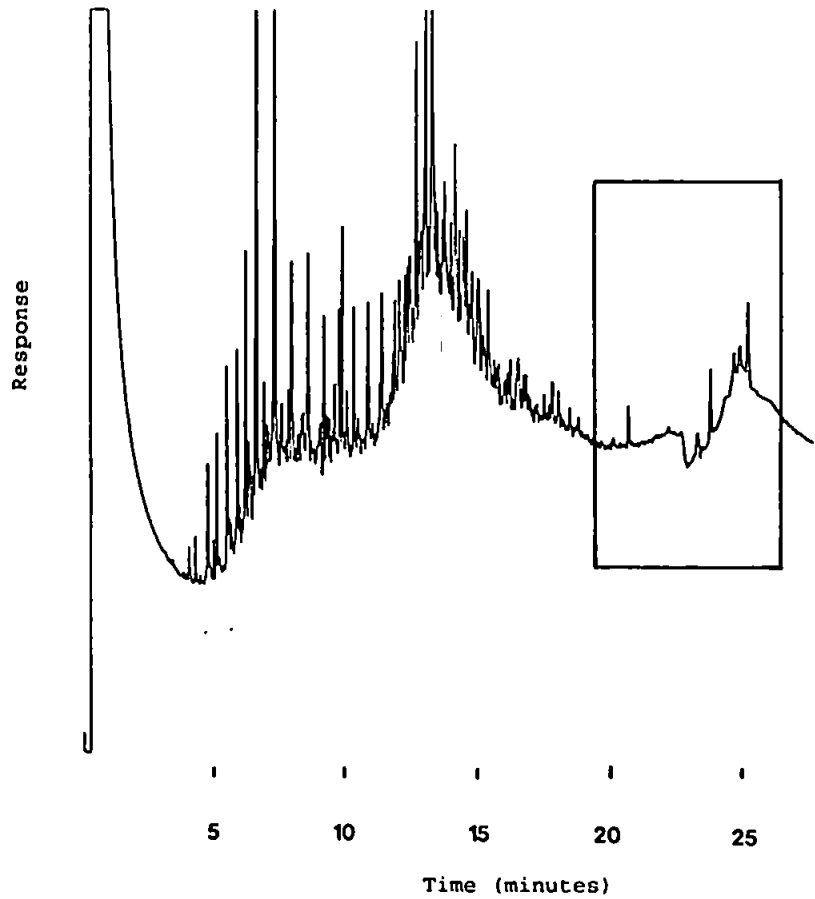
**Figure 3.24:** HTGC-FID of Marl Slate nickel porphyrins (3.2 $\mu$g on column) on 9 m HT-5, 50°C to 350°C at 15°C/min, 350°C to 410°C at 10°C/min, 3 min isothermal

## 3.5.1. HTGC-FID:

The HTGC-FID chromatogram of the nickel and vanadyl porphyrin mixture is shown in Figure 3.25 (a). The chromatogram has three major peaks superimposed on what seems to be excessive column "bleed". The "bleed" was not column phase but the slow elution of the vanadyl porphyrins from the HT-5 column as observed with the Julia Creek vanadyl fraction on HT-5 phase. The nickel porphyrin peaks have retention indices ranging from 6150 to 6791 (Table 3.15). The chromatogram is simpler than that obtained for the geoporphyrins of other the shales examined.

## 3.5.2. Probe-MS and HTGC-MS:

Probe-MS and HTGC-MS data of the nickel and vanadyl porphyrins is shown in Figures 3.26 and 3.27 [Figure 3.25 (b)]. The probe-MS spectrum reflects the complexity of the mixture. Since the porphyrin mixture (vanadyl and nickel) could undergo trans-metallation during probe-MS, the HTGC-MS data was considered more reliable in this case.

The HTGC-MS spectra showed that both the vanadyl and nickel species were present, which makes interpretation difficult. These difficulties are overcome by the examination of the mass chromatograms for the various macrocycles (Table 3.16), which confirm the presence of A, A-2 and A-4 macrocycles. A type macrocycles from $C_{26}$-$C_{35}$ (maximum $C_{27}$), A-2 from $C_{28}$-$C_{32}$ (maximum $C_{32}$) and A-4 from $C_{27}$-$C_{29}$ (maximum $C_{29}$). The A-2 type macrocycle
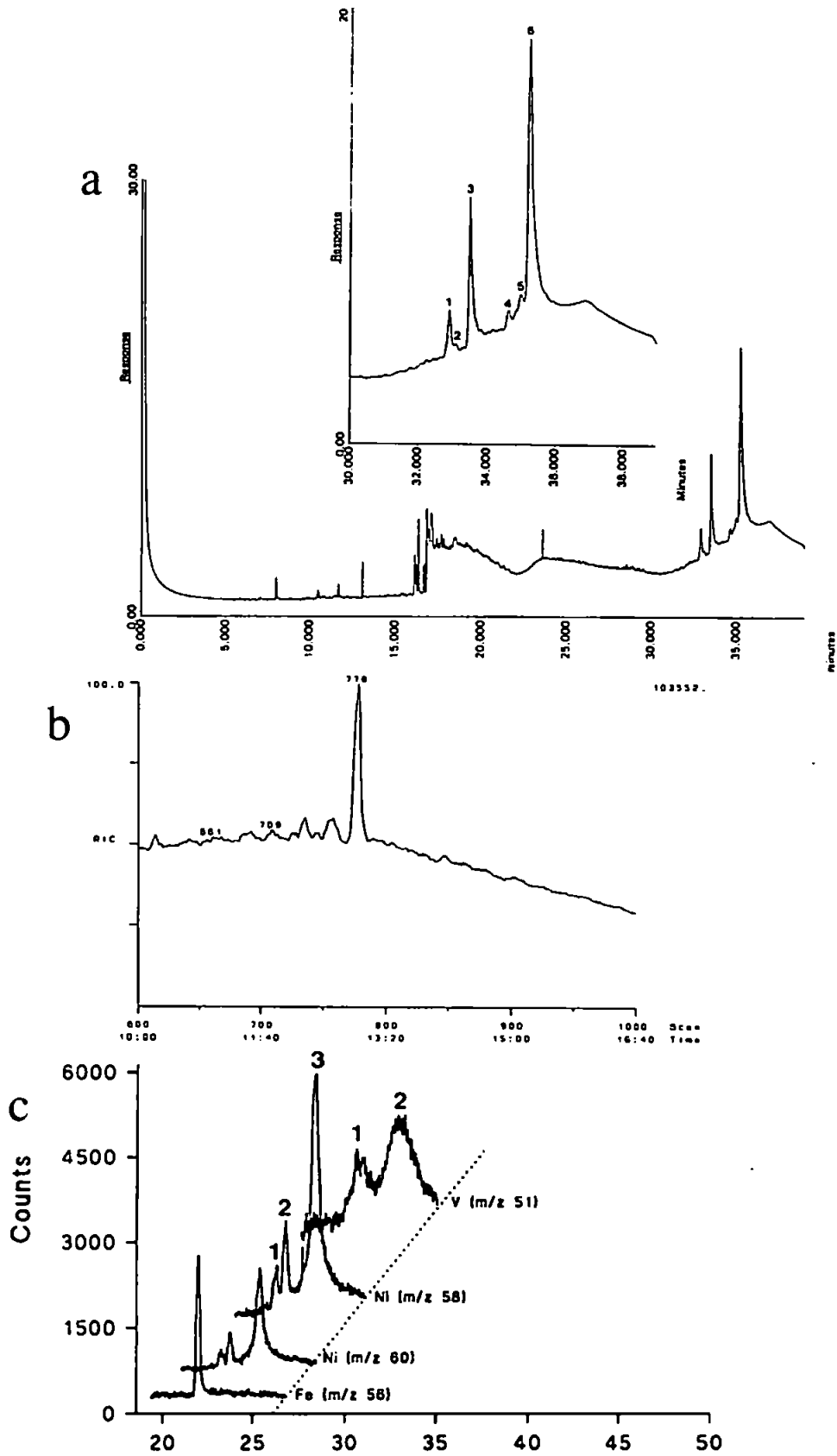
**Figure 3.25:** HTGC of Green River nickel and vanadyl porphyrins on 12 m HT-5

(a) HTGC-FID conditions as in Figure 3.1 (3.7 μg on column)

(b) HTGC-MS conditions as in Figure 3.5 (3.1 μg on column)

(c) HTGC-ICP-MS, conditions as in Figure 3.21(c), (4.0 μg and 10 ng iron OEP on column)

| Retention time | Integrated area (%) |
|---|---|
| 21.1 (1) | 2.66 |
| 21.3 (2) | 12.12 |
| 22.2 (3) | 16.35 |
| 23.8 (4) | 63.44 |
| 25.84 (5) | 5.42 |

**Table 3.14:** HTGC-ICP-MS retention and integration data

for Marl Slate nickel porphyrins

shown in Figure 3.21 (c)

| Retention Time (min) | Retention Index | Integrated Area (%) | Elution Temp. (°C) |
|---|---|---|---|
| 32.89 (1) | 6150 | 7.73 | 378 |
| 33.13 (2) | 6234 | 0.34 | 383 |
| 33.48 (3) | 6312 | 23.41 | 384 |
| 34.64 (4) | 6431 | 3.97 | 396 |
| 35.00 (5) | 6737 | 2.27 | 400 |
| 35.20 (6) | 6791 | 60.20 | 402 |

**Table 3.15:** HTGC-FID chromatogram of Green River

nickel and vanadyl porphyrin mixture
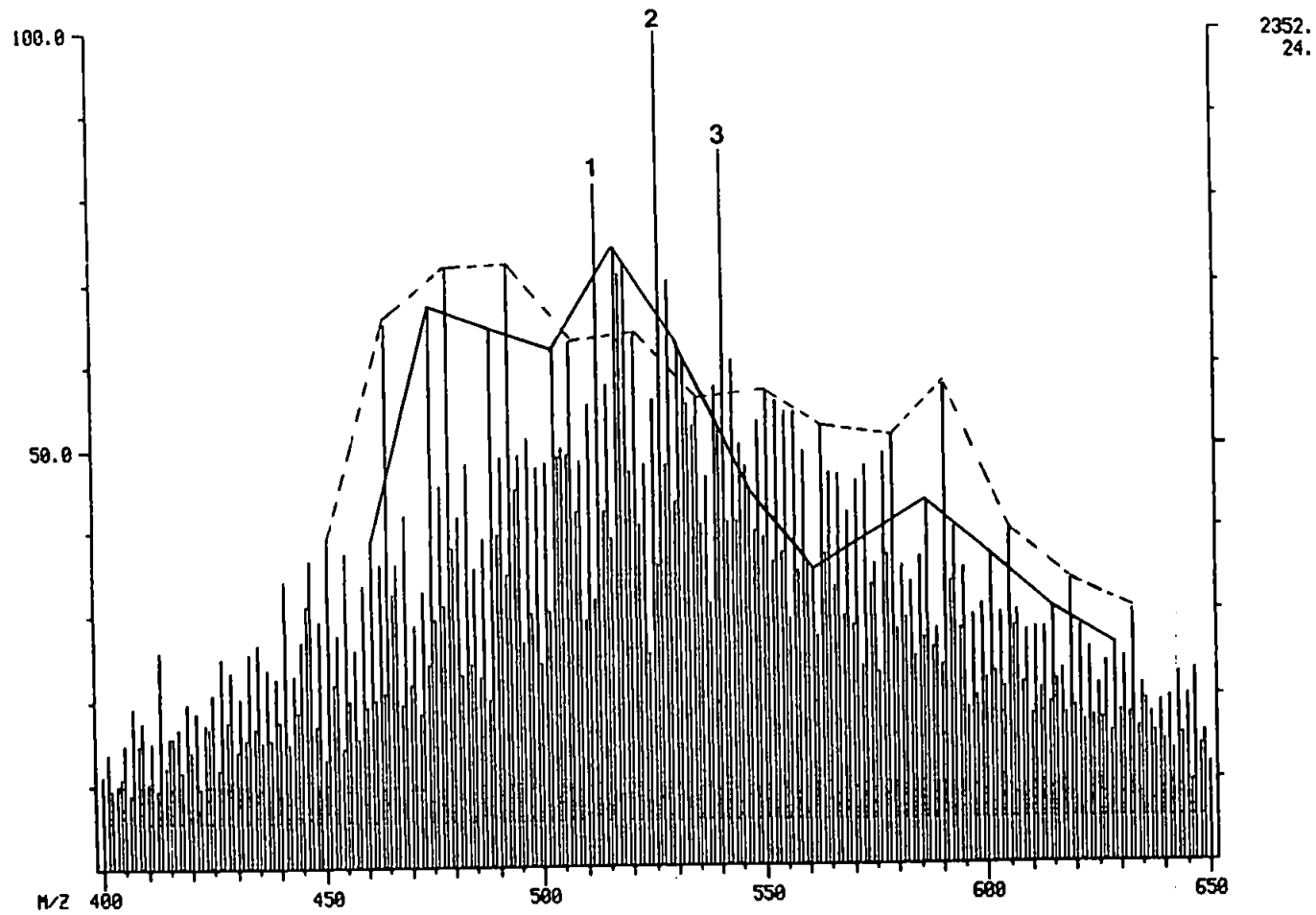
**Figure 3.26:** Probe mass spectrum of Green River nickel and vanadyl porphyrins at 16eV; 1= A-2 V=O $C_{30}$, 2= A-2 V=O $C_{31}$, 3= A-2 $C_{32}$; -- A macrocycles, — A-2 macrocycles

## Green River Total Ion Current
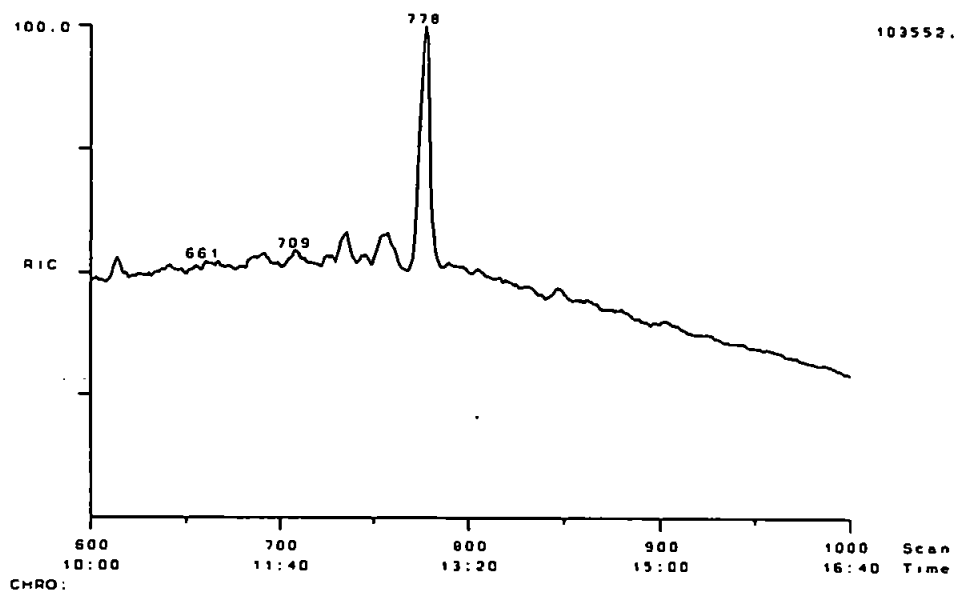


## Scan 735
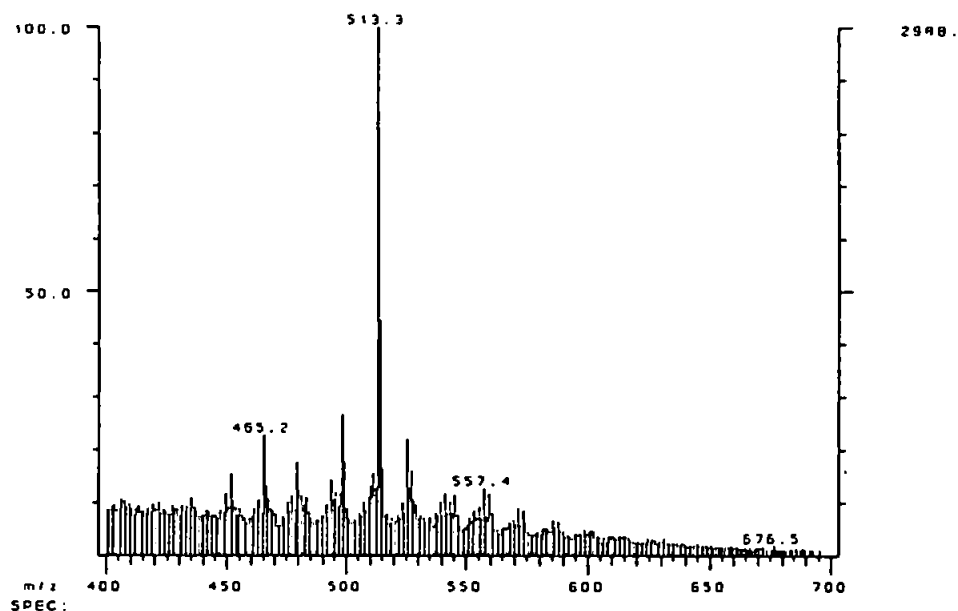


**Figure 3.27:** HTGC-MS of Green River nickel and vanadyl porphyrins (3.3 μg on column), conditions as in Figure 3.5, selected mass spectra shown

## Scan 756
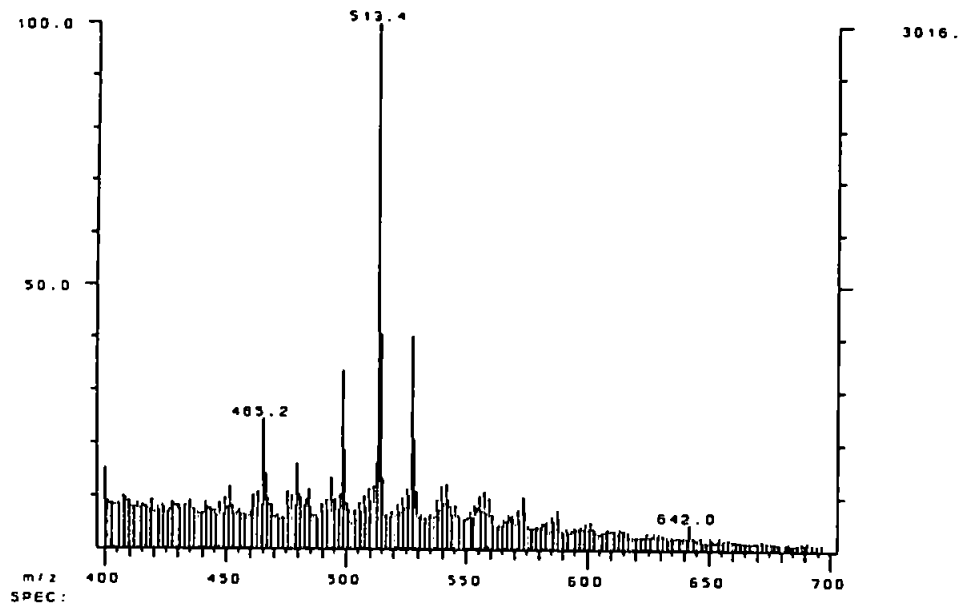


## Scan 778
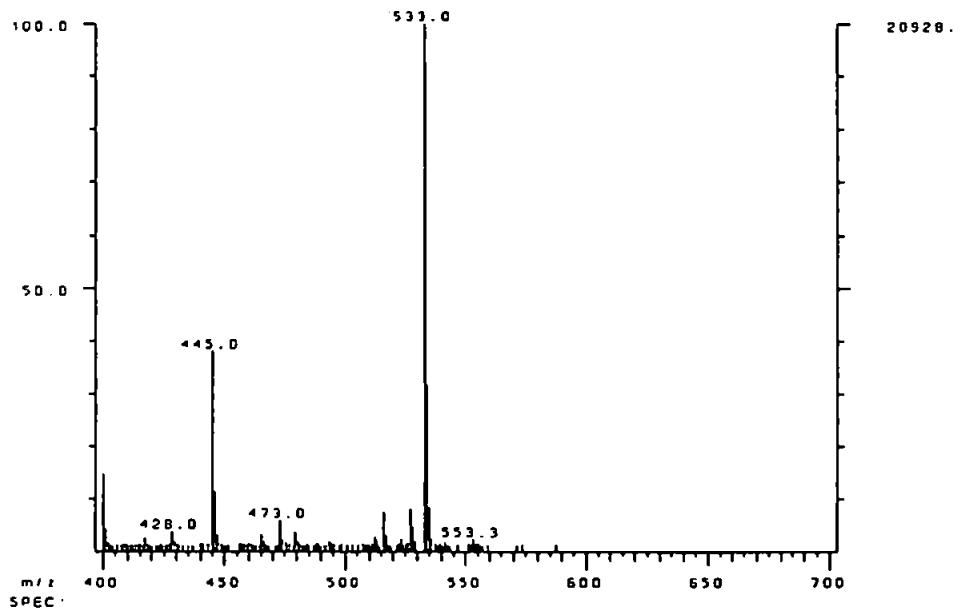


**Figure 3.27: continued**

| Retention Time/ Scan no. | Macrocycle Type and Molecular Ion Observed |
|---|---|
| 10.93 (656) | $C_{26}$ A (452), $C_{27}$ A (466), $C_{31}$ A-2 (518), $C_{29}$ A-4 (488) |
| 11.55 (693) | $C_{26}$ A (452), $C_{27}$ A (466), $C_{28}$ A (480), $C_{28}$ A-2 (476), $C_{30}$ A-2 (504), $C_{31}$ A-2 (518) |
| 11.80 (708) | $C_{27}$ A (476), $C_{28}$ A (480) |
| 12.25 (735) | $C_{27}$ A (462), $C_{28}$ A (480), $C_{29}$ A (494), $C_{31}$ A (522), $C_{28}$ A-2 (476) |
| 12.60 (758) | $C_{26}$ A (452), $C_{27}$ A (466), $C_{28}$ A (480), $C_{28}$ A-2 (476) |
| 12.96 (778) | $C_{27}$ A (466), $C_{28}$ A (480), $C_{29}$ A (494), $C_{30}$ A (508), $C_{31}$ A (522), $C_{32}$ A (536), $C_{26}$ A-2 (448), $C_{27}$ A-2 (462), $C_{31}$ A-2 (518), $C_{32}$ A-2 (5$_{32}$), $C_{33}$ A-2 (546), $C_{27}$ A-4 (460), $C_{28}$ A-4 (474), $C_{29}$ A-4 (488) |

Table 3.16: Nickel porphyrin distribution in HTGC-MS chromatogram of Green River nickel and vanadyl porphyrin mixture

is the most abundant with the $C_{32}$ being the dominant component of the nickel porphyrin fraction.

The three major vanadyl porphyrin macrocycles can be seen in the probe-MS (A-2 type $C_{30}-C_{32}$) [Figure 3.26].

### 3.5.3. HTGC-ICP-MS:

The nickel and vanadyl mixture was analysed using selected ion recording of m/z 51 (V), 56 (Fe), 58 (Ni) and 60 (Ni), as shown in Figure 3.25 (c). The sample was spiked with ~10 ng of iron octaethylporphyrin chloride as internal standard, in order to obtain a quantitative estimate of the amount of nickel and vanadium eluting from the column.

The chromatogram consisted of three peaks for the nickel porphyrins and a bimodal "hump" for the vanadyl porphyrins (Table 3.17). The distribution of the nickel porphyrin was similar to that obtained by HTGC-FID. The vanadyl distribution could not be compared to that obtained with the HTGC-FID due to slow elution the vanadyl porphyrins from the column.

The ratio of $^{58}$Ni : $^{60}$Ni was 0.721:0.279 and these values agree closely with the natural ratio (0.722:0.278). The nickel to vanadyl ratio[1] was 0.42 which is higher than that calculated previously (0.28,[134]).

---

[1] Calculated from $^{51}$V/($^{51}$V + $^{58}$Ni + $^{60}$Ni)

## 3.6. Analysis of an Iron Porphyrin Fraction from Bagworth Coal:

The iron porphyrins were analysed by HTGC-FID, HTGC-MS and HTGC-ICP-MS.

### 3.6.1. HTGC-FID:

The HTGC-FID chromatogram is shown in Figure 3.28. The chromatogram has only two peaks at retention index of 6325 and 6723, with a ratio of 0.222 to 0.778.

### 3.6.2. Probe-MS and HTGC-MS:

Probe-MS and HTGC-MS data are shown in Figures 3.29 and 3.30. The HTGC-MS and probe-MS confirmed the presence of iron ETIO porphyrins with a distribution from $C_{28}$ to $C_{32}$. The mass chromatograms shown in Figure 3.31 confirm this distribution. The distribution of the porphyrins is shown in Table 3.18.

Although iron porphyrins were complexed with chloride according to the method of Bonnett et al. [10], the porphyrins identified by HTGC-MS were not the chloride complexes. The molecular ions detected had masses corresponding to that of the iron porphyrin, without axial chloride ligands (Figure 3.30).
The differences in the distributions obtained were probably due to the different methods used i.e. probe-MS by Bonnett et al. [10] and HTGC-MS herein (Table 3.18).

The two peaks observed at scan 985 and 1029 contained the iron

| Retention time | Integrated area (%) Nickel porphyrins | Integrated area (%) Vanadyl porphyrins |
|---|---|---|
| 21.5 | 5.17 | 26.58 (Ret. time=22.4 min) |
| 22.0 | 11.84 | 73.42 (Ret. time=25.2 min) |
| 24.0 | 82.98 | / |

**Table 3.17:** HTGC-ICP-MS retention and integration data for Green River Shale nickel and vanadyl porphyrin mixture shown in Figure 3.25 (c)

| Iron ETIO Porphyrin | Distribution (% of mixture) |
|---|---|
| $C_{29}$ | 10.12 (9.8) |
| $C_{30}$ | 24.37 (44.9) |
| $C_{31}$ | 22.28 (7.4) |
| $C_{32}$ | 46.02 (37.9) |
| $C_{33}$ | 0.76 (/) |

(Values in brackets are the distribution calculated by Bonnett *et al.* from probe-MS data [24])

**Table 3.18:** Distribution of the iron ETIO porphyrins occurring in Bagworth coal obtained from integration of mass chromatograms in Figure 3.31

132
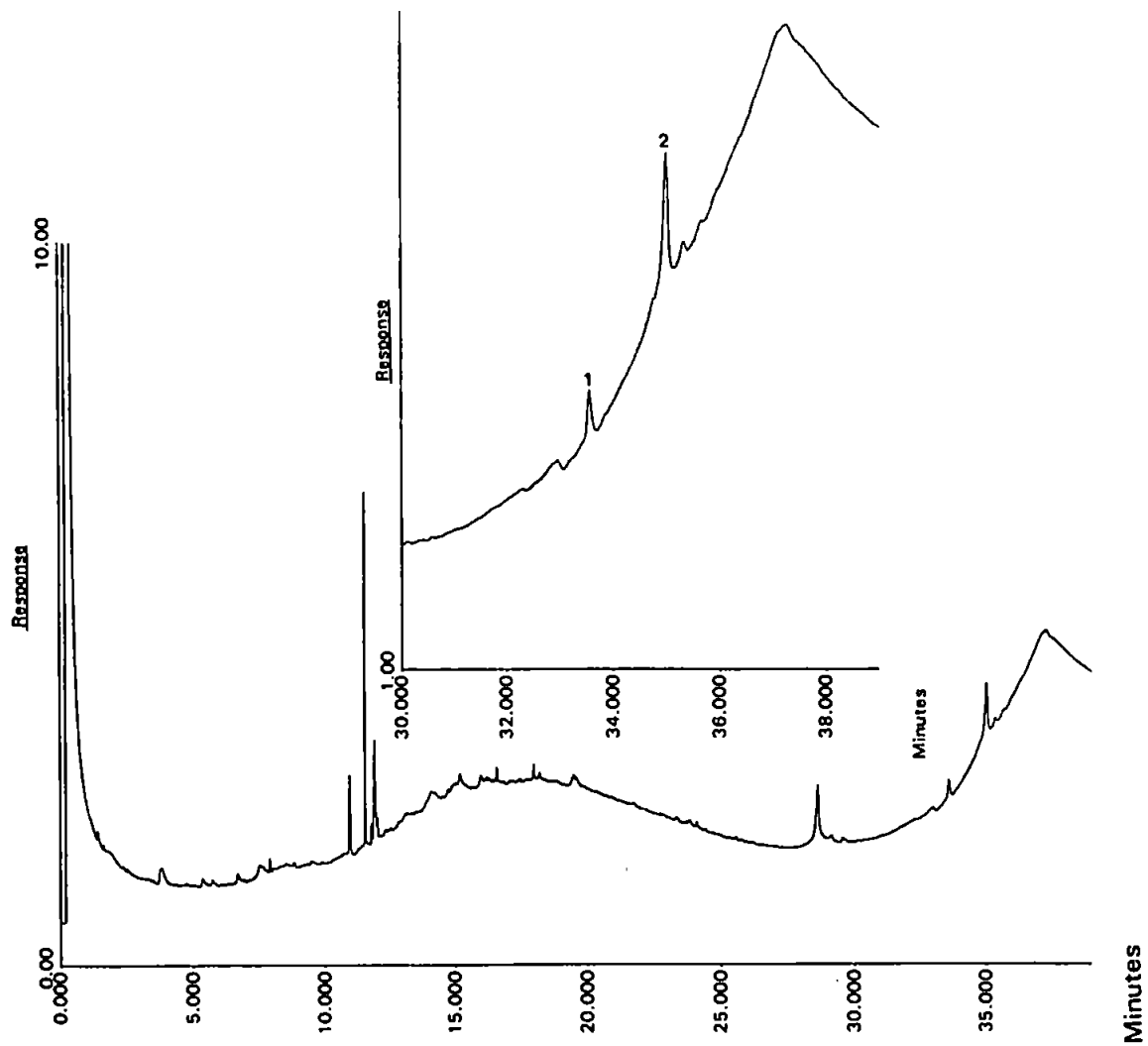
**Figure 3.28:** HTGC-FID of Bagworth coal iron porphyrins (5.0 μg on column), conditions as in Figure 3.1
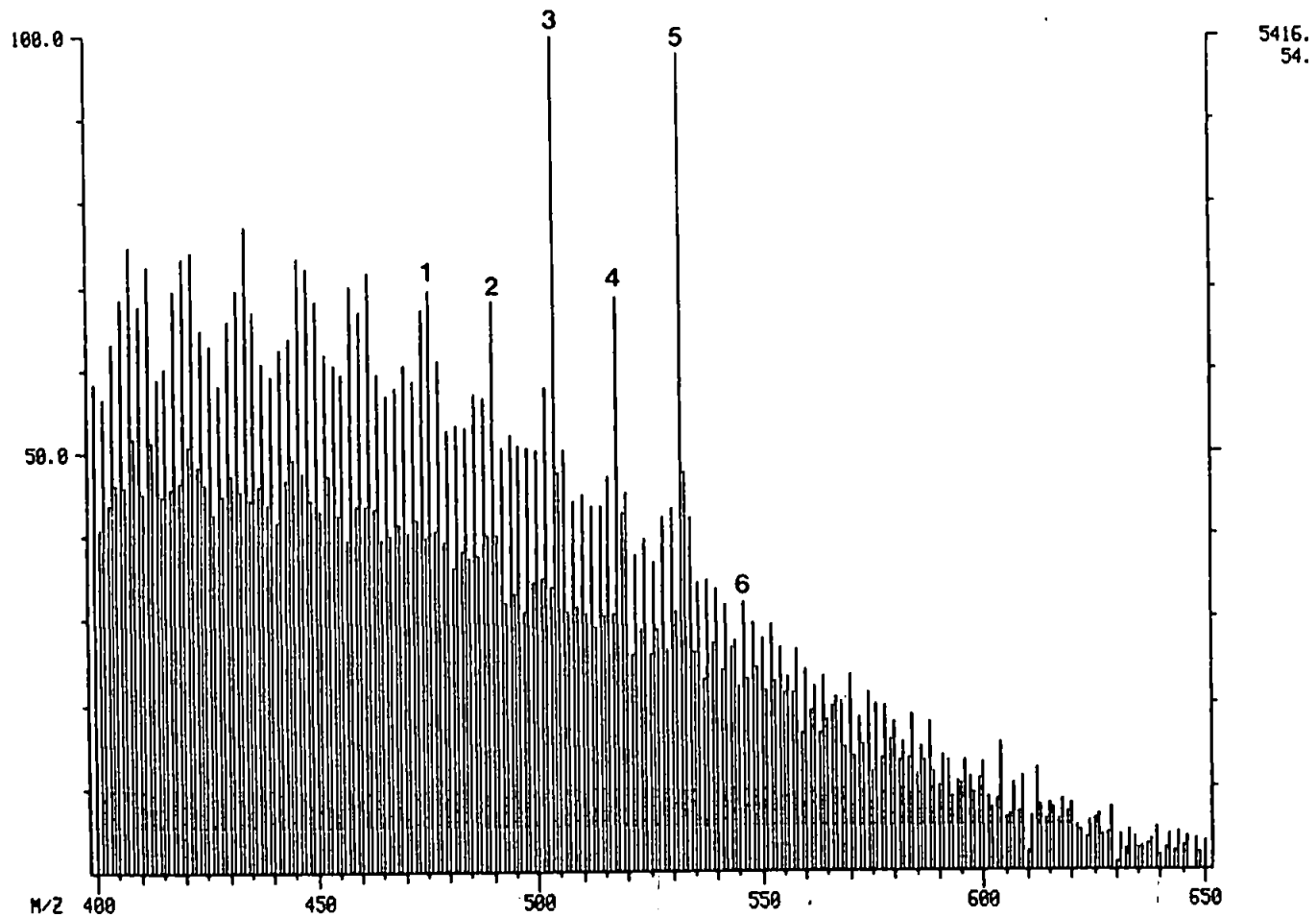
**Figure 3.29:** Probe mass spectrum of Bagworth coal iron porphyrins at 16eV, 1= A $C_{28}$, 2= A $C_{29}$, 3= A $C_{30}$, 4= A $C_{31}$, 5= A $C_{32}$, 6= A $C_{33}$

## Bagworth Coal Total Ion Current
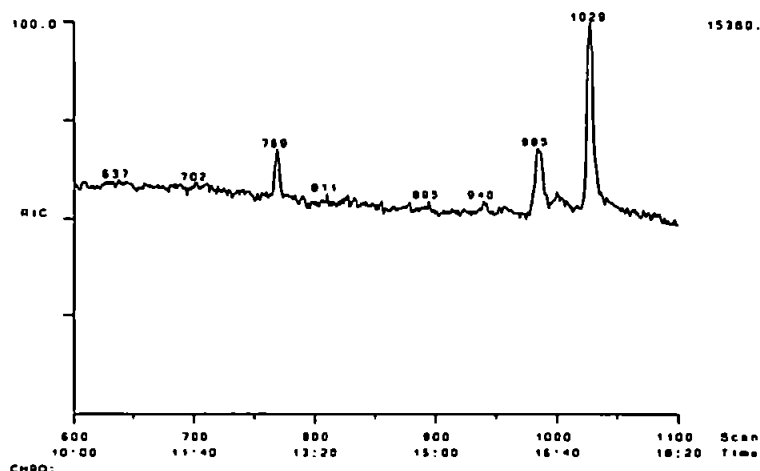


Scan 984
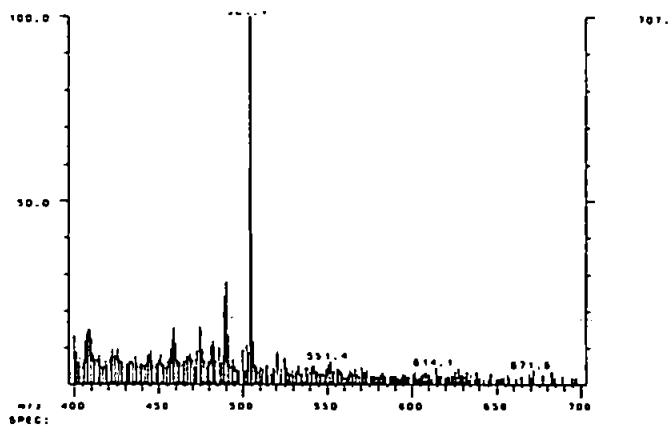
Scan 1027
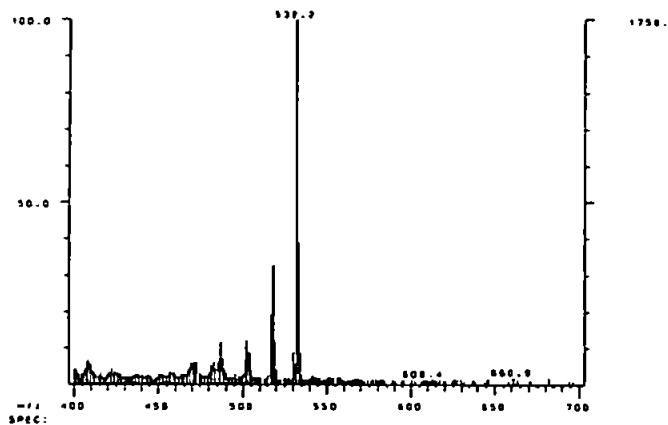
**Figure 3.30:** HTGC-MS of Bagworth coal iron porphyrins (5.2 μg on column), conditions as in Figure 3.5, selected mass spectra shown
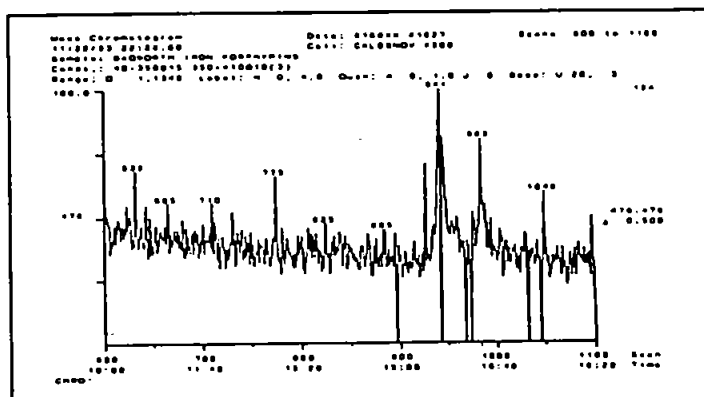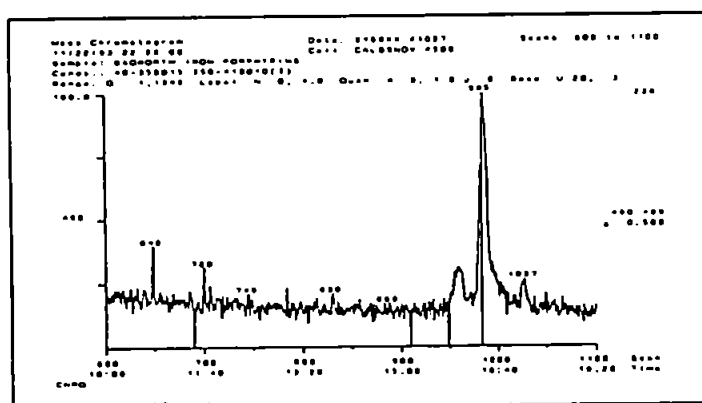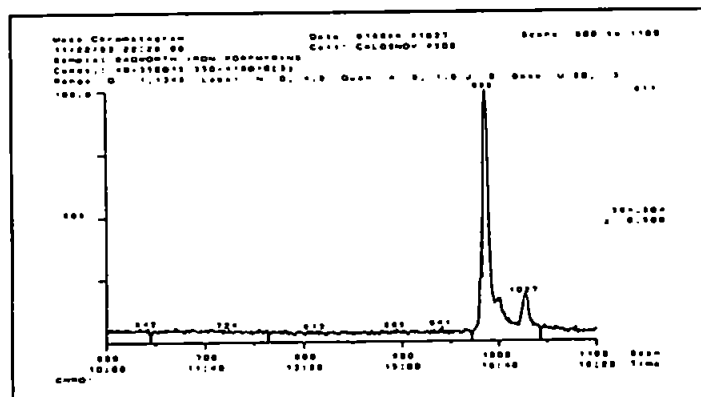
Figure 3.31: Single mass chromatograms obtained from HTGC-MS (Figure 3.30), showing A ($C_{28}-C_{33}$) macrocycles present in Bagworth coal iron porphyrin fraction
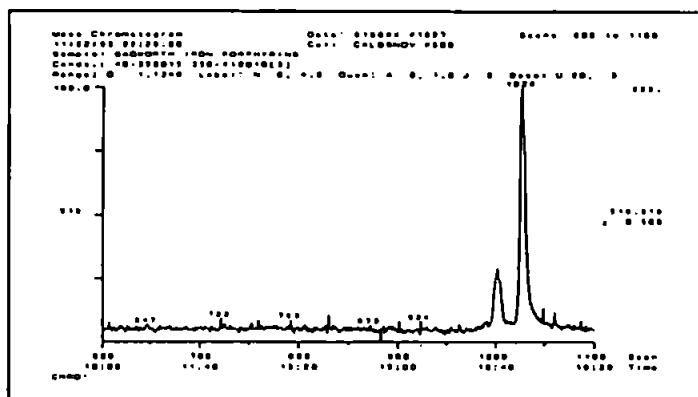
C₃₁ A
(m/z 518)
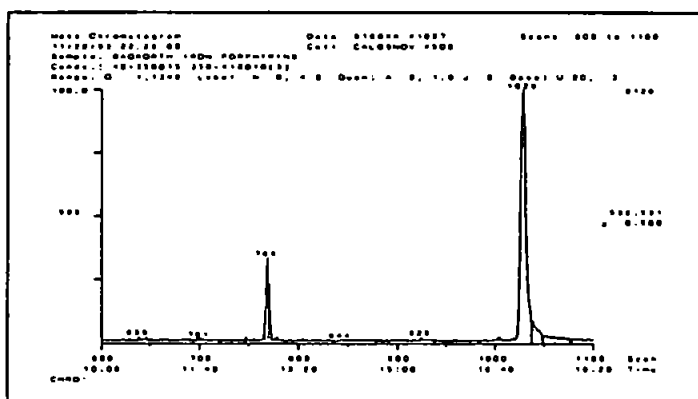
C₃₂ A
(m/z 532)
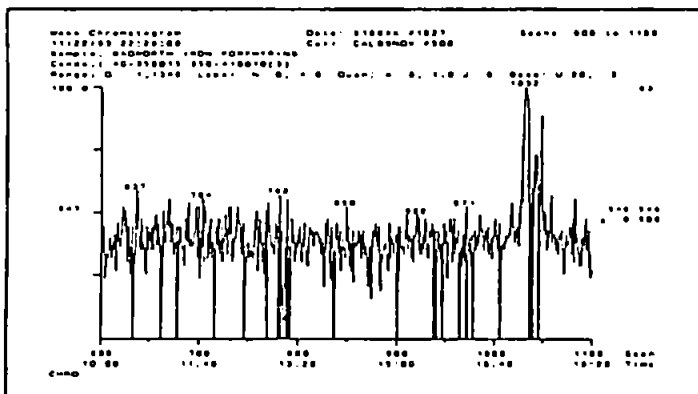
C₃₃ A
(m/z 546)

**Figure 3.31:** A $C_{31}$ to $C_{33}$

137

ETIO porphyrins. The peak at scan 985 contained the $C_{29}$ to $C_{31}$ iron ETIO porphyrins, while the peak at scan 1029 contained the $C_{29}$ to $C_{33}$ iron ETIO porphyrins. The ratio of the two peaks was 0.282 (scan 985) : 0.718 (scan 1029).

### 3.6.3. HTGC-ICP-MS:

Selected ion HTGC-ICP-MS chromatograms are shown in Figure 3.32. The chromatograms in Figure 3.32 show a comparison of the crude extract (no TLC purification) prior to the TLC clean-up step with the iron porphyrins separated using one preparative TLC step. The ratios of the peaks are 0.090(1):0.196(2):0.714(3) [Figure 3.32 (a)] and 0.045(1):0.298(2):0.657(3) [Figure 3.32 (b)]. The ratios in Figure 3.32 show good agreement with those obtained using HTGC-FID and HTGC-MS. The TLC clean-up seems to have a slight effect on the distribution of the iron porphyrins, probably due to some demetallation on the silica absorbent.

### 3.7. Chromatographic Behaviour of Synthetic and Geological Metalloporphyrin Mixtures:

Given the apparent utility of HTGC for geoporphyrin analysis demonstrated herein and in other studies [34-37,64,65,121,122] and the importance of porphyrins in petroleum geochemistry [135], it is surprising that the method has not found more
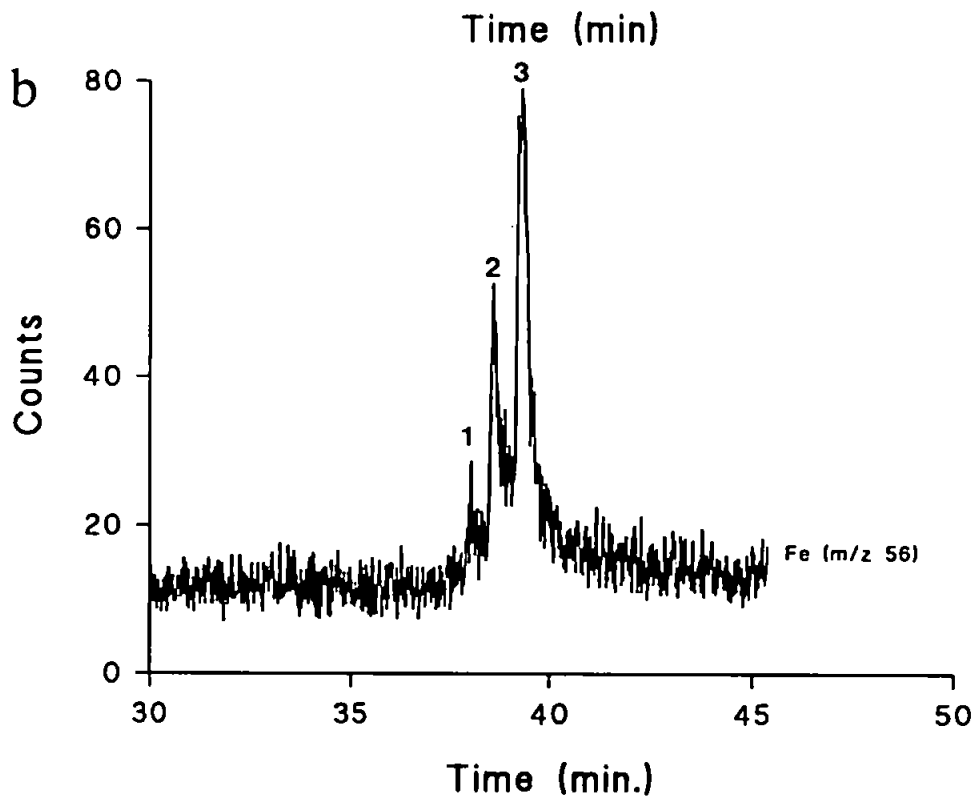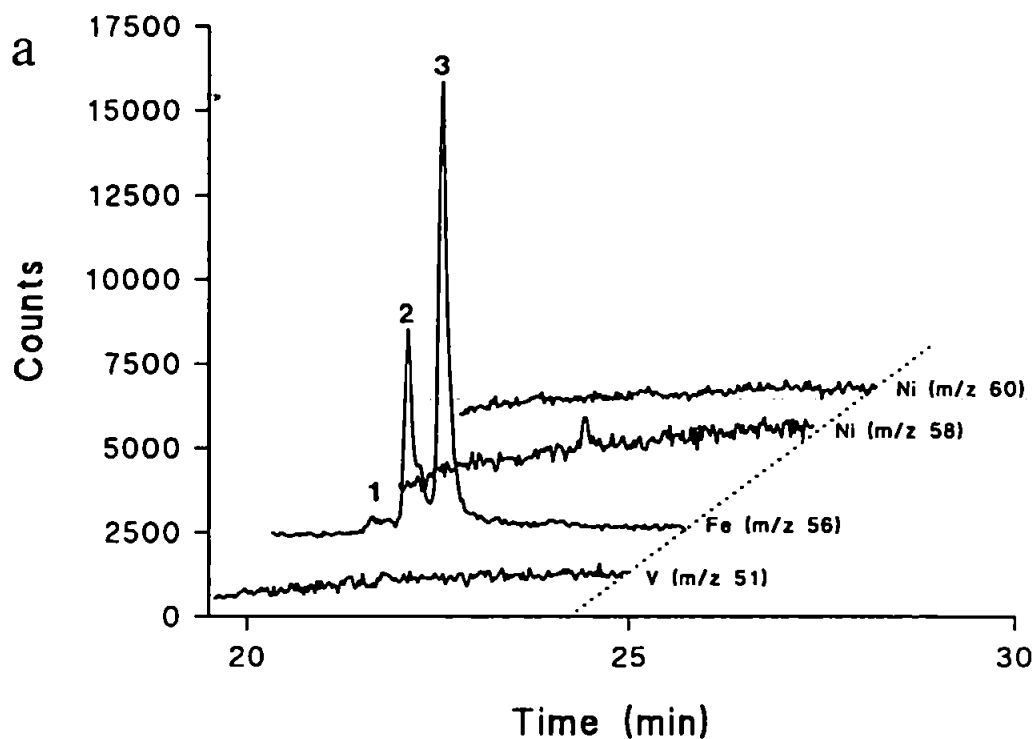
**Figure 3.32:** HTGC-ICP-MS of Bagworth coal iron porphyrins

(a) Prep-TLC fraction (3.7 μg on column), conditions as in Figure 3.21 (c)

(b) Crude coal extract (7.3 μg on column), conditions as in Figure 3.11

widespread use in the ~5 years that the columns have been available. Whilst porphyrins are known to be rather difficult analytes and early studies by packed column GC were fraught with difficulties (reviewed by Gill [136]), modern capillary HTGC, at first sight, appears to be a more practicable method. However, a close examination of the literature and personal experience of the author suggests that "...something is rotten in the state of Denmark..." [137].

For example, a recent publication [37] was the first to state the quantity of porphyrins examined by HTGC. Analysis of 200 mg of Boscan oil (1.4 mg of porphyrins) by injection of 1 ml of solution was required in order to produce a chromatogram, using the GC-MIP-AED (Hewlett Packard). Given the column dimensions (5 m x 0.5 mm i.d.) this represents 40,000 times more than recommended sample loading [138] and the amount of solvent injected would have filled 50 % of the column volume! Even so, or perhaps as a consequence, porphyrins appeared as broad "humps" rather than peaks. The question then arises as to why such large quantities were required? A significant deterioration in chromatographic resolution and detector response (whichever detector was used) was also noted by the present author when repeat analyses of the geoporphyrins of shales and coals (Sections 3.2-3.6) was attempted. In an effort to obtain statistically validated results, this prompted a systematic investigation of the HTGC column stability.

Obviously a routine HTGC method for geoporphyrin analysis should avoid such drastic measures if possible. During the

studies made herein it became apparent to the author that column stability was a problem for routine analysis. An attempt was made to assess the stability of the HTGC columns by the construction of calibration curves for various authentic, pure metalloporphyrin compounds. The calibration curves showed good linearity (correlation coefficients between 0.9994-0.9998), the retention times of both the internal standard and analyte were constant and good peak shapes were maintained (Figure 3.33). The results obtained from the analysis of the authentic reference compounds herein thus seemed to indicate that new HTGC columns were suitable for the analysis of geoporphyrins. The columns were pre-treated by injection of metalloporphyrin standards (~3 injections; 1 $\mu$l of 70 ppm vanadyl, nickel and iron octaethylporphyrin) and these injections were intended to "passivate" any active sites on the column surfaces.

However, severe problems were encountered with column stability with subsequent analyses of geoporphyrins. The elution of the geoporphyrins varied from analysis to analysis. For example, Figure 3.34 shows a sequence of injections on a HT-5 column (used only 10 times previously i.e. ~10 prior injections), the response for the geoporphyrins including the internal standard (tetraphenyl porphyrin, last peak on chromatograms= i; retention time 37.8 min.) decreased from analysis 11 to 12 until virtually no detector response was obtained by analysis 13. This problem was temporarily solved by removal of the first ~1 metre of column (analysis 14), but this was only successful once or twice per column. By the time that removal of two
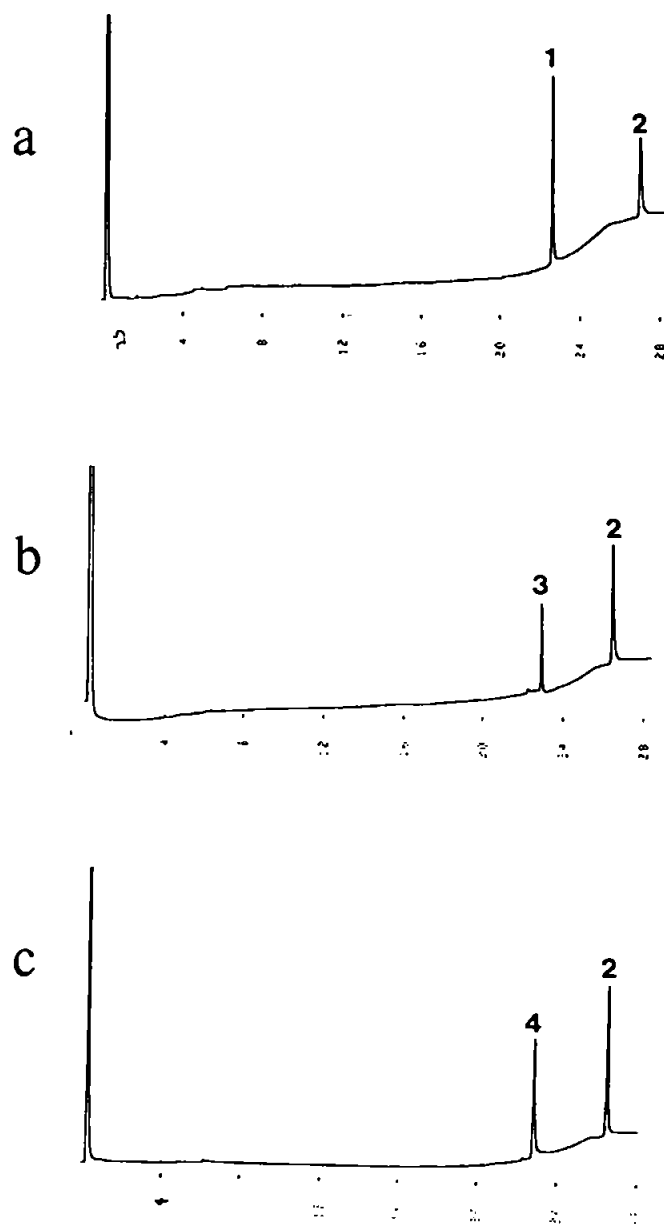
Figure 3.33:   HTGC-FID of porphyrin standards on 12 m HT-5,

50°C to 420°C at 15°C/min

(a) 1= OEP (40 ng on column), 2= TPP (20 ng on column)

(b) 3= NiOEP (20 ng on column)

(c) 4= FeOEP (20 ng on column)
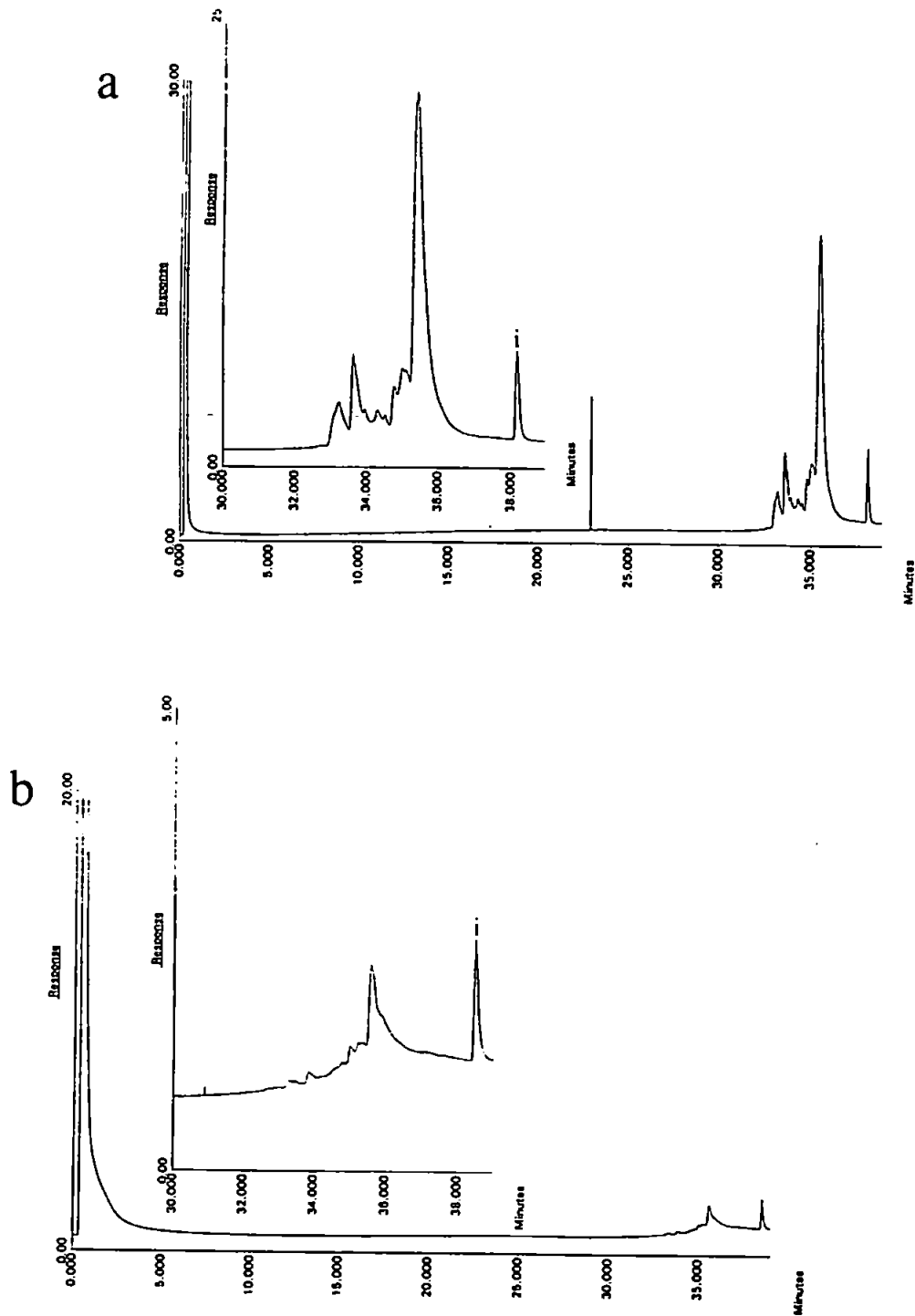
**Figure 3.34:** HTGC-FID of Kupfershiefer nickel porphyrins on 12m HT-5, conditions as in Figure 3.1 (2.0 μg on column);(a) Injection 1, (b) Injection 2

143
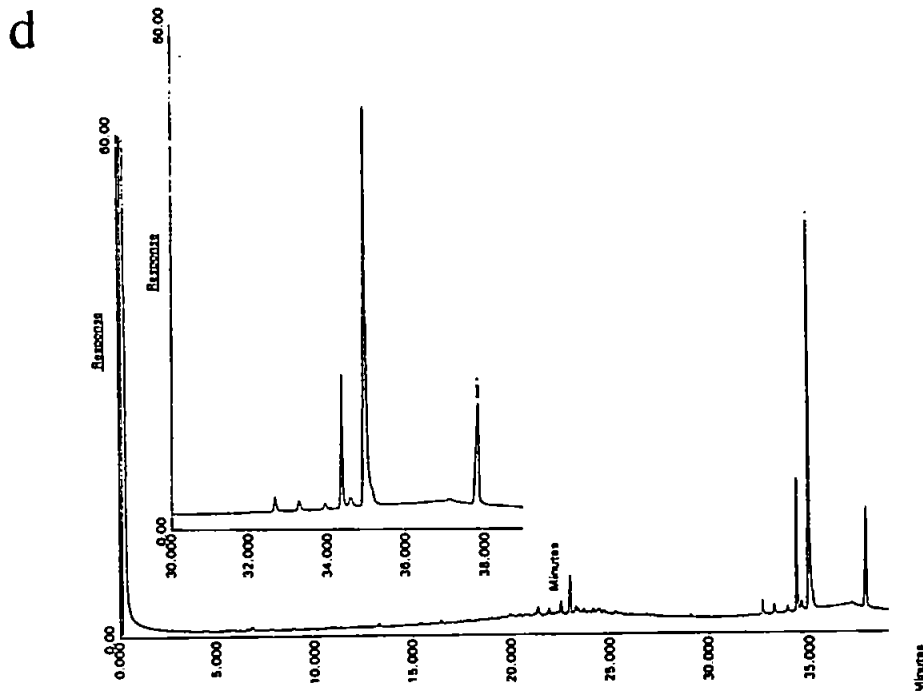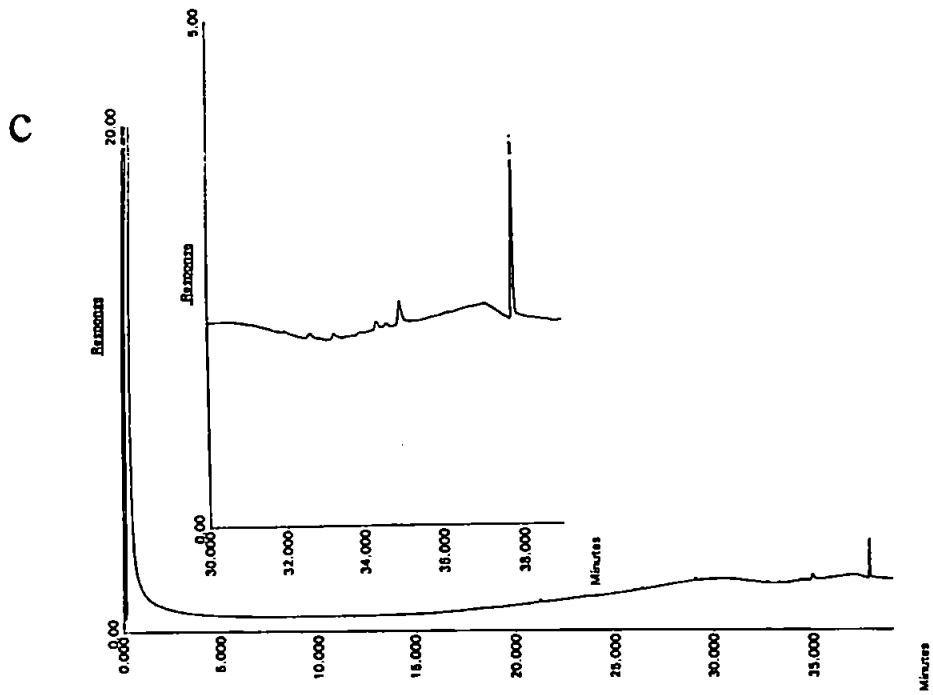
**Figure 3.34:** (continued) (c) Injection 3, (d) Removed ~1 m of
column from injector end directly after injection
3 and injected

metres of column had become necessary, the column had generally become too badly degraded for further analyses and the chromatograms resembled those obtained from a column exhibiting excessive phase bleed (both HT-5 and DB-1 ht columns). This phenomenon was observed with both the MS and ICP-MS detection (Figure 3.35). The mass spectrum of this column "bleed" [Figure 3.35 (b)] showed that it consisted of porphyrins slowly eluting from the column.

The performance of the columns (HT-5 and DB-1 ht) also varied from column to column, which lasted at best for 15 injections and at worst for only 5 injections!

Problems with the chromatography were often mistakenly thought to be related to the HTGC-ICP-MS interface. The Mark VII interface design was as a result of this mistaken notion. These results were similar to those obtained by Kim [134], who also reported variations in retention times with successive injections. The problems encountered by Kim were probably due to the large amounts injected (typically 600 ng on column) onto a 0.32 mm, 25 m (HT-5) column, which proved necessary because of column deterioration [135]. Following these discoveries subsequent HTGC analyses of porphyrins were curtailed pending improvements in column technology.

## 3.8. Conclusions:

Analysis of various geoporphyrin samples by HTGC with new
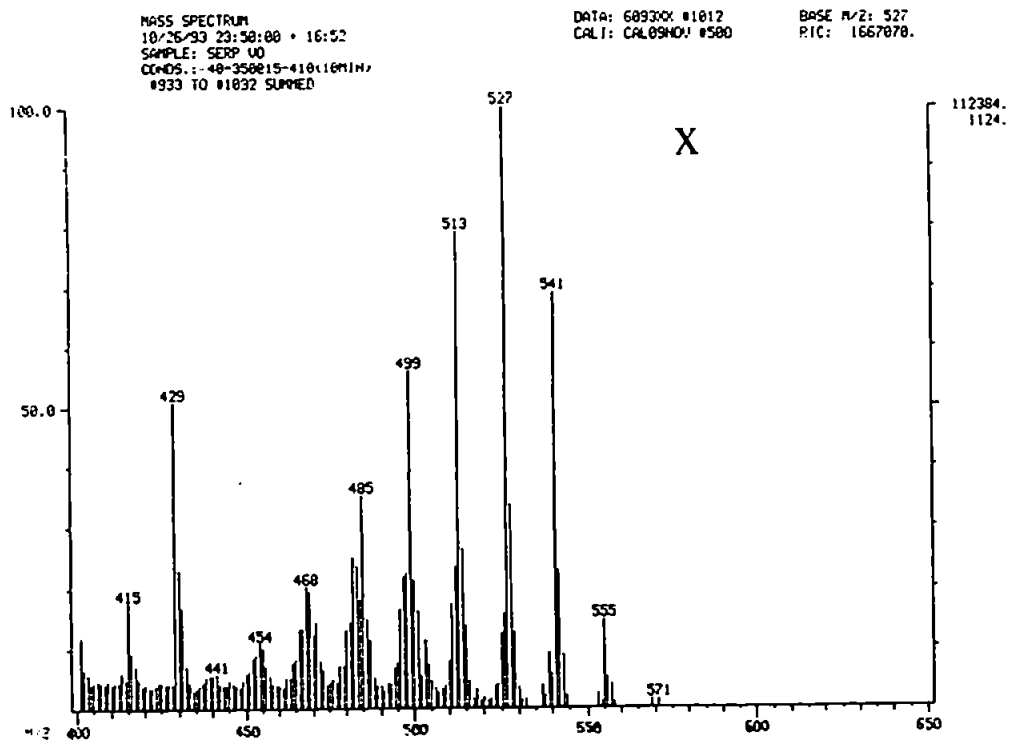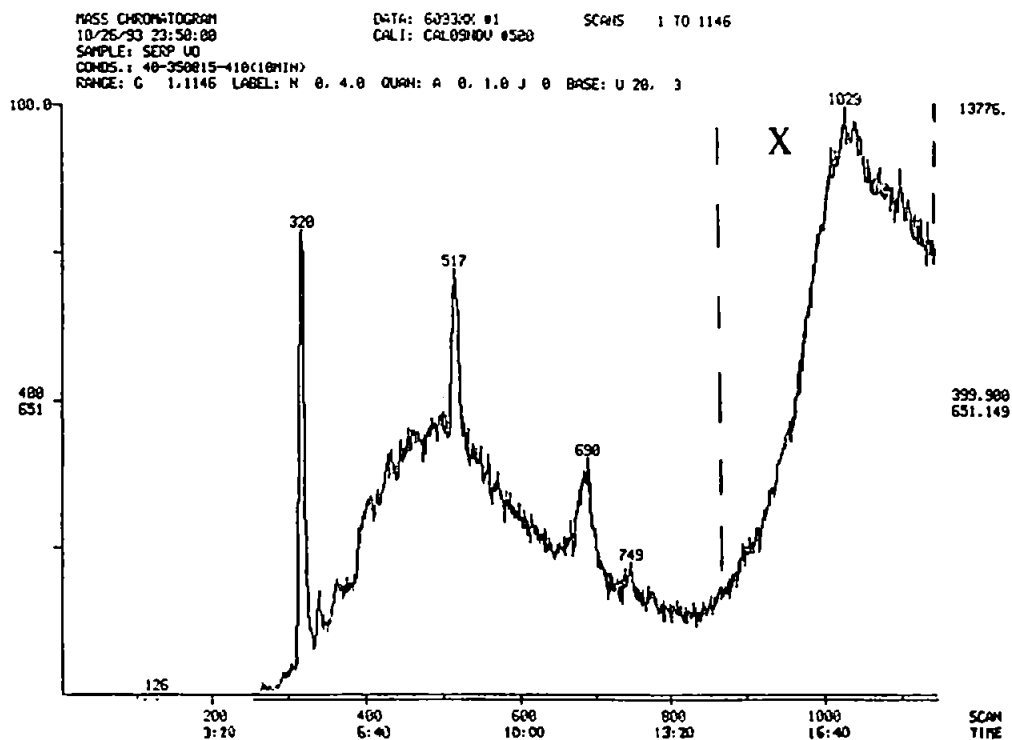
**Figure 3.35: Illustration of degraded column (DB-1 ht) elution of porphyrin**

(a) Serpiano vanadyl porphyrins (0.7 μg on column), conditions as in Figure 3.4 (b)

(b) Mass spectrum of "bleed" (scans 933-1092 summed)

146

columns showed the potential of the technique. The distributions of the various macrocycles could be determined by HTGC-MS and mass chromatography whilst HTGC-ICP-MS provided a new tool for the investigation of the metals chelated to the porphyrin macrocycles. The tentative identification of titanium porphyrins in Julia creek Oil Shale and Marl Slate, in which they have not been reported previously, demonstrates the power of the method. Although these compounds co-eluted with the more common and abundant nickel porphyrins they could nevertheless be distinguished easily from the latter by selected ion chromatography. The close similarity in chromatographic behaviour of the nickel and titanium porphyrins possibly explains the lack of previous reports since less selective detection methods would not reveal their presence. The use of HTGC-ICP-MS also allowed the determination of the nickel isotope ratios ($^{58}Ni$:$^{60}Ni$) for the Green River Shale and Marl Slate.

Unfortunately, whilst the aforementioned results are very encouraging, the unreliability of the chromatographic behaviour of present day HTGC columns for the analysis of geoporphyrins probably precludes routine use of the method at present. This was demonstrated by successive HTGC analyses of a standard mixture. A rapid deterioration of column characteristics was observed for both HT-5 and DB-1 ht phases.

Reverse phase HPLC-ICP-MS, a technique also demonstrated for separation of geoporphyrins in the present work, may prove a more reliable and robust method of analysis, until further

research into column stationary phases presents the analyst with more durable HTGC materials.

# 4.0 HPLC ANALYSIS OF GEOPORPHYRINS:

## 4.1 Introduction:

Gas chromatographic separation of geoporphyrins revealed extensive co-elution of different porphyrin macrocycles (see Section 3.2). The inability of HTGC to separate A type porphyrin macrocycles from A-2 macrocycles was a major problem given the abundance of these in geological samples. The majority of porphyrins occur as A-2 macrocycles (in both the nickel and vanadyl porphyrins) which were not separated, the $C_{30}$ to $C_{32}$ porphyrins co-eluting as a single peak in the HTGC chromatograms. The major differences in the distributions of the A-2 macrocycles, visible in the probe-MS spectra, were not apparent in the HTGC chromatograms. HTGC-MS mass chromatography overcame this problem to some extent.

In the 1980's Sundararaman and Boreham et al. developed reverse phase HPLC methods for the separation of both vanadyl and nickel geoporphyrins [19,20]. Such methods allowed the separation of A from A-2 porphyrin macrocycles. Boreham et al. showed that the vanadyl porphyrins required higher efficiency columns for complete separation of A (ETIO) and A-2 (DPEP) macrocycles, since their separation was less dependent on the macrocycle structure, than that of nickel porphyrins [56].

Reverse phase HPLC has been used with ICP-MS for the analysis of a variety of metal complexes (Table 1.2) and such methods

149

should be amenable to the separation of nickel geoporphyrins with an element specific detector like ICP-MS [23,24].

In this chapter the HPLC-ICP-MS and HPLC-UV/VIS analysis of gallium and nickel geoporphyrins is described.

## 4.2 Experimental:

### 4.2.1 HPLC:

HPLC was performed with a Constametric pump (LDC Analytical) and a Waters (6000 A) pump. Injections were performed with a Rheodyne injector (model 7125) fitted with a 200 $\mu$l loop. UV/VIS detectors used were a modified LC-UV (Pye Unicam) and Hitachi L-4200, at a wavelength of 400 nm (Soret absorption of porphyrin macrocycles) [3]. The data handling and processing was performed using a PE Nelson (Perkin Elmer) integration software package.

The nickel and gallium porphyrins were separated using a 300 mm (3.9 mm i.d.), $C_{18}$ (4 $\mu$m) Novapak column (Waters).
The mobile phase used for the gallium porphyrins was 15 % 1 mM tetrabutylammonium dihydrogen phosphate in methanol, at a flow rate of 1.0 ml/min. The mobile phase used for the nickel porphyrins was 0.2 % pyridine in methanol, at a flow rate of 1.0 to 1.2 ml/min.

### 4.2.2. HPLC-ICP-MS interface:

The ICP-MS instrument used was a VG PlasmaQuad II. Operating conditions for HPLC-ICP-MS are given in Table 4.1.

The HPLC column eluent was nebulized using an Ebdon V-groove nebulizer, into a Scott double pass spray chamber (VG Elemental). The spray chamber was chilled to -10°C by a refrigerated bath (Techne RB-5) and circulator (Techne TE-8A). The nickel sampler and skimmer cones (VG Elemental) had orifices of 1.0 mm and 0.7 mm, respectively. The desolvation system, used with the gallium analyses consisted of a 300 mm x 20 $\mu$m silicone membrane (PS Analytical) mounted in a polypropylene tube, with an argon purge of 1.6 to 3.0 L/min [139].

The nebulizer gas was mixed with oxygen (~2.0 to 3.0 %) which helped reduce carbon deposition on the sampler and skimmer cones. The HPLC-ICP-MS system is shown schematically in Figure 4.1. The loss in efficiency in the HPLC-ICP-MS system compared with the HPLC-UV/VIS system was < 10 %, calculated, using the equation:

$$N = 16 \ (t_r/w_b)^2 \qquad \text{(Equation 4.1 [140])}$$

Where $N$ is the efficiency, $t_r$ is the uncorrected retention time and $w_b$ is the width of the peak at baseline. The latest eluting peak in the gallium porphyrin chromatograms was used for these calculations.
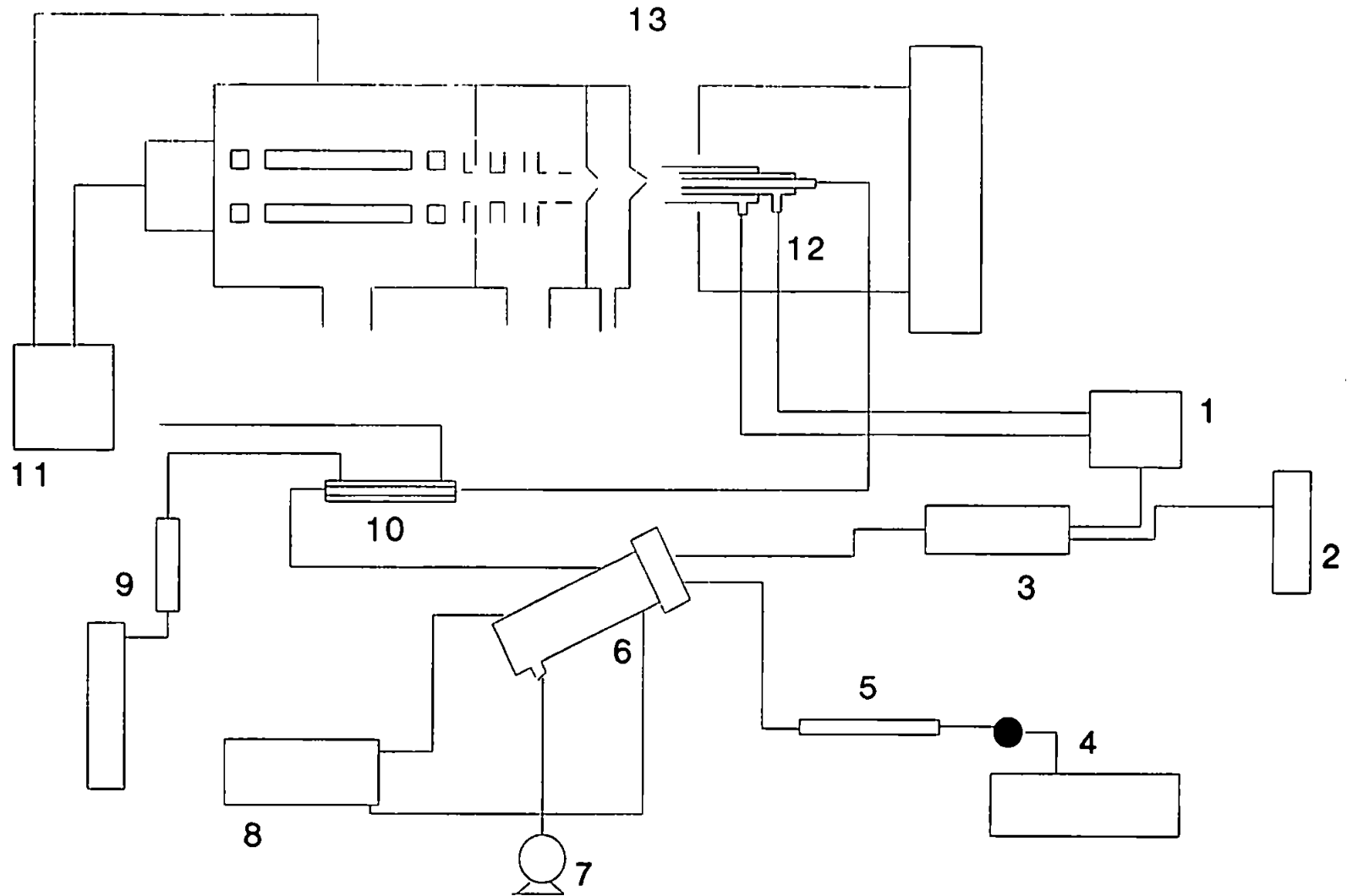
**Figure 4.1:** HPLC-ICP-MS interface: 1. argon tank; 2. oxygen cylinder; 3. gas blender; 4. HPLC pump and injector; 5. HPLC column; 6. spray chamber and nebulizer; 7. drain pump; 8. chiller unit; 9. argon purge flowmeter; 10. membrane separator; 11. ICP-MS computer; 12. Fassel type plasma torch; 13. ICP-MS

| | |
|---|---|
| Cooling gas | 15 L/min |
| Auxiliary gas | 1.0 L/min |
| Nebulizer gas | 0.85 L/min |
| Oxygen bleed | 2.5 % |
| Forward Power | 1.75 kW |
| Reflected power | 25 W |
| Mode | Single ion monitoring $^{71}$Ga (39.8 %); $^{58}$Ni (67.8 %) |
| Dwell | Typically between 1.3 s to 2.6 s |
| Channels | Typically between 2700 to 4000 |
| Data acquisition time | Between 75 and 120 min |
| Spray Chamber Temperature | -10°C |

Table 4.1: HPLC-ICP-MS Operating conditions

## 4.3 HPLC of Gallium Porphyrins from British Coals:

Coals obtained from British Coal (Stoke Orchard) were sampled, homogenised and stored using standard methods and are therefore termed "standard coals" [141]. Coals were chosen since no other suitable standard reference materials for geoporphyrins were available. Since they are readily available, these coals could be analysed by other workers and the results compared with those reported herein. Indeed, Bagworth coal was chosen precisely for this reason, since Bonnett *et al.* has already analysed the same material [4,5,10,142].

Gallium porphyrins were extracted from the coals and isolated using preparative and analytical TLC procedures [10,142]. Work-up procedures are described in detail in Chapter 7. Gallium porphyrin fractions were dissolved in dichloromethane. HPLC-UV/VIS analyses were performed in duplicate and HPLC-ICP-MS in triplicate over a 24 hour period. The gallium signal was monitored at m/z 71 ($^{71}$Ga, 39.8 % abundance), due to a polyatomic interference at m/z 69 ($^{69}$Ga, 60.2 % abundance), possibly due to $^{40}$Ar$^{12}$C$^{16}$OH$^{+}$ and/or $^{37}$Cl$^{16}$O$_2^{+}$.

Chromatograms of the porphyrin distributions obtained by HPLC-UV/VIS and HPLC-ICP-MS are shown in Figures 4.2-4.4. The difference in retention times between the two methods was caused by the use of two different HPLC pumps for the two methods.

Bagworth coal which has been analysed previously by Bonnett et
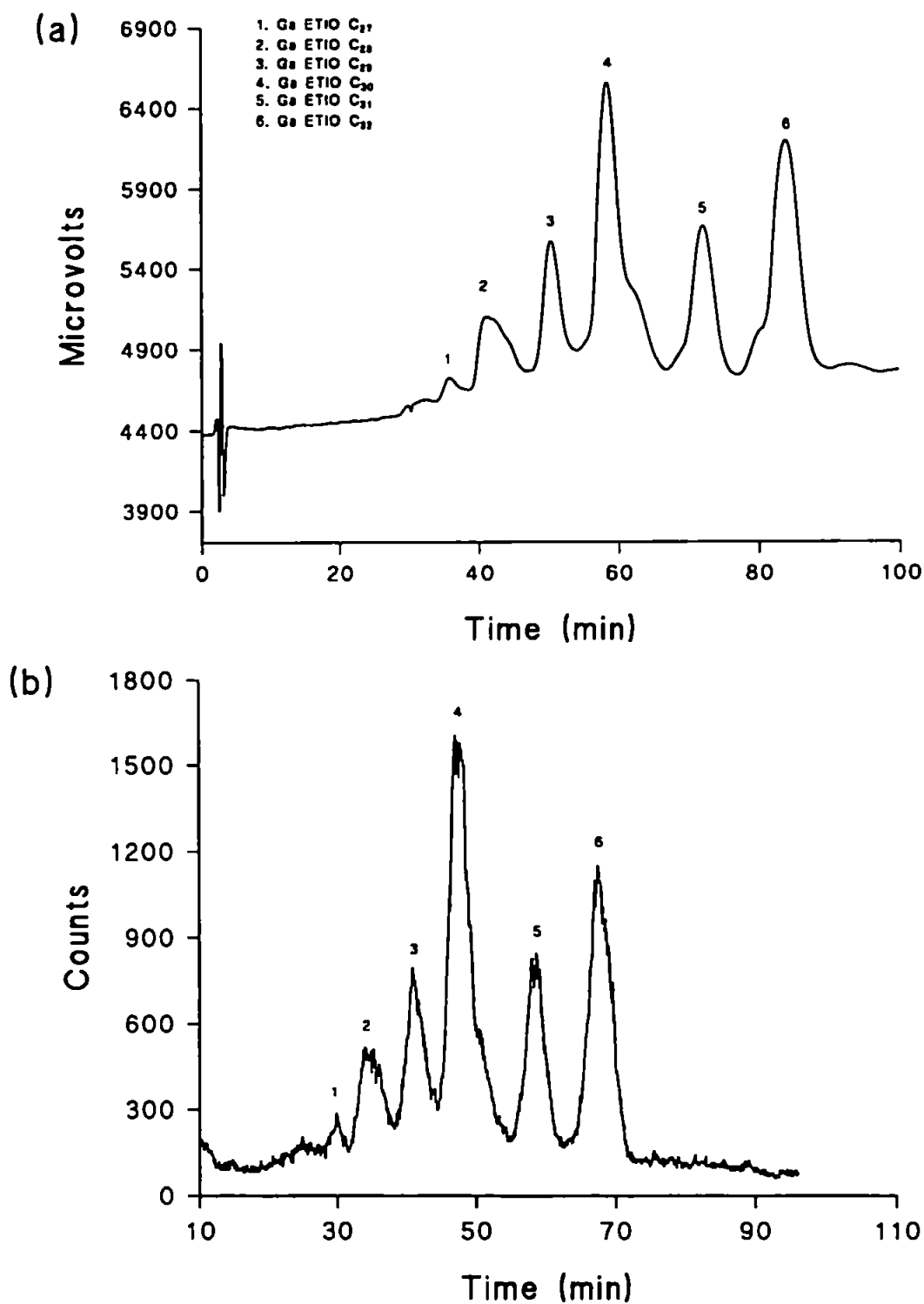
**Figure 4.2:** Comparison of HPLC-UV/VIS (a) and HPLC-ICP-MS (b) chromatograms for Bagworth coal gallium porphyrins (0.57 μg injected)
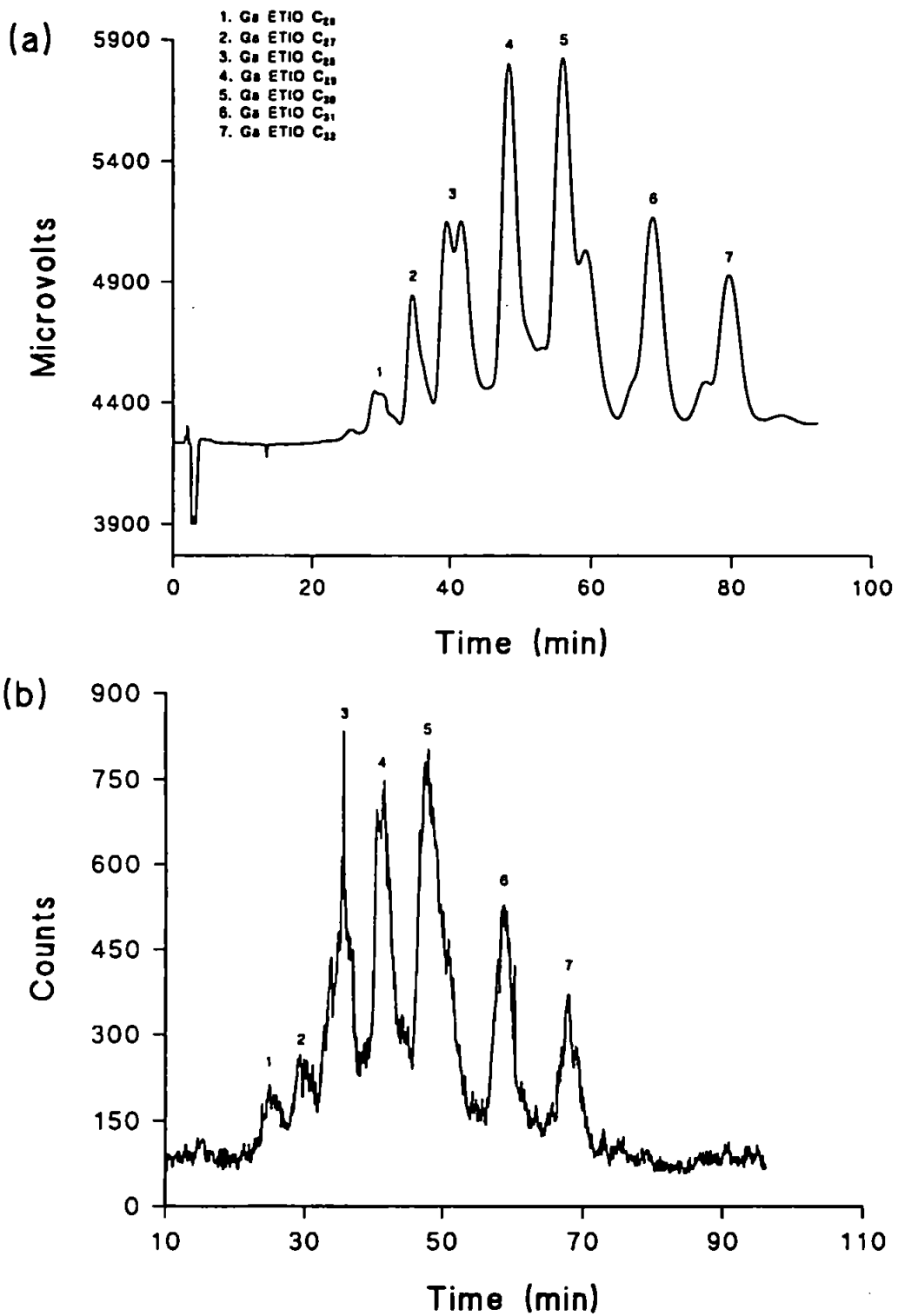
**Figure 4.3:** Comparison of HPLC-UV/VIS (a) and HPLC-ICP-MS (b)
chromatograms for Markham Main coal gallium
porphyrins (0.25 µg injected)

(a)

1. Ga ETIO C₁₆
2. Ga ETIO C₁₇
3. Ga ETIO C₁₈
4. Ga ETIO C₁₉
5. Ga ETIO C₃₀
6. Ga ETIO C₃₁
7. Ga ETIO C₃₂
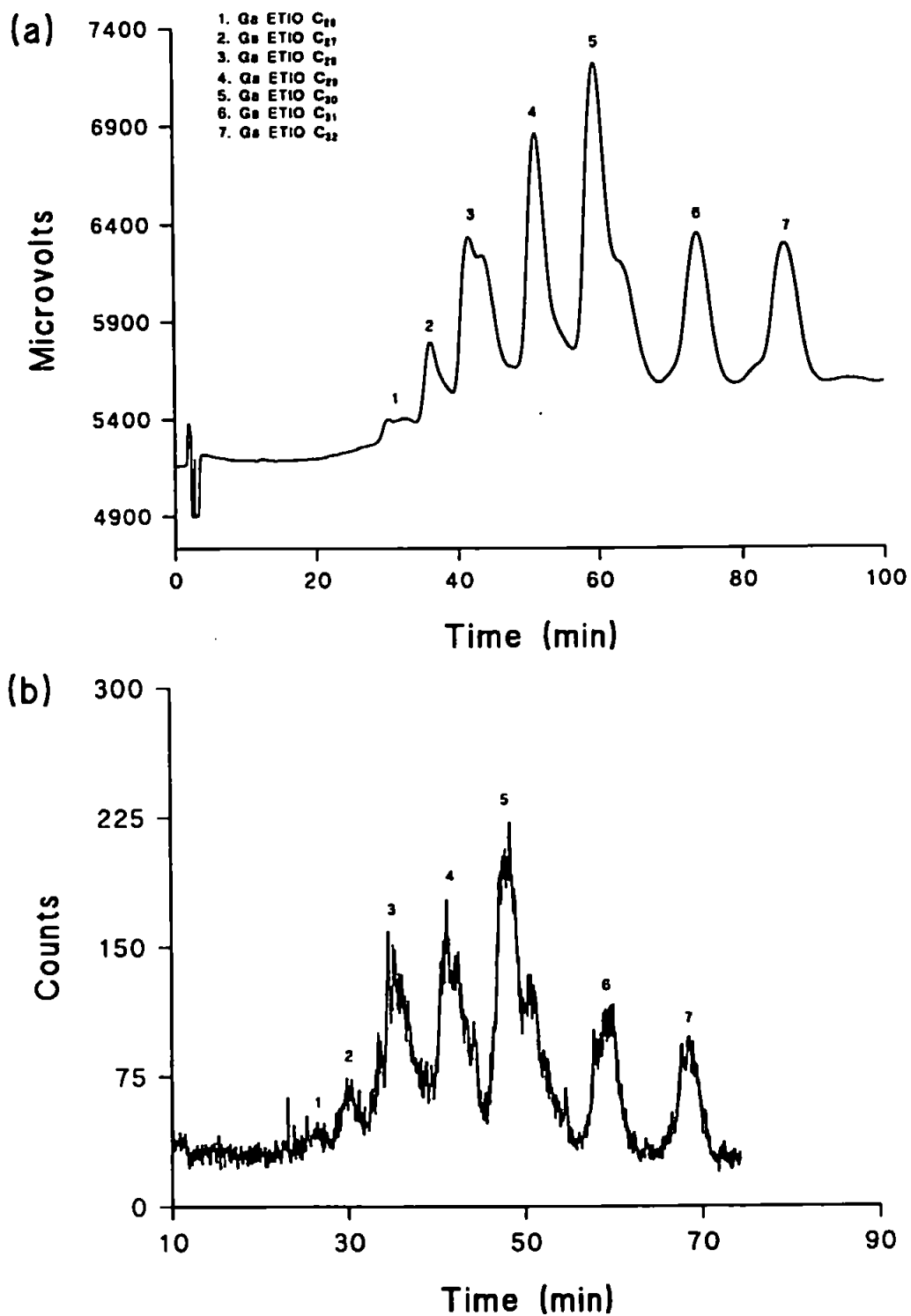
**Figure 4.4:** Comparison of HPLC-UV/VIS (a) and HPLC-ICP-MS (b) chromatograms for Gedling coal gallium porphyrins (0.53 μg injected)

*al.* and was used as a standard against which to compare the other gallium porphyrin distributions [10]. Figure 4.5 shows a qualitative comparison of the results obtained by Bonnett *et al.* and those obtained in this study. Since the results agree closely it was possible to tentatively identify the gallium porphyrins (carbon number) in those coals which had not been previously analysed (Figures 4.3,4.4).

The distributions obtained for the gallium porphyrins using HPLC-UV/VIS and HPLC-ICP-MS were qualitatively very similar. The high efficiency of the separation was maintained by the HPLC-ICP-MS coupling. Figures 4.5-4.7, allow the gallium porphyrin homologue distributions obtained by the two methods to be compared. The jagged peaks obtained for the Gedling HPLC-ICP-MS chromatogram (Figure 4.4) was due to carbon deposition on the sampler and skimmer cones of the ICP-MS which caused a degradation in the signal to noise ratio. However, the close agreement of the two methods was particularly pleasing and the m/z 71 ion chromatogram confirmed the presence of gallium in all the porphyrin macrocycles (only inferred previously from UV/VIS). The close agreement between the UV/VIS and ICP-MS results indicates that the ICP-MS signal was stable over the elution window.

The concentrations of gallium porphyrins in the coals were measured by HPLC-ICP-MS using gallium octaethylporphyrin as an external standard. Gallium octaethylporphyrin was flow-injected (by-passing the HPLC column) before and after each chromatographic run.

**% Distribution**

**Porphyrin homologue (carbon number)**

—•— HPLC-UV/VIS [1]     —+— HPLC-ICP-MS [1]
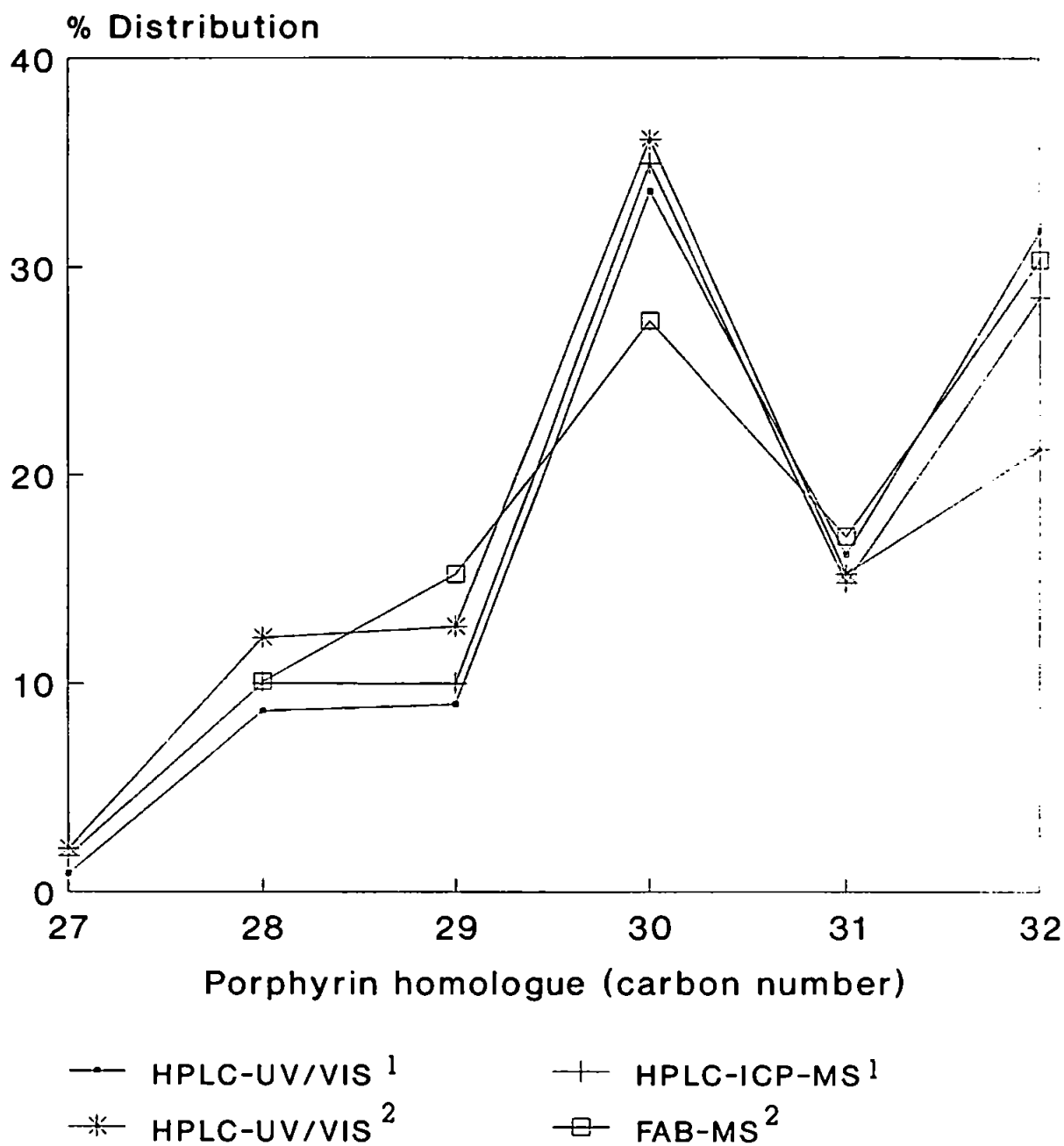
—※— HPLC-UV/VIS [2]     —▫— FAB-MS [2]

1. This work
2. Bonnett et al. (10)

**Figure 4.5:** Comparison of Bagworth coal gallium porphyrin distributions obtained using HPLC-UV/VIS (this work and [10]), HPLC-ICP-MS (this work) and FAB-MS ([10])

159
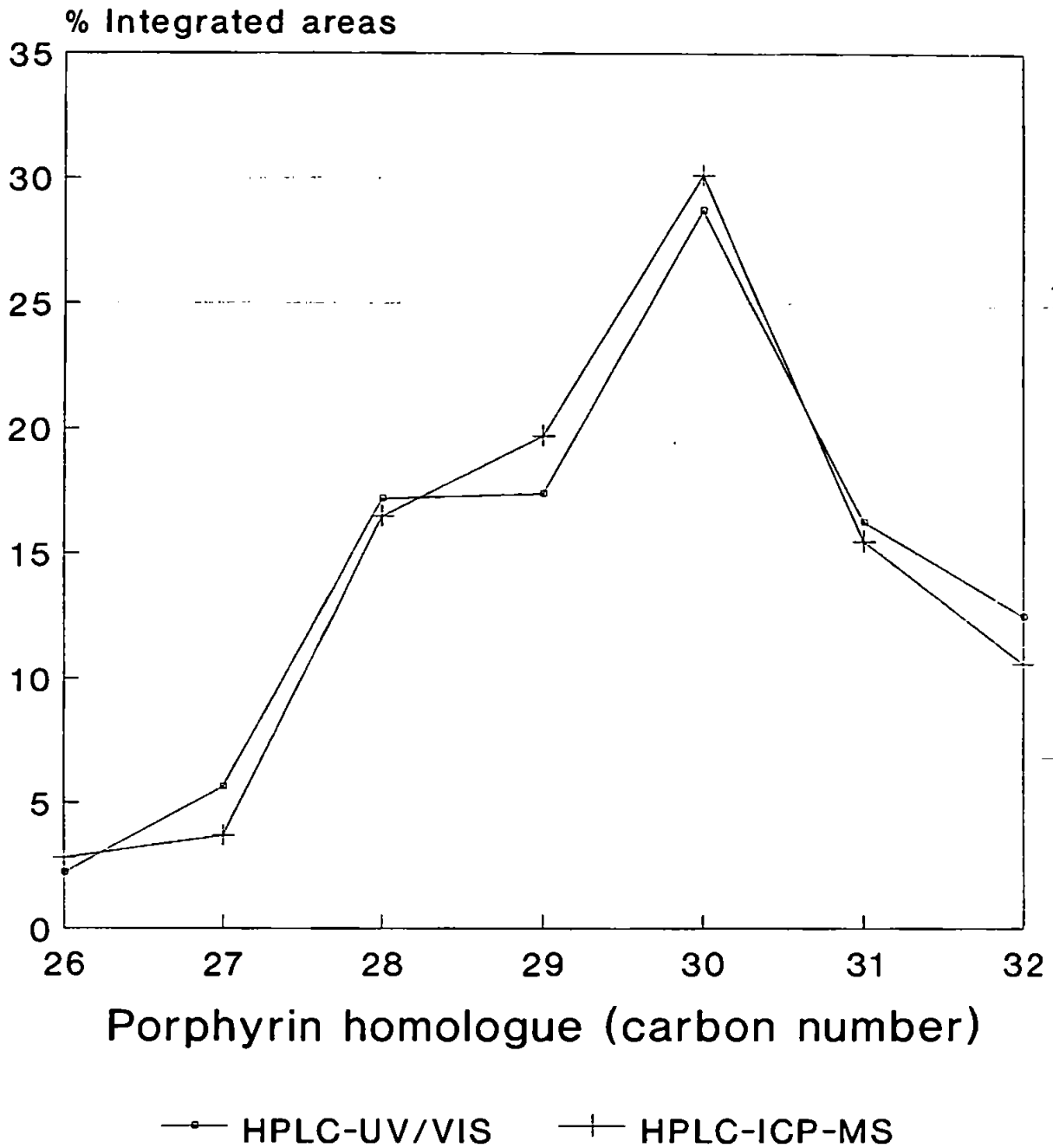
**Figure 4.6:** Comparison of Markham Main coal gallium porphyrin distributions obtained using HPLC-UV/VIS and HPLC-ICP-MS
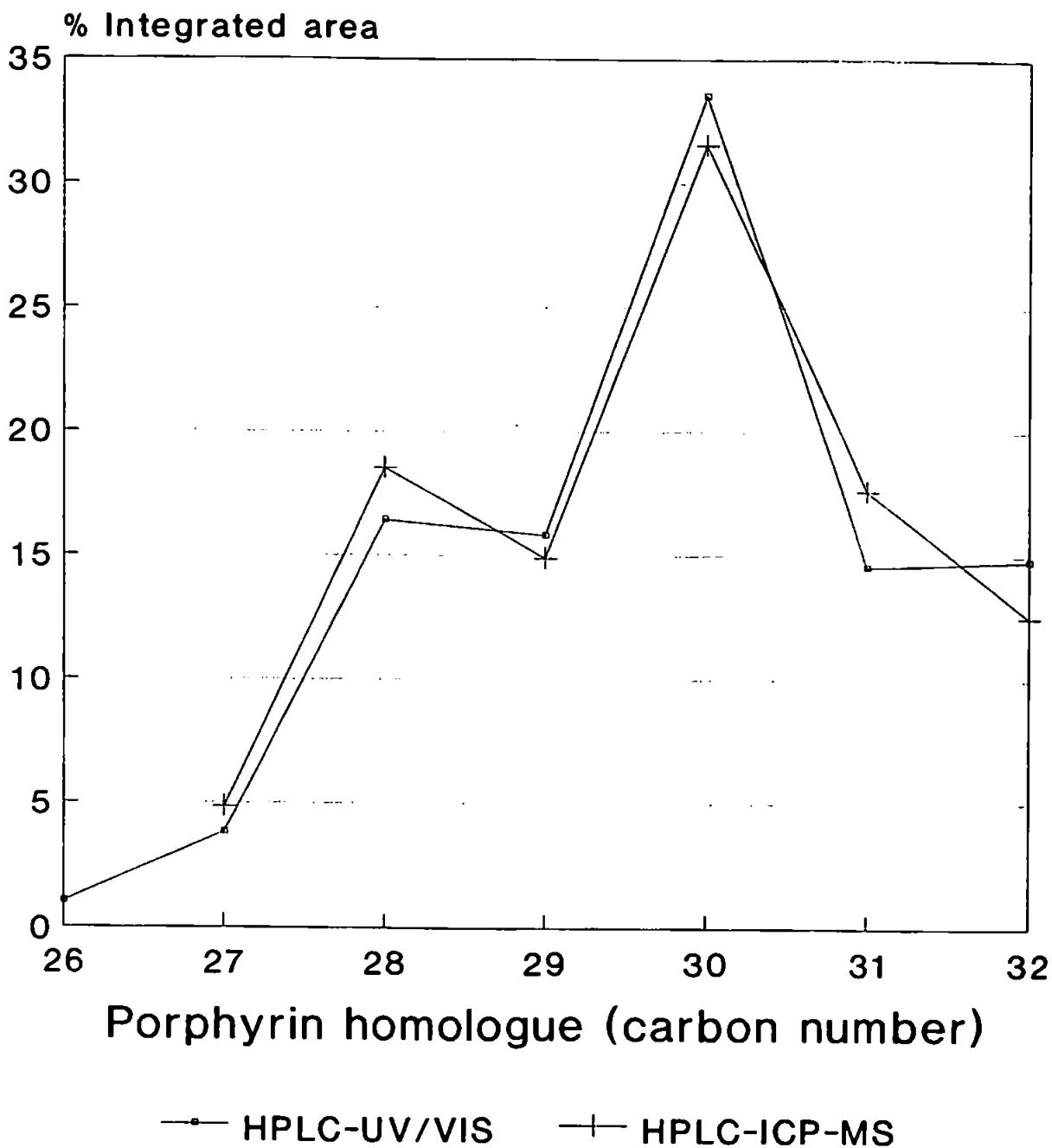
**Figure 4.7:** Comparison of Gedling coal gallium porphyrin distributions obtained using HPLC-UV/VIS and HPLC-ICP-MS

The quantitative data obtained are shown in Table 4.2. UV/VIS was used previously to estimate the concentration of the gallium porphyrins [4,5,10,142] and the data from those studies can also be compared with that obtained herein. The HPLC-ICP-MS results indicate a 3-4 fold higher gallium content than estimated both herein and previously using UV/VIS, but the gallium concentration obtained previously by UV/VIS for Bagworth coal (0.85 $\mu$g/g [10]) agreed closely with the value obtained in the present work (0.84 $\mu$g/g) by the same method. Thus, the UV/VIS method seems to be reproducible between different laboratories and analysts. However, UV/VIS estimations were calculated using an assumed extinction coefficient and a fixed molecular mass for the mixture [4,5,10,142]. This may account for the discrepancy between the values obtained by UV/VIS and HPLC-ICP-MS since the extinction coefficient will vary depending on the purity of the standard gallium porphyrin used to calculate it. For example, extinction coefficients used for the calculation of nickel and vanadyl geoporphyrin concentrations have been found to vary by a factor of ~2 [135,136,143-145].

The estimated detection limit for HPLC-ICP-MS of the gallium porphyrins was 64 pg/sec, calculated at $3\sigma$, but there was a 60% non-linear variation in the signal obtained for the standard injections over a period of 24 hours, as shown in Figure 4.8. The variation was probably due to carbon deposition and general cone wear as the analyses proceeded. The expansion pressure in the first stage vacuum of the ICP-MS was constant throughout

| COAL | Ga-porphyrin content[1] (UV/VIS) | Ga-Porphyrin content (HPLC-ICP-MS) | Relative standard deviation for (HPLC-ICP-MS) |
| --- | --- | --- | --- |
| Bagworth | 0.84 (0.85)[2] | 2.87 | 12.6 % (n=3) |
| Markham Main | 0.19 | 0.73 | 9.4 % (n=3) |
| Gelding | 0.12 | 0.38 | 21.4 % (n=3) |

1. Calculated using method in reference [10]

2. 0.85 $\mu$g/g from reference [10]

**Table 4.2:** Concentrations ($\mu$g/g) of gallium porphyrins in "standard" British coals using UV/VIS (400nm) and HPLC-ICP-MS (m/z 71) detection
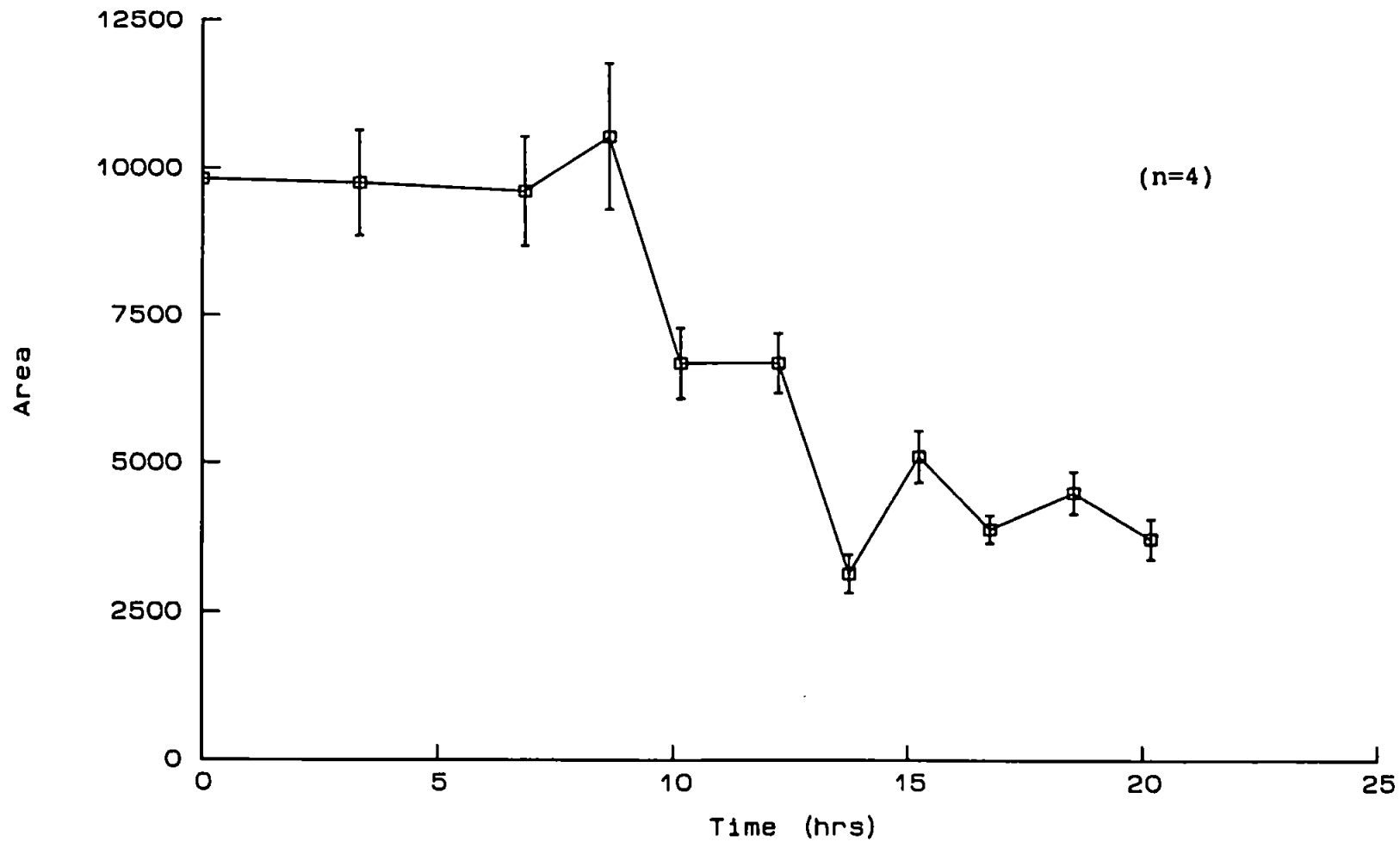
**Figure 4.8:** Drift of flow injected standard response over 24 hour period

the experiment which seemed to indicate no carbon deposition on the sampler cone, but on removal of the sampler cone substantial carbon build-up was evident and deposition of carbon behind the skimmer cone was later confirmed. The variation in RSD increased with the chronological order in which the samples were analysed. This variation, combined with the degradation in external standard signal with time is further evidence that carbon build up between the cones and/or cone wear are significant factors in causing a reduction in signal to noise ratio.

## 4.4 HPLC of Nickel Porphyrin Fractions of Julia Creek, Serpiano and Green River Oil Shales:

The shales were Soxhlet-extracted for 48 hours with a mixture of methanol and dichloromethane. The extract was then submitted to column chromatography using various solvents. The sample work-up procedures are described in detail in Chapter 7.

The HPLC-UV/VIS and HPLC-ICP-MS analyses were performed using the sample interface described earlier (Section 4.2.2), except that the silicone membrane was not used. A higher oxygen concentration was used in the nebulizer gas (3.0 %), which resulted in improved signal stability (6.95 % RSD for 12 flow-injections over 6 hours), but also resulted in accelerated cone wear. The nickel porphyrins were quantified by flow injection of [4,4′(ethane-1,2-diyldiimino)bis(pent-3-enonato)] nickel

(II) before and after each HPLC-ICP-MS chromatogram [146,147].

The nickel porphyrin distributions were complex, compared with those of the gallium porphyrins. The nickel is complexed to A, A-2 and A-4 porphyrin macrocycles (Section 3.2.2). However reverse phase HPLC allows the separation of A, A-2 and A-4 porphyrins and separation of homologues and isomers of these macrocycles. Nickel geoporphyrins appear not to have been analysed by HPLC-MS to date. Preliminary studies suggest they are too involatile and are therefore not vaporized by thermospray HPLC interfaces [102]. HPLC-MS using electrospray interfaces may however solve this problem, but as yet no work on this has been published. Thus, for identification of the various macrocycles co-injection studies are normally employed. No suitable authentic geoporphyrins were available to the author. Boreham *et al.* injected a number of authentic nickel porphyrins and correlated the retention times to identify the geoporphyrins in Julia Creek oil shale [19,56]. Thus, in the present work correlation of the data to that of Boreham *et al.*, using the same chromatographic conditions allowed a comparison to be made [19,56]. Probe-MS and HTGC-MS data were also used to verify these correlations. Without comparison with the mass chromatography, the assignments would not be possible, due to the large number of possible A-2 isomers and their variation in retention time [19,56].

Figures 4.9-4.11 show the HPLC chromatograms for the shales analysed, with tentative compound assignments. The distributions of the macrocycles in Julia Creek oil shale are
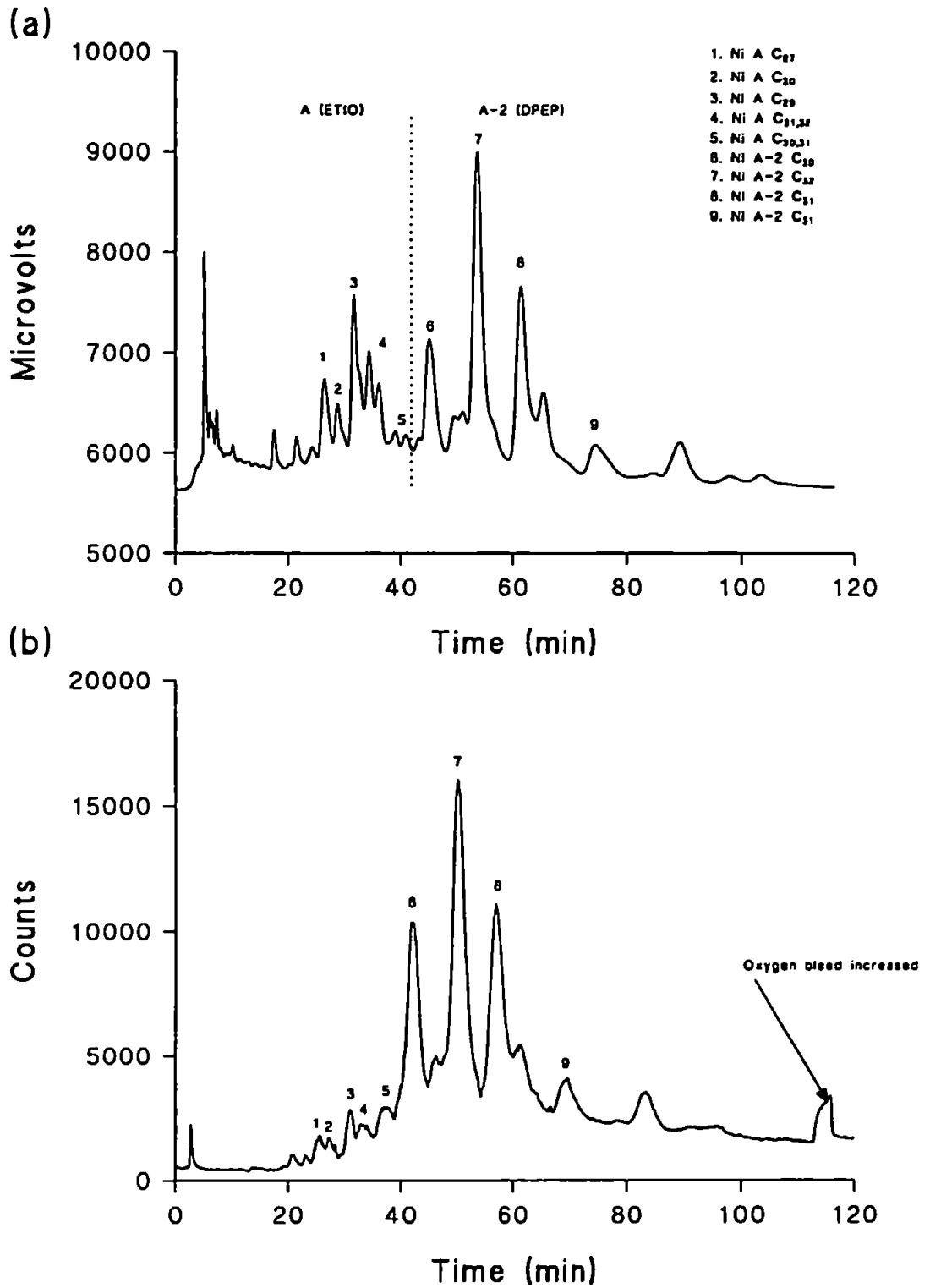
**Figure 4.9:** Comparison of HPLC-UV/VIS (a) and HPLC-ICP-MS (b) chromatograms for Julia Creek nickel porphyrins (108 $\mu$g injected)

**(a)**

A (ETIO)

A-2 (DPEP)

1. NI A $C_{27}$
2. NI A $C_{28}$
3. NI A $C_{29}$
4. NI A $C_{30,31,32}$
5. NI A-2 $C_{29}$
6. NI A-2 $C_{28}$
7. NI A-2 $C_{32}$
8. NI A-2 $C_{31}$

**(b)**
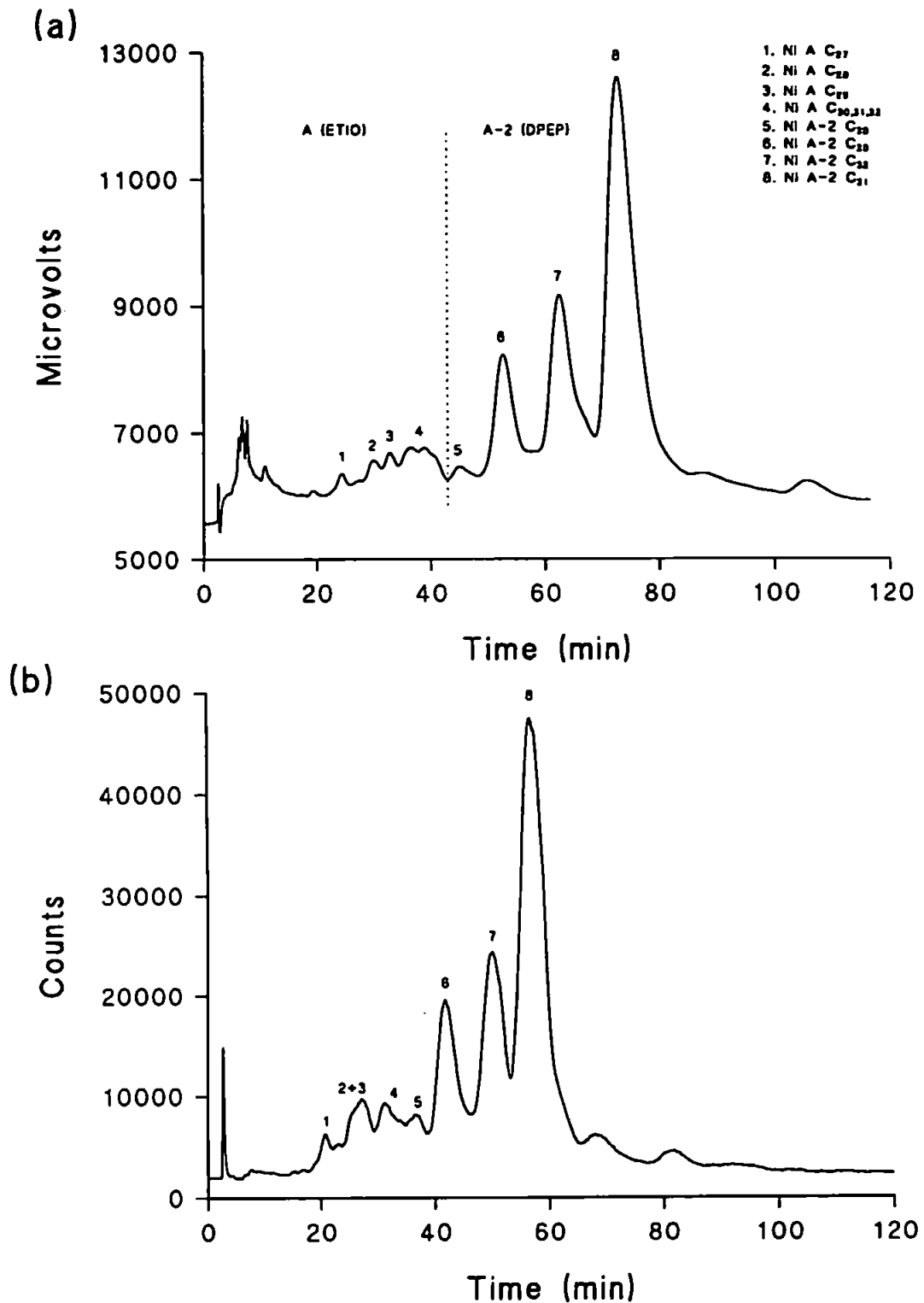
**Figure 4.10:** Comparison of HPLC-UV/VIS (a) and HPLC-ICP-MS (b) chromatograms for Serpiano nickel porphyrins (170 $\mu$g injected)
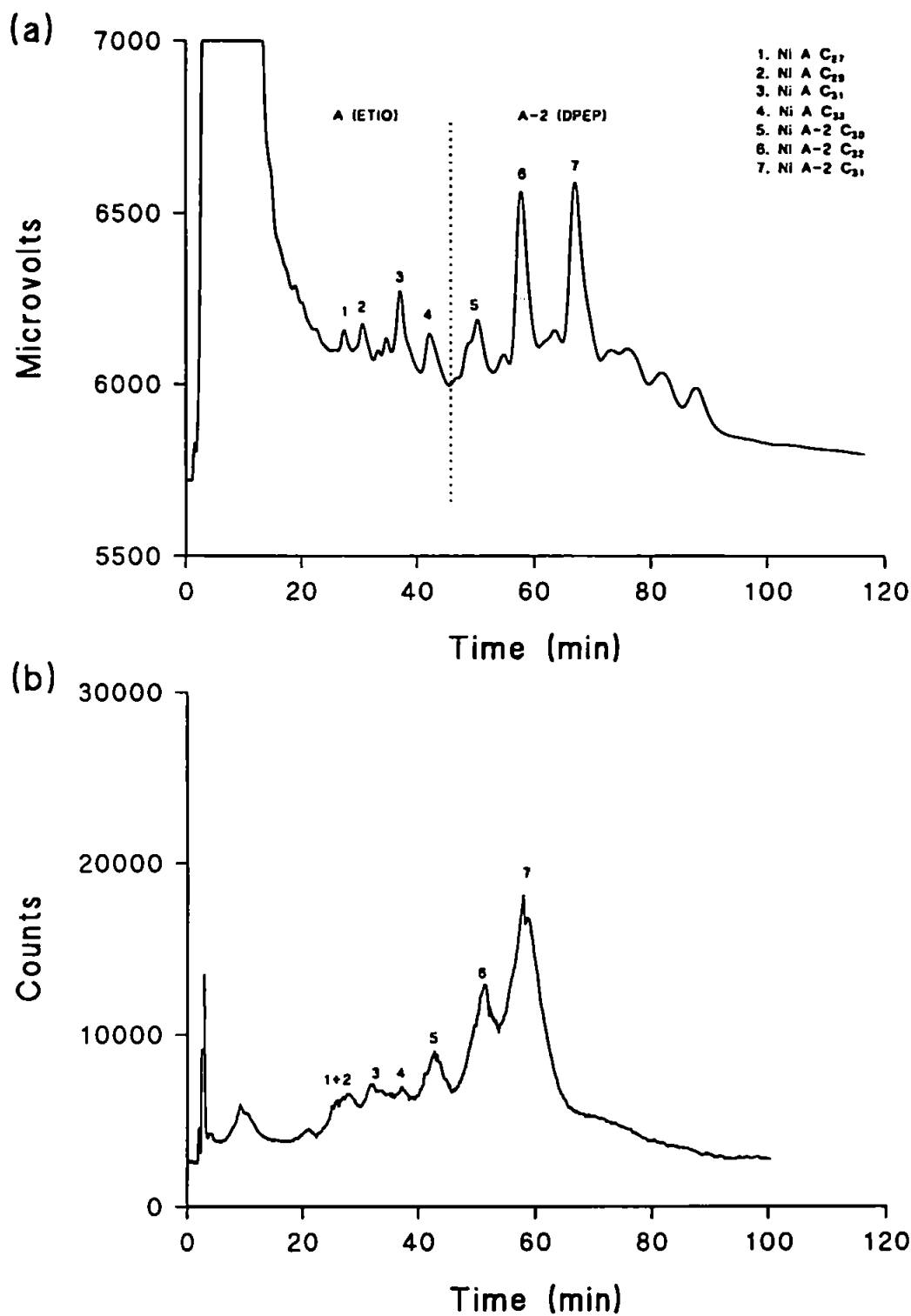
**Figure 4.11:** Comparison of HPLC-UV/VIS (a) and HPLC-ICP-MS (b) chromatograms for Green River nickel porphyrins (148 μg injected)

dominated by the A-2 macrocycles and the distribution of the A-2 $C_{30}$-$C_{32}$ (maximum $C_{32}$) can also be seen. The Serpiano distribution is also dominated by the A-2 macrocycles $C_{30}$-$C_{32}$ (maximum $C_{31}$), as is Green River Shale ($C_{30}$ to $C_{32}$; maximum $C_{30}$, $C_{32}$).

HPLC-ICP-MS and HPLC-UV/VIS analyses produced similar distributions for the Julia Creek and Serpiano oil shales, but the Green River Shale HPLC-ICP-MS and HPLC-UV/VIS did not correlate well. The distributions of the major A-2 homologues in the HPLC analyses are compared in Figure 4.12. The reason for the latter discrepancy was the fact that the "nickel" fraction analysed actually consisted of a mixture of both vanadyl and nickel porphyrins. The co-elution of vanadyl porphyrins in the UV/VIS chromatogram could possibly account for the differences between the UV/VIS and the ICP-MS chromatograms, since vanadyl and nickel porphyrins were both detected at 400 nm.

The quantitative results obtained from the HPLC-ICP-MS and UV/VIS (Chapter 7) are shown in Table 4.3. The results for the two methods do not agree, but this can probably be ascribed to the variation in the UV/VIS methods used (i.e. variation of extinction coefficient values). The extinction coefficient used to calculate the concentration of the nickel porphyrins was 22000, but values between 34000-22000 have been used [143-145,149,150]. Thus the UV/VIS results can be considered approximations of the actual concentration.
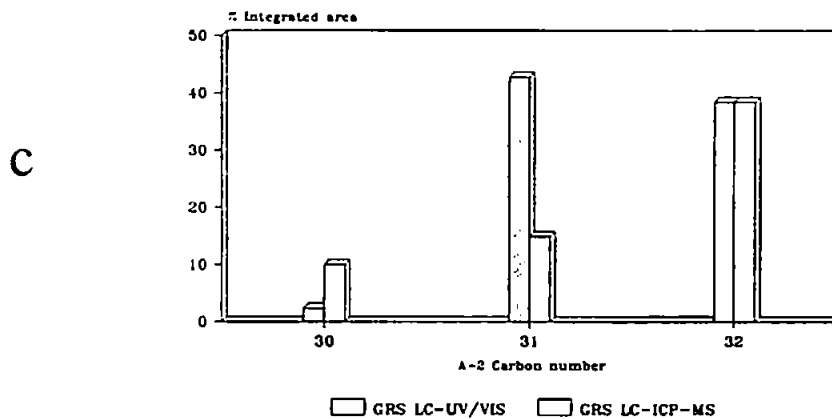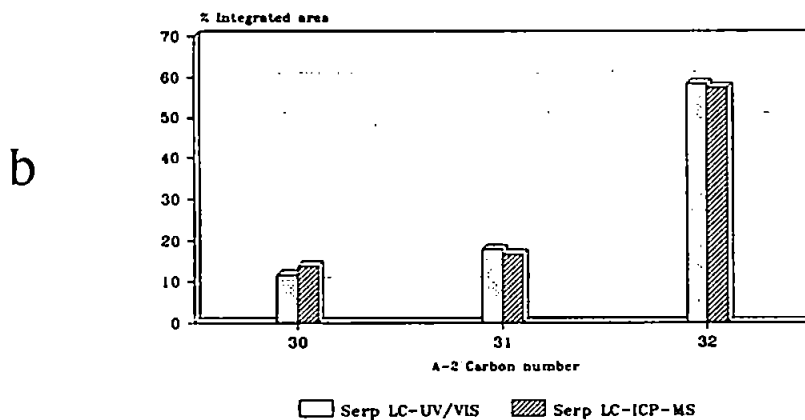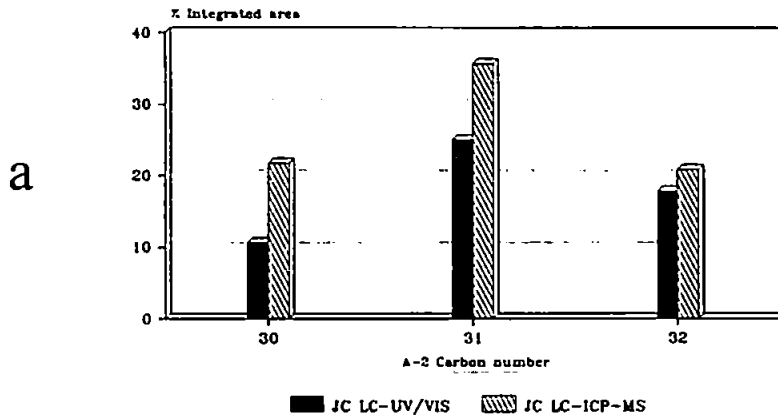
**Figure 4.12:** Comparison of nickel porphyrins, A-2 macrocycle ($C_{30}$ to $C_{32}$) distribution obtained from HPLC-UV/VIS and HPLC-ICP-MS (a) Julia Creek; (b) Serpiano; (c) Green River

| Shale | Nickel porphyrins $\mu$g/g Shale from HPLC-ICP-MS[1] | Nickel porphyrins $\mu$g/g Shale from UV/VIS[2] |
|---|---|---|
| Julia Creek | 14.9 | 16.3 |
| Serpiano | 119.8 | 51.5 |
| Green River | 2.5 | n/d |

1. Using average molecular mass of 532 (A-2 $C_{32}$)

2. Using extinction co-efficient of 2.2 x $10^4$ $cm^2mol^{-1}$ (550 nm) and average molecular mass 532 [149]

Table 4.3: Comparison of HPLC-ICP-MS and UV/VIS quantitative data for shales

Attempts to verify the presence of titanium porphyrins in Julia Creek oil shale were not successful; only the nickel porphyrins were detected. However, this may have been due to the chromatographic conditions, which were developed for optimal separation of nickel porphyrins. Hence titanium porphyrins may have been retained on the column [151].

## 4.5 Conclusions:

The separation of vanadyl porphyrins was not attempted since this would require the use of a mobile phase consisting of acetonitrile (47.5 %), methanol (47.5 %) and water (5 %). This mobile phase would not allow normal operation of the plasma, for reasons explained in Section 1.3 (plasma instability). HPLC-ICP-MS was thus used to analyse gallium and nickel geoporphyrins in coals and shales. The high efficiency of the chromatographic separations observed by HPLC-UV/VIS was maintained, with less than 10 % loss in efficiency due to the interfacing of HPLC with ICP-MS. This represents significantly better chromatography-ICP-MS than previously reported for metallo-species.

The presence of gallium porphyrins in three British coals was confirmed and quantified. The distributions of the porphyrin macrocycles was also determined and showed excellent agreement with the HPLC-UV/VIS distributions.

The nickel porphyrin fractions of Julia Creek, Serpiano and

Green River oil shales were quantified. The distributions of these obtained for Julia Creek and Serpiano with HPLC-ICP-MS and HPLC-UV/VIS showed good agreement.

The problems encountered with the nebulization of the methanol mobile phase into the plasma were solved by the use of higher oxygen/argon mixtures in the nebulizer gas. This solved the problems encountered with instrumental drift, but also considerably shortened the lifetime of the nickel sampling cones.

# 5.0 GC-LOW PRESSURE-ICP-MS:

## 5.1 Introduction:

Gas chromatography coupled to low pressure-plasma-MS with helium microwave induced plasmas has been investigated by a number of workers [151-153] but there appears to have been only one study of an argon inductively coupled plasma-MS [110]. The low pressure $^4$He plasma has probably been preferred to the $^{40}$Ar plasma because the former results in reduced polyatomic interferences [154].

The main advantage of using a low pressure helium or argon plasma is a reduction in the number of polyatomic species formed by entrainment of air [154]; hence the background for chlorine, phosphorus and sulfur are reduced (Table 1.2). The reduction of the background occurs because of the reduced concentration of nitrogen and oxygen polyatomics formed in the low pressure system. These elements occur in important analytes in the environment. A further advantage of using a low pressure plasma source is that the plasma can be generated at a lower power than under atmospheric conditions. Typically 1.5 kW is required for generation of an ICP under atmospheric conditions whereas only 10-350 W are required for generation of a low pressure ICP.

Another advantage of low pressure argon plasmas is that only

minor modifications to standard ICP-MS instrumentation are required, whereas with helium at least the plasma matching network and torch box have to be replaced.

Most research with GC-low pressure plasma-MS has focused on the use of the source for element selective analysis [151-154,110]. However, the use of lower powers with low pressure plasma sources has enabled a number of workers to use low pressure-MIP-MS for "soft" ionization [155-157]. Heppner *et al.* investigated a MIP formed with helium and hydrogen at between 30-150 W forward power and a pressure of 10-20 torr (1.3-2.6 kPa) [155]. The analytes were introduced into the MIP via a capillary GC column and the plasma gas sampled by a mass spectrometer. The sampled gas was ionized using electron impact conditions and the fragments analysed using a mass spectrometer. The fragments detected were essentially $CH^+$, $CH_4^+$, $CO^+$, which suggested that the analytes were destroyed in the MIP, with recombination of the constituent elements occurring in the sampling region. Poussel *et al.* utilized a MIP formed with argon, xenon or krypton at powers of 25-50 W and at pressures between 0.02-0.06 mbar (2-6 Pa) [156]. The analytes were introduced into the tail-flame of the MIP discharge where they fragmented and ionized. The fragments where then extracted into a mass spectrometer through a skimmer cone. The spectra obtained for the analytes were similar to those obtained with EI ionization. Olson *et al.* also introduced analytes into the tail flame of a MIP discharge and obtained spectra similar to EI spectra [157]. However, when the analytes were introduced through the whole length of the MIP discharge,

molecular ions disappeared and mono-atomic ions where observed.

Thus MIP-MS systems have the potential to produce both atomic and molecular ions, but no work of this nature appears to have performed previously using low pressure ICP-MS.

## 5.2 Design and Construction of a Gas Chromatography-Low Pressure-Inductively Coupled Plasma-Mass Spectrometry interface :

The ICP-MS instrument used was a VG PlasmaQuad II modified in several ways. The pumping rate at the interface was increased from 44 L/min to 75 L/min by the addition of a second pumping port at 135° to the original port, linked to the same rotary vacuum pump (Edwards E1M-18, Edwards High Vacuum).

The standard sampling cone was replaced with a low pressure sampler machined from aluminium (Machine Shop, University of Plymouth, U.K.), with a 2 mm orifice and a threaded male fitting onto which a ½" *Ultra-Torr*$^{tm}$ (Swagelok, U.S.A.) fitting was attached (Figure 5.1) [151-153]. The *Ultra-Torr* fitting consists of a silicone o-ring compressed onto the silica tube by a stainless steel ferrule, providing a vacuum seal. Using this design it was possible to form a vacuum seal between the low pressure torch and sampler.

The torch was constructed from ½" silica tubing (140 mm long)

with a ¼" sidearm through which the plasma gases were introduced (Figure 5.1). The vacuum was maintained in the torch using a ½" to 1/16" *Ultra-Torr* reducing union for the end of the torch and ¼" *Ultra-Torr* union was used for the sidearm. A 1/16" stainless steel tube was inserted into the torch and extended to within 25 mm of the plasma. This served to support and centralize the GC capillary column. The capillary column was connected to the 1/16" stainless steel tube using a 1/16" Swagelok union.

The transfer line was that used in the original interface design of the atmospheric system (Section 2.1, Figure 2.2). The GC system was as described in Section 2.2. To eliminate dead volume, no switching valve system was used to vent solvent, in this work

Typical operating conditions and data acquisition parameters are shown in Table 5.1.

## 5.3 Optimisation of the GC-Low Pressure-ICP-MS System:

GC carrier gas and plasma gas flow had pronounced effects on the performance of the system.

Initially the GC was operated at a carrier gas head pressure of 42.5 kPa. At this pressure the carrier gas caused a slight indentation at the base of the plasma. The peaks obtained using this head-pressure were ~20 seconds wide [base peak width; Figure 5.2 (a)]. On increasing the head pressure to 54.5 kPa,
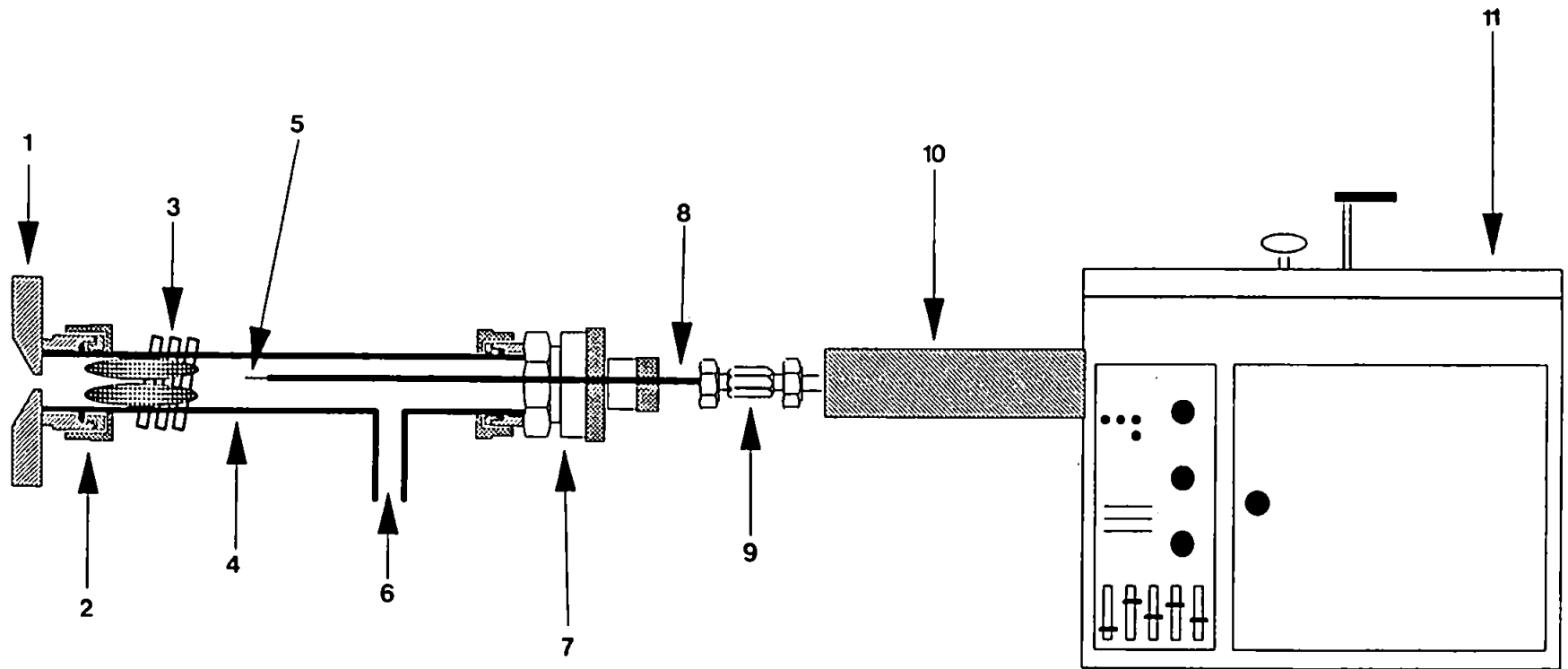
**Figure 5.1:** GC-LP-ICP-MS interface: 1. aluminum sampler cone; 2. $\frac{1}{2}$ inch ultra torr fitting; 3. load coil; 4. $\frac{1}{2}$ inch silica torch; 5. tip of capillary column; 6. side arm argon inlet; 7. $\frac{1}{2}$-$\frac{1}{4}$ inch ultra torr reducing union; 8. s/steel tube for supporting capillary column; 9. zero dead volume union; 10. transfer line; 11. GC

| | Element selective detection | Molecular fragmentation |
|---|---|---|
| Forward power (W) | 200 | 20-50 |
| Reflected power (W) | 35 | 7-30 |
| Plasma gas flow (l/min Ar) | 1.0 | 0 |
| Pressure in interface (mbar) | 2.1 | not measured |
| Pressure in torch (mbar) | 13 | not measured |
| Mode | Single ion | Peak jumping |
| No. of masses | 1 | 150 |
| Points per mass | n/a | 1 |
| Mass range (m/z) | n/a | 60-209 |
| Dwell time (ms) | 164 | 1.28 |
| No. of sweeps per time slice | n/a | 2 |
| No. of channels | 4096 max | n/a |

**Table 5.1:** Typical operating conditions used for LP-ICP-MS.
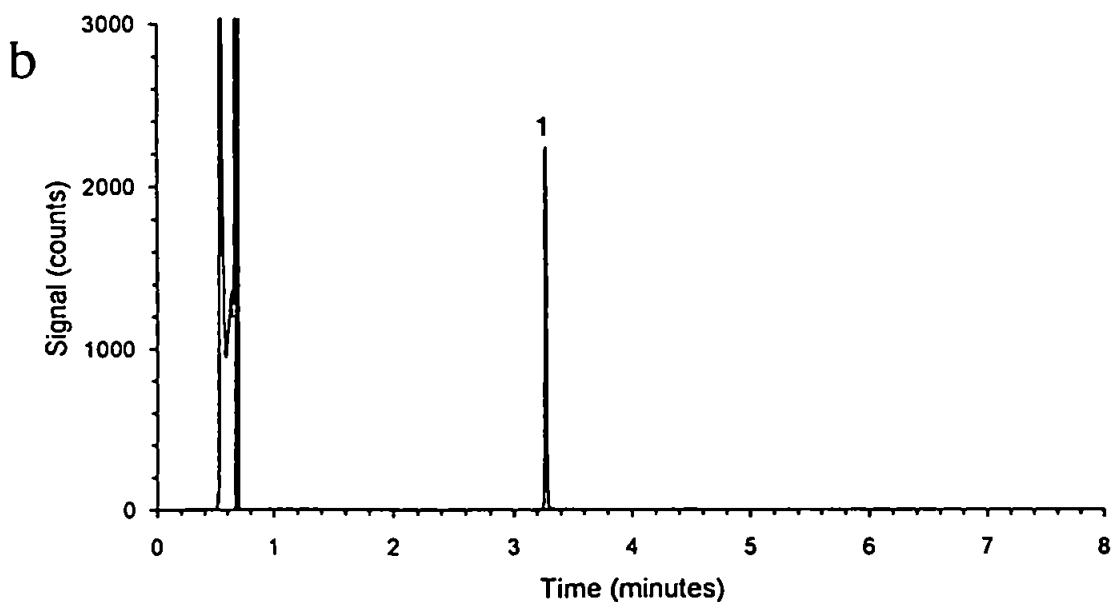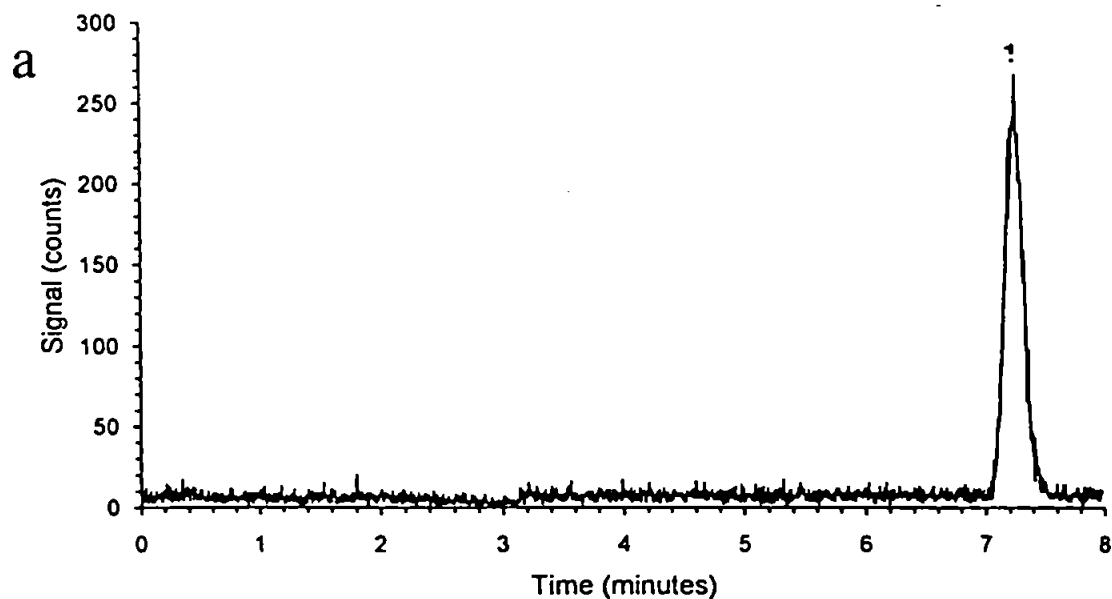
**Figure 5.2:** Effect of helium carrier gas head pressure on band broadening; chromatograms for tetraethyl lead (1; 10 ng on column at) (a) 42.5 kPa (~2.5 ml/min) and (b) 54.5 kPa (~3.0 ml/min); DB-5 column (30 m, $0.1 \mu m$ film thickness), 50°C to 210°C at 20°c/min

the carrier gas punctured the plasma and an annular shaped plasma was obtained which was clearly visible when the solvent eluted from the column. The peak width at 54.5 kPa was decreased to ~3 seconds [Figure 5.2 (b)], thus the column efficiency was increased from ~7500 (~195°C) to ~69500 (~116°C) plates (calculated using equation 4.1, p. 151). The increased flow rate (due to the increase head-pressure) caused increased column efficiency but this increase cannot account completely for the ~ 9 fold increase in efficiency. The band broadening due to the dead volume in the plasma torch must also have been reduced due to the plasma being punctured. This also contributed towards the increased efficiency of the column, thus a head-pressure of 54.5 kPa was used.

The plasma gas flow rate was a critical parameter with regard to the analytical utility of the low-pressure ICP. The effect of plasma gas flow on the elemental signals for bromobenzene (monitored at m/z 79) and tetraethyl lead (monitored at m/z 208) are shown in Figure 5.3.

Evidently the effect on signal was dependent on the analyte. The signal for tetraethyl lead was not detectable below a flow rate of 0.600 L/min, whereas the bromobenzene signal was unaffected, and was considerably enhanced when the flow was reduced to 0.200 L/min. A similar effect was observed for chloro- and iodobenzene. Several explanations may be offered for the contradictory behaviour of the two compounds, but first a few descriptive notes on the effect of gas flow on the plasma are necessary. At a gas flow of 0.200 L/min the plasma was
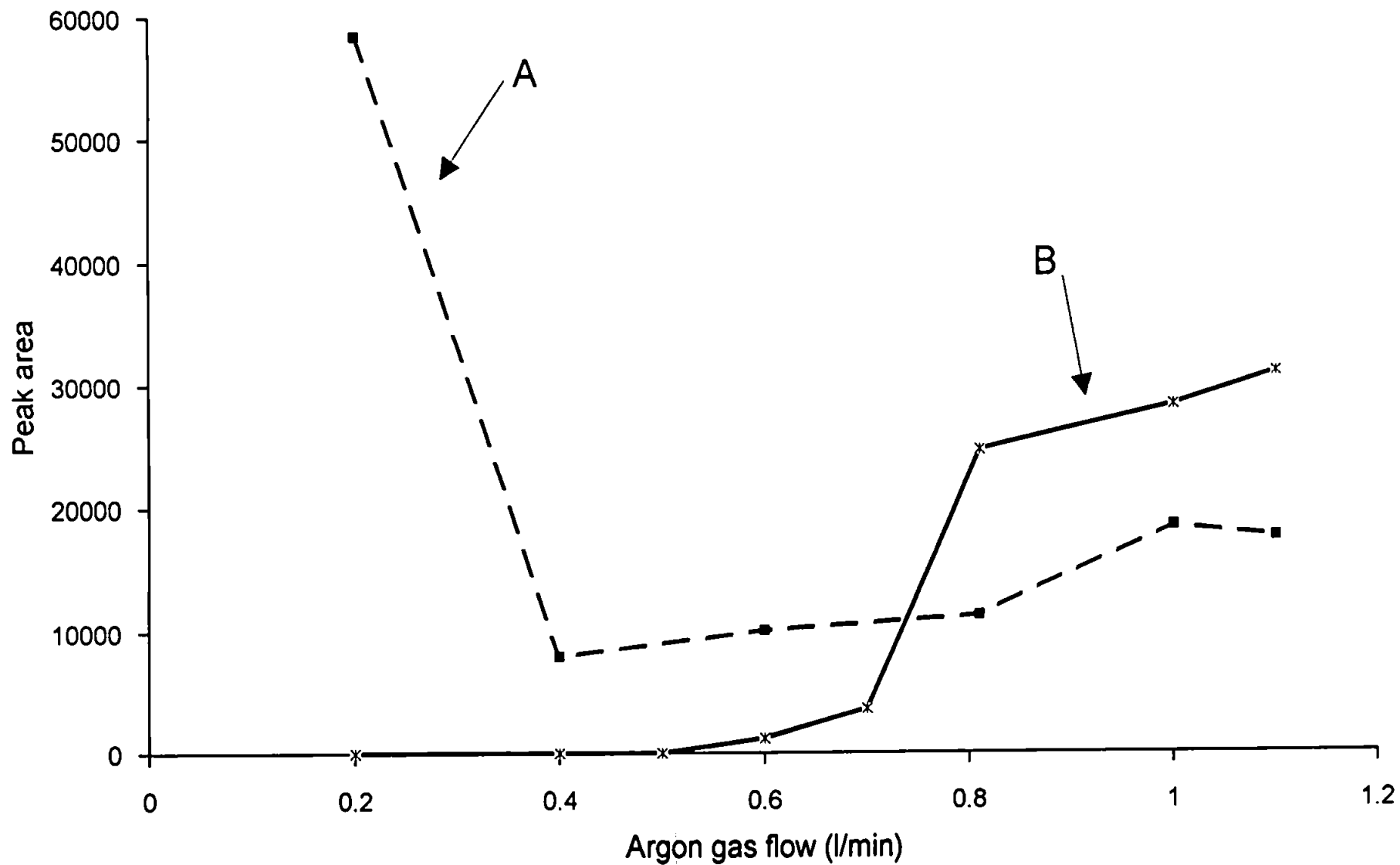
**Figure 5.3:** Effect of plasma gas flow on peak area; A= Bromobenzene monitored at m/z 79 (10 ng on column), B= Tetraethyl lead monitored at m/z 208 (10 ng on column); Gc conditions as in Figure 5.2

quite diffuse and extended to the tip of the GC column. As the gas flow rate was increased, the base of the plasma was pushed further forward and the plasma became progressively denser and brighter, until it was confined completely within the load coil at a gas flow greater than 0.800 L/min. Hence, the effect of the gas flow was to condense the plasma at higher flows, thereby increasing the energy density and number density of electrons and ions. This could have affected the ionisation of these analytes.

The effect of the gas flow on the sampling and skimming processes of ions from the plasma into the mass spectrometer must be considered as a possible explanation for the differing behaviour of the two analytes. The sampling/skimming interfaces for plasma-MS were designed using criteria derived from molecular beam studies [69]. The plasma gas is sampled from a relatively high pressure environment through an orifice into a low pressure expansion chamber. In the expansion chamber the gases undergo adiabatic expansion and form a barrel shock region. Within the barrel shock region is the so-called "zone of silence" which is thought to be representative of the sampled plasma gases. The barrel shock takes the form of a cone with the apex at the orifice of the sampler cone. At the base of the cone is a diffuse collisional region, where the expanding gas meets the background gas, known as the "Mach disc". In order to obtain the greatest ion throughput to the mass spectrometer, the gases must be sampled within the zone of silence and upstream of the Mach disc. The position of the Mach disc is dependent on the pressure differential between the

sampled gas and the gas in the expansion chamber; and the orifice diameter, as shown below [73].

$$X_m = 0.67 \ D_0 \ (P_o/P_1)^{\frac{1}{2}} \quad \text{Equation 5.1}$$

Where $X_m$ is the distance of the Mach disc downstream of the sampling orifice in metres; $D_0$ is the diameter of the sampling orifice in metres, i.e. 0.002 m; $P_0$ is the pressure in the torch in pascals; and $P_1$ is the pressure in the expansion stage of the interface.

In this work, pressure measurements were made in the low-pressure torch and the expansion chamber at different plasma gas flows using a Pirani gauge and the position of the Mach disc calculated using the above equation. The effect of gas flow on the position of the Mach disc is shown in Figure 5.4. It is evident that the gas flow had very little effect on the position of the Mach disc (i.e. the $P_0/P_1$ ratio remained relatively constant).

The skimming distance used for this work was ~4.5 mm, so the expanding gases were skimmed downstream of the Mach disc. This means that the skimmed ions were not necessarily representative of those in the sampled plasma because of the likelihood of collisional processes occurring outside the zone of silence.

Apart from illustrating that skimming was performed non-optimally in this work, this illustrates the possibility that many processes may be contributing to ion formation and
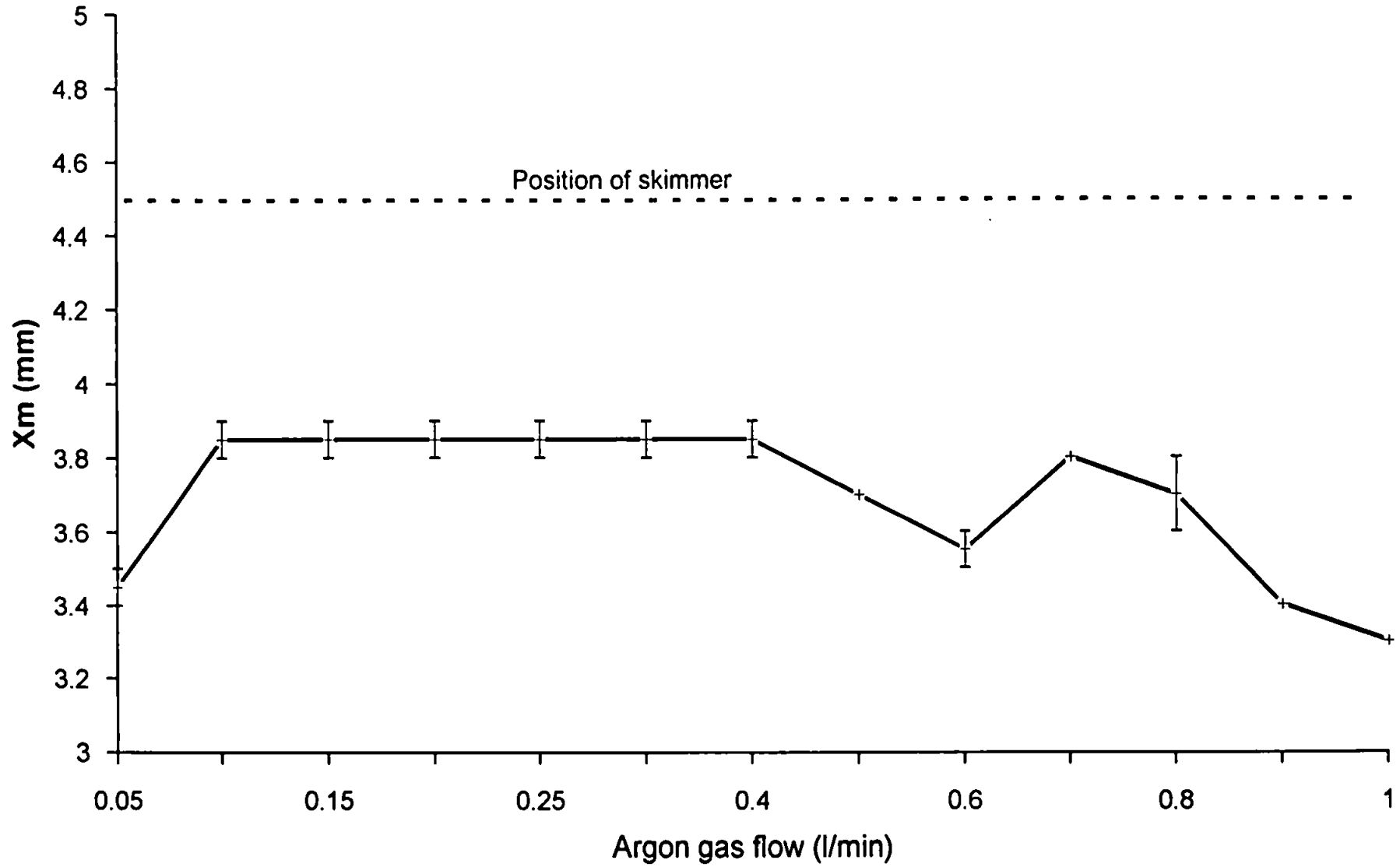
**Figure 5.4:** Effect of plasma gas flow on the position of the "Mach disc"

collisional recombination, both in the plasma itself and in the expansion chamber may be occurring. Hence it is conceivable that the compounds could behave differently and undergo varying degrees of dissociation and/or recombination when skimmed outside the zone of silence.

Another possible explanation is that the bromobenzene was not completely converted into the constituent elements. Thus the benzene ring could have been partially hydrogenated to form a molecular fragment with a mass of m/z 79.

## 5.4    Element Selective Analysis:

### 5.4.1    Analysis of Chlorobenzene, Bromobenzene, Iodobenzene, Ferrocene, Tetrabutyl-tin and Tetraethyl lead:

Table 5.2 shows the results of the analysis of chlorobenzene, bromobenzene, benzylbromide, iodobenzene, ferrocene tetrabutyl-tin and tetraethyl lead. The detection limits were all below 1 ng on-column. Typical chromatograms for ferrocene, tetrabutyl-tin, chlorobenzene, bromobenzene, benzylbromide and iodobenzene are shown in Figure 5.5 (a)-(e). The peaks within the first minute of each chromatogram are due to elution of solvent and are presumably caused by a combination of the quenching effect of the solvent on the plasma, dissociation, and subsequent recombination in the expansion stage. The solvent perturbed the plasma, but did not extinguish it and the plasma returned to its normal state after the solvent had
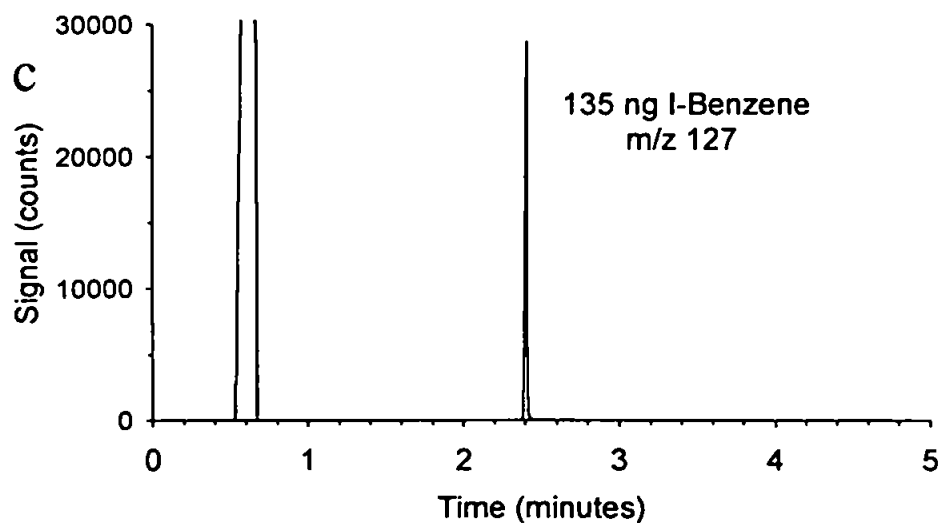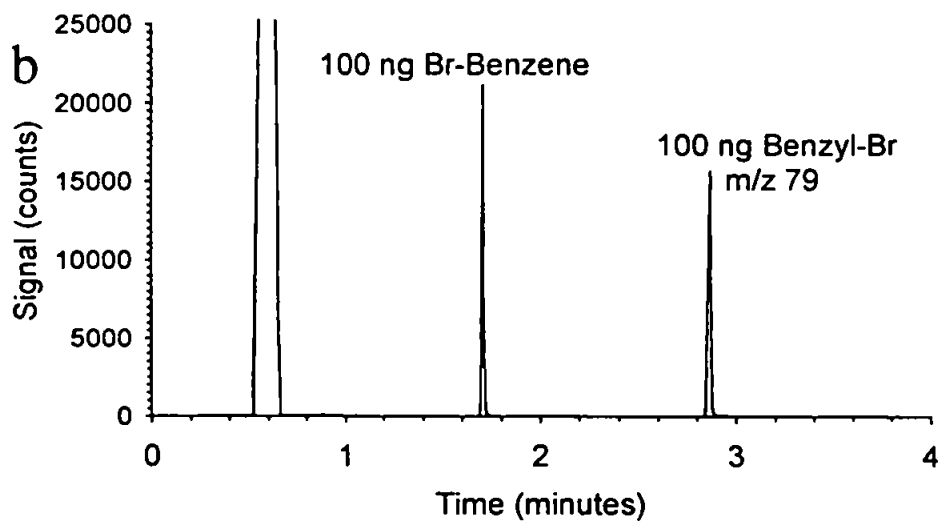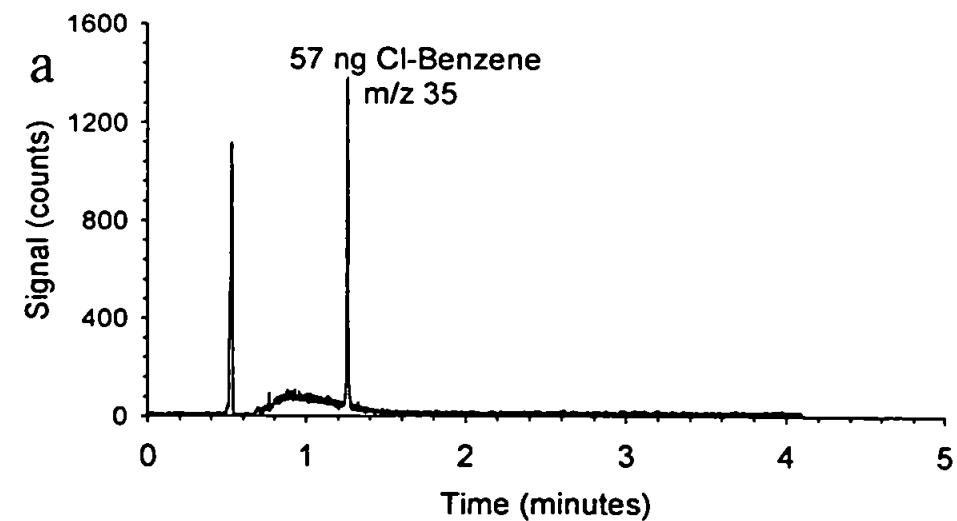
**Figure 5.5:** Typical chromatograms obtained for (a) chlorobenzene; (b) bromobenzene and benzyl bromide; (c) iodobenzene; (d) ferocene; (e) tetrabutyl tin

d

**10 ng Ferrocene**
**m/z 56**

e

**55 ng Tetrabutyl-Sn**
**m/z 120**
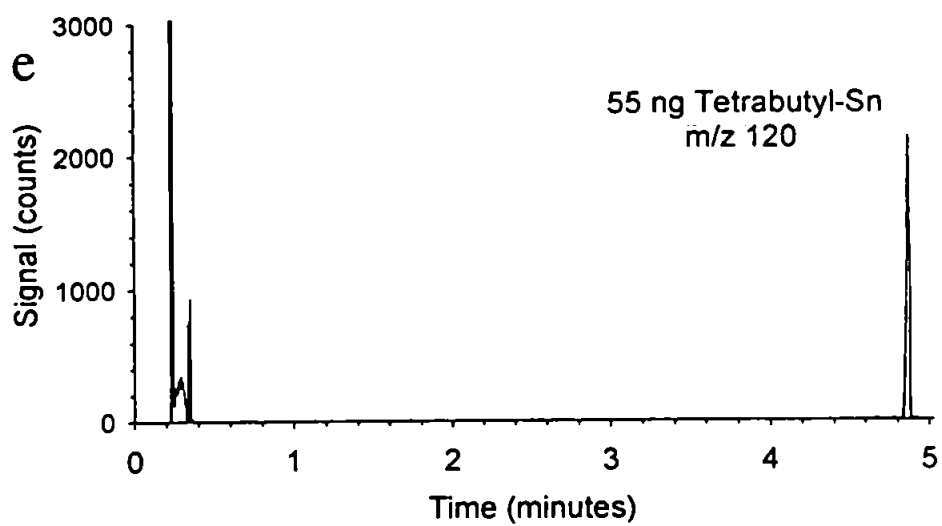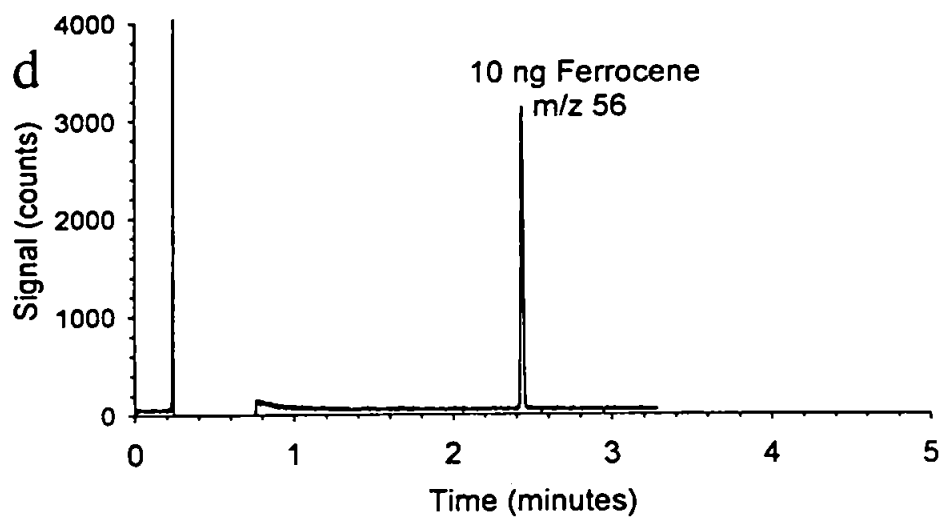
**Figure 5.5:** (continued)

| Compound | m/z monitored | Detection limit (pg) |
|---|---|---|
| Chlorobenzene | 35 | 500[*] |
| Ferrocene | 56 | 33[#] |
| Bromobenzene | 79 | 50[*] |
| Tetrabutyl-tin | 120 | 35[#] |
| Iodobenzene | 127 | 25[*] |
| Tetraethyl lead | 208 | 13[#] |

[*] 3X signal to noise; [#] 3X standard deviation of blank

**Figure 5.2:** Detection limits obtained for a selection of standards, using element specific detection.

eluted. This offers a significant advantage over the MIP system for which solvent venting has to be employed [151-153].

A calibration curve for tetraethyl lead was linear over 2 orders of magnitude (Figure 5.6). The relative standard deviation in peak area over a five hour period for repeat injections of tetraethyl lead was 6.1 %. The signal stability for the low-pressure system was monitored over several days with the peak area remaining within 15 %. This is considerably more stable than the atmospheric GC-ICP-MS [158].

### 5.4.2 Analysis of lead in naphtha and petrol:

Chromatograms for a naphtha and a petrol sample monitored at m/z 208 (major lead isotope) and m/z 12 (major carbon isotope) are shown in Figures 5.7 and 5.8, respectively.

The GC-FID chromatogram for the naphtha sample is shown in Figures 5.7 (c). This closely resembles the m/z 12 mass chromatogram obtained, thus illustrating the minimal band broadening obtained with the GC-LP-ICP-MS interface. The high background for the m/z 12 chromatograms may have been due in part to residual carbon deposited on the torch walls by the solvent.

### 5.5 Analysis of Metalloporphyrins:

The interface was modified for the analysis of metalloporphyrins by use of a shorter torch (100 mm) and
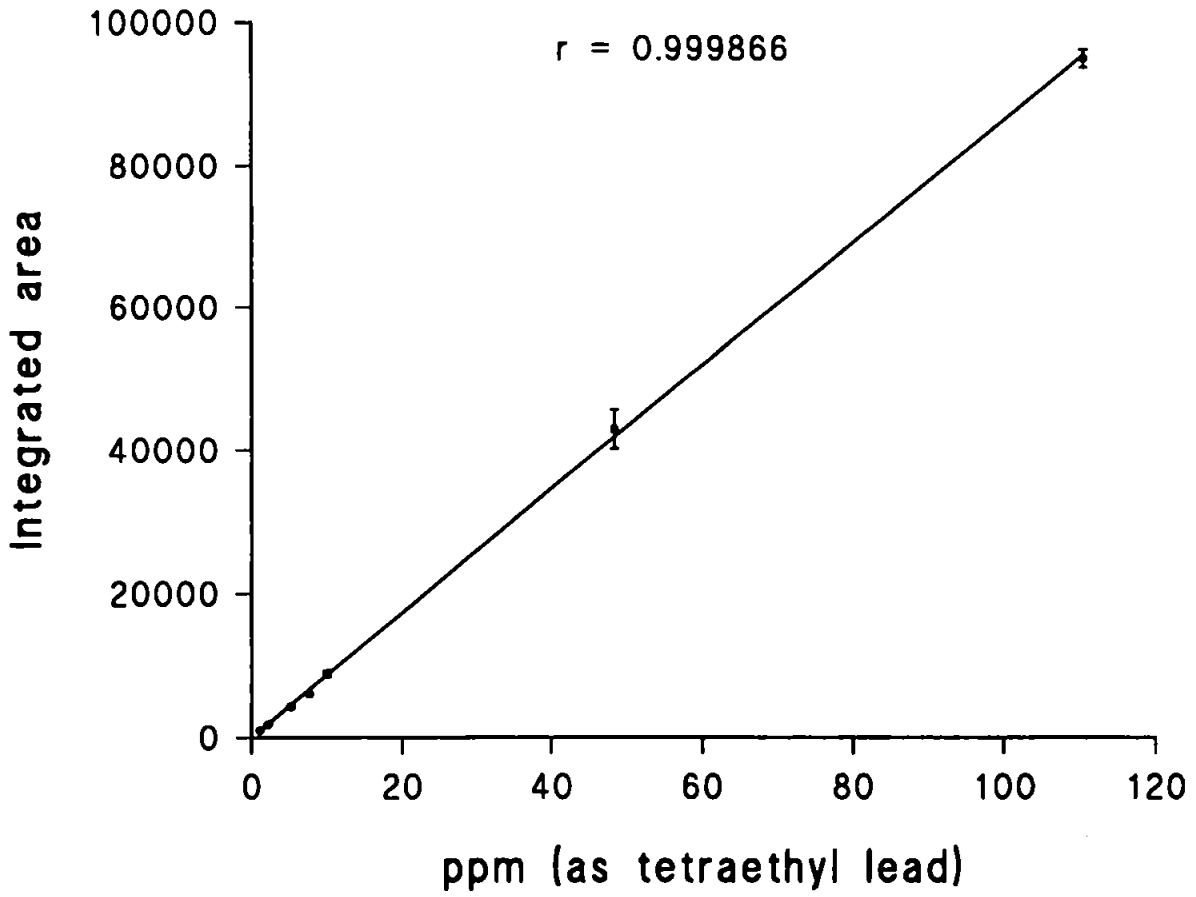
**Figure 5.6:** Calibration curve for tetraethyl lead (monitored at m/z 208)
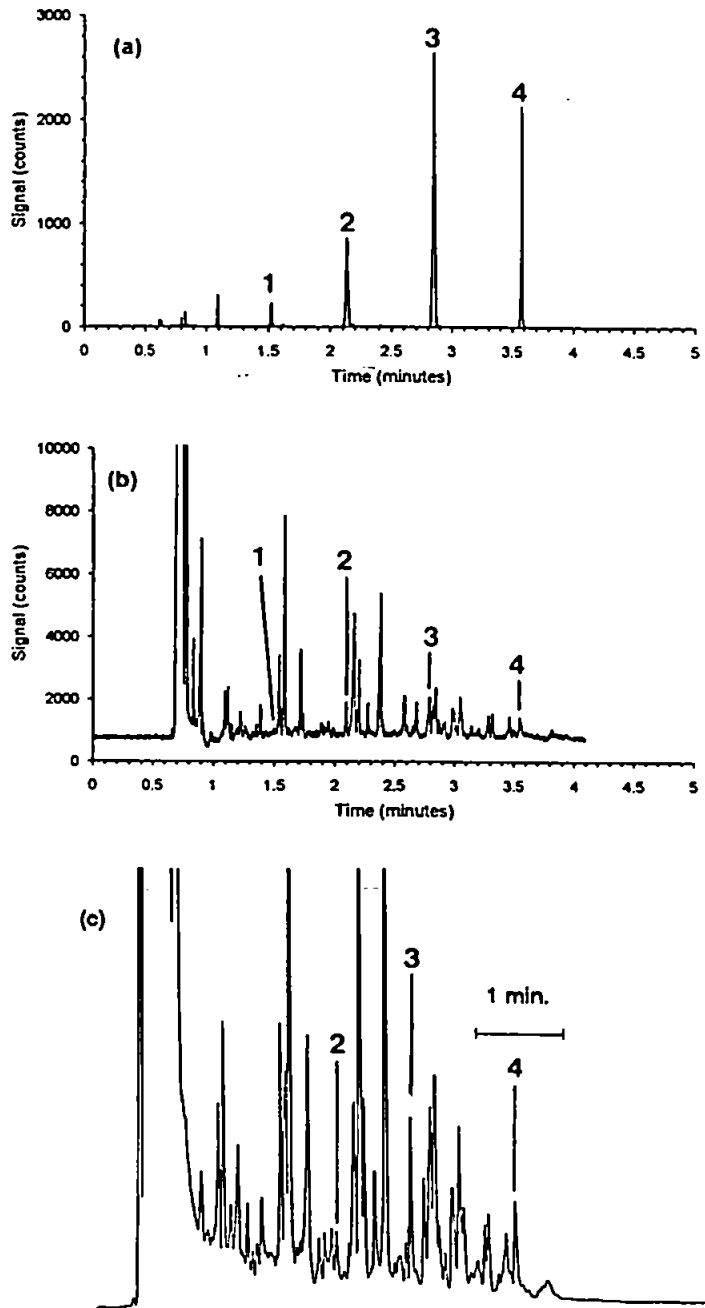
**Figure 5.7:** Lead species in Naphtha; monitored at (a) m/z 208 for lead; (b) m/z 12 for carbon and (c) with GC-FID for comparison with m/z 12; 1= $PbEtMe_3$, 2= $PbEt_2Me_2$, 3= $PbEt_3Me$, 4= $PbEt_4$; GC conditions as in Figure 5.2
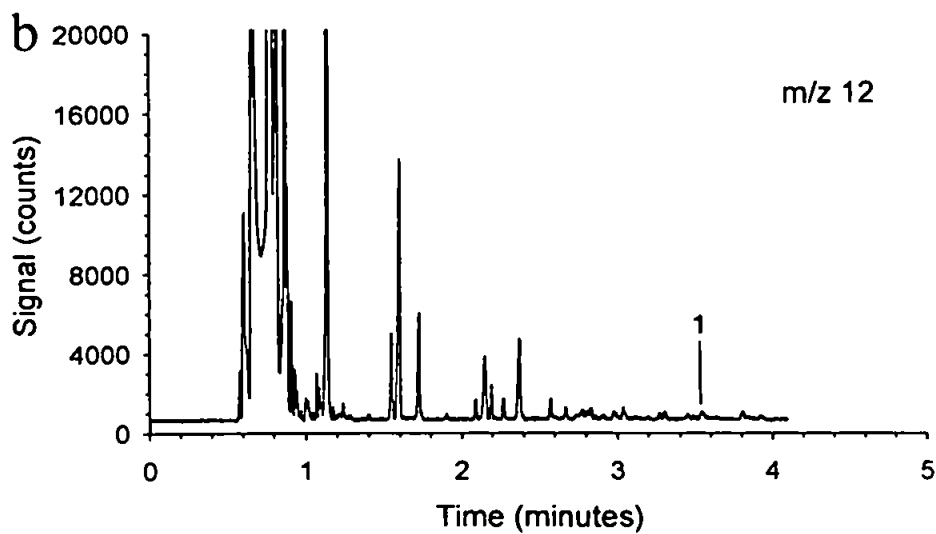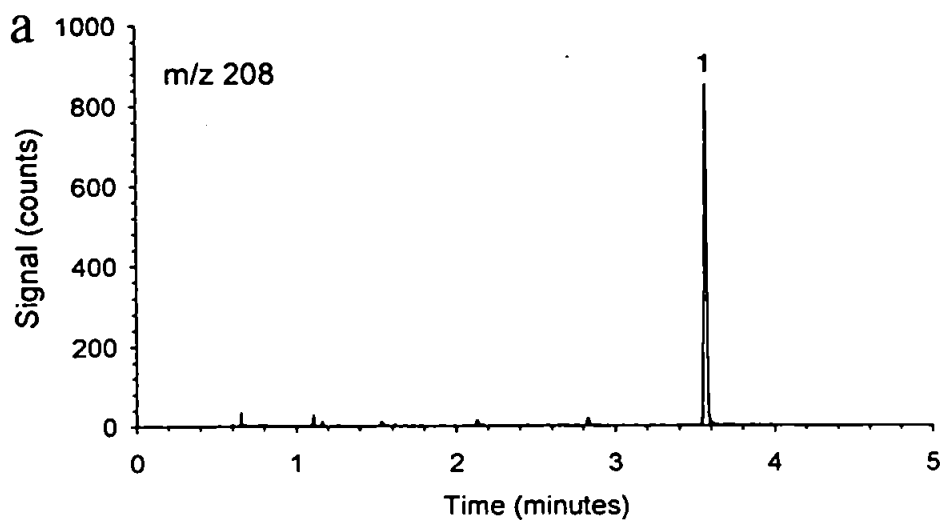
**Figure 5.8:** Tetraethyl lead in petrol; monitored at m/z 208 and m/z 12; 1= PbEt$_4$; GC conditions as in Figure 5.2

insulation of the torch as far as possible with industrial pipe lagging.

The attempts to analyse porphyrins with the GC-LP-ICP-MS system proved fruitless. The unreliablity of the gas chromatography (Section 3.7) made it difficult to assess whether the interface and/or the chromatography was the problem. Analysis of metalloporphyrins was therefore not pursued further.

## 5.6 Molecular Fragmentation Studies:

The low-pressure plasma can be sustained using powers < 50 W. Thus, if the power could be lowered to a point where the plasma no longer causes atomization and ionization of the analyte, it should be possible to observe molecular species of the compound. The work that follows is a preliminary investigation into this possibility.

The fragmentation of four compounds was studied using helium and in one case argon, as the plasma gas. The main problem encountered with the low pressure argon plasma was the polyatomic interferences that arose due to combination of the analyte fragments with argon. The spectra obtained were difficult to interpret due to the presence of these polyatomic species. Figure 5.9 shows the spectrum obtained for bromobenzene with the argon plasma. It was necessary to inject a large amount of analyte in order to study the fragments, since the majority of the analyte was destroyed. Although the spectra were complex and difficult to interpret, some fragments

195
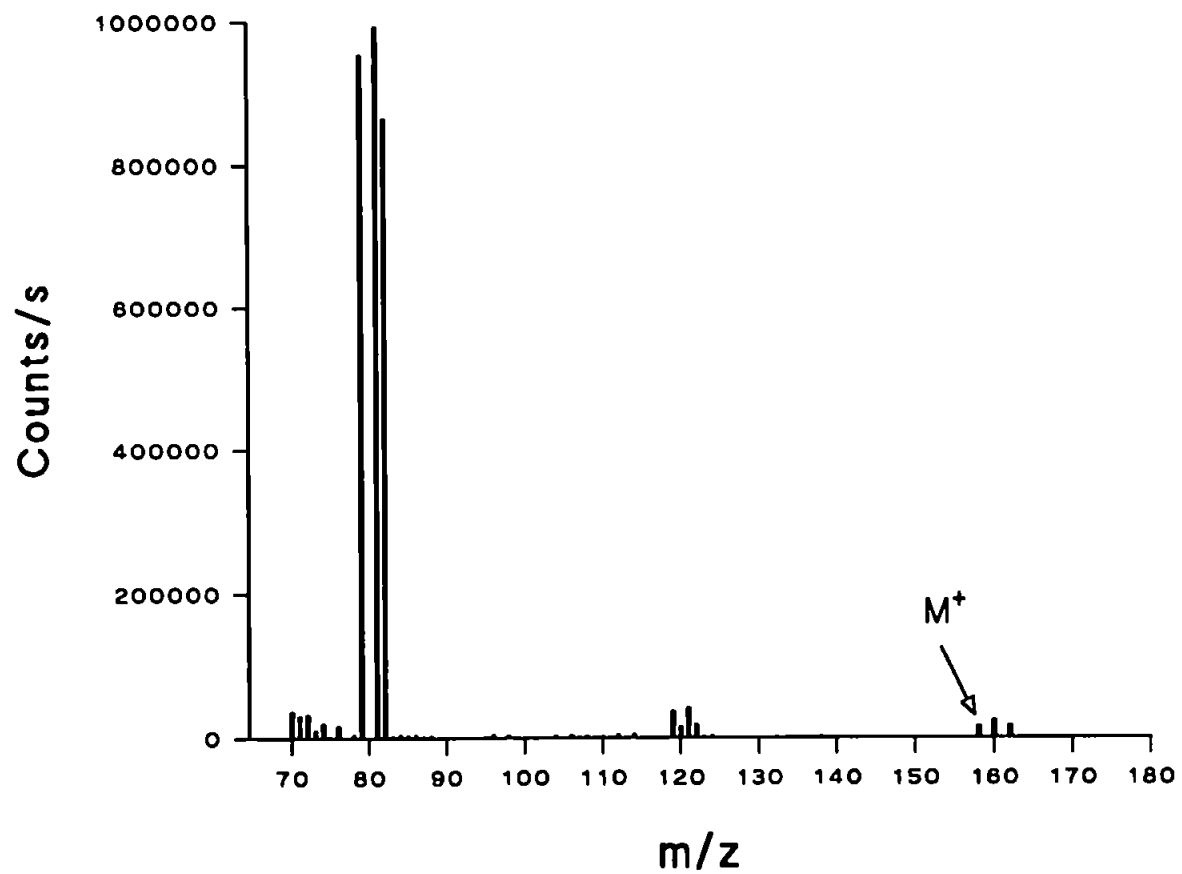
**Figure 5.9:** Fragmentation pattern obtained for bromobenzene (1000 ng on column) using an argon plasma (0.2 L/min at 125 W forward power)

could be observed. The results obtained with the argon plasma were encouraging and the use of helium was the next logical step.

In the case of helium the flow from the capillary column was used to sustain the plasma at powers between ~10 and 50 W. The advantage of the helium plasma was that the mass spectra were simpler due to the mono-isotopic nature and low mass number of helium (m/z 4). The inductively coupled plasma radio frequency power supply had the standard matching network used for high power argon plasmas. This limited the use of higher flow rates of helium, since the matching network would not allow the plasma to be sustained for any length of time at higher helium flows. Thus the helium flow from the capillary column was used to form the plasma. This resulted in a diffuse plasma at the sampler orifice and enabled the use of lower plasma powers (i.e. down to 10 W).

The helium plasma yielded analyte fragmentation patterns similar to that obtained with EI ionization, as can be seen in Figure 5.10. The molecular ions for chloro-, bromo- and iodobenzene can be seen at 112 (76 %) and 114 (24 %), 156 (49 %) and 158 (49 %), and 204 (100 %) m/z, with the isotope patterns matching that of the chlorine and bromine. The loss of the halogens to yield the phenyl ion at m/z 77 can also be seen. The fragmentation was shown to be concentration and power dependent as can be seen in Figure 5.11. The concentration dependence of the fragmentation may be related to the plasma
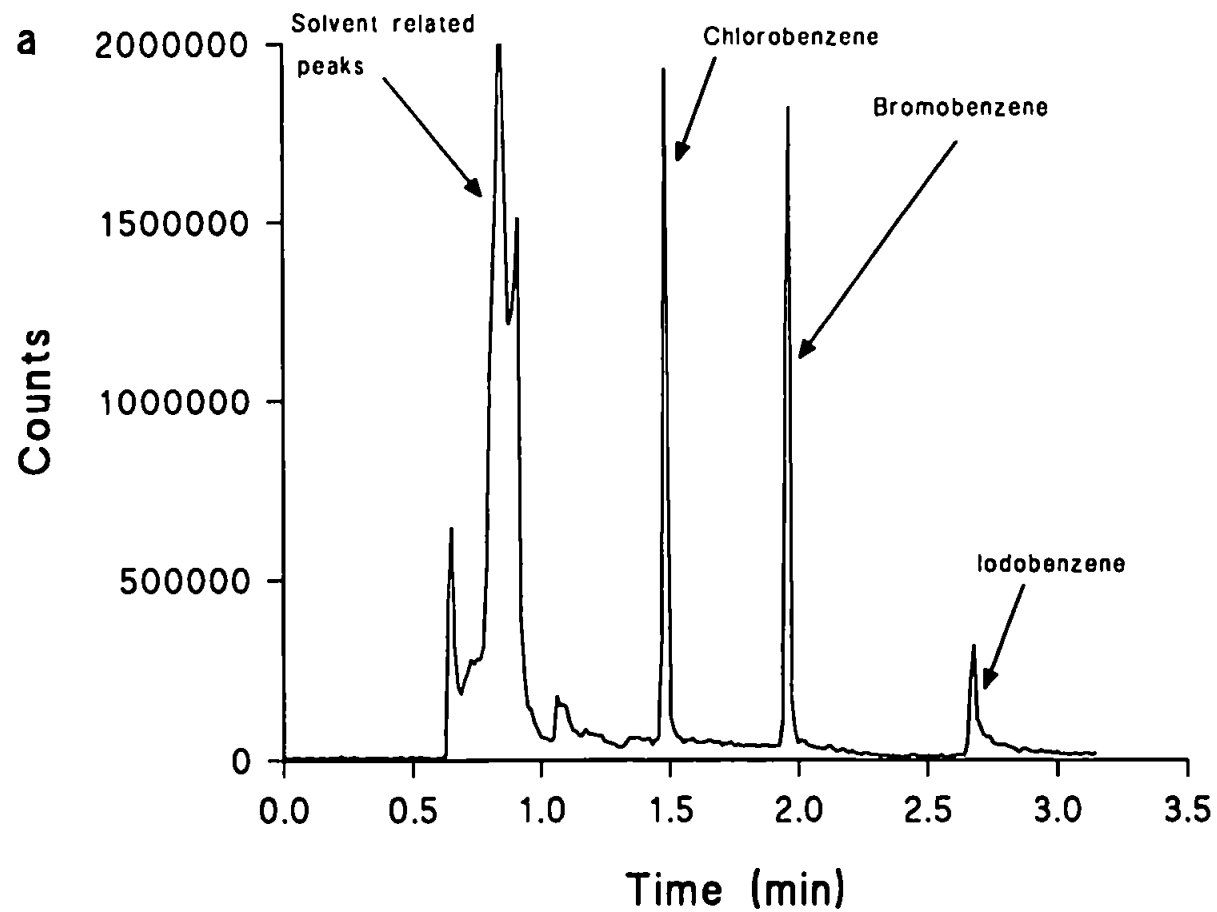
**Figure 5.10 (a):** GC-LP-ICP-MS chromatogram of chloro-, bromo- and iodobenzene (125 ng on column of each); plasma forward power 10 W; GC conditions as in Figure 5.2
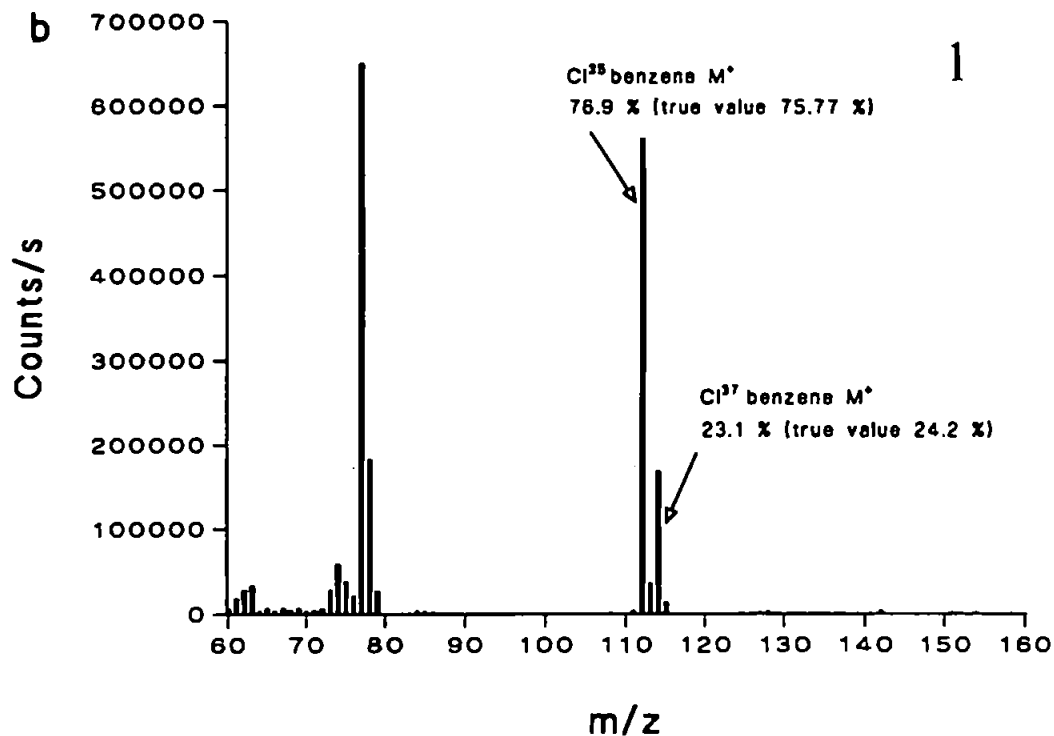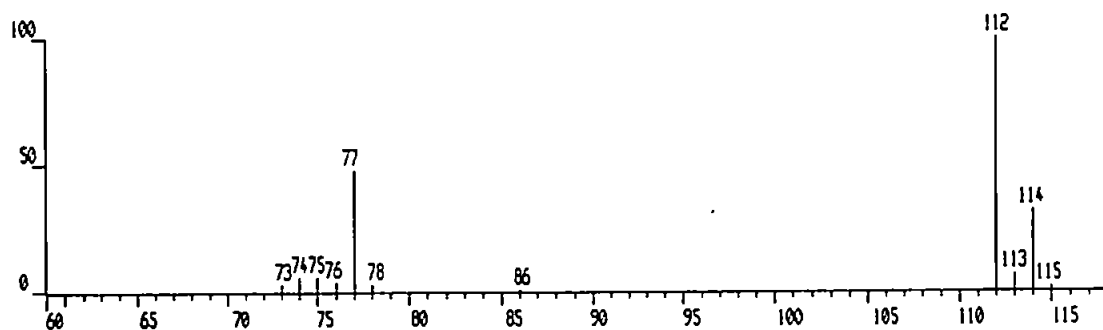
**Figure 5.10 (b):** Comparison of mass spectra of chlorobenzene; (1) fragmentation pattern obtained from GC-LP-ICP chromatogram in Figure 5.10 (a); (2) conventional electron impact fragmentation pattern

199
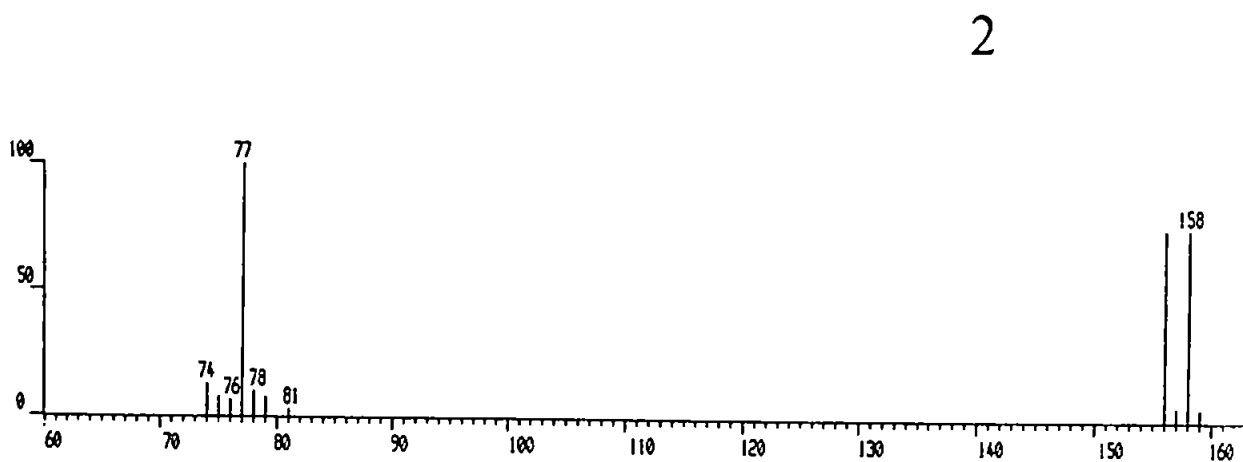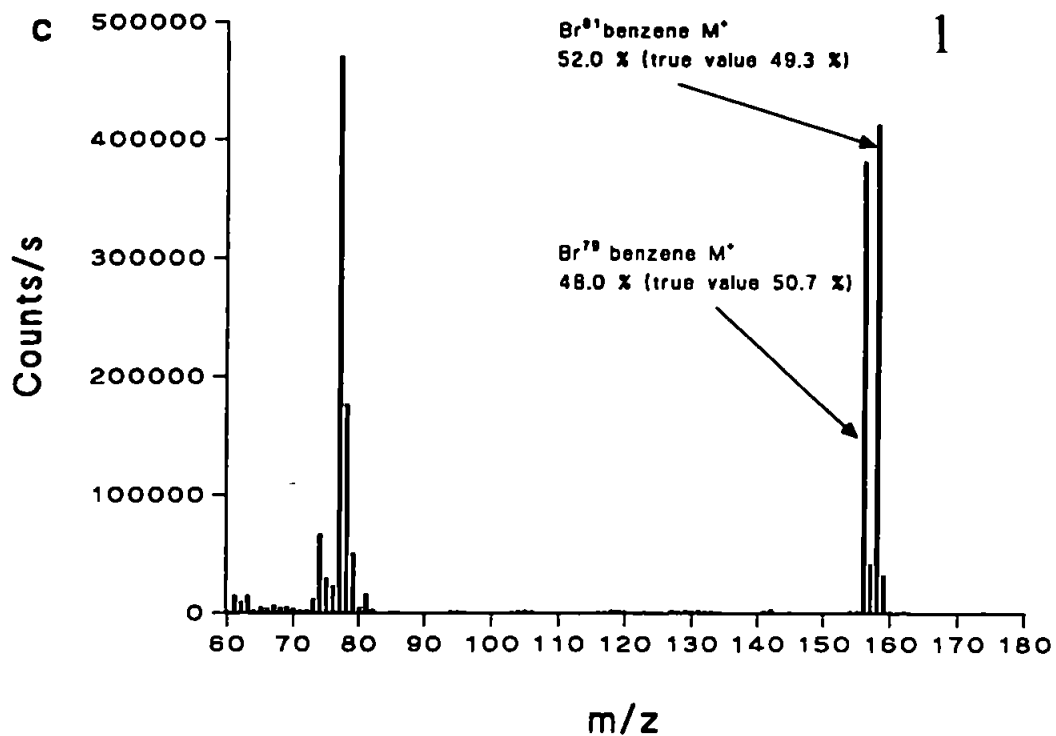
Figure 5.10 (c): Comparison of mass spectra of bromobenzene;
(1) fragmentation pattern obtained from GC-LP-ICP
chromatogram in Figure 5.9 (a); (2) conventional
electron impact fragmentation pattern

d
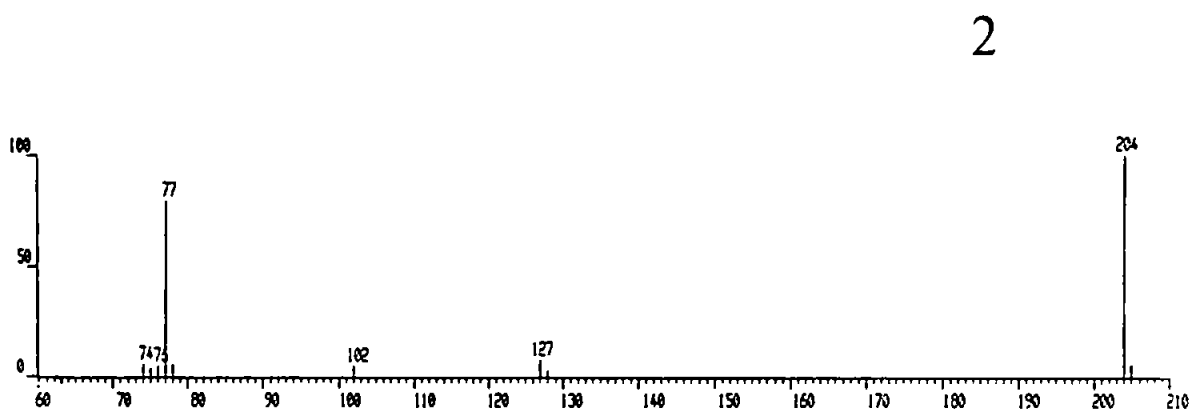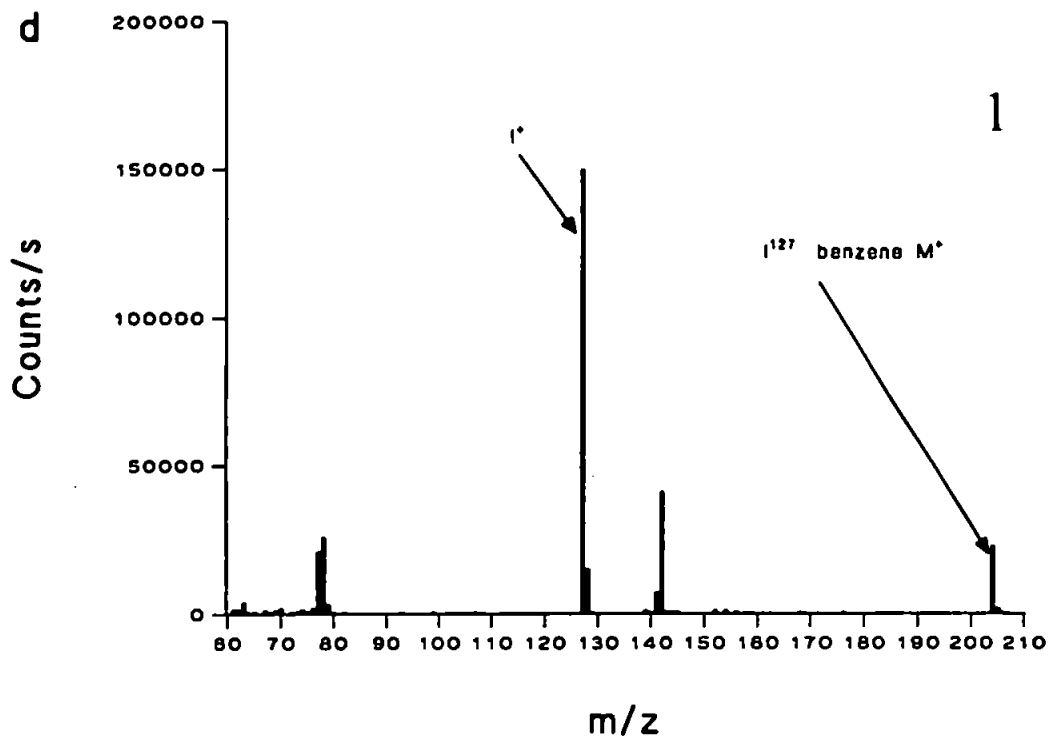


Figure 5.10 (d): Comparison of mass spectra of iodobenzene; (1)
fragmentation pattern obtained from GC-LP-ICP
chromatogram in Figure 5.9 (a); (2) conventional
electron impact fragmentation pattern
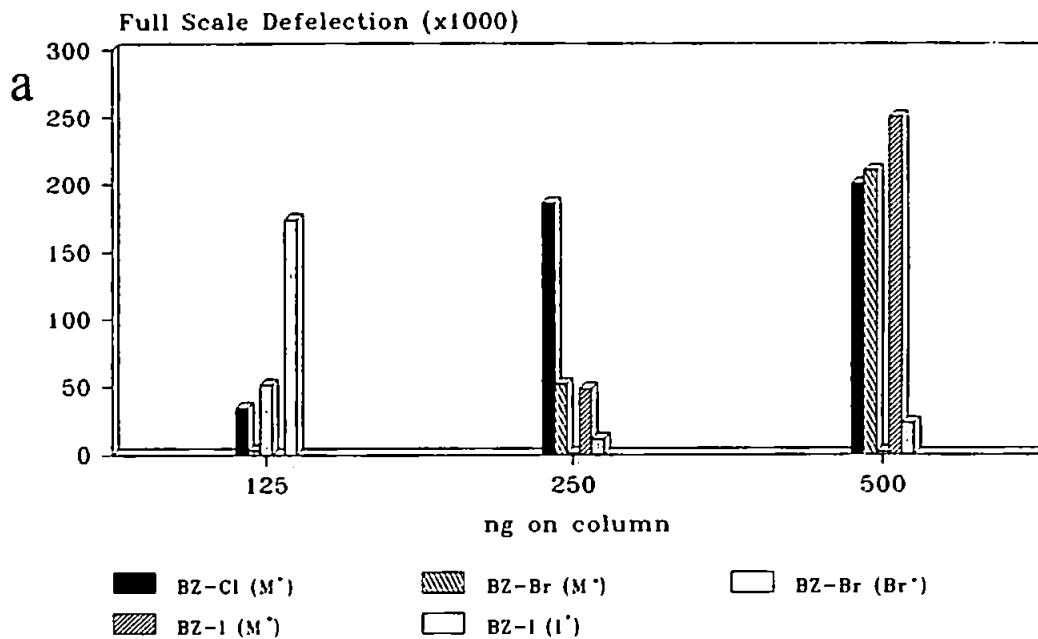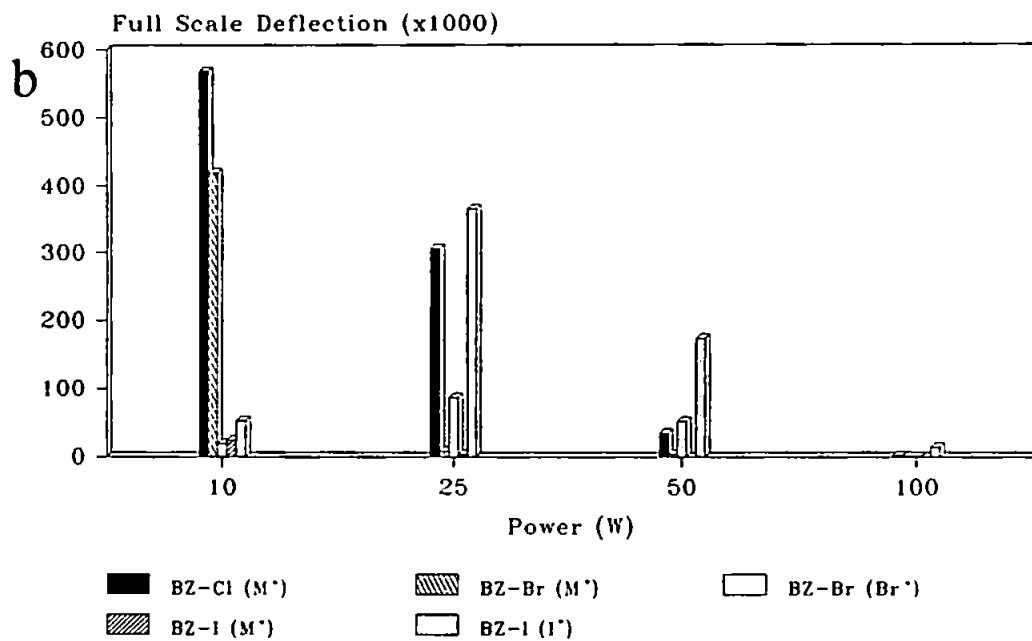
Figure 5.11: (a) Variation of molecular and atomic ion
intensities obtained with various amounts of
analytes injected;(b) Variation of molecular and
atomic ion intensities obtained at various plasma
forward powers; both using carrier gas (~3 ml/min
He) as plasma gas, GC conditions as in Figure 5.2

loading. The greatest response for the molecular ions was obtained with the lowest power used, while the maximum element selective detection occurred at higher powers. The molecular ion for chlorobenzene was observed for concentrations as low as 10 ng (at 10 W). The fragmentation of halobenzenes was related to the electron impact ionization potentials of the halo-benzenes, which increase in the order I (9.05 eV), Br (9.45eV) and Cl (9.55eV) [159]. Thus, the trend observed with the fragmentation versus element selective detection agrees with the trend in the ionization potentials of the halobenzenes, with iodobenzene and bromobenzene tending to produce $I^+$ and $Br^+$ ions derived from the halobenzene more readily than chlorobenzene.

In the initial experiments up to 5000 ng was injected on-column. This probably overloaded the plasma, whereas later experiments used 10-500 ng, which are closer to normal plasma operating conditions. The fragmentation of organic molecules using an MIP-MS was achieved by Olsen et al., by the introduction of pure analyte compounds into the tail flame of the plasma. This also probably overloaded the plasma [157]. That work was limited to high concentrations and no comments on the concentration dependence of the system were made.

## 5.7 Conclusions:

Initial experiments proved that by controlling the power of a

low pressure radio frequency plasma it was possible to obtain both atomic and molecular fragmentation spectra for a number of compounds.

The best results for the element selective analyses were obtained at higher powers (200 W) and for fragmentation were obtained at lower powers (10 W).

The ionization/fragmentation mechanism for both the helium and argon plasmas is complex and possibly involves a combination of electron impact, chemical and charge transfer ionizations. The mean free path of electrons in a low pressure plasma is longer than in atmospheric systems and consequently the electron is accelerated longer in a low pressure plasma compared with an atmospheric plasma. Hence the electrons in a low pressure plasma acquire higher energy than in an atmospheric plasma, even though the kinetic temperatures are much lower. The recombination energy of $He^{+}$ is 24.5 eV which is sufficient to fragment most organic molecules, hence the dominant processes would seem to be electron impact and charge transfer mechanisms [160].

# 6.0 CONCLUSIONS AND SUGGESTIONS FOR FUTURE WORK:

## 6.1 HGTC-ICP-MS:

A previously designed GC-ICP-MS interface was successfully modified to allow analysis of metalloporphyrins for the first time by this method. The modified interface gave detection limits in the low nanogram range (0.1-0.5 ng) for the metalloporphyrins, with minimal chromatographic band broadening. A new interface designed specifically for the HTGC-ICP-MS analysis of metalloporphyrins gave similar detection limits and minimal band broadening, but was easier to assemble and operate.

The HTGC-ICP-MS system allowed selected ion recording of 10 elements or more during a single chromatographic analysis. This enabled the analysis of geoporphyrins *via* HTGC-ICP-MS and illustrated the versatility of the system.

HTGC-ICP-MS showed the presence of previously unreported titanium porphyrins in Julia Creek oil shale and Green River shale. The titanium porphyrins could easily be distinguished from the co-eluting nickel porphyrins by the element specific detection of ICP-MS. Indeed, even the nickel isotope ratio ($Ni^{58}:Ni^{60}$) could be calculated, showing the potential of the system for positive identification of metallic elements present

in the analytes. The vanadium to nickel ratio, which has been suggested as an important maturity parameter for oils, was also calculated, further illustrating the potential of the system.

The first HTGC analysis of iron porphyrins in coal was reported herein, for Bagworth coal. HTGC-MS allowed identification of a number of ETIO porphyrin pseudohomologues and HTGC-ICP-MS confirmed these were iron containing porphyrins.

Unfortunately, HTGC-ICP-MS was restricted to qualitative analyses by the rapid degradation of gas chromatographic columns when analysing geoporphyrins. The degradation of HTGC columns has also been observed by Blum [162], with columns lasting only 20-30 injections. The lack of accurate reporting of information on the use/applicability of HTGC to the analysis geoporphyrins has compounded the misconception that geoporphyrins can be routinely analysed by HTGC.

The future of HTGC-ICP-MS for the analysis of geoporphyrins rests on further investigation of the nature of the column degradations and development of more robust phases. The development of bonded and cross-linked silicon porphyrin phases may be a starting point.

The HTGC-ICP-MS system could be applied to the screening of other geological samples for the presence of other volatile metallated species.

## 6.2 HPLC-ICP-MS:

HPLC-ICP-MS was successfully applied to the determination of gallium and nickel geoporphyrins in a number of coals and shales. The presence of nickel and gallium was confirmed and the system provided an alternative to the use of HTGC-ICP-MS, (particularly for quantitative work) but was limited in that only gallium and nickel could be analysed with the interface used. This limitation was due to the plasma being unstable with eluents containing high concentrations of volatile organic compounds, such as acetonitrile.

The integrity of the chromatography was maintained during the interfacing of HPLC to ICP-MS. This has not been achieved previously for metalloporphyrins. The maintenance of good chromatographic separation allowed the quantification of various porphyrin macrocycles. The UV/VIS results for the gallium porphyrins showed good agreement with that obtained previously [4,5,10,142], however UV/VIS results for the nickel porphyrins could not be compared with those obtained by other workers (due to the various extinction coefficients quoted for nickel porphyrins). The HPLC-ICP-MS and HPLC-UV/VIS results for porphyrins compared well. However, the quantitative results of the HPLC-ICP-MS and UV/VIS did not agree, probably due to the different extinction coefficients used by various workers [143-145,149,150]. This highlights the need for a standard reference material certified for metalloporphyrins and the use of standardized extinction coefficients.

Future work on the HPLC-ICP-MS system should concentrate on the development of an efficient desolvation interface, which would allow the use of common reverse phase HPLC eluents (acetonitrile and tetrahydrofuran). This would allow the development of chromatography for analysis of all possible metalloporphyrins in the geosphere. The analysis of other metallated species such as those reported by Fish et al. could be undertaken [25,26].

## 6.3 GC-Low Pressure-ICP-MS:

Metalloporphyrins did not successfully elute from the GC-LP-ICP-MS. The system was used for both element selective and molecular fragmentation of smaller molecules, by alteration of the gas flow, composition and the RF power of the plasma. The molecules fragmented (chloro-, bromo- and iodobenzene) showed the potential of this system.

The system needs further development, with the optimization of the interface and power being the most important criteria. Once this has been completed the fragmentation processes should be studied, this may require the use of a quadrupole that has a higher mass range (VG PlasmaQuad II limited to 256 amu). Ideally this could lead to a universal interface for HPLC and GC, which could be used for both element selective and molecular fragmentation.

# 7.0 EXPERIMENTAL:

## 7.1. Reagents and chemicals:

The reagents used were all AnalaR grade or, in the case of solvents HPLC glass distilled grade. MilliQ grade water was used throughout.

All porphyrins were obtained from Aldrich (U.K.), except gallium octaethylporphyrin (>98 % purity) which was obtained from Porphyrin Products Inc. (U.S.A.).

## 7.2. Extraction and Purification of Geoporphyrins from Oil Shales:

The shales used were Julia Creek (Eromanga Basin, Queensland, Australia, Cretaceous 105 million years) and Serpiano (Monte San Giorgio, Serpiano, Switzerland, Triassic 215 million years) and were supplied by Professor J.R. Maxwell (University of Bristol, U.K.).

Shales were extracted using the method described by Chicarelli et al. [122]. The shale was ground to < 75 $\mu$m, sieved and dried at 50°C (2 hours). Shale (20 g) was Soxhlet extracted with a mixture of dichloromethane and methanol (70:30; 48 hrs). The total organic extract was weighed and submitted to flash chromatography using hexane, hexane:dichloromethane (50:50), dichloromethane and dichloromethane:methanol (50:50). Fractions

were collected, weighed and the porphyrin content quantified using UV/VIS (Table 7.1).

The sample of nickel porphyrins from Marl Slate (Co. Durham, U.K., Permian, 250 million years) was provided by Dr. A.J.G Barwise (BP Research, Sunbury, U.K.). A porphyrin extract of Green River Shale (Colorado, U.S.A, Eocene, 50 million years) was obtained from Dr. A.W. Kim (University of Plymouth, U.K.).

The geoporphyrin samples were stored in vials covered with aluminium foil at 4°C prior to use. Sub-samples used for HTGC and HPLC were dissolved in dichloromethane and injected on-column.

The probe-MS and HTGC-MS data acquisition parameters used for the analysis of geoporphyrins are shown in Table 7.2.

The retention indices for the porphyrins were calculated using:

$$I = 100i \left[ (t'_{r(x)} - t'_{r(n)})/(t'_{r(n+i)} - t'_{r(n)}) \right] + 100n \quad \text{(Equation 7.1)}$$

Where I (retention index), i (difference in numbers of carbon atoms of the n-alkane references), t', (adjusted retention time), x (compound of interest and n (number of atoms in n-alkane) [161].

## 7.3. Extraction and Purification of Geoporphyrins from Coals:

| Shale/Coal | Nickel Porphyrins $(\mu g/g)$[1] | Vanadyl Porphyrins $(\mu g/g)$[2] | Gallium Porphyrins $(\mu g/g)$[3] |
|---|---|---|---|
| Julia Creek | 16.3 | 458 | / |
| Serpiano | 51.5 | 1334 | / |
| Bagworth | / | / | 0.84 |
| Markham Main | / | / | 0.19 |
| Gedling | / | / | 0.13 |

1.  Calculated using extinction coefficient of 22000 L/mol.cm (550 nm) and molecular mass of 532 [148]

2.  Calculated using extinction coefficient of 26000 L/mol.cm (570 nm) and molecular mass of 541 [143]

3.  Calculated using extinction coefficient of 400000 L/mol.cm (400 nm) and molecular mass of 600 [10]

**Table 7.1:** UV/VIS Quantification of nickel, vanadyl and gallium porphyrins

| Parameter | GC-MS | Probe |
|---|---|---|
| Ion source temperature | 170°C | 170°C |
| Electron energy | 70 eV | 16 eV |
| Emission current | 300 $\mu$A | 300 $\mu$A |
| Scan range/time | 400-700 (in 1 sec.) | 50-700 (in 3 sec.) |

**Table 7.2:** GC-MS and Probe-MS conditions

Coals were obtained from the British Coal Bank (British Coal, Glos., U.K.) and were received ready ground to 75 $\mu$m, data on these coals are shown in Tables 7.3-7.5.

The method developed by Bonnett *et al.* was used for extraction of porphyrins from the coal samples [10].

Coal (~ 100 g) was placed in a conical flask wrapped in aluminium foil to exclude light. Sulphuric acid (7%, 300 ml) in methanol was added, the flask sealed and the mixture stirred for 48 hours. The sulphuric/methanol mixture was filtered and extracted three times with 40 ml portions of chloroform. The chloroform was then washed with 50 ml of saturated sodium bicarbonate solution, followed by 50 ml of water. The extract was evaporated to dryness and submitted to thin layer chromatography (TLC).

TLC plates (1 mm or 0.25 mm x 300 mm) were prepared in-house using Merck silica gel H. The plates were pre-eluted with methanol/chloroform (50:50). The TLC work up procedure for the gallium and iron porphyrins is shown in Figure 7.1.

Concentrations of gallium porphyrin were determined using the UV/VIS method developed by Bonnett *et al.* and the results are shown in Table 7.1.

**7.4. Preparation of nickel (II) [4,4'(ethane-1,2-diyldiimino)bis(pent-3-enonato)]:**

**COAL: BAGWORTH**

**Proximate analysis, (% ad)**

| | |
|---|---|
| Moisture | 13.7 |
| Ash | 7.6 |
| Volatile matter | 34.1 |
| Fixed carbon | 44.6 |
| Volatile matter (dmmf) | 44.2 |

**Caking properties**

| | |
|---|---|
| Swelling index | ½ |
| Gray-King coke type | B |

**Calorific value**

| | |
|---|---|
| kJ/kg (daf) | 32640 |

**Ash fusion range (°C)[*]**

| | |
|---|---|
| Deformation temperature | 1180 |
| Hemisphere temperature | 1210 |
| Flow temperature | 1330 |

**Ultimate analysis, %**

| | | |
|---|---|---|
| Carbon | (dmmf) | 80.6 |
| Hydrogen | (dmmf) | 5.4 |
| Oxygen | (dmmf) | 11.8 |
| Nitrogen | (dmmf) | 1.37 |
| Sulphur organic | (db) | 0.69 |
| Sulphate as S | (db) | 0.03 |
| Pyritic sulphur as S | (db) | 0.51 |
| Chlorine | (db) | 0.10 |
| Carbon Dioxide | (db) | 0.88 |
| Mineral matter | (db) | 10.57 |

**Maceral analysis**

| | | |
|---|---|---|
| % Volume[2] | Vitrinite | 72 |
| | Exinite | 5 |
| | Inertinite | 23 |

**Mean maximum reflectance[3]**

| | |
|---|---|
| % - | 0.731 |
| sd % - | 0.062 |

**Ash analysis (% on ash)**

| | |
|---|---|
| $Na_2O$ | 1.6 |
| $K_2O$ | 1.0 |
| CaO | 16.0 |
| MgO | 1.2 |
| $Fe_2O_3$ | 9.2 |
| $Al_2O_3$ | 20.8 |
| $SiO_2$ | 33.2 |
| $SO_3$ | 12.4 |
| $TiO_2$ | 1.4 |
| $Mn_3O_4$ | 0.13 |
| $P_2O_5$ | 2.2 |

[*] Test atmosphere - reducing
(50% $CO_2$/50% $H_2$)
[2] Mineral matter/coal shale free
basis
[3] Total no. of points - 100
Oxygen by difference

| | |
|---|---|
| ad | - as analysed basis |
| db | - dry basis |
| daf | - dry, ash free basis |
| dmmf | - dry, mineral matter free |

**Table 7.3:** Petrographic data for Bagworth coal [141]

**COAL: MARKHAM MAIN**

### Proximate analysis, (% ad)

| | |
|---|---|
| Moisture | 8.4 |
| Ash | 3.4 |
| Volatile matter | 33.1 |
| Fixed carbon | 55.1 |
| Volatile matter (dmmf) | 37.9 |

### Caking properties

| | |
|---|---|
| Swelling index | 1 |
| Gray-King coke type | C |

### Calorific value

| | |
|---|---|
| kJ/kg (daf) | 33600 |

### Ash fusion range (°C)*

| | |
|---|---|
| Deformation temperature | 1070 |
| Hemisphere temperature | 1080 |
| Flow temperature | 1150 |

* Test atmosphere - reducing (50% $CO_2$/50% $H_2$)

2 Mineral matter/coal shale free basis

### Ultimate analysis, %

| | | |
|---|---|---|
| Carbon | (dmmf) | 82.4 |
| Hydrogen | (dmmf) | 5.2 |
| Oxygen | (dmmf) | 9.3 |
| Nitrogen | (dmmf) | 1.81 |
| Sulphur organic | (db) | 0.97 |
| Sulphate as S | (db) | 0.03 |
| Pyritic sulphur as S | (db) | 0.46 |
| Chlorine | (db) | 0.66 |
| Carbon Dioxide | (db) | 0.37 |
| Mineral matter | (db) | 4.73 |

### Maceral analysis

| | | |
|---|---|---|
| % Volume2 | Vitrinite | 80 |
| | Exinite | 7 |
| | Inertinite | 13 |

### Mean maximum reflectance

| | | |
|---|---|---|
| | % - | 0.50 |
| sd | % - | 0.08 |

### Ash analysis (% on ash)

| | |
|---|---|
| $Na_2O$ | 7.1 |
| $K_2O$ | 0.9 |
| CaO | 7.5 |
| MgO | 0.9 |
| $Fe_2O_3$ | 22.4 |
| $Al_2O_3$ | 23.9 |
| $SiO_2$ | 30.1 |
| $SO_3$ | 4.6 |
| $TiO_2$ | 1.1 |
| $Mn_3O_4$ | <0.1 |
| $P_2O_5$ | 2.2 |

| | | |
|---|---|---|
| ad | - | as analysed basis |
| db | - | dry basis |
| daf | - | dry, ash free basis |
| dmmf | - | dry, mineral matter free |
| mmf | - | mineral matter free |

**Table 7.4:** Petrographic data for Markham Main coal [141]

COAL: GEDLING

**Proximate analysis, (% ad)**

| | |
|---|---|
| Moisture | 10.0 |
| Ash | 2.0 |
| Volatile matter | 34.5 |
| Fixed carbon | 53.5 |
| Volatile matter (dmmf) | 39.4 |

**Caking properties**

| | |
|---|---|
| Swelling index | 1 |
| Gray-King coke type | C |

**Calorific value**

| | |
|---|---|
| kJ/kg (daf) | 33580 |

**Ash fusion range (°C)\***

| | |
|---|---|
| Deformation temperature | 1050 |
| Hemisphere temperature | 1130 |
| Flow temperature | 1180 |

**Ultimate analysis, %**

| | | |
|---|---|---|
| Carbon | (dmmf) | 81.6 |
| Hydrogen | (dmmf) | 5.2 |
| Oxygen | (dmmf) | 10.3 |
| Nitrogen | (dmmf) | 1.70 |
| Sulphur organic | (db) | 0.89 |
| Sulphate as S | (db) | 0.02 |
| Pyritic sulphur as S | (db) | 0.07 |
| Chlorine | (db) | 0.46 |
| Carbon Dioxide | (db) | 0.28 |
| Mineral matter | (db) | 2.76 |

**Maceral analysis**

| | | |
|---|---|---|
| % Volume[2] | Vitrinite | 72 |
| | Exinite | 8 |
| | Inertinite | 20 |

**Mean maximun reflectance[3]**

|  |  |
|---|---|
| % - | 0.638 |
| sd % - | 0.078 |

**Ash analysis (% on ash)**

| | |
|---|---|
| $Na_2O$ | 10.0 |
| $K_2O$ | .0.4 |
| CaO | 13.3 |
| MgO | 3.8 |
| $Fe_2O_3$ | 10.0 |
| $Al_2O_3$ | 19.3 |
| $SiO_2$ | 23.4 |
| $SO_3$ | 17.4 |
| $TiO_2$ | 0.62 |
| $Mn_3O_4$ | 0.34 |
| $P_2O_5$ | 0.09 |

\* Test atmosphere - reducing (50% $CO_2$/50% $H_2$)

[2] Mineral matter/coal shale free basis

[3] Total no. of points - 100
Oxygen by difference

| | |
|---|---|
| ad | – as analysed basis |
| db | – dry basis |
| daf | – dry, ash free basis |
| dmmf | – dry, mineral matter free |

**Table 7.5:** Petrographic data for Gedling coal [141]

216

Raw coal extract

TLC (Silica gel H, 1mm x 300 mm plate)
1. Toluene
2. 2% MeOH-Ammonia/Toluene
3. 15 % MeOH-Ammonia/Toluene

Gallium Porphyrins

Free-base Porphyrins
(Trace amounts)

TLC (Silica gel H, 0.25mm x 300mm plate)
1. 50-100 % Ethyl acetate/Toluene
2. 2-4 % MeOH-Ammonia/Ethyl acetate

Iron Porphyrins

2 Molar HCl

Gallium/Iron Porphyrin Chloride Complexes
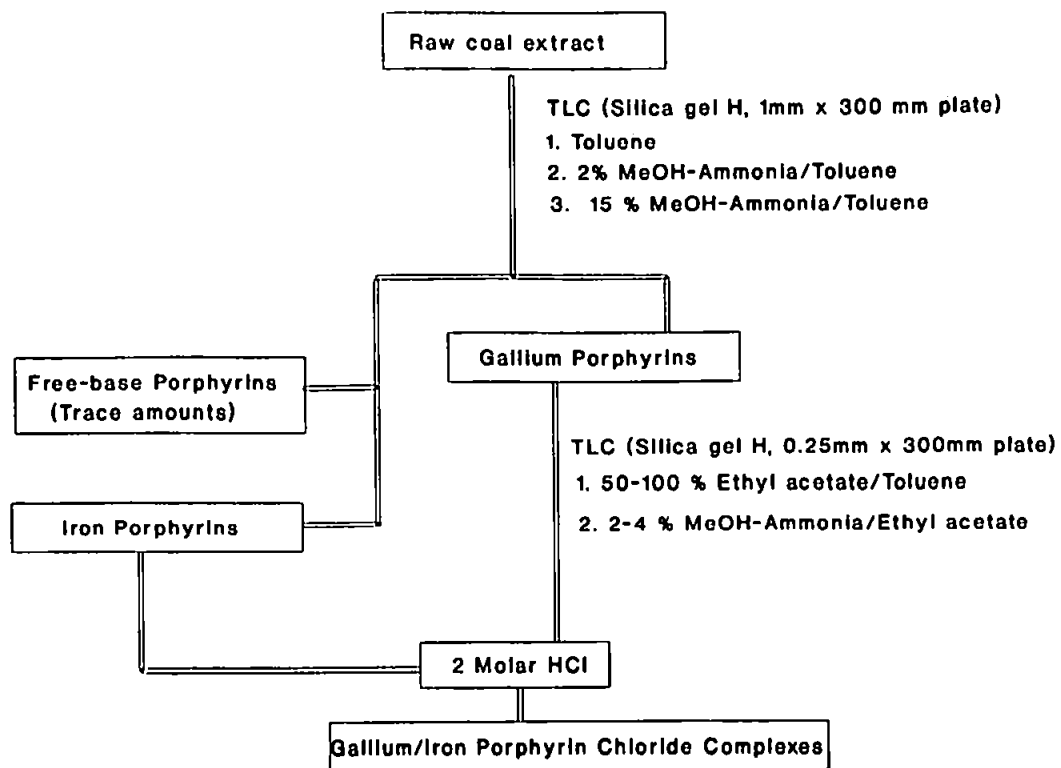
**Figure 7.1:** TLC procedures used for the separation of gallium and iron porphyrins from crude coal extract

Both nickel and vanadyl chelates were synthesised and purified, for use as internal standards for the HTGC-ICP-MS analysis of the geoporphyrin fractions. Unfortunately, use was pre-empted by the problems with HTGC column stability. The nickel chelate was however used as the standard for HPLC-ICP-MS determinations.

Both 4,4'-(ethane-1,2-diyldiimino)bis(pent-3-en-2-one) (AAED) and Nickel AAED were synthesised using a method described by Dilli *et al.* [146,147]. AAED was synthesised by the condensation of ethylene diamine with acetylacetone using ethanol as solvent.

AAED (2.24 g) dissolved in 10 ml of ethanol was added to a mixture of nickel acetate (2.487 g) dissolved in 30 ml of 1 M ammonium hydroxide. The mixture was maintained at 50°C for 30 minutes. The product was filtered and weighed (yield 49 %).

Crude product was sublimed at 150°C and 0.6 torr. The product was analysed by GC and shown to be > 98% pure.

Purified product was analysed using FTIR, GC-MS and $^1$H (Figure 7.2). The relevant peaks are shown below:

**FTIR:** 3050 (alkene), 2900 (alkane), 1600 (carbonyl), 1425 (alkane), 1300 (tertiary amine) $cm^{-1}$

**MS:** $M^{+\cdot}$ 280, 282 m/z ($^{58}Ni$ $C_{14}H_{20}N_2O_2$, $^{60}Ni$ $C_{14}H_{20}N_2O_2$)

$(M-111)^{+\cdot}$ 169, 171 m/z ($^{58}Ni$ $C_6H_9NO$, $^{60}Ni$ $C_6H_9NO$)
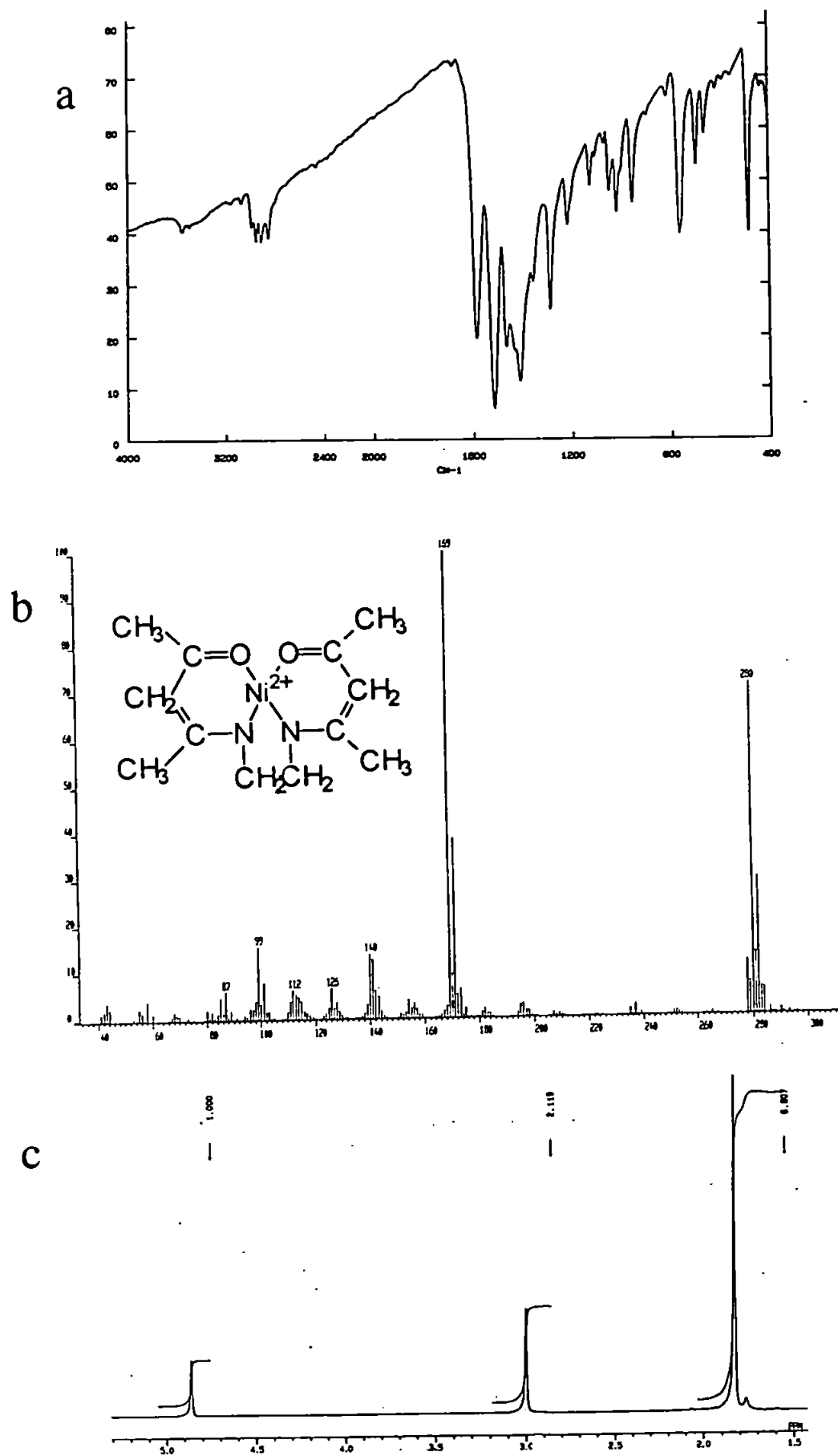
**Figure 7.2:** FTIR (a), MS (b) and $^1$H NMR (c) of [4,4'(ethane-1,2-diyldiimino) bis (pent-3-enonato)] Nickel (II)

218

$(M-140)^{+\cdot}$ 140,142 m/z ($^{58}$Ni C$_4$H$_6$NO, $^{60}$Ni C$_4$H$_6$NO)

$(M-168)^{+\cdot}$ 112 m/z (C$_6$H$_8$NO)

$(M-181)^{+}$·99 m/z (C$_5$H$_9$NO)

$^1$H NMR: 1.83 ppm (-CH$_3$), 3.0 (-CH$_2$ alkane), 4.86 (-CH$_2$ alkene)

# REFERENCES:

1. Treibs A., *Justus Liebig's Annalen der Chemie*, (1934), **510**, p. 42.

2. Filby R.H. and van Berkel G.J. in *"Metal Complexes in Fossil Fuels"*, ed. Filby R.H. and Branthaver J.F., (1987), ACS Symposium Series, **344**, New York, U.S.A., Chapter 1, p. 2-39.

3. Baker E.W. and Louda J.W., *Org. Geochem.*, (1984), **6**, p. 183.

4. Bonnett R. and Czechowski F., *Nature*, (1980), **283**, p. 465.

5. Bonnett R., Burke P.J., Czechowski F. and Rezka A., *Org. Geochem.*, (1984), **6**, p. 177.

6. Treibs A., *Angew. Chemie*, (1936), **49**, p. 682.

7. Corwin A.H., *Proc. 5ᵗʰ World Petroleum Congress*, (1960), Paper V-10, Section V, 119, New York.

8. Barwise A.J.G. and Roberts I., *Org. Geochem.*, (1984), **6**, p. 167.

9. Sudararaman P. in *"Biological Markers in Sediments and Petroleums"* ed. Moldowan J.M., Albrecht P. and Philp R.P., (1992), Prentice-Hall, Engelwood Cliffs, New York, U.S.A., Chapter 16, p. 313.

10. Bonnett R., Czechowski F. and Hughes P.S., *Chem. Geol.*, (1991), **91**, p. 193.

11. Gransh J.A. and Eisma E. in *"Advances in Organic Geochemistry 1966"* ed. Hobson G.D. and Speers G.C., (1970), Pergamon Press, Oxford, U.K., p. 69.

12. Hajibrahim S.K., Quirke J.M.E. and Eglinton G., *Chem. Geol.*, (1981), **32**, p. 173.

13. Barwise A.J.G., Park P.J.P. in *"Advances in Organic Geochemistry 1981"* ed. Bjoroy M., (1983), John Wiley, London, U.K., p. 668.

14. Moldowan J.M., Sundararaman P. and Schoell M., *Org. Geochem.*, (1986), **10**, p. 915.

15. Branthaver J.F. in *"Metal Complexes in Fossil Fuels"*, ed. Filby R.H. and Branthaver J.F., (1987), ACS Symposium Series, **344**, New York, U.S.A., Chapter 12, p. 189.

16. Quirke J.M.E., Eglinton G. and Maxwell J.R., *J. Amer. Chem. Soc.*, (1979), **101**, p. 7693.

17. Hajibrahim S.K., Tibbetts D.J.C., Watts C.D., Maxwell J.R. and Eglinton G., *Anal. Chem.*,(1978), **50**, p. 549.

18. Xu H. and Lesage S., *J. Chromatogr.*, (1992), **607**, p. 139.

19. Boreham C.J. and Fookes C.J.R., *J. Chromatogr.*, (1989), **467**, p. 195.

20. Sundararaman P., *Anal. Chem.*, (1985), **57**, p. 2204.

21. Sundararaman P., Biggs W.R., Reynolds J.G. and Fetzer J.C., *Geochim. Cosmochim. Acta*, (1988), **52**, p. 2337.

22. Mc Fadden W.H., Bradford D.C., Eglinton G., Hajibrahim S.K. and Nicoliades N., *J. Chromatogr. Sci.*, (1979), **17**, p. 518.

23. de Waal W.A.J., Heemstra S., Kraak J.C. and Jonker R.J., *Chromatographia*, (1990), **30**, p. 38.

24. de Waal W.A.J., Kuiper C.C., Maessen F.J.M. and Kraak J.C., *J. Chromatogr.*, (1989), **462**, p. 115.

25. Fish R.H. and Komlenic J.J., *Anal. Chem.*, (1984), **56**, p. 510.

26. Fish R.H., Komlenic J.J. and Wings B.K., *Anal. Chem.*, (1984), **56**, p. 2452

27. Boylan D.B., Alturki Y.I. and Eglinton G. in *"Advances in Organic Geochemistry 1968"* ed. Schenck P.A. and Havenaar I., (1969), Pergamon Press, Oxford, U.K., p. 227.

28. Marriott P.J., Gill J.P. and Eglinton G., *J. Chromatogr.*, (1982), **249**, p. 291.

29. Eckardt C.B., Dyas L., Yendle P.W. and Eglinton G., *Org. Geochem.*, (1988), **13**, p. 573.

30. Gill P.J., Evershed R.P., Chicarelli M.I., Wolff G.A., Maxwell J.R. and Eglinton G., *J. Chromatogr.*, (1985), **350**, p. 37.

31. Gill P.J., Evershed R.P. and Eglinton G., *J. Chromatogr.*, (1986), **369**, p. 281.

32. Marriott P.J., Gill P.J., Evershed R.P., Hein C.S. and Eglinton G., *J. Chromatogr.*, (1984), **301**, p. 107.

33. Marriott P.J., Gill J.P. and Eglinton G., *J. Chromatogr.*, (1982), **236**, p. 395.

34. Blum W., Ramstein P. and Eglinton G., *HRC and CC*, (1990), **13**, p. 85.

35. Hausler D.W. and Renfro D.H., *Symposium on Modern Analytical Techniques for the Analysis of Petroleum*, ACS Div. Pet. Chem. Meeting, New York, (1991), **36 (2)**, p. 225.

36. Quimby B.D., Dryden P.C. and Sullivan J.J., *HRC*, (1991), **14**, p. 110.

37. Zeng Y., Seeley J.A., Dowling T.M., Uden P.C. and Khuhawar M.Y., *HRC*, (1992), **15**, p. 669.

38. W. Blum, *PhD Thesis*, Bristol University, U.K., (1989), Chapter 5, p. 166.

39. S.M. Fields, PhD Thesis, Brigham Young University, Provo, Utah, U.S.A., p. 177 in [38] Chapter 2, p. 47.

40. Alturki Y.I., Eglinton G. and Pillinger C.T., in *"Advances in Organic Geochemistry 1971"* ed. von Gaertner H.R. and Wehner H., (1972), Pergamon Press, Oxford, U.K., p. 135.

41. Baker E.W., Yen T.F., Dickie J.P., Rhodes R.E. and Clark L.F., *J. Amer. Chem. Soc.*, (1967), **89**, p. 3631.

42. Wolff G.A., Chicarrelli M.I., Shaw G.J., Evershed R.P., Quirke J.M.E. and Maxwell J.R., *Tetrahedron*, (1984), **40**, p. 3777.

43. Quirke J.M.E., Eglinton G. and Maxwell J.R., *J. Amer. Chem Soc.*, (1979), **101**, p. 7693.

44. Wolff G.A., Murray M., Maxwell J.R., Hunter B.K. and Sanders J.K.M., *J. Amer. Chem. Soc. Comm.*, (1983), p. 922.

45. Ekstrom A., Fookes C.J.R., Hambley T., Loeh H.J., Miller S.A. and Taylor J.C., *Nature*, (1983), **306**, p. 173.

46. Quirke J.M.E. in *"Metal Complexes in Fossil Fuels"*, ed. Filby R.H. and Branthaver J.F., (1987), ACS Symposium Series, **344**, New York, U.S.A., Chapter 20, p. 308.

47. Chicarelli M.I. and Maxwell J.R., *Trends Anal. Chem.*, (1987), **6**, p. 158.

48. Quirke J.M.E., Eglinton G., Palmer S.E. and Baker E.W., *Chem. Geol.*, (1982), **35**, p. 69.

49. Baker E.W. and Plamer S.E. in *"The Porphyrins"* ed. Dolphin D., (1978), Academic Press Inc., New York, U.S.A., Chapter 11, p. 485.

50. Hood A., Carlson E.G. and O'Neal M.J. in *"Encyclopedia of Spectroscopy"* ed. Clark G.L., (1960), Nostrand-Reinhold, Princeton, New York, U.S.A., p. 616.

51. Blumer M. and Rudrum M., *J. Inst. Pet.*, (1970), **56**, p. 99.

52. Baker E.W. and Plamer S.E. in *"The Porphyrins"* ed. Dolphin D., (1978), Academic Press Inc., New York, U.S.A., p. 498.

53. Barwise A.J.G., Evershed R.P., Wolff G.A., Eglinton G. and Maxwell J.R., *J. Chromatogr.*, (1986), **368**, p. 1.

54. Chen J.H. and Philp R.P., *Chem. Geol.*, (1991), **91**, p. 139.

55. Ping'an P., Eglinton G., Jiamo F. and Guoying S., *Energy & Fuels*, (1992), **6**, p. 215.

56. Boreham C.J. in *"Biological Markers in Sediments and Petroleums"* ed. Moldowan J.M., Albrecht P. and Philp R.P., (1992), Prentice-Hall, Engelwood Cliffs, New York, U.S.A., Chapter 15, p. 301.

57. Sundararaman P. and Boreham C.J., *Geochim. Cosmochim. Acta*, (1993), **57**, p. 1367.

58. Eckardt C.B., Carter J.F. and Maxwell J.R., *Energy & Fuels*, (1990), **4**, p. 741.

59. Boylan D.B. and Calvin M., *J. Amer. Chem. Soc.*, (1967), **89**, p. 5472.

60. Gill J.P., *PhD Thesis*, (1984), Bristol University, Bristol, U.K., Chapter 2, p. 73-143.

61. Klesper E., Corwin A.H. and D.A. Turner, *J. Org. Chem.*, (1962), **27**, p. 700.

62. Karayannis N.M., Corwin A.H., Baker E.W., Klesper E. and Walter J.A., *Anal. Chem.*, (1968), **40**, p. 1736.

63. Karayannis N.M. and Corwin A.H., *J. Chromatogr.*, (1970), **47**, p. 247.

64. Gallegos E.J., Sundararaman P., Seifert W.K. and Treibs A., *Am. Chem. Soc. Meeting*, Geochemistry Division, Washington D.C., Sept., (1983)

65. Gallegos E.J. and Fetzer J.C., *Energy & Fuels*, (1991), **5**, p. 376.

66. Spencer-Smith J.L., *Phil. Mag.*, (1935), **19**, p. 1016.

67. Lynt R.W. and Gregg A.H., *Trans. Faraday Soc.*, (1940), **36**, p. 1062.

68. O'Halloran G.J., Fuegge R.A., Betts J.F., Everett W.L. and Walker L.W., *A.F Materials Laboratory ASP-TDR-62-644*, (1964), Parts I and II

69. Gray A.L., *Spectrochim. Acta*, (1985), **40 B**, p. 1525.

70. Boorn A.W., Fulford J.E. and Wegscheider W., *Mikrochim. Acta*, (1985), **2**, p. 171.

71. Dean J.R., Massey R.C. and Ebdon L., *J. Anal. Atom. Spectrom.*, (1987), **2**, p. 369.

72. Marshall J., Francis J., Abel I. and Tye C., *J. Anal. Atom. Spectrom.*, (1991), **6**, p. 145.

73. Horlick G. and Shao Y. in *"Inductively Coupled Plasmas in Analytical Atomic Spectometry: Second Edition"* ed. Montaser A. and Golightly D.W., (1992), VCH Publishers, New York, U.S.A., Chapter 12, p. 551.

74. Pretorius W., Foulkes M.E., Ebdon L. and Rowland S., *HRC*, (1993), **16**, p. 157.

75. Evans E.H., *Personal Communication*, (1993), University of Plymouth, U.K.

76. Thompson J.J. and Houk R.S., *Anal. Chem.*, (1986), **58**, p. 2541.

77. Jiang S.J., Palmieri M.D., Fritz J.S. and Houk R.S., *Anal. Chim. Acta*, (1987), **200**, p. 559.

78. Dean J.R., Munro S., Ebdon L., Crews H.M. and Massey R.C, *J. Anal. Atom. Spectrom.*, (1987), **2**, p. 607.

79. Beauchemin D., Bednas M.E., Berman S.S., Mc Laren J.W., Siu K.W.M. and Sturgeon R.E., *Anal. Chem.*, (1988), **60**, p. 2209.

80. Bushee D.S., *Analyst*, (1988), **113**, p. 1167.

81. Jiang S.J. and Houk R.S., *Spectromchim. Acta*, (1988), **43 B**, p. 405.

82. Branch S., Ebdon L., Hill S. and O'Neill P., *Anal. Proc.*, (1989), **26**, p. 401.

83. Shibata Y. and Morita M., *Anal. Sciences*, (1989), **5**, p. 107.

84. Beauchemin D., Siu K.W.M., Mc Laren J.W. and Berman S.S., *J. Anal. Atom. Spectrom.*, (1989), **4**, p. 285.

85. Crews H.M., Dean J.R., Ebdon L. and Massey R.C., *Analyst*, (1989), **114**, p. 895.

86. Heitkemper D., Creed J., Fricke F.L. and Caruso J., *J. Anal. Atom. Spectrom.*, (1989), **4**, p. 279.

87. Suyani H., Heitkemper D., Creed J. and Caruso J., *Appl. Spectrosc.*, (1989), **43**, p. 962.

88. Matz S.G., Elder R.C. and Tepperman K., *J. Anal. Atom. Spectrom.*, (1989), **4**, p. 767.

89. Brown M.A., Kim I.S., Roehl R., Sasinos F.I. and Stephens R.D., *Chemoshpere*, (1989), **19**, p. 1921.

90. Sheppard B.S., Shen W.L, Caruso J., Heitkemper D.T. and Fricke F.L., *J. Anal. Atom. Spectrom.*, (1990), **5**, p. 431.

91. Gercken B. and Barnes R.M., *Anal. Chem.*, (1991), **63**, p. 283.

92. Mc Laren J.W., Siu K.W.M., Lam J.W., Willie S.N., Maxwell P.S., Palepu A., Koether M. and Berman S.S., *Fresenius J. Anal. Chem.*, (1990), **337**, p. 721.

93. Al-Rashdan A., Heitkemper D. and Caruso J.A., *J. Chromatogr. Sci.*, (1991), **29**, p.98.

94. Al-Rashdan A., Vela N.P., Caruso J.A. and Heitkemper D., *J. Anal. Atom. Spectrom.*, (1992), **7**, p. 551.

95. Kawabata K., Kishi Y., Kawaguchi O., Watanabe Y. and Inoue Y., *Anal. Chem.*, (1991), **63**, p. 2137.

96. Owen L.M.W., Crews H.M., Hutton R.C. and Walsh A., *Analyst*, (1992), **117**, p. 649.

97. Sheppard B.S., Caruso J.A., Heitkemper D.T. and Wolnik K.A., *Analyst*, (1992), **117**, p. 971.

98. Braverman D.S., *J. Anal. Atom. Spectrom.*, (1992), **7**, p. 43.

99. Shum S.C.K., Neddersen K. and Houk R.S., *Analyst*, (1992), **117**, p. 577.

100. Shum S.C.K., Ping H. and Houk R.S., *Anal. Chem.*, (1992), **64**, p. 2444

101. Beauchemin D., Micklethwaite R.K., Van Loon G.W. And Hay G.W., *Chem. Geol.*, (1992), **95**, p. 187.

102. Carter J., *Personal Communication*, (1993), Bristol University, U.K.

103. Wolf W.R., Irgolic K., Ludwicki R.J., Mehlhorn R.J., Mertz W., Mills C.F., Oehichen U., Piscator M., Sadler P.J., Thorneley R.N.F., Weber G. and Zeppezauer in *"Importance of Chemical Speciation in Environmental Processes"* ed. Bernhard M., Brinkman F.E. and Sadler P.J., (1986), Springer-Verlag, Berlin, Germany, p. 17.

104. van Loon J.C., Alcock L.R., Pinchin W.H. and French B., *Spectro. Lett.*, (1986), **19**, p. 1125.

105. Chong N.S. and Houk R.S., *Appl. Spectrosc.*, (1987), **41**, p. 66.

106. Peters G.R. and Beauchemin D., *J. Anal. Atom. Spectrom.*, (1992), **7**, p. 965.

107. Peters G.R. and Beauchemin, *Anal. Chem.*, (1993), **65**, p. 97.

108. Kim A., Foulkes M.E., Ebdon L., Hill S., Patience R.L., Barwise A. and Rowland S.J., *J. Anal. Atom. Spectrom.*, (1992), **7**, p. 1147.

109. Kim A., Hill S., Ebdon L. and Rowland S.J., *HRC*, (1992), **15**, p. 665.

110. Evans E.H. and Caruso J.A., *J. Anal. Atom. Spectrom.*, (1993), **8**, p. 427.

111. Kim A.W., *Ph.D. Thesis*, (1993), University of Plymouth, Plymouth, U.K., Chapter 2, p. 52-88.

112. De Zeeuw J., *Chrompack News*, (1990), **17**, p. 3.

113. Chrompack Reprint *"High Temperature Gas Chromatography"*, (1990), **no. 503551**.

114. Chrompack Reprint *"Unbreakable Unimetal columns for high temperature and process applications"*, (1992), **no. 503560**.

115. Beens J., *Hewlett-Packard Third AED Users Meeting*, May 1993, Riva del Garda, Italy.

116. Sundararaman P., Biggs W.R., Reynolds J.C. and Fetzer J.C., *Geochim. Cosmochim. Acta*, (1988), **52**, p. 2337.

117. van Berkel C.J., Quirke J.M.E. and Filby R.H., *Org. Geochem.*, (1989), **14**, p. 119.

118. Ocampo R., Bauder C., Callot H.J. and Albrecht P., *Geochim. Cosomochim. Acta*, (1992), **56**, p. 745.

119. Sundararaman P. and Moldowan J.M., *Geochim. Cosomochim. Acta*, (1993), **57**, p. 1379.

120. Blum W. and Eglinton G., *HRC*, (1989), **12**, p. 290.

121. Blum W., Richter W.J. and Eglinton G., *HRC*, (1988), **11**, p. 148.

122. Chicarelli M.I., Eckardt C.B., Owen C.R., Maxwell J.R., Eglinton G., Hutton R.C. and Eaton A.N., *Org. Geochem.*, (1990), **15**, p. 267.

123. Hutton R.C., *J. Anal. Atom. Spectrom.*, (1986), **1**, p. 259.

124. Al Swaidan H.M., *Anal. Letters*, (1988), **21**, p. 1487.

125. Fookes C.J.R., *J. Chem. Soc. Chem. Comm.*, (1983), p. 1472.

126. Fookes C.J.R., *J. Chem. Soc. Chem. Comm.*, (1983), p. 1474.

127. Fookes C.J.R. and Loeh H.J., *Proc. 1" Australian Workshop on Oil Shales*, May 1983, Lucas Heights, p. 65.

128. Boreham C.J., Fookes C.J.R., Popp B.N. and Hayes J.M., *Geochim. Cosomochim. Acta*, (1989), **53**, p. 2451.

129. W. Blum, *PhD Thesis*, Bristol University, U.K., (1989), Chapter 2, p. 91-92.

130. Yen T.F., Boucher C.J., Dickie J.P., Tynan E.C., Vaughan G.B., *J. Inst. Pet. (London)*, (1969), **55**, p. 87.

131. Saitoh K., Kiyohara C. and Suzuki N., *J. Chromatogr.*, (1992), **603**, p. 231.

132. Mango F.D., *Geochim. Cosomochim. Acta*, (1992), **56**, p. 553.

133. Lynch A.W., *Appl. Catal.*, (1986), **24**, p. 227.

134. Kim A.W., *Ph.D. Thesis*, (1993), University of Plymouth, Plymouth, U.K., Chapter 4, p. 141-169.

135. Eglinton G., Maxwell J.R., Evershed R.P. and Barwise A.J.G., *Interdisciplinary Science Reviews*, (1985), **10**, p. 222.

136. Gill J.P., *PhD Thesis*, (1984), Bristol University, Bristol, U.K., Chapter 1, p. 40-46.

137. Shakespeare, "*Hamlet*", 1 b.

138. "*SGE Chromatogaphy Products*", 1992/93 Catalogue, SGE U.K., p. 40.

139. Hill S.J., Hartley J. and Ebdon L., *J. Anal. Atom. Spectrom.*, (1992), 7, p. 23.

140. Rood D., "*A Practical Guide to the Care, Maintenance and Troubleshooting of Capillary Gas Chromatographic systems*", (1991), Huthig, Heidelberg, Germany.

141. Burchill P. and Way D.S., "*Coal Research Establishment: The CRE Coal Sample Bank: A Users Handbook*", (1993), British Coal, Cheltenham, U.K.

142. Bonnett R. and Czchowski F., *J. Chem. Soc. Perkin Trans. I*, (1984), p. 125.

143. Barwise A.J.G. and Whitehead E.V. in "*Advances in Organic Geochemistry 1979*" ed. Douglas A.G. and Maxwell J.R., (1980), Pergamon Press, Oxford, U.K., p. 181.

144. Popp B.N. and Hayes J.M., *Energy & Fuels*, (1993), 7, p.

145. Waring J.R., *PhD Thesis*, (1991), Bristol University, Bristol, U.K., Chapter 7, p. 206.

146. Dilli S. and Pastalides E., *J. Chromatogr.*, (1977), **130**, p. 251.

147. Dilli S. and Pastalides E., *Aust. J. Chem.*, (1981), **34**, p. 1579.

148. Gibbson R., *Personal Communication*, (1993), Bristol University, U.K.

149. Chicarelli M.I., *PhD Thesis*, (1985), Bristol University, Bristol, U.K.

150. Gill J.P., *PhD Thesis*, (1984), Bristol University, Bristol, U.K., Chapter 7, p. 386.

151. Creed J.T., Davidson T.M., Shen W.C. and Caruso J.A., *J. Anal. Atom. Spectrom.*, (1990), **5**, p. 109.

152. Story W.C., Olson L.K., Shen W.L., Creed J.T. and Caruso J.A., *J. Anal. Atom. Spectrom.*, (1990), **5**, p. 467.

153. Story W.C. and Caruso J.A., *J. Anal. Atom. Spectrom.*, (1993), **8**, p. 427.

154. Vela N.P., Olson L.K. and Caruso J.A., *Anal. Chem.*, (1993), **65**, p. 585 A.

155. Heppner R.A., *Anal. Chem.*, (1983), **55**, p. 2170.

156. Poussel E., Mermet J.M., Deruaz D. and Beaugrand C., *Anal. Chem.*, (1988), **60**, p. 923.

157. Olson L.K., Story C.W., Creed J.T., Shen W.C. and Caruso J.A., *J. Anal. Atom. Spectrom.*, (1990), **5**, p. 471.

158. Kim A.W., *Ph.D. Thesis*, (1993), University of Plymouth, Plymouth, U.K., Chapter 3, p. 94.

159. Loudon A.G. in *"The chemistry of the carbon-halogen bond: Part 1"*, ed. Patai S., (1973), John Wiley and Sons, London, U.K., Chapter 4, p. 223.

160. Chapman J.R., *"Practical Organic Mass Spectrometry"*, (1986), John Wiley & Sons, Chichester, U.K., Chapter 3, p. 46.

161. van den Dool H. and Kratz P.D., *J. Chromatogr.*, (1963), **11**, p. 463.

162. W. Blum, *PhD Thesis*, Bristol University, U.K., (1989), Chapter 6, p. 171.

# APPENDIX A

**MOLECULAR IONS FOR NICKEL AND VANADYL GEOPORPHYRINS:**

| Carbon number | Ni A | Ni A-2 | Ni A-4 | V=O A | V=O A-2 | V=O A-4 |
|---|---|---|---|---|---|---|
| $C_{25}$ | 436 438 | 434 436 | 432 434 | 445 | 443 | 441 |
| $C_{26}$ | 450 452 | 448 450 | 446 448 | 459 | 457 | 455 |
| $C_{27}$ | 464 466 | 462 464 | 460 462 | 473 | 471 | 469 |
| $C_{28}$ | 478 480 | 476 478 | 474 476 | 487 | 485 | 483 |
| $C_{29}$ | 492 494 | 490 492 | 488 490 | 501 | 499 | 497 |
| $C_{30}$ | 506 508 | 504 506 | 502 504 | 515 | 513 | 511 |
| $C_{31}$ | 520 522 | 518 520 | 516 518 | 529 | 527 | 525 |
| $C_{32}$ | 534 536 | 532 534 | 530 532 | 543 | 541 | 539 |
| $C_{33}$ | 548 550 | 546 548 | 544 546 | 557 | 555 | 553 |
| $C_{34}$ | 562 564 | 560 562 | 558 560 | 571 | 569 | 567 |
| $C_{35}$ | 576 578 | 574 576 | 572 574 | 585 | 583 | 581 |
| $C_{36}$ | 590 592 | 588 590 | 586 588 | 599 | 597 | 595 |

*Molecular ions for both major isotopes of nickel shown ($^{58}$Ni, $^{60}$Ni)*

# APPENDIX B

**PUBLICATIONS:**

1. W. Pretorius, M. Foulkes, L. Ebdon and S. Rowland, *"HPLC Coupled with ICPMS for the determination of Metalloporphyrins in Coal Extracts"*, Journal of High Resolution Chromatography, (1993), **16**, p. 157-160.

2. W.G. Pretorius, L. Ebdon and S.J. Rowland, *"Development of a high temperature gas chromatography-inductively coupled plasma mass spectrometry interface for the determination of metalloporphyrins"*, Journal of Chromatography, (1993), **646**, p. 369-375.

3. E.H. Evans, W.G. Pretorius, L. Ebdon and S.J. Rowland, *"Low pressure inductively coupled plasma ion source for molecular and atomic spectrometry"*, submitted to Analytical Chemistry (1994)

4. L. Ebdon, W.G.Pretorius and S.J. Rowland, *"HPLC-ICP-MS and HTGC-ICP-MS of geoporphyrins"*, submitted to Journal of Analytical Atomic Spectrometry (1994)

# APPENDIX C

1. *"GC and HPLC coupled to ICP-MS for element selective detection"*, South African Chemical Society (Eastern Cape region), Seminar, University of Port Elizabeth, November 1992. **(Oral presentation)**

2. *"Development of a High Temperature Gas Chromatography-Inductively Coupled Plasma-Mass Spectrometry interface"*, Fifteenth International Symposium on Capillary Chromatography, Riva del Garda, Italy, May 1993. **(Poster presentation and travel award)**

3. *"HPLC and HTGC-ICP-MS analysis of metalloporphyrins"*, Annual British Organic Geochemical Society Meeting, University of Plymouth, July 1993. **(Oral presentation)**

4. *"HTGC and HPLC-ICP-MS for the analysis of geoporphyrins"*, 1994 Winter Conference on Plasma Spectrochemistry, San Diego, California, January 1994. **(Poster presentation)**

**Related Presentation:**

H.E. Evans, W. Pretorius, P.J. Worsfold, L. Ebdon and S. Rowland, paper FL6.1 presented at XXVIII Colloquium Spectroscopicum Internationale, July 1993. **(Oral presentation by H.E. Evans)**

# APPENDIX D

**LECTURES ATTENDED:**

1. Weekly Seminars at University of Plymouth, 1992-1994

2. Fortnightly Seminars at Plymouth Marine Laboratory, 1992-1993

3. Royal Society: Analytical Division (South West), Lectures, 1992-1994